Master's thesis

2019

Kristine Glomsås Nymoen

NTNU
Norwegian University of
Science and Technology
Faculty of Engineering
Department of Geoscience and Petroleum

Kristine Glomsås Nymoen

Palaeoproterozoic Tectonomagmatic Evolution and Crustal Architecture of the SW Margin of Fennoscandia

A geochronological, geochemical and isotope study of Grytøya, Bjarkøya, Sandsøya and Krøttøya, Troms, Norway.

NTNU
Norwegian University of
Science and Technology

NTNU

Norwegian University of
Science and Technology

Palaeoproterozoic Tectonomagmatic Evolution and Crustal Architecture of the SW Margin of Fennoscandia

A geochronological, geochemical and isotope study of Grytøya, Bjarkøya, Sandsøya and Krøttøya, Troms, Norway.

Kristine Glomsås Nymoen

Geology
Submission date: May 2019
Supervisor: Trond Slagstad
Co-supervisor: Bjørn Eske Sørensen

Norwegian University of Science and Technology
Department of Geoscience and Petroleum

Abstract

The study area comprises the four islands Grytøya, Bjarkøya, Sandsøya and Krøttøya in Troms, Norway, located on what was the SW margin of the Fennoscandian Shield in late Paleoproterozoic time. The lithologies found in this area are graphite- and sulphide-bearing supracrustal rocks (quartzite, amphibolite, slate, meta-arkose, calc-silicates) intruded by Paleoproterozoic meta-gabbros, granodiorites and granites overthrusted by the Caledonian nappes from the west. The oldest lithology found in this area consists of gneissic supracrustal rocks found at Bjarkøya and as xenoliths at Sandsøya, that resemble the supracrustal rocks in Rombak Tectonic Window (RTW). From field observations it is found that these supracrustals are intruded by younger granitic rocks. The supracrustal rocks of RTW were deformed during the Svecofennian Orogeny (D_1+D_2) in a compressional tectonic setting, before they were intruded by voluminous granitic rocks.

Comprehensive U-Pb geochronology analytical work by LA-ICP-MS and SHRIMP has been performed and shows that the supracrustal rocks at Bjarkøya (1869 ± 42 Ma) have similar ages as the supracrustal rocks of Kiruna in Sweden (1.88 Ga). The intrusive rocks of the RTW (1.80-1.79 Ga) show similar ages as the intrusive rocks of the study area (1811 ± 52 Ma to 1770 ± 16). Whole-rock geochemistry from the volcanic and intrusive rocks of the RTW and the intrusive rocks of the study area show variations in the major element concentrations within rocks from the same units. Trace elements for the volcanic and intrusive rocks of RTW and the intrusive rocks from the study area show a general subduction zone signature in chondrite- and primitive mantle-normalized diagrams (high concentration of the LILE, low concentrations of the HFSE and negative Na and Tb anomalies). Isotopic data have been obtained from both zircon and whole-rock, indicating a primarily crustal melt source for both the intrusive rocks of the RTW (ε_{Nd}=-3.4 to -6.9) and the intrusive rocks from the study area (ε_{Nd}=-7.2 to -8.7, ε_{Hf}=-3.0 to -13), with the intrusive rocks from the study area showing a lower degree of mixing/and or assimilation by depleted mantle melt than the intrusive rocks of RTW. The volcanic rocks from the RTW show a slightly more juvenile composition (ε_{Nd}=-2.8 to -6.4) and are interpreted to have a subduction-related origin and reflect the establishment of a continental arc that was intruded shortly after formation, by crustally derived intrusive granitic rocks.

In light of the new geochronological, geochemical and isotopic data from the study area, a comparison with similar rocks found in the RTW, West-Troms Basement Complex, Lofoten Vesterålen area and Central Nordland Basement Windows indicates that the 1.8 Ga granitic rocks from the study area were part of a short-lived but geographically widespread magmatic regional event. The differences in SiO_2, MgO and FeO and isotopic data between the volcanic rocks in RTW and the intrusive rocks of RTW and the study area and the absence of D_1 and D_2 structures in the intrusive rocks suggest a change in the tectonic setting for the intrusive rocks. This thesis suggests delamination as an explanation for the short-lived, voluminous magmatism taking place at 1790-1800 Ma. A compression resulting in thickening of the crust probably formed cold, dense eclogitic rocks at a lower crustal/lithospheric level that delaminated and sank. This process led to asthenosphere ascending towards the base of the crust and melting it. Isotope data supports the idea of an Archean-Paleoproterozoic boundary south of the study area but gives no further constraint regarding its exact position. Most richly mineralised regions in Sweden are located in 1.88 Ga metasupracrustal rocks. The field and geochronological data from the study area show that although such rocks may have extended further west into Norway, they are intruded by ca. 1.80 Ga granites. Gravity maps show that the mineralised areas in Sweden are located in high-gravity regions that do not continue into Norway. This is presumably due to the presence of voluminous 1.8 Ga granites in Norway that has removed

most of the potentially mineralised rocks. The potential of finding economically sustainable mineralisations in the supracrustals in Norway is therefore believed to be low.

Sammendrag

Feltområdet omfatter de fire øyene Grytøya, Bjarkøya, Sandsøya og Krøttøya i Troms, Norge, lokalisert på den tidligere sørvestlige marginen av det Fennoskandiske skjold i sen-paleoproterozoisk tid. Litologiene som finnes der består av grafitt- og sulfid-førende suprakrustaler (kvartsitt, amfibolitt, skifer, meta-arkose, kalk-silikater) intrudert av paleoproterozoiske meta-gabbroer, granodioritter og granitter med kaledonske skyvedekker skøvet over disse bergartene fra vest. Den eldste litologien funnet i området består av suprakrustale gneisser funnet på Bjarkøya og som opptrer i xenolitter på Sandsøya, som viser likhetstrekk med suprakrustalene funnet i det tektoniske vinduet i Rombak (RTW). Fra feltobservasjoner finner man at disse suprakrustalene er intrudert av yngre granittiske bergarter. Suprakrustalene fra RTW ble deformert under den svekofenniske orogenesen (D_1+D_2) i en tektonisk setting dominert av kompresjon, før de ble intrudert av omfangsrike granittiske bergarter.

Omfattende U-Pb geokronologisk analytisk arbeid ved LA-ICP-MS og SHRIMP har blitt utført og viser at suprakrustalene på Bjarkøya (1869±42 Ma) har liknende aldre som suprakrustalene i Kiruna, Sverige (1.88 Ga). De intrusive bergartene i RTW (1.80-1.79 Ga) viser liknende aldre som de intrusive bergarter i feltområdet (1811±52 Ma til 1770±16). Bulkkjemien til de vulkanske og intrusive bergartene i RTW og de intrusive bergartene fra feltområdet viser variasjon i hovedelementene innenfor samme litologi. Sporelementene for de vulkanske bergartene i RTW og de intrusive bergartene fra RTW og feltområdet viser en generell subduksjonssonesignatur i kondrittisk- og primitiv mantel-normaliserte diagrammer (høy konsentrasjon av LILE, lav konsentrasjon av HFSE og negative Nb and Ta anomalier). Isotopdata fra både zirkon og bulksammensetning, indikerer primært en skorpesmeltekilde for både intrusivene i RTW (ε_{Nd}=-3.4 to -6.9) og de intrusive bergartene i feltområdet (ε_{Nd}=-7.2 to -8.7, ε_{Hf}=-3.0 to -13). Intrusivbergartene fra feltområdet viser en mindre grad av miksing og/eller assimilering med en utarmet mantelsmelte enn intrusivbergartene i RTW. De vulkanske bergartene fra RTW viser en mer juvenil sammensetning (ε_{Nd}=-2.8 to -6.4) og er tolket til å ha en subduksjonsrelatert opprinnelse og reflekterer etablering av en kontinentalbue som kort tid senere ble intrudert av skorpederiverte granittiske bergarter.

I lys av de nye geokronologiske, geokjemiske og isotopdataene fra feltområdet kan det gjøres en sammenligning med liknende bergarter funnet i RTW, West-Troms Basement Complex, Lofoten-Vesterålen og Central Nordland Basement Window som indikerer at 1.8 Ga bergartene fra feltområdet var del av en geografisk utbredt, men tidsbegrenset magmatisk hendelse. Forskjellene i SiO_2, MgO og FeO og isotopdata mellom de vulkanske bergartene og de intrusive bergartene i RTW og feltområdet, samt fravær av D_1 og D_2 strukturer i de intrusive bergartene antyder en endring i det tektoniske miljøet for de intrusive bergartene. Denne avhandlingen foreslår delaminering som en forklaring på den tidsbegrensede, omfangsrike magmatismen som fant sted mellom 1790-1800 Ma. En kompresjon med påfølgende skorpefortykning førte sannsynligvis til dannelse av kald, tung eklogitt-bergarter ved nedre skorpe/litosfære som delaminerte og sank. Denne prosessen førte til at astenosfæren steg opp mot og smeltet nedre del av skorpen. Isotopdata støtter idéen om en arkeisk-paleoproterozoisk grense sør for feltområdet men gir ingen eksakt posisjon for hvor den er plassert. Områder rike på mineraliseringer i Sverige er funnet i 1.88 Ga meta-suprakrustaler. Feltdata og geokronologi viser at selv om slike bergarter strekker seg vestover i Norge, så er disse intrudert av 1.8 Ga granitter. Gravitasjonskart viser at mineraliseringene er funnet i høy-gravitasjonsregionene i Sverige, og disse

fortsetter ikke videre inn i Norge. Dette er antatt å være fordi Norge har hatt stor utbredelse av 1.8 Ga granitter som har fjernet de fleste av potensielle mineraliserte bergarter. Potensialet for å finne økonomisk drivverdige mineraliseringer i suprakrustaler i Norge anses derfor som liten.

Acknowledgements

This thesis was carried out at the Geological Survey of Norway (NGU) in collaboration with the Department of Geoscience and Petroleum at the Norwegian University of Science and Technology (NTNU), as part of my master's degree in Geology. Dr. Trond Slagstad (NGU) has been the supervisor of this project, with Prof. Bjørn Eske Sørensen being co-supervisor.

First of all, I would like to thank my two supervisors, Trond and Bjørn, for their endless guidance, help and support throughout this project. Not only have they always held an open door for me, they've also spent over a week with me in the field to get me started with the mapping. A big thanks to Nolwenn Coint for helping me during the fieldwork and for providing me with information and educational discussions regarding the regional geology.

I want to thank the Mineral Resources group at NGU for a warm welcome and practical help regarding the microscopy lab and the SEM-lab. I would also like to thank Benjamin Berge, Øyvind Skår and Anne Nordtømme for training at the Mineral lab and Bengt Johansen for preparing thin-sections. Also, thank you Arild Monsøy and Kjetil Eriksen at the thin section laboratory at the Department of Geoscience and Petroleum at NTNU and NGU for preparing thin-sections.

A big thanks also goes to the Department of Geoscience and Petroleum at NTNU and the GEMMS project lead by Rune Berg-Edland for sponsoring me a one semester scholarship, giving me the opportunity to be an exchange student at Texas Tech University, Texas, USA. In that context I would like to thank Dr. Calvin Barnes and Dr. Callum Hetherington for their interest and help with the examination of my thin-sections. I will forever be grateful for the experiences and knowledge that I was provided with during this exchange. Also, thank you to the Department of Geoscience and Petroleum at NTNU for sponsoring of my trip to Australia where I got to accomplish the dating work with help from Dr. Chris Kirkland and the rest of the people working at the LA-ICP-MS lab at Curtin University.

In the end I would like to thank my fellow students at NTNU that I've had the pleasure to travel around the world with and creating a highly educational environment. My time as a geology student would not have been the same without you. Finally, I would like to thank my family and friends for their infinite encouragement and support through all these years of hard work and fun.

Kristine Glomsås Nymoen

Trondheim, May 2019

Table of contents

List of figures

List of tables

List of equations

Abbreviations

BSE	Backscatter electron image
CL	Cathodoluminescent
CNBW	Central Nordland Basement Window
HREE	Heavy Rare Earth Elements
LA-ICP-MS	Laser Ablation Inductively Coupled Plasma Mass Spectrometer
LREE	Light Rare Earth Elements
NGU	Norges Geologiske Undersøkelse (Geological Survey of Norway)
NTNU	Norwegian University of Science and Technology
PPL	Plane-polarized light
REE	Rare Earth Elements
RTW	Rombak Tectonic Window
SHRIMP	Sensitive High-Resolution Ion Microprobe
WTBC	West-Troms Basement Complex
XPL	Cross-polarized light

1 Introduction

1.1 Background and aim for the study

This thesis is a regional geological study that aims to give a better understanding of Paleoproterozoic tectonic and magmatic processes of the southwestern margin of the Fennoscandian Shield, in the West Troms Basement Complex. Geological mapping, U-Pb geochronology, whole-rock and zircon geochemistry together with isotopic data forms the foundation of this study.

The study area is located at the southwestern of what was the Fennoscandian margin at ca 1.8 Ga in the central portion of the WTBC. The study area is located outside the city of Harstad, in Troms county. The area comprises Precambrian rocks that record Svecofennian (ca. 2.0 to 1.8 Ga) magmatic and metamorphic events, and later events during the Caledonian orogen. Archean crust is evident from supracrustal rocks, whilst the main rock type of this area, the granitic rocks, are dated to Paleoproterozoic time (1.8 Ga). These granitic rocks were formed during a voluminous intrusion of granitic melt. The geological data suggest a tectonic setting with different processes in conjunction to an active margin. These changes in tectonic settings have left traces of both extensional and compressional structures in the rocks (Angvik, 2014).

Samples have been collected from Grytøya, Bjarkøya, Sandsøya, Krøttøya and Meløyvær (Figure 1.1). Isotopic data from the West Troms Basement Complex (WTBC), Lofoten-Vesterålen, Altevatn, Rombak Tectonic Window (RTW) and Central Nordland Basement Windows (CNBW) have been used for comparison to the isotopic data from the study area, to put the tectonomagmatic evolution into a regional scale. U-Pb geochronology was performed on the LA-ICP-MS and SHRIMP II at Curtin University, Perth. The lab at the Norwegian Geological Survey (NGU), British Geological Survey (BGS), ALS Chemex and at the Department of Geology at Curtin University also provided isotopic-, major- and trace element data.

The thesis investigates the tectonic setting where the large volumes of 1.8 Ga melt were formed and compare these Paleoproterozoic rocks with the 1.8 Ga volcanites and intrusive rocks from Rombak Tectonic Window, to demonstrate the similarities on a regional scale. The Svecofennian deformation and the following magmatic events are studied to reveal what tectonic setting these large extent intrusive rocks were formed at. To be able to create such a large volume of melt, it demands a tectonic setting that allows for mantle sources to create such a large heating that it allows for magma to be transported through the crust and out on the surface. The thesis also attempts to contribute to the interpretation of the Archean-Paleoproterozoic boundary and explain why it is difficult to define a sharp boundary. It also compares the supracrustal rocks that forms the well-known Kiruna-Gällivare ores with the supracrustal rocks found at Bjarkøya, which is part of the study area. Good descriptions from the field combined with geochemical- and isotopic data from both the study area and from a larger regional scale has been necessary to construct a reasonable tectonic model for the magmatic evolution. These data have also been used to constrain the location of the Archean-Paleoproterozoic boundary, and to understand how the supracrustal belts found on Bjarkøya do not show the same mineralization as the ones in Kiruna-Gällivare. Hopefully the new data and results can be used in further research to understand the geological history of this area.

1.2 Description of the study area

The study area is in the centre of the WTBC, relatively close to the previously proposed Archean-Proterozoic boundary. The rocks that are present in the area are mainly from around 1.9 to 1.8 Ga, related to a magmatic event that has an extent from the WTBC in the north and possibly down to Grong (Nord-Trøndelag) in the south. Fieldwork was done on the four islands of Grytøya, Bjarkøya, Sandsøya and Krøttøya (Figure 1.1). The geological mapping was mainly carried out along the shore and at road cuts, as the rocks were best exposed there. The four islands make up a large area, but Grytøya is the only island to have mountains ranging up to 1012 meters above sea level. However, thick vegetation cover and rugged ground in addition to steep mountain sides did set limits for some parts of the study area.

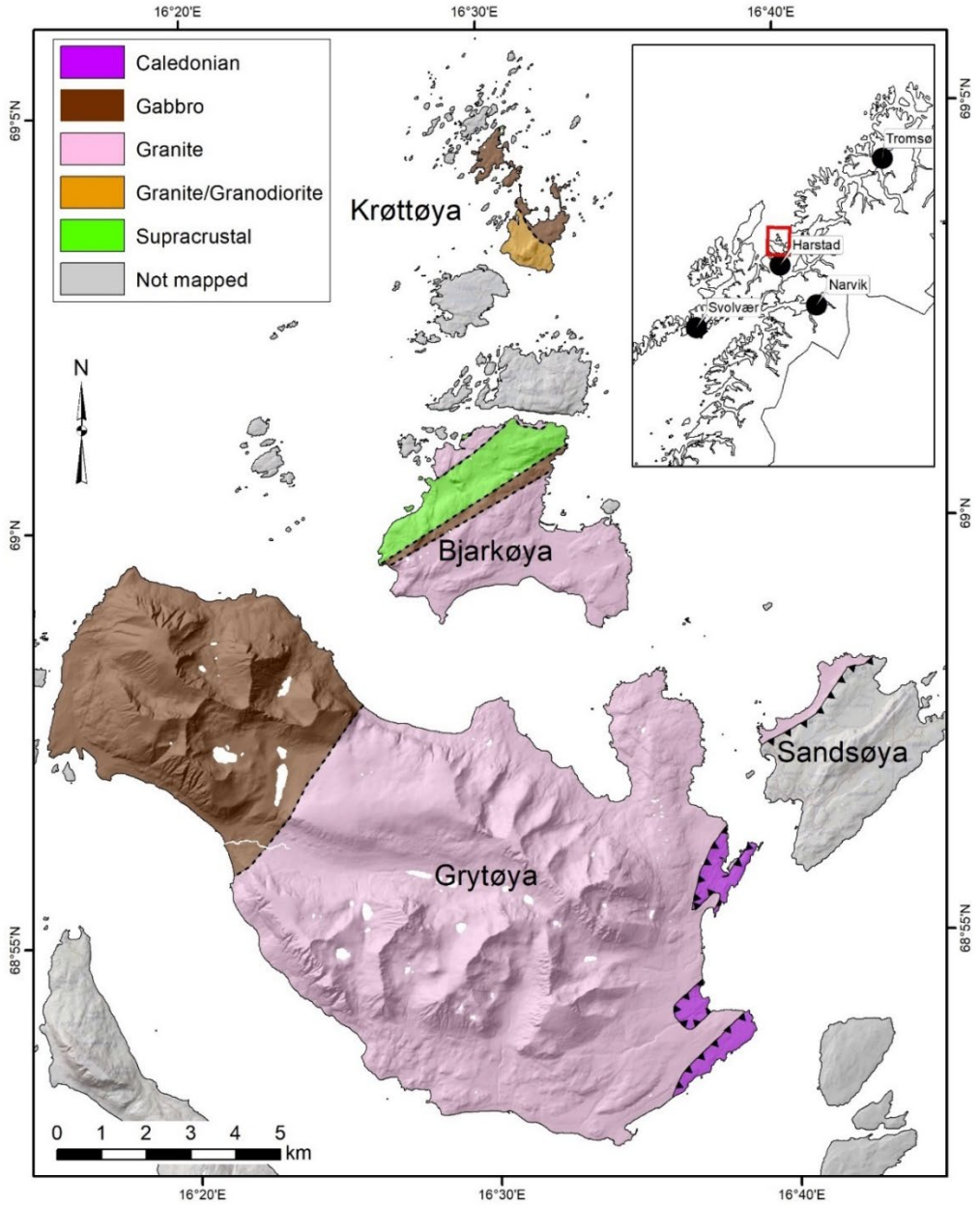

Figure 1.1: *Geological map of the four islands of Grytøya, Sandsøya, Bjarkøya and Krøttøya based on the mapping done in the summer of 2018.*

2 Regional geology

The study area is in the central portion of the West Troms Basement Complex (WTBC) and comprise the four islands of Grytøya, Sandsøya, Bjarkøya and Krøttøya. To understand the former geological events of these islands it is important to have knowledge about the regional geology, to hopefully find its place in the regional tectonomagmatic framework. A geological map with the study area and the associated regional geological areas are found in Figure 2.1.

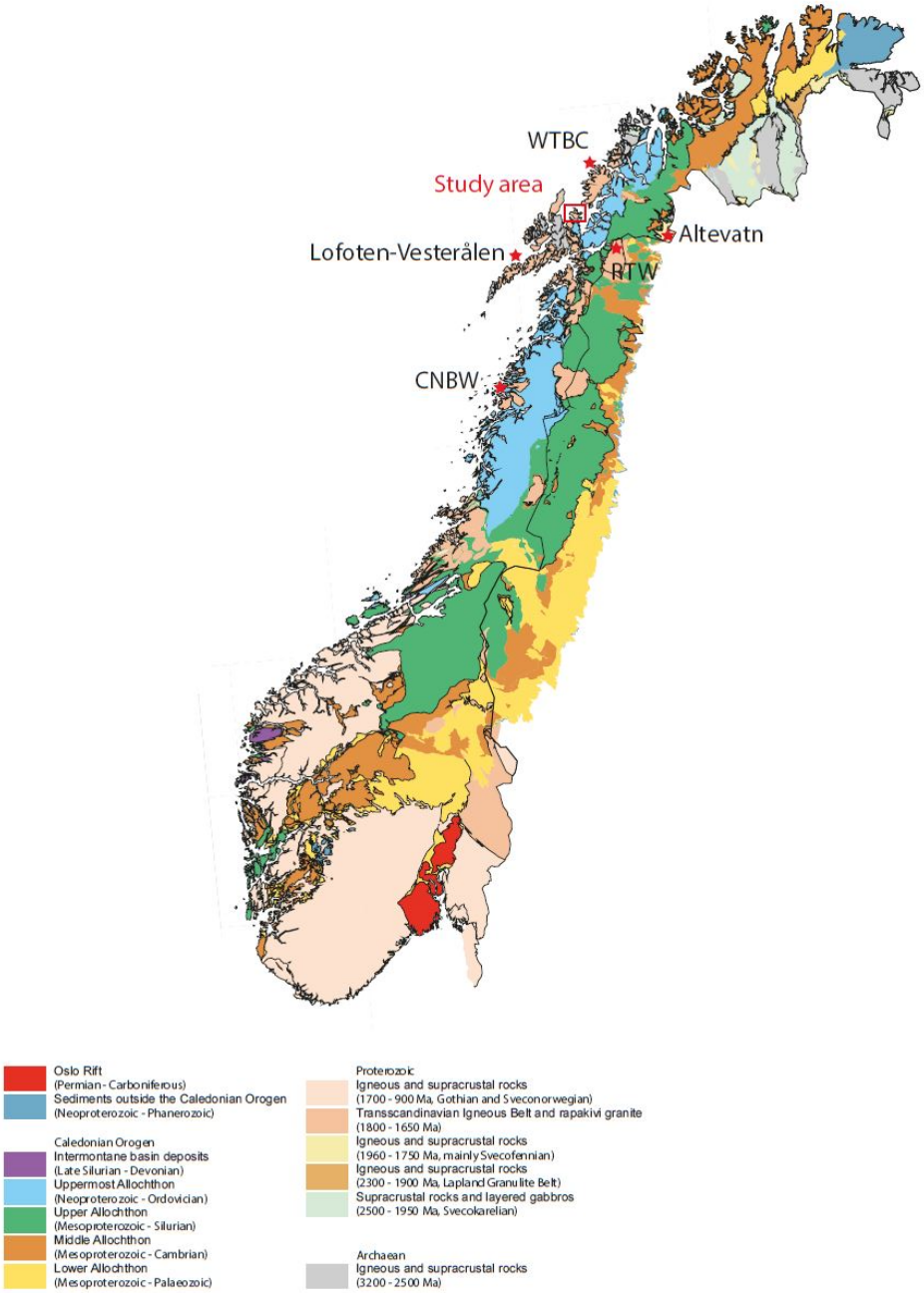

Figure 2.1: *Geological map of Norway showing the different lithologies with associated age estimates. The red box indicates the location of the study area. Abbreviations: WTBC- West Troms Basement Complex, RTW- Rombak Tectonic Window, CNBW- Central Nordland Basement Windows. Figure from (Slagstad et al., 2011), modified after Solli and Nordgulen (2006).*

2.1 Fennoscandian Shield Evolution and Svecofennian Orogeny

To be able to understand the geology that we are looking at in the field today, a good understanding of the past is required. The Fennoscandian Shield comprises the peninsula of Norway, Sweden, Finland, Karelia and Kola, an area that contributed to the two former supercontinents of Columbia (2.5-1.5 Ga) and Rodinia (1.1-0.9 Ga) during Paleoproterozoic through early Neoproterozoic time (Roberts and Slagstad, 2014, Zhao et al., 2002). The Fennoscandian Shield formed during the amalgamation of the supercontinent Columbia around 1.9 Ga through accretion of Archean and younger Paleoproterozoic crust (Roberts and Slagstad, 2014). The southwestern margin (present-day coordinates) is thought to have been the outer edge of the Columbia supercontinent, and during the Rodinia supercontinent it may have been part of the interior (Roberts and Slagstad, 2014). These interpretations have been made based on the understanding of plate tectonics and geochemistry, mainly isotopic data. The location of the Fennoscandian Shield as it is thought to have been in late Palaeoproterozoic time is illustrated in Figure 3.

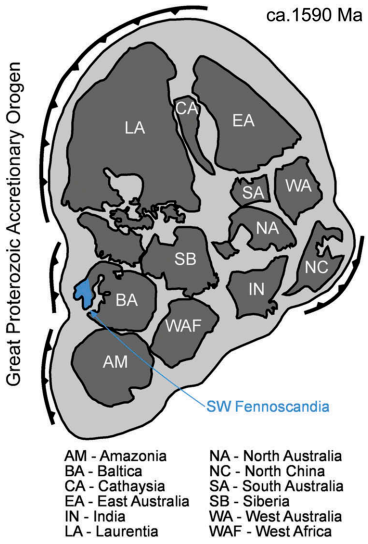

Figure 2.2: *The Columbia supercontinent (a.k.a. Nuna) shown at 1590 Ma. From Roberts and Slagstad (2014), modified after Zhang et al. (2012). SW Fennoscandia is marked in blue showing its location on the southwestern margin of Baltica.*

In the northwestern part of Norway, tectonic windows that have preserved Archean and Paleoproterozoic crust exist. These windows hold geological history that goes back to 2.7 Ga and has been important in the study of the tectono-magmatic evolution of the Fennoscandian Shield (Laurent et al., 2019). The basement outliers are located between the NE trending Caledonides at the eastern side and Mesozoic basins offshore to the western side (Blystad, 1995). Bergh et. al (2014) have constructed a table with a summary of tentative correlations of age constraints, main component characteristics and tectonic events that are found in the West Troms Basement Complex (WTBC) and the Lofoten-Vesterålen area (Figure 2.3).

West Troms Basement Complex		Lofoten-Vesterålen province	
Age (Ga)	**Components and events**	**Age (Ga)**	**Components and events**
2.92–2.77 Ga	*Neoarchaean cratonization:*		*Neoarchaean cratonization:*
	Tonalite crystallization (Dåfjord & Kvalsund gneisses)	2.85–2.7 Ga	Accretion, convergence and crustal thickening
2.85–2.83 Ga	*Volcanism and sedimentation:*		
	Ringvassøya greenstone belt: calc-alkaline and tholeiitic metabasalts, paragneisses and sulphide-rich schists	2.75–2.68 Ga	Tonalite magmatism
2.75–2.7 Ga	*Continued Neoarchaean cratonization*		
2.75–2.67 Ga	Mafic plutonism (Bakkejord diorite) in the southwest	2.72–2.66 Ga	*Neoarchaean deformation and metamorphism:*
2.73–2.58 Ga	*Main Neoarchaean deformation and metamorphism:*		Various orthogneisses (e.g. Bremnes gneiss) formed by crustal shortening
	Magmatism, migmatization (Gråtind migmatite) and ductile shearing (in *Dåfjord* and *Kvalsund* gneisses)		
	Main gneissic foliation (initially flat-lying), ductile shear zones, tight folds and ENE-directed stretching lineation		
	Medium/high-grade metamorphism, ENE-WSW crustal contraction and thickening by accretion and/or underplating		
2.69-2.58 Ga	High-grade granulite facies metamorphism and resetting	2.64 Ga	Emplacement of tonalites, followed by high-grade metamorphism and localized migmatization and ductile crustal shearing (*Sigerfjord migmatite, Ryggedalen granulite*)
2.69 Ga	Granitoid and alkaline intrusions		
2.58–2.57 Ga	Late-stage mafic intrusion (*Bakkejord pluton*)		
2.40 Ga	*Crustal extension and intrusion* of the *Ringvassøya* mafic dyke swarm	?	
2.4–2.2 Ga	*Deposition* of *Vanna group* clastic sediments in a marine subsiding basin	?	*Deposition* of supracrustal units, heterogeneous mafic gneisses, banded iron formations, quartzite, marbles, graphite schists
2.22 Ga	*Intrusion* of Vanna diorite sill	?	
2.2–1.9 Ga	*Deposition of Mjelde-Skorelvvatn*, Torsnes and possibly the *Astridal* supracrustal belts		
1.993 Ga	*Intrusion/volcanism* in the Mjelde-Skorelvvatn belt	1.87-1.86 Ga	Precursory stage magmatism, AMCG-suite
1.80 Ga	*Magmatism/intrusion* of granites and norite in Senja	1.8-1.79 Ga	Main stage intrusion of AMCG-suite plutonic rocks
1.79 Ga	*Magmatism/intrusion* of *Ersfjord Granite* in Kvaløya	1.77 Ga	Intrusion of granite pegmatite dykes
c. 1.9–1.7 Ga	*Palaeoproterozoic/Svecofennian deformation*		*Svecofennian deformation*

Figure 2.3: *Tectono-magmatic evolution summary of the Archean and Paleoproterozoic outliers west of the Scandinavian Caledonides. From Bergh et al. (2014).*

The rocks of Archean age found in the WTBC comprise mainly tonalite-trondhjemite-granodiorite (TTG) -gneisses, supracrustal rocks and intrusive gabbroid and granitoids. The TTG gneisses experienced at least three episodes of deformation, magmatism and metamorphism during Neoarchean time ending in a high-grade metamorphic event at 2.6 Ga (Myhre et al., 2013). These events have been dated by U-Pb techniques and the crustal accretion is believed to have been caused by plate convergence (Figure 2.3). The convergent tectonic setting of the Fennoscandian Shield was followed by rifting (2.85-2.83 and 2.4-1.9 Ga), and later magmatism, deformation and metamorphism during the Svecofennian orogeny (1.9-1.7 Ga).

Bergh et al. (2014) have suggested that the basement outliers found in this northern part of Norway can be correlated with the Archean Karelian province found east of the WTBC and Lofoten-Vesterålen area, based on structural evidence (Figure 2.4). Both NW-SE ductile shear zones and NW-SE greenstone belts shows a linkage, indicating that the basement outliers found in North Norway has a similar Archean evolution as the Swedish Archean rocks.

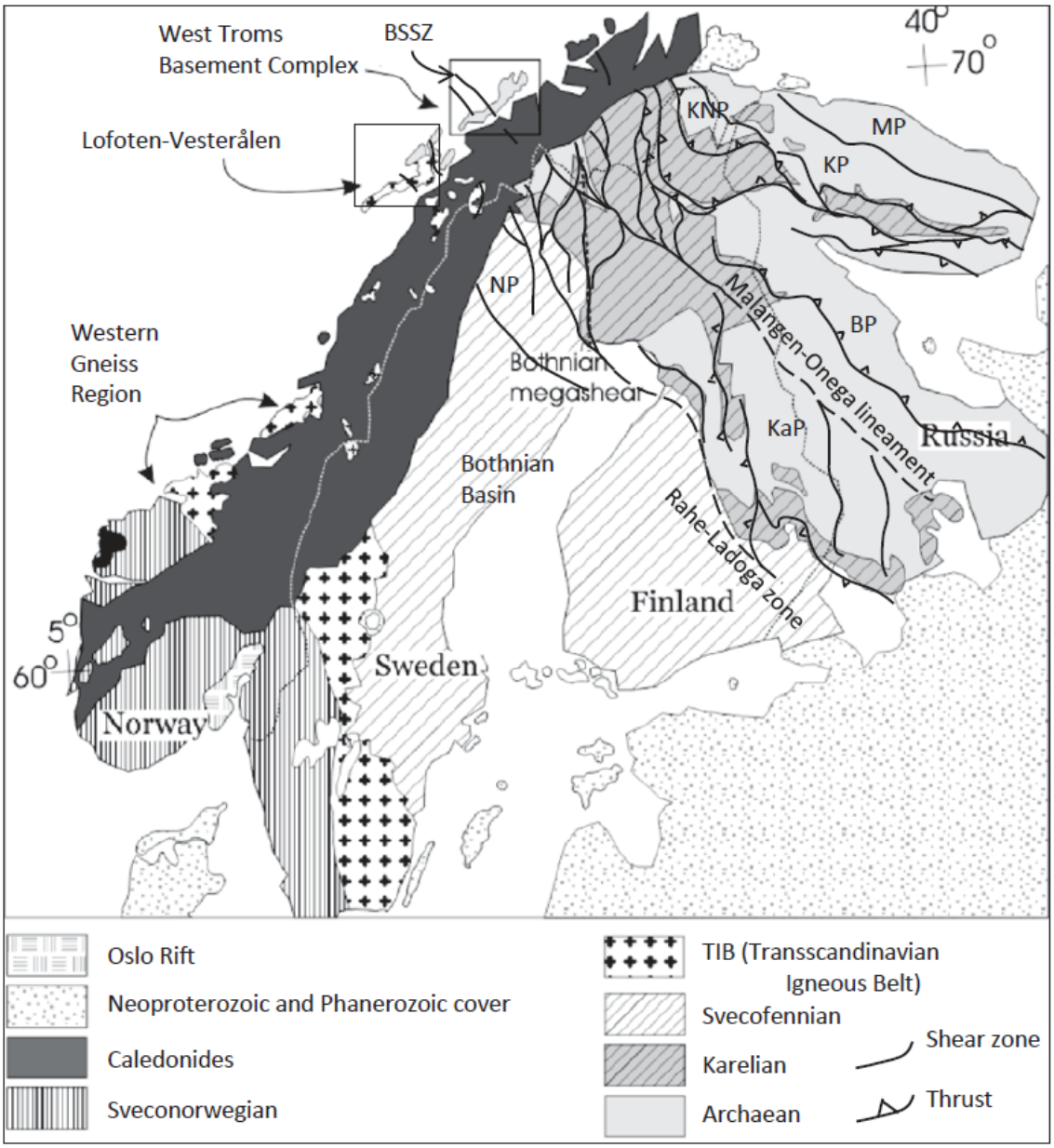

Figure 2.4: *Geological overview map showing the Fennoscandian Shield with location of the West Troms Basement Complex (WTBC) and the Lofoten-Vesterålen area representing tectonic outliers to the west of the Scandinavian Caledonides. Archean and younger provinces and major ductile shear zones are included for the Fennoscandian Shield to the east of the Caledonides. Abbreviations: BP=Belomorian Province, BSSZ= Bothnian-Senja Shear Zone, MP= Murmansk province, KaP= Karelian province, KNP= Kola-Norwegian province, KP= Kola province, NP= Norrbotten province. Figure and caption from Bergh et al. (2014)*

2.2 Svecofennian Orogeny

The Svecofennian Orogeny affected the southwestern margin of Fennoscandia and was followed by post-Svecofennian events that can be divided into four phases- all contributing to continental growth; formation of the Transscandinavian Igneous Belt (TIB), the Gothian orogeny, the Telemarkian orogeny and the Sveconorwegian orogeny. The TIB formed between 1.86 and 1.66 Ga and comprised plutonic and volcanic activity that affected the region of the northwestern Norwegian coast stretching to the southeastern Swedish coast, shown in Figure 2.4 (Roberts and Slagstad, 2014). The TIB rocks are mainly granitoids that are geochemically alkali-calcic and can be classified as I-and A-type (Högdahl et al., 2004). The evolution of the TIB is often put into TIB-0-, TIB-1- and TIB-2/3 units that reflect the different ages of the rocks involved, where the two earlier units are thought to overlap with the later stages of the Svecofennian deformation (Roberts and Slagstad, 2014). The geological setting of the TIB has been discussed for a long time and the tectonic setting that is supported by most workers is a convergent margin that comprise both compressional and extensional regimes as a result of subduction zone migration (Roberts and Slagstad, 2014). The full extent of the TIB is shown in Figure 2.4.

The Gothian orogeny followed TIB domain formation and took place between 1.66 and 1.52 Ga and is believed to reflect a tectonic setting of island arcs and continental arc formation with rifting and accretion processes (Åhäll and Connelly, 2008). The rocks related to this event are divided into: 1) deformed remnants of volcanic arc complexes belonging to the eastern part (Brewer et al., 1998, Gaál and Gorbatschev, 1987, Åhäll et al., 1995) and 2) supracrustal units consisting of meta-greywackes belonging to the western part (Åhäll and Daly, 1989, Åhäll, 1984). The third of the main stages in the Fennoscandian Shield evolution is the Telemarkian orogeny, an event that lasted between 1.52 and 1.48 Ga (Roberts and Slagstad, 2014). As for the TIB and the Gothian domain this period consisted of continental growth of the Fennoscandian Shield. The tectonic setting found to dominate in this period is an island- or continental arc (Åhäll and Connelly, 2008). Figure 2.5 is a cartoon showing the three-main accretionary orogenies, in addition to two younger orogenies known as the Hallandian-Danopolonian orogeny and the Sveconorwegian orogeny. The Svecofennian period stopped or overlapped with the TIB, resulting in a long-lived accretionary orogen contributing most importantly to crustal growth on the southwest Fennoscandian margin.

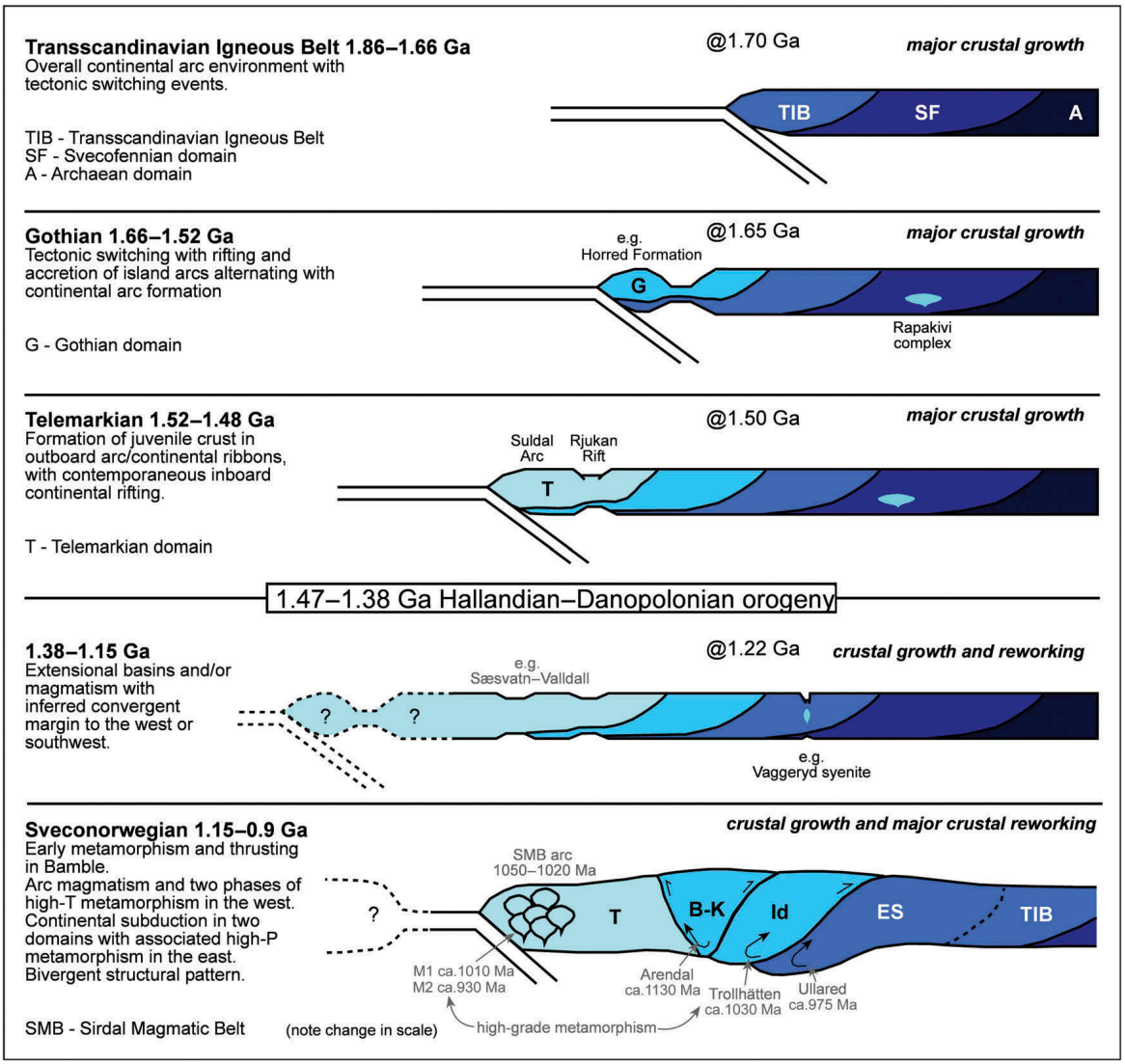

Figure 2.5: *Cartoon tectonic cross-sections of southwest Fennoscandia at various time periodshighlighting the westward younging of crustal domains, formed along an accretionary convergent margin. For simplicity, a single subduction zone with consistent polarity is maintained, and along-margin movement between domains are ignored. The final Sveconorwegian period is a composite of major diachronous events shown in one section, with the geometry of crustal boundaries being largely inferred from the metamorphic gradients. Figure and caption from Roberts and Slagstad (2014).*

2.3 Lofoten-Vesterålen Area

The Lofoten-Vesterålen islands are very interesting because of their geographic location and the rocks that are found there. It is the westernmost exposure of the basement rocks found in northern Norway and comprises both Archean and Palaeoproterozoic rocks that cover the geological history from around 2.7 to 1.8 Ga. Rocks that are found southwest on the islands are dominantly Archean whilst the northwestern parts are mostly ca. 1.8 Ga intrusive rocks related to an anorthosite-mangerite-charnockite-granite (AMCG) suite. The AMCG-suite is extra interesting because such suites are believed to be an exclusive feature of Proterozoic crust (Corfu, 2004). Fernando Corfu (2004) has done U-Pb geochronology in Lofoten-Vesterålen to reveal whether they are significant in the study of crustal growth during the Svecofennian orogen. By studying Figure 2.6 it is evident that the Lofoten-Vesterålen area is composed of Archean and Palaeoproterozoic crust, that was later overthrusted by allochthonous N-NE-trending Caledonian nappes.

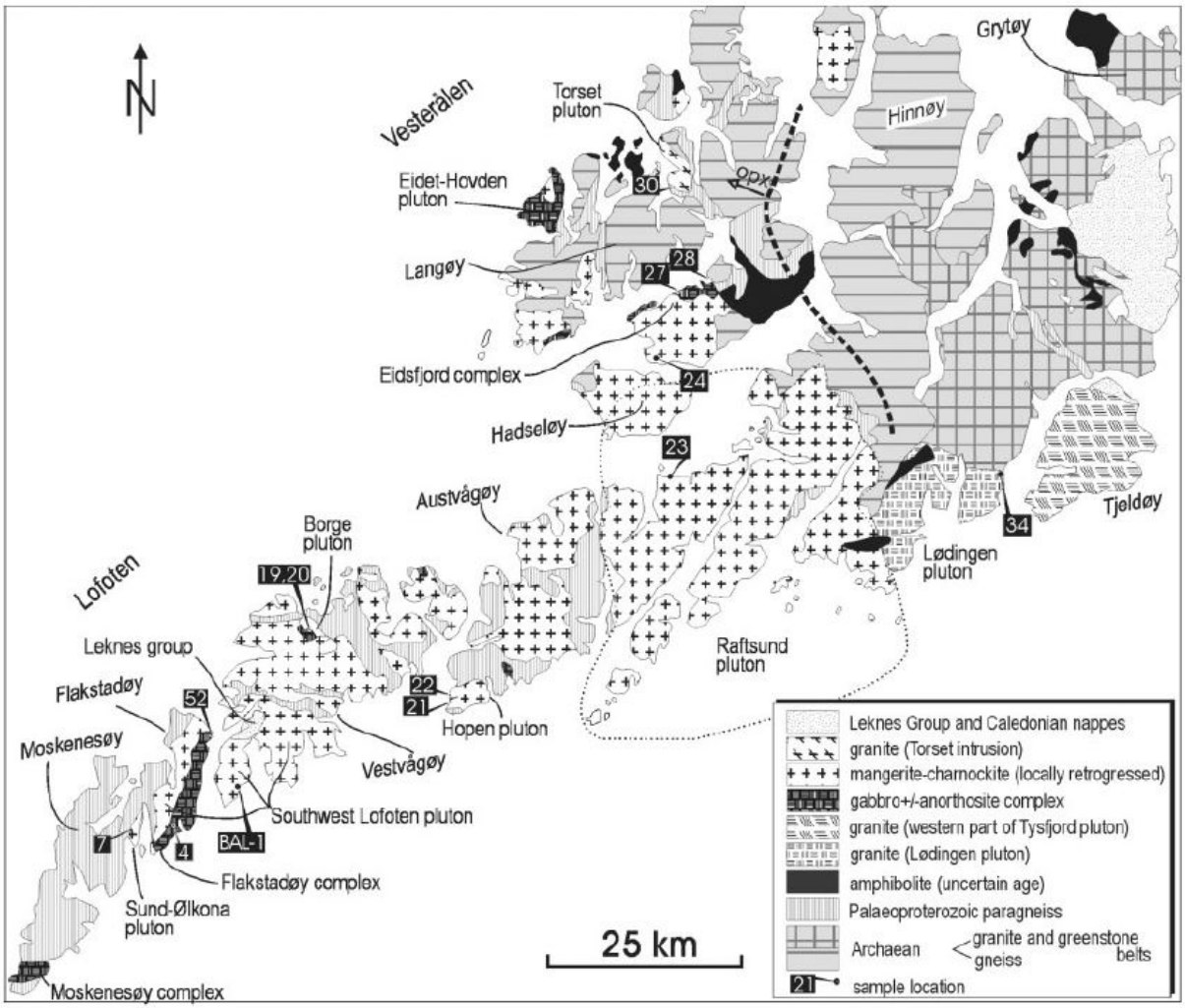

Figure 2.6: *Overview map of the lithologies found in the Lofoten-Vesterålen area. Figure from Corfu (2004).*

The plutons studied by Corfu (2004) show magmatic crystallization ages varying between 1790 and 1800 Ma, with the granitic plutons recording a metamorphic event around 422±5 Ma resulting in formation or resetting of titanite(Corfu, 2004). Based on the work of Corfu (2004) the Proterozoic evolution can be divided into four different events. The events cover both similar and different geological processes. The first event took place in the period of 1870-1860 Ma, with the emplacement of the Lødingen granite and Hopen pluton. The Hopen pluton consists of gabbro, mangerite and charnockite (Corfu, 2004). The previous ages found for the Lødingen granite are younger than the ages found using the newer dating technique of U-Pb geochronology. The explanation is most likely due to Caledonian overprinting influencing the Rb-Sr system which they used for the earliest dating (Corfu, 2004). The second event, being the most important one, is related to the emplacement of the largest amounts of the AMCG-suite in Lofoten-Vesterålen around 1800-1790 Ma. The AMCG-suite was most likely a result of a complex magmatic process, where the magma was presented in multiple magma batches that differentiated in sequences and ended up with a magma characterized by mixing and crustal assimilation (Corfu, 2004). The third event has been called "Late- to post-magmatic stage" by Corfu (2004), it took place at 1769±11 Ma and represents hydration of relatively dry AMCG-suites. The fourth and last event recognized by U-Pb age dating is high-grade metamorphism, which is found to have been active around 1800 Ma (Corfu, 2004). The rocks in Lofoten-Vesterålen have been

exposed to both prograde and retrograde metamorphism, making it complicated to decide whether the metamorphic grade that is observed today is a result of contact- or regional metamorphism.

Formation of the AMCG-suite is divided into two specific magmatic geological environments: the first at 1870-1860 Ma is related to a collisional and arc amalgamation setting related to the Caledonian orogeny and the second at 1800-1780 Ma is associated with more distant continental collision processes (Corfu, 2004). The rocks in the Lofoten-Vesterålen has also undergone a multistage metamorphic evolution that has been described by Corfu (2007). This evolution was also revealed by U-Pb data in accessory minerals. It has been found that the western and southwestern part of the area consists of granulite facies rocks, whilst the eastern part of the area consists of amphibolite facies rocks (Corfu, 2007). Geophysical investigation have identified large magnetic and gravity anomalies in the western part resulting from dense rocks and an elevated Moho discontinuity, probably due to the uplift and extension that the area was exposed to during the Caledonian orogeny (Corfu, 2007). This transition from granulite facies rocks in the west and amphibolite facies rocks to the east is the basis for geological discussions related to whether the transition is due to a single metamorphic event, a metamorphic progression with westward increasing pressure and temperature, or more recently, a tectonic boundary. Corfu (2007) confirms the current understanding of the crustal history of the area, regarding two major periods of crust accretion and stabilization in Archean- and Late Paleoproterozoic time. The granulite facies rocks were metamorphosed during Archean and Proterozoic time. The oldest event happened at 2640 Ma and involve intrusions of diorite bodies and anatexis. In Proterozoic time the Lofoten-Vesterålen area was exposed to a three-stage high-grade metamorphic event. Two of the stages are directly connected to the emplacement of the AMCG magmatism, and the last one took place at 1880-1810 Ma. Out of the three alternatives describing the reasoning for the metamorphic transition, only the last one that consider a tectonic boundary can be supported. This is due to Proterozoic granulites bordering Archean migmatites, excluding the probability of having one single metamorphic event present (Corfu, 2007).

Markl et al. (2003a) have carried out geochemistry of the AMCG-suite and found that the Sm-Nd isotopes for these rocks shows an $\varepsilon_{Nd(t)}$ varying from -4.2 to -8.8 for a T_{DM} set at 2.5 Ga to 2.8 Ga. The trend is that the higher the T_{DM}, the more negative the $\varepsilon_{Nd(t)}$ gets. Gabbros, leuco-gabbros and ferrodiorites from the same area were also analysed and shows an $\varepsilon_{Nd(t)}$ between 2.2 to -6.2 (Markl and Höhndorf, 2003a).

2.4 West Troms Basement Complex

The West-Troms Basement Complex (WTBC) comprises the basement outliers located in between high-grade metamorphic suites towards the southwest and rocks affected by the Caledonian Orogeny to the east (Figure 2.7). The rocks present in the WTBC can be divided into four main groups: 1) Neoarchean gneisses of varying compositions, 2) Neoarchean and Paleoproterozoic supracrustals, 3) Early Paleoproterozoic mafic dyke swarms and 4) Paleoproterozoic granitic and mafic plutons (Bergh et al., 2010, Laurent et al., 2019).

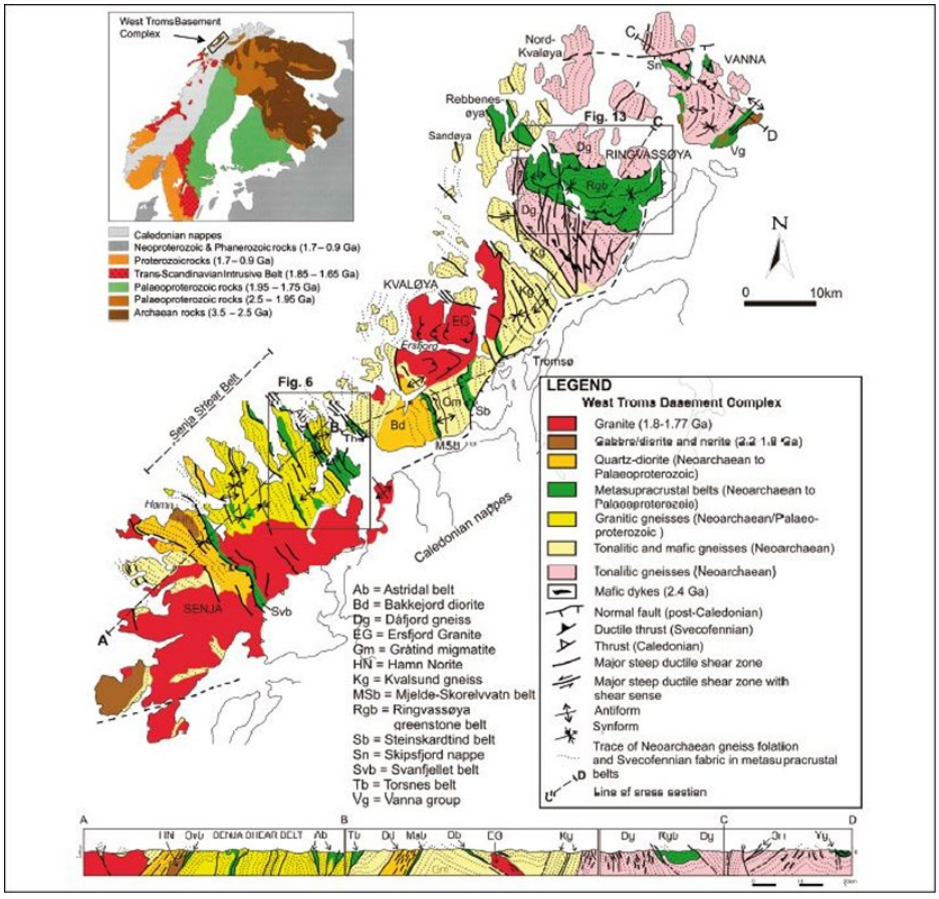

Figure 2.7: *Regional geologic-tectonic map and cross-section of the West Troms Basement Complex. Revised after Kullerud et al. (2006b) and Bergh et al. (2007). The index map shows the location of the WTBC relative to the Fennoscandian Shield, with its broad division of provinces by age after Nordgulen and Andresen (2008). Figure and caption from Bergh et al. (2010).*

The Neoarchean gneisses have been dated to 2.89-2.56 Ga (Bergh et al., 2010, Corfu et al., 2003, Kullerud et al., 2006a, Zwaan and Tucker, 1996). The relative ages of these rocks are identified by cross-cutting relationships between their foliation and the Svecofennian mylonitic fabrics and granitic intrusions. These relations have also been confirmed by U-Pb dating that has given crystallization- and resetting ages (Bergh et al., 2010). The gneisses are mainly tonalitic in composition and borders to NW-SE trending Svecofennian deformed supracrustal belts accompanied by shear zones (Bergh et al., 2010). The latest proven geological event that this group experienced was intrusion of granitic rocks around 1.8 Ga. Another unit of rocks described from the WTBC includes Neoarchean to Paleoproterozoic supracrustal belts found to have an age of 2.85 to 1.97 Ga (Kullerud et al., 2006a, Motuza et al., 2001). Most of the belts are trending NW-SE, and they vary from being continuous to being disjointed folded inliers or dismembered enclaves (Bergh et al., 2010). These supracrustal belts underwent high-grade metamorphism during the Svecofennian orogeny and the lithology of some of the rocks within these belts therefore show a metamorphic texture. According to U-Pb titanite ages the Svecofennian deformation was active in the WTBC affecting the gneiss and the supracrustal belts around 1768±4 Ma to 1751±8 Ma(Bergh et al., 2010, Corfu et al., 2003). Structural studies done on the many supracrustal belts of this area has revealed information about the metamorphic grades the rocks have been exposed to and constrain a time-frame for the deformation and the effect on the different lithologies. A group of Paleoproterozoic mafic dyke swarms has been dated to be 2.40 to 2.22 Ga (Kullerud et al., 2006a) in the WTBC

and comprise doleritic to gabbroic/noritic compositions. Geochemistry has been used to reveal the tectonic setting in which these dyke swarms were formed, and according to trace elements they are found to plot between mid-ocean-ridge basalt (MORB) and within-plate basalts (Kullerud et al., 2006b). The last major event that the WTBC experienced was intrusion of Svecofennian igneous suites. These suites are mostly of granitic composition and holds a U-Pb zircon age of 1.80 to 1.76 Ga (Corfu et al., 2003). Compared to the TIB rocks, the Svecofennian igneous suites in the WTBC are S- and I-types instead of I- and A-types. It has been suggested to reflect a crustal melt from a reworking in a transtensional/transpressional domain rather than a crustal thickening as for the TIB rocks, leading to an interpretation of an accretionary orogenesis origin (Roberts and Slagstad, 2014). A proposed tectonic evolution is shown in Figure 2.8.

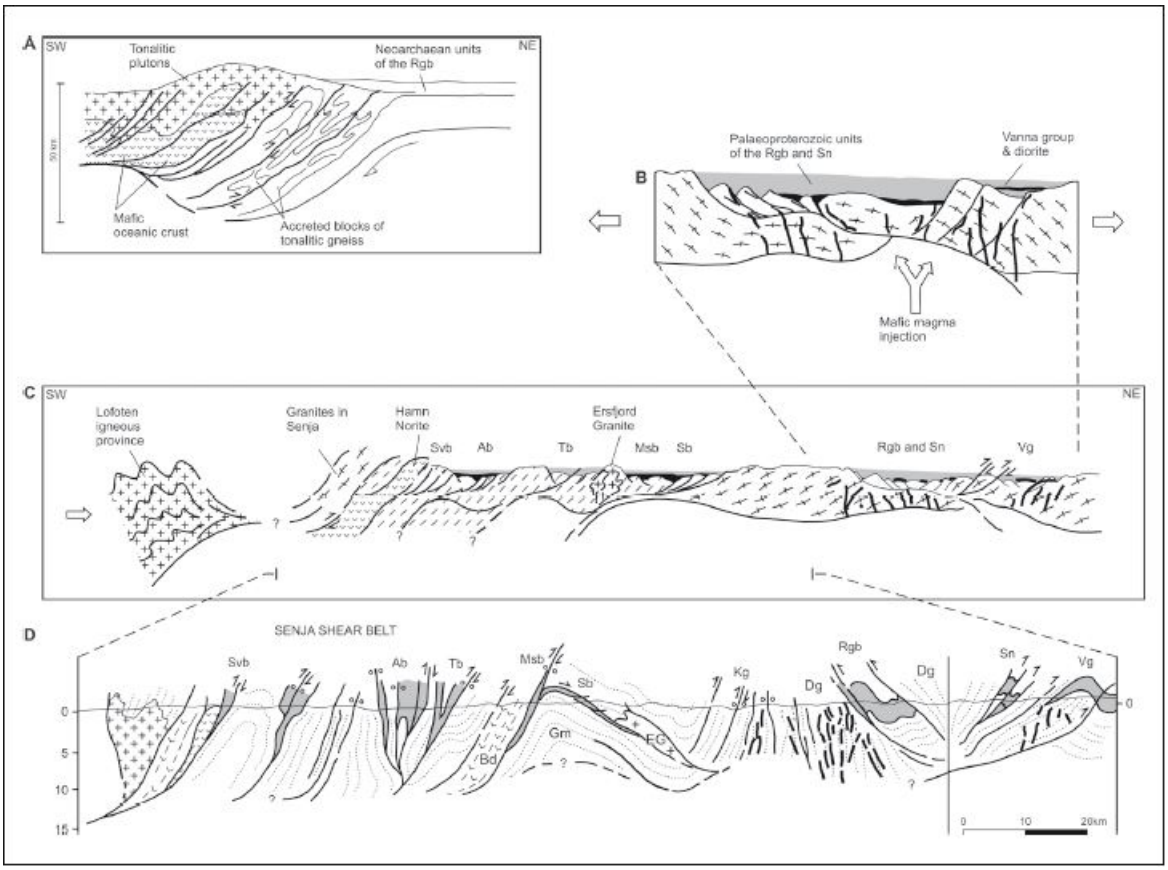

Figure 2.8: *SW-NE oriented cartoon sections illustrating the Neoarchaean to Paleoproterozoic tectonic evolution of the West Troms Basement Complex. (A) Tentative Neoarchaean (2.9-2.6 Ga) tonalitic gneiss generating event which may have involved crustal accretion and thickening due to underplating. Note position of possible precursory volcanic basin deposits as early units of the Ringvassøya greenstone belt. (B) Early Paleoproterozoic (2.4-2.2 Ga) crustal extension, basin formation and mafic dyke swarm injection, followed by (C) Svecofennian (1.8-1.75 Ga) continental contraction and probable magmatic arc accretion in the southwest (including the Lofoten igneous province). (D) Section illustrating the compiled result of Svecofennian crustal contraction, accretion and continent-continent collision with increasing transpressive deformation through time. Figure and captions from Bergh et al. (2010). Abbreviations are those used in Figure 7 in Bergh et al. (2010).*

The tectono-magmatic evolution of the West Troms Basement Complex can be summarized with a Neoarchean crustal contraction with following thickening and/or underplating leading to metamorphism. The geological environment then changed to rifting during the

Palaeoproterozoic time resulting in dyke swarms and deposition of volcano-sedimentary units. The last tectonic event to affect the WTBC was the Svecofennian orogeny that is characterized by crustal shortening and arc-related contraction leading to metamorphism and shearing, ending with geological denudation and retrogressive resetting (Bergh et al., 2010). An important question that has been raised during the study of the WTBC is how it is possible that the rocks are left with so very few mineralogical and structural effects that are directly related to Caledonian continent-continent collision, affecting the area in Silurian-Devonian time (Myhre et al., 2011). This lack of mineralogical and structural effects has led to debates of whether the WTBC is an extension of the Fennoscandian Shield or if it could be allochthonous. A study of the geophysical and structural features, together with geological and geochronological records has been done by Myhre et al. (2011) to see which interpretation fits best. The supracrustal belts that were investigated were the Steinskardtind belt, Mjelde-Skoreelvvatn belt, Torsnes belt and Astridal belt. The results from the study show that the Mjelde-Skorelvvatn and Torsnes belts are correlative of rocks formed in a global extensional regime, with the difference being that the Torsnes belt is deposited directly on the felsic gneisses with a lack of Svecofennian zircons, which implies that it must have been deposited before Svecofennian orogenesis (Myhre et al., 2011).

Recent studies of the West Troms Basement Complex by Laurent (2019) comprise of both U-Pb age data and Lu-Hf isotopic data. One tonalite-trondhjemite sample from Vanna was dated to 2865 Ma with a ε_{Nd} of +2.9, four tonalite-trondhjemite samples from Ringvassøya was dated with an age between 2831 and 2920 Ma and ε_{Nd} values in the range of +2.5 to +3.0 (Laurent et al., 2019). Three tonalite-trondhjemite samples from Kvaløya had an U-Pb age between 2744 to 2957 Ma with associated ε_{Nd} values in the range of +3.0 to -0.9 (Laurent et al., 2019). Two quartz diorite-granodiorite-granites samples from Kvaløya are dated to 2744 and 2957 Ma and gives a ε_{Nd} of -1.0 and -3.8. The same rock type is found on Senja where three samples have been dated in the range of 2665 to 2678 Ma with ε_{Nd} values from +0.9 to +1.9. The quartz monzonite-(monzo) diorite on Kvaløya show two samples with a U-Pb age of 1800 and 1861 Ma with slightly more mafic ε_{Nd} values of -8.3 and -10.0. On Senja the same rock is found with an age between 1790 and 1869 and ε_{Nd} values in the range of -7.0 to -12.0. Monzo-syenogranite is the last rock type that was checked for this study and is found on Kvaløya and Senja, the one sample found on Kvaløya is dated to 1791 Ma with a ε_{Nd} value of -11.8. The three other samples on Senja have an U-Pb age between 1759 to 1789 Ma and a ε_{Nd} from -10 to -12 (Laurent et al., 2019). The data suggest that the younger the rocks get the more negative the ε_{Nd} values get, implying that they have a larger contribution from a crustal melt.

2.5 Rombak Tectonic Window

The Rombak Tectonic Window (RTW) is an area located near the southern margin of the Archean Domain (Pharaoh & Pearce 1984, Öhlander et al., 1987). The tectonic window holds rocks that are dated back to Early Proterozoic time, including supracrustal belts that are shown to have turbidites and mafic to felsic volcanites within them (Korneliussen and Sawyer, 1989). A simplified geological map for the RTW is provided in Figure 2.9.

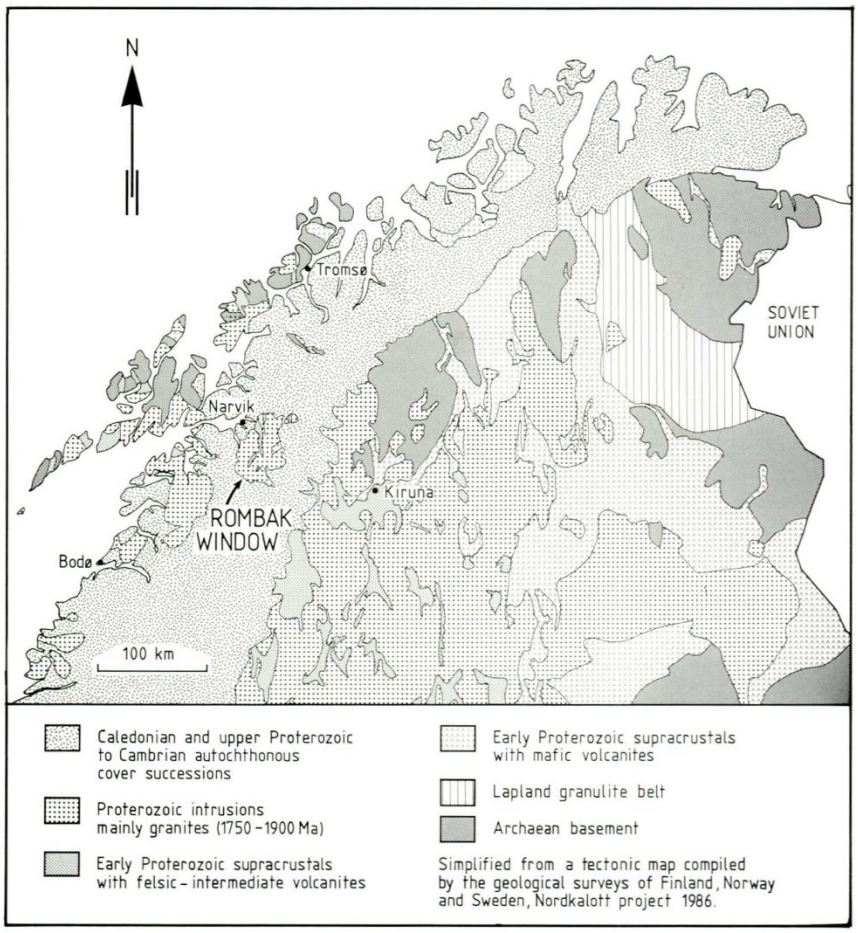

Figure 2.9: *Major geological units of the northern part of the Baltic Shield in Norway, Sweden and Finland. Simplified from a tectonic map compiled by the geological surveys of Finland, Sweden and Norway, Nordkalott Project 1986. Figure from Korneliussen & Sawyer (1989).*

The geological history runs back to 2.4 Ga when the Archean craton was fragmented during rifting, leading to formation of greenstone belts (Gaál and Gorbatschev, 1987). Korneliussen and Sawyer (1989) has done studies on the geochemistry of the metavolcanic rocks of RTW and found that the rocks seem to have formed in a geological environment characterized by a magmatic arc overlying a subduction zone. Using Rb-Sr dating techniques, the Swedish supracrustal belts have been dated to 1.91-1.88 Ga. With the same technique, the intrusions of the granitic rocks are found to have taken place around 1.78-1.69 Ga (Korneliussen and Sawyer, 1989). These dates have been updated with the more precise U-Pb dating techniques. The new geochronological data shows a more constrained age range between 1-79 and 1.80 Ga, from Angvik (2014) and (Slagstad et al., unpublished data, 2019). The N-S trending linear, inhomogeneous supracrustal belts are preserved between extensive younger plutonic rocks presenting a mineral assemblage linked to metamorphic events in the lower amphibolite facies (Korneliussen and Sawyer, 1989). The RTW can be subdivided based on different metamorphic grades. The central, western and southwestern part has been exposed to amphibolite facies conditions whilst the rest show metamorphism in the greenschist facies (Korneliussen and Sawyer, 1989). To complicate things, rocks of the same area underwent retrograde metamorphism during the Caledonian Orogeny. This retrograde metamorphism has left traces of greenschist-facies that overprints the rocks to various degrees (Korneliussen and Sawyer, 1989). The rocks that are found in RTW are shown together with their abbreviations in Figure 2.10. The Sørdalen Supracrustal Belt (S) is an area dominated by porphyritic, mafic, intermediate

and felsic volcanites (Korneliussen and Sawyer, 1989). Stasjonsholmen-Rombak Supracrustal Belt (SH) comprises a graded sequence of pelite-greywacke turbidites with interlayering of tuffitic layers, whilst the Muohtaguobla area (M) consists of mafic and intermediate lavas, felsic tuffs, pelites and graphitic schists that show complex intermixing of crossbedded quartzites and conglomerates (Korneliussen and Sawyer, 1989). The Ruvssot-Sjangeli Supracrustal Belt (RS) includes mafic and ultramafic volcanites, fine-grained biotite schists, greywackes and carbonates, that bear a resemblance to greenstone belts (Korneliussen and Sawyer, 1989). Gautelis Supracrustal Belt (G) is dominated by a turbiditic sequence , and Stasjonsholmen (SH) unit shows thin horizons of tuffitic mafic and felsic volcanites interlayered with conglomerates and debris flows (Korneliussen and Sawyer, 1989).

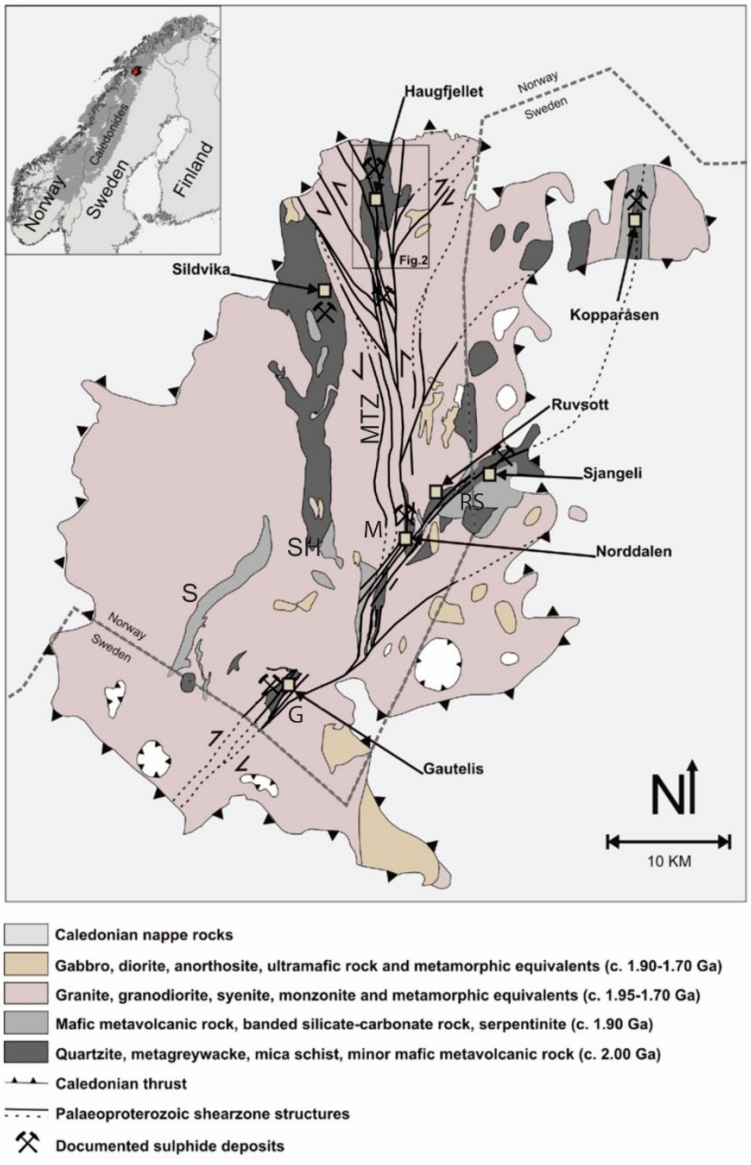

Figure 2.10: *Generalized geological map of the Rombak Tectonic Window. Abbreviations used in the text with precise locations: S- Sørdal, G- Gautelis, SH- Stasjonsholmen, M- Muohtaguobla, MTZ- Muohtaguobla Tectonic Zone, RS- Ruvssot-Sjangeli. Figure modified after Angvik (2014).*In the work on the geochemistry, Korneliussen & Sawyer (1989) separated the rocks into extrusive and intrusive. The (Na_2O+K_2O) versus SiO_2 plot shows that the extrusive rocks from the southwestern and central part are more alkaline than the rest of the RTW and the interpretation of the diagram favours an andesitic composition (Korneliussen and Sawyer,

1989). Studying the Na_2O versus K_2O plot made for the same area shows three important compositional differences within the volcanites: a) The Ruvssot-Sjangeli extrusives are K2O-deficient and have variable, but low Na2O contents; b) The Gautelis felsic volcanites from the Tonalite Complex have a higher Na2O/K2O ratios than the other volcanites from the west of the Muohtaguobla Tectonic Zone; and c) within the Sørdal-, Stasjonsholmen-, Muohtaguobla- and Rombaksvatn volcanites the mafic members have higher Na2O/K2O ratios than the associated volcanites (Korneliussen and Sawyer, 1989). Based on the findings in the major element chemistry the Rombak Window Supracrustals can be divided into three types: 1) The RS-type; low-K2O mafic to ultramafic sub alkaline extrusives from the 2.3 Ga supracrustal belt. 2) The G-type; low-K2O, high Na2O rhyodacitic to rhyolitic volcanites. 3) The SN-type; a suite of mafic to felsic, generally K2O-rich extrusives (Korneliussen and Sawyer, 1989). The major elements can therefore be said to indicate an andesitic composition of the extrusives that favours a calc-alkaline affinity (Korneliussen and Sawyer, 1989). With the help from trace elements it is possible to distinguish between the three volcanite types, commonly they all show a REE-trend indicating a calc-alkaline suite. The geochemistry has also been checked for the intrusive rocks of the RTW, and the major elements generally plot along a calc-alkaline trend like the extrusive rocks. The trace elements display a REE-pattern with negative Ta, Nb and Ti anomalies that according to (Best, 1975), (Hawkesworth et al., 1977a) and (Sun and Nesbitt, 1978) implies subduction-related magmas. The geochemistry of both the extrusive and intrusive rocks of RTW concludes that the area can be geochemistry divided into an eastern and western part based on the geochemistry. The eastern part contains remnants of the early stages of an intra-oceanic arc volcanism that seem to have occurred at around 2.3 Ga and is hence the oldest part. The western part contains remnants of a younger (ca 1.78 Ga) mature volcanic arc located on thicker, continental crust (Korneliussen and Sawyer, 1989).

It is important to note that the ages dated by Angvik (2014) and Slagstad et al. (unpublished data,2019) have been carried out by the newer and more precise technique of U-Pb dating. Korneliussen and Sawyer (1989) used Rb-Sr to do the same dating, in which the system is more vulnerable for errors due to changes of the system. These changes are mostly caused by hydrothermal processes under metamorphism or magmatism. The hydrothermal processes cause the Rb and Sr to be more mobile and therefore move around, and also introduce new Rb and Sr into the rock, such that the event of the alteration can be dated- but not the age at which the rock formed. Therefore, the most accurate ages for the intrusion of the granites would be 1.79 to 1.80 Ga (Angvik, 2014). Isotopic data regarding the Sm-Nd system was examined by Romer (1992). The $\varepsilon_{Nd(t)}$ was found to be in the range of +2.5 to -12.6 for the granites covering the area from Kvaløya to Sjona, with an age set to 1.71 to 1.78 Ga (Romer et al., 1992). The Early Proterozoic mantle is believed to have had an ε_{Nd} of +4 (Huhma, 1986), whilst the Archean crust had an ε_{Nd} of approximately -12 (Skiöld, 1988) with a modelling age of 1.8 Ga for these rocks.

2.6 Altevatn area

The Altevatn area is in eastern Troms, the second northernmost county of Norway. The area has gained interest due to the MINN programme, a short name for Mineral Resources in Northern Norway, which was initiated by the Norwegian Geological Survey in 2011. The ambition of the programme was to renew geophysical and geological information of this part of the country, to find out if the area has any considerable mineral resources (Slagstad et al., 2015). The choice of location is not random, as the Altevatn area is the northwesternmost, undisputed autochthonous part of the Fennoscandian Shield (Slagstad et al., 2015). The area belongs to the north-western part of the Norrbotten Province (Figure 2.11) that is known for its mineral resources linked to among others, the world-known Kirunavaara apatite-iron deposit.

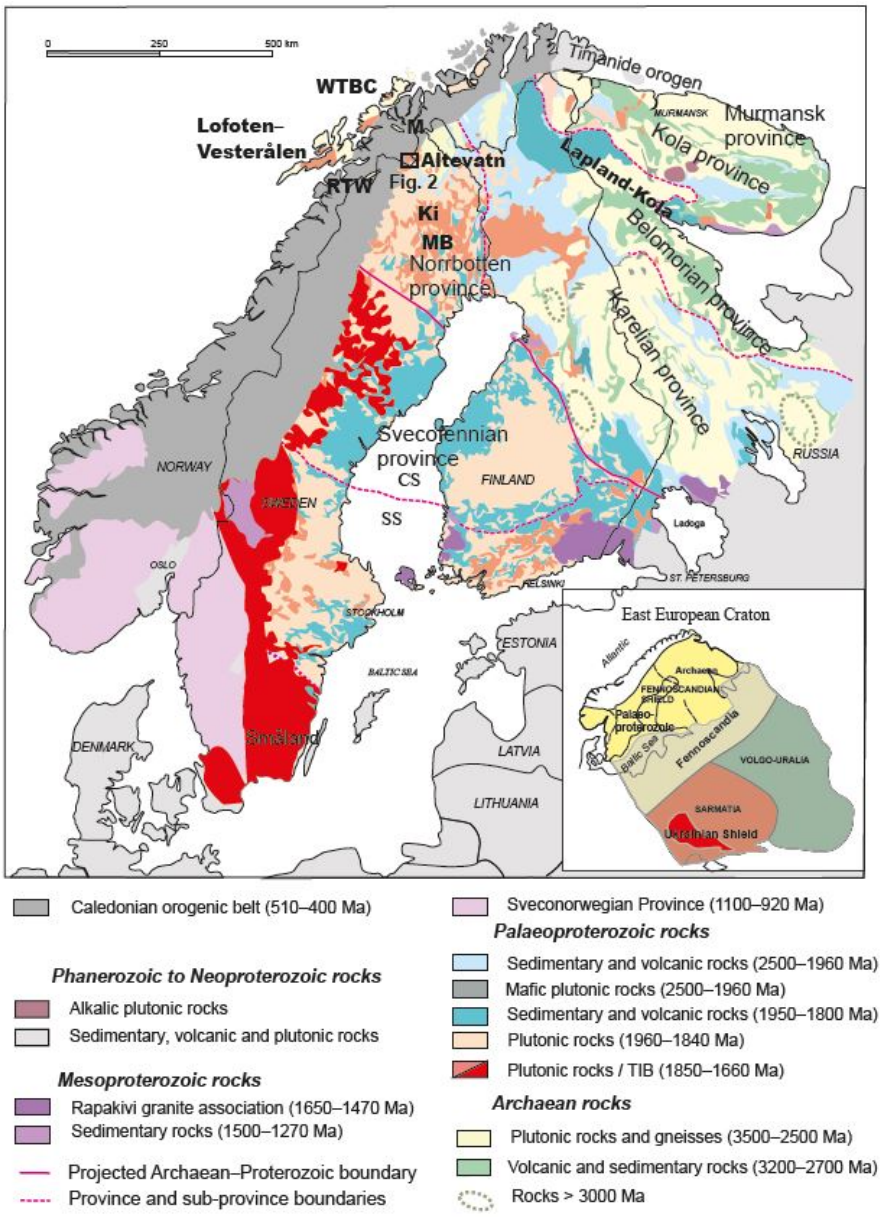

Figure 2.11: *Fennoscandia and its location within the East European Craton. Simplified geological map based on Koistinen et al. (2001) and inset map based on Gorbatschev & Bogdanova (1993). Abbreviations: CS- Central Svecofennia, SS- Southern Svecofennia, Ki-Kiruna, M- Mauken, MB-Malmberget, RTW- Rombak Tectonic Window, WTBC- West Troms Basement Complex. Modified from Lahtinen (2012).*The Altevatn area is located within the Norrbotten Province as shown in

Figure 2.11. Due to a thick cover of moraine the area lacks exposures and fresh outcrops of the geology, except from around the shore of the Altevatn lake and elevations in the surrounding terrain (Slagstad et al., 2015). Geophysical data has therefore been a very important contribution in the interpretation of the tectonic elements that are hidden below the moraine. The rocks that constitute the Altevatn area are found to be Archean migmatitic rocks, monzonite, granite and gabbro that appear as intrusions. Only the migmatitic rocks are found in fresh outcrops as they are preserved in the lichenfree outcrops along the shore of the regulated lake. The other rocks are found at more weathered outcrops away from the Altevatn area (Slagstad et al., 2015). A geological map of the Altevatn area is shown in Figure 2.12.

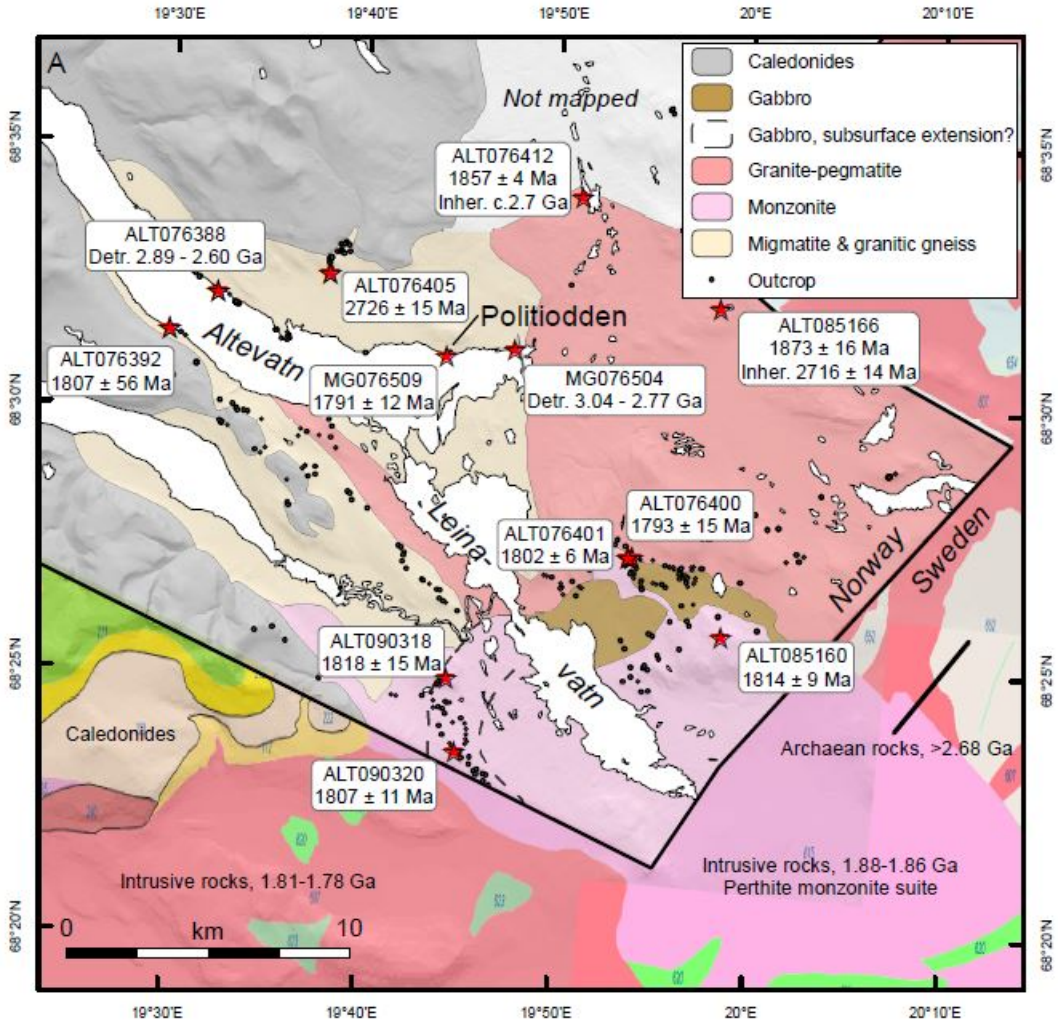

***Figure 2.12**: Geological map of the Altevatn area with associated lithologies. Sample locations with dating results are also plotted. Figure from Slagstad et al. (2015).*

The migmatitic rocks are described as gneisses that may have both supracrustal and plutonic protoliths, but due to high degree partial melting it is hard to identify the protoliths (Slagstad et al., 2015). Slagstad et al. (2015) divides the Archean rocks into metatexites and diatexites. The metatexites are defined as medium to coarse grained foliated biotite gneisses with gneissic textures and granitic leucosomes, that incorporates fine-grained homogenous amphibolite thought to be former mafic dykes (Slagstad et al., 2015). On the basis of the textures and structures found within the metatexites and the association with quartzite, the protolith at least for some of the migmatites is supracrustal (Slagstad et al.,

2015). The diatexites shows less continuation of structures and contain biotite-rich schliren and rotated blocks of resister lithologies and in contrast to the metatexites the amphibolite sheets appear as disrupted fragments (Slagstad et al., 2015). The amphibolite fragments are commonly found to be surrounded by pegmatites (Slagstad et al., 2015). The Archean granitic gneisses and granites are described as heterogenous and typically includes lenses of metatexite and in some cases extend into biotite-schliren (Slagstad et al., 2015). The younger, intrusive rocks are dated to be Paleoproterozoic (ca.1.80 Ga) and comprise gabbro, monzonite and granite-pegmatite. The gabbro shows a variation in its composition, ranging from leucogabbro to melagabbro (Slagstad et al., 2015). The rock is coarse-grained and shows a subophitic texture under the microscope with a high magnetic susceptibility indicated by the geophysical data (Slagstad et al., 2015). The monzonite is also described as coarse-grained and consists of 60-90% ternary feldspar with quartz being interstitial. Mafic minerals appear as clusters and the opaque minerals are rimmed by titanite, leading to an interpretation of the rock experienced greenschist facies metamorphism (Slagstad et al., 2015). Like the gabbro, the monzonite has a relatively high magnetic susceptibility shown on the geophysical map. The granite-pegmatite unit, as suggested by its name, gradually varies from coarse-grained granite to pegmatite and consists mostly of plagioclase, K-feldspar and quartz. Mafic minerals are sparse and shows retrogression connected to fluid circulation with static recrystallization (Slagstad et al., 2015). Unlike the gabbro and monzonite, the granite-pegmatite unit is found to have a relatively intermediate to low magnetic susceptibility (Slagstad et al., 2015). Fine-grained granitic undeformed dykes that cut the Archean migmatites are also observed in the same area (Slagstad et al., 2015).

The Norrbotten province comprises both Archean and Proterozoic rocks. The Archean rocks are mainly tonalitic, granodioritic, quartzdiorittic and supracrustal. The Paleoproterozoic rocks are both mafic-ultramafic intrusions, metavolcanics, metasedimentary- and supracrustal rocks. The metallic deposits within these rocks are of four types: 1) stratiform-strata bound base metals and iron, 2) apatite iron ores, 3) epigenetic base metals and 4) other metals (Slagstad et al., 2015). This province is the one used to compare the mineral resource potential of the Altevatn area. Geochronological results from the monzonites, gneisses, granites and granitic dykes found in Altevatn provides information of the same geological events that are described for the Norrbotten province. The supracrustal rocks of Altevatn are dated to 1.96-1.85 Ga (Bergman et al., 2001), the same as found for the supracrustal rocks in the Kiruna area. Even though the Altevatn area constitutes of similar rocks and a geological record that is similar to the Swedish part of the Fennoscandian Shield remnants, no economically resources have yet been found in Altevatn.

2.7 Central Nordland Basement Window and the extension of the Fennoscandian Shield, the Archean-Proterozoic boundary

Tectonic basement windows are not particular just for the northernmost part of Norway, they are also found in Nordland. The importance of the study done on these tectonic basement windows can be attributed to the Archean-Proterozoic boundary giving an idea of how far southwest the Archean rocks of the Fennoscandian Shield stretched. For the time being this boundary has been drawn on a straight line from the east to the west side of the Norwegian border, south of the Lofoten islands and Salten (Figure 2.13).

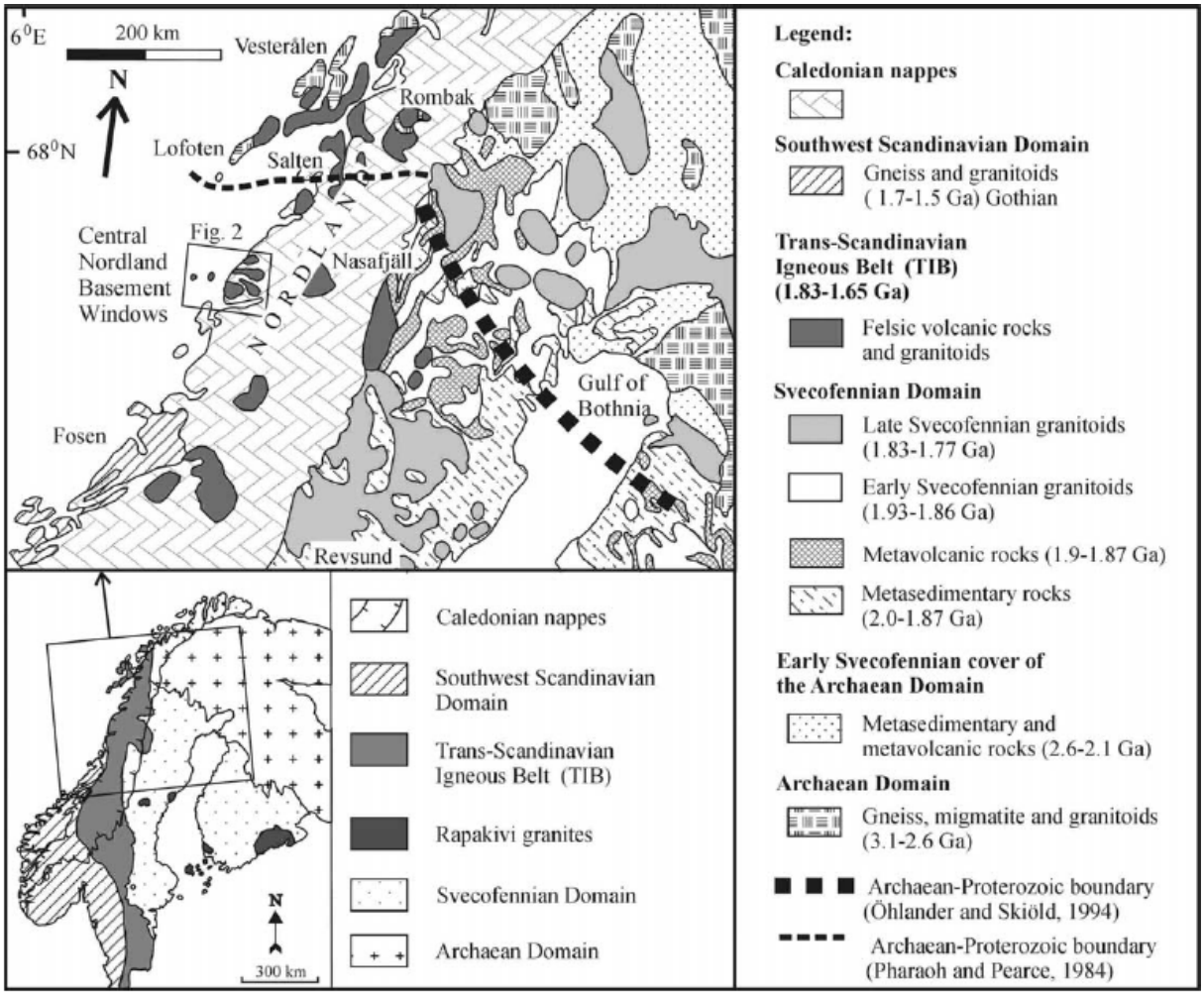

Figure 2.13: *Geological map of northern Scandinavia showing the main lithological units and the Archean-Proterozoic boundary defined from Sm-Nd isotopes. After Gaál and Gorbatschev (1987).*

Gaàl and Gorbatschev (1987) used Sm-Nd isotope geochemistry to constrain a boundary for Archean-Proterozoic rocks, this boundary is shown in Figure 2.13. From the Norwegian border there is little or no published Sm-Nd data to continue this boundary. Figure 2.13 and 2.14 show the many tectonic basement windows that are found along the central to northern parts of Norway, four of them being Glomfjord-, Svartisen-, Høgtuva and Sjona Window.

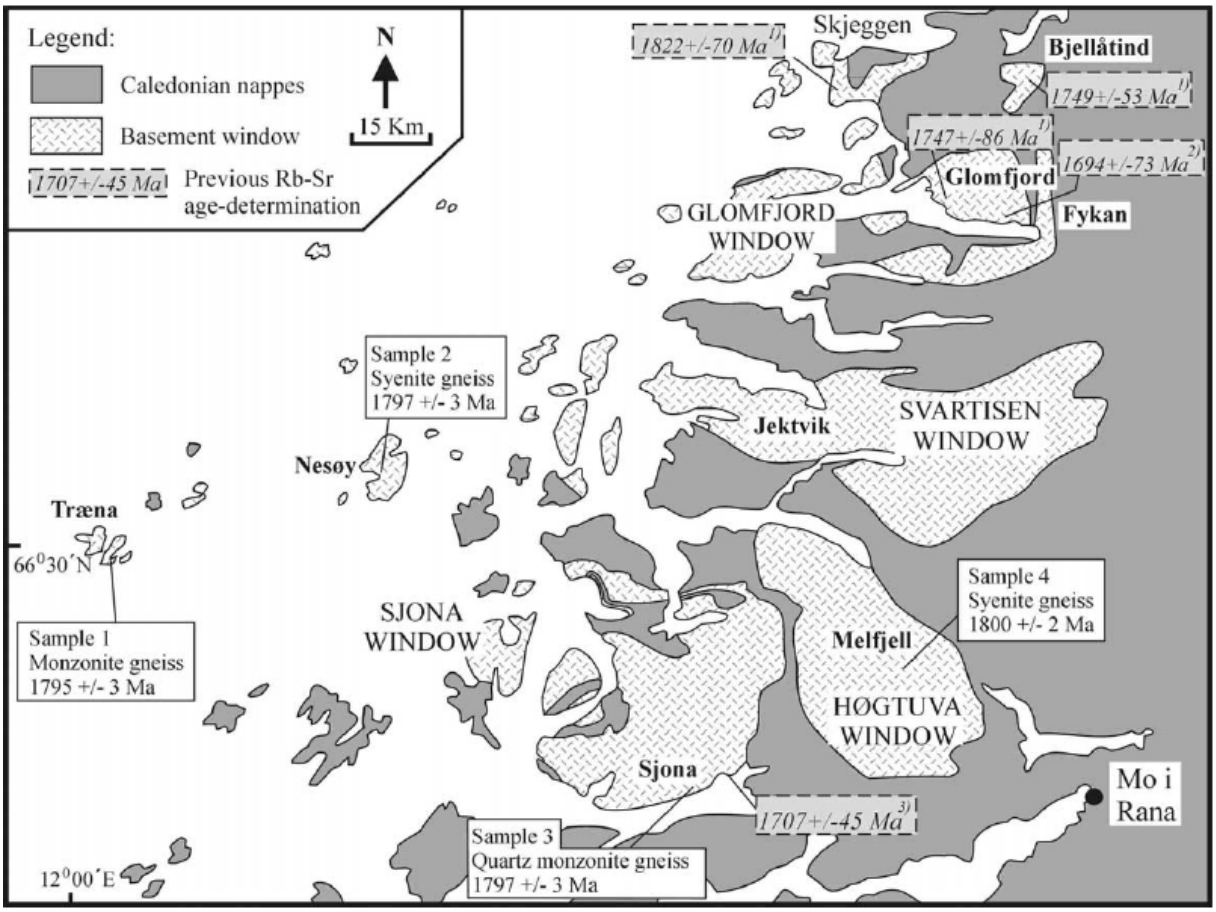

Figure 2.14: *Central Nordland Basement Windows. Interpreted isotopic ages are shown together with the U-Pb sample locations, after (Skår, 2002). Previous age determinations: (1) (Cribb, 1981); (2) (Wilson and Nicholson, 1973); (Wilberg, 1987).*

Skår (2002) has done field work in these four tectonic basement windows and carried out both geochronology and geochemistry to reveal whether these rocks are similar to the basement rocks found at the Lofoten-Vesterålen islands and in the RTW. The Glomfjord Window is described to expose red microcline gneisses, grey gneisses, foliated microcline granite in the northern part and granite-monzonite gneisses and grey granodioritic gneisses in the southern and central part (Skår, 2002). The Svartisen Window show exposures of granitic and tonalitic gneisses, where the granitic gneisses form zones of non-foliated granite and the tonalitic gneisses contain lenses of amphibolite (Skår, 2002). Both gneisses vary in degree of deformation and appear with granitic pegmatites (Skår, 2002). The Høgtuva Window comprises foliated equigranular granitic gneisses with concordant biotite schist with a foliation parallel to the overlying Caledonian nappes (Skår, 2002). The fourth and southernmost basement window is the Sjona Window, which exposes rocks that vary in composition between monzonite and granite, in addition to some gabbroic rocks (Skår, 2002).

U-Pb geochronology shows that samples collected from Træna, Nesøy and Sjona in the Sjona Window have upper intercept ages of 1793±5, 1797±3 and 1796±11 Ma, respectively, and lower intercept ages of 392±13, 359±64 and 426±12 Ma, respectively (Skår, 2002). One sample collected from the Høgtuva Window shows an upper intercept age of 1800±2 Ma and a lower intercept age of 414±10 Ma (Skår, 2002). The upper intercept ages are interpreted to be the crystallization age of the protoliths and the lower intercept ages are interpreted to reflect the Caledonian metamorphism (Skår, 2002). These

ages are comparable to the ages found in the Lofoten-Vesterålen area and RTW, and there is reason to believe that they have experienced the same magmatic and metamorphic events. The geochemistry of the coeval granitoids are at least as important, especially in the search for the Archean-Paleoproterozoic boundary. Initial $\varepsilon_{Nd(t)}$ values have been calculated for the four basement windows and are found to be in the range of +0.3 to -3.4 calculated with a T_{DM} of 1.8 Ga, except from three samples taken from the easternmost windows that are in the range of -5.0 to -6.5 (Skår, 2002). Compared with the initial $^{\varepsilon}Nd(t)$ of basement window rocks in Sweden varying from +0.3 to -6.5, most of the samples are in the range of 0 to -4. And from the Archean crustal evolution (-11 to -13) defined from Nd isotope signatures of 1.90 Ga granitoids, the basements windows in Nordland seem to fit in to the southwest, younger side of the Archean-Proterozoic boundary (Skår, 2002).

3 Theory

3.1 Geochronology

3.1.1 Uranium-lead geochronology

The decay of uranium (U) and thorium (Th) to stable lead isotopes is the foundation of several dating techniques. Thorium (Z=90) and U (Z=92) have similar electron configurations and therefore similar chemical properties (Faure and Mensing, 2005). Because they both are concentrated in the liquid phase during partial melting and have an affinity for silica-rich minerals, they are more enriched in the continental crust than the upper mantle (Faure and Mensing, 2005). Three naturally occurring U isotopes exist in nature, ^{238}U, ^{235}U and ^{234}U. They are all radioactive and emit energy in the form of radiation resulting in alpha, beta and gamma rays. Thorium occurs primarily as radioactive ^{232}Th, whilst lead occurs as radiogenic ^{206}Pb, ^{207}Pb, ^{208}Pb and non-radiogenic ^{204}Pb. Uranium and thorium are both parental isotopes and do not decay directly to stable lead isotopes, but go through a chain of radioactive daughter isotopes (Figure 3.1) emitting alpha and beta rays (Faure and Mensing, 2005). The half-lives of the parental isotopes are much longer than their radioactive daughter isotopes making them the target during isotope measurements. ^{238}U has a half-live of 4.468×10^9 years and ^{235}U has a half-life of 0.7038×10^9 years (Steiger and Jäger, 1977). The decay of uranium and thorium to stable lead isotopes are shown in Equation 1-3. α is the alpha particle, β is the beta particle and E is the energy released during decay (Schoene, 2014).

$$^{238}U \rightarrow {}^{206}Pb + 8\alpha + 6\beta + E \qquad \text{Eq. 1}$$

$$^{235}U \rightarrow {}^{207}Pb + 7\alpha + 4\beta + E \qquad \text{Eq. 2}$$

$$^{232}Th \rightarrow {}^{208}Pb + 6\alpha + 4\beta + E \qquad \text{Eq. 3}$$

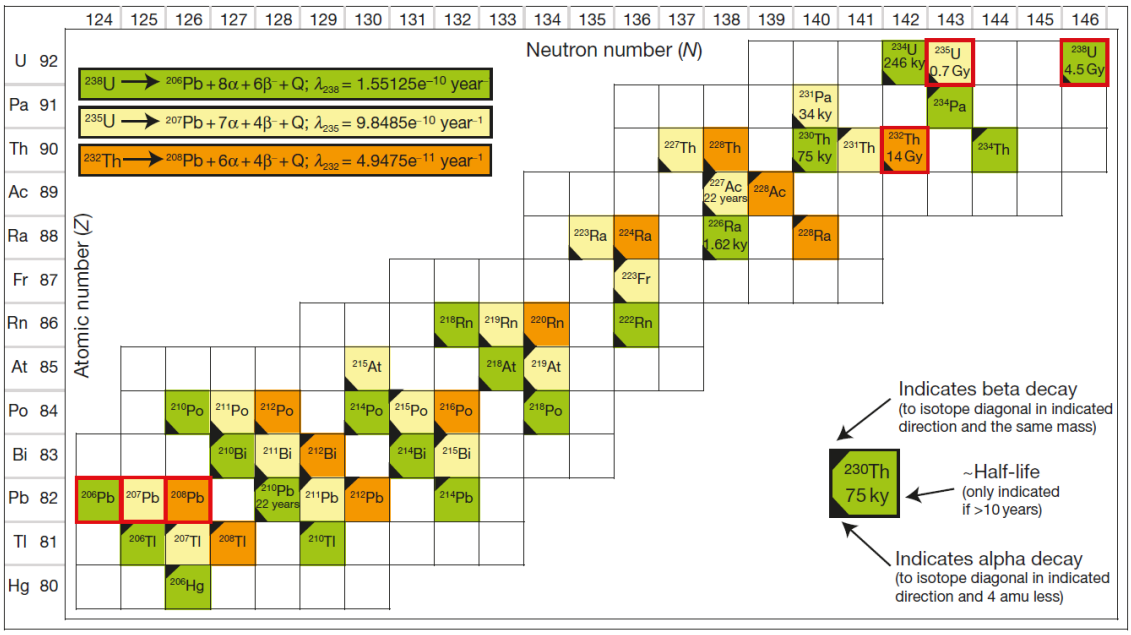

Figure 3.1: *An illustration of the U-Th-Pb decay chains. Each isotope occurring in a given decay chain is color-coded to its parent isotope, which is outlined in red, as are the stable daughter isotopes of Pb. See inset for description of symbols used in each box. Figure and caption after Schoene*

*(2014).*Due to their long half-lives, both ^{238}U, ^{235}U and ^{232}Th satisfy the requirements of a secular equilibrium decay chain meaning that the product of the abundance of an isotope and its decay constant are equal among all intermediate daughter products and the parent isotope (Schoene, 2014). The uranium and thorium isotopes can therefore be treated as if they decayed directly to the respective stable lead isotopes. An important aspect of U-Pb and Th-Pb dating applies to ^{204}Pb, also known as common lead. This isotope is non-radiogenic and can cause a low U/Pb or Th/Pb ratio that again affects the dating of the calculated age.

Uranium and thorium occur and can be thought of as both trace elements and contributors in accessory minerals, such as zircon ($ZrSiO_4$) in this study. Zircon is a favoured mineral for U-Pb dating techniques as it is highly resistant to weathering and has a high closure temperature that preserves information about the rocks history by avoiding loss of uranium and thorium.

3.1.2 U-Pb Concordia Plots

For visualisation of the U-Pb data gained from LA-ICP-MS and SHRIMP it is common to construct a U-Pb Concordia plot. A concordia plot is helpful in visualizing how assembled or spread a dataset is and thereby get a hint of the quality of the dataset. Things such as multiple zircon populations or possible reasons of discordance are easier to observe on a plot than in a data sheet. There are two very common plots for U-Pb dating, the Tera-Wasserburg Plot and the Wetherill Plot. The preferred plot for this study is the Terra-Wasserburg (TW) diagram. The advantages of this diagram are that all the isotopes are measured in the instruments (^{207}Pb, ^{206}Pb and ^{238}U), in the Wetherill diagram the ^{235}U isotope is calculated from the other isotopes which could cause a slight uncertainty. The second advantage of the TW diagram is that it is easier to spot if there is common lead present. This is easier to observe because the TW has one axis with the $^{207}Pb/^{206}Pb$ ratio and one axis with the $^{238}U/^{206}Pb$ ratio, the common lead could therefore be traced in the $^{207}Pb/^{206}Pb$ ratio. In the Wetherill diagram there is two ratios which both are measured between a Pb and U ratio. For this reason, it is also easier to observe fractionation in the TW diagram. The only advantage of the Wetherill diagram is that one can anchor in 0. The most common types of discordance in TW plots are shown in Figure 3.2, with an arrow indicating the direction which the data points tend to move in each case of discordance. Note that samples can be discordant by one or more reasons, making it harder to know the exact reason for the discordance (e.g. both common lead and lead loss). An example of a Wetherill concordia diagram is provided in Figure 3.3.

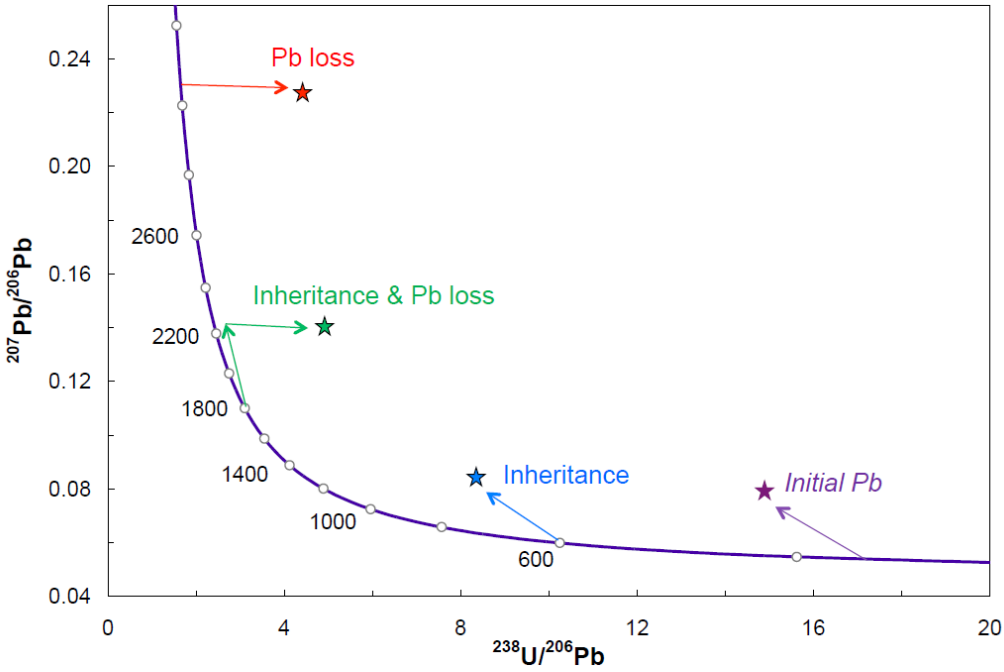

Figure 3.2: *Tera-Wasserburg plot showing the trends of respectively Pb-loss, Inheritance & Pb-loss, Inheritance and Initial Pb. Figure borrowed Paul Sylvester from a lecture given in 2018 at Texas Tech University, Texas, USA.*

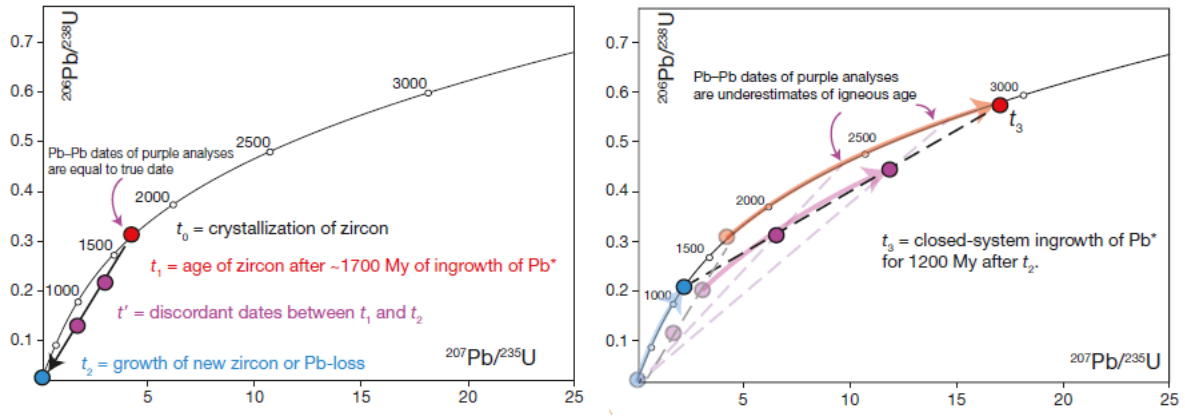

Figure 3.3: *Graphical representation of zircon growth history in the Wetherill Concordia diagram (a, b). (a) Example of a 1700 Ma zircon losing Pb or mixing with metamorphic overgrowth. t0 is the crystallization age of the zircons; after 1700 My of closed-system ingrowth of Pb, the zircons appears on concordia at t1; at t2 the zircon suffers Pb loss or growth of new zircon around old core; t0 represents zircons that are discordant following partial Pb loss or mineral overgrowth at t2. (b) The same data after the system has closed again and continues to evolve up the concordia curve. The discordia line defined by purple analyses now has an upper intercept with Concordia representing the original igneous crystallization event at t1, and a lower intercept age representing t2, the time before the present at which Pb loss or overgrowth occurred Figure and caption from Schoene (2014).*

Independent of what Concordia plot that is chosen for a presentation of U-Pb ages it is common to calculate the discordance of the data (Eq.4). Usually the $^{206}Pb/^{238}U$ age is designated the younger rocks and the $^{207}Pb/^{235}U$ for the older rocks, this is due to the low abundance of ^{207}Pb in younger rocks.

$$\% - discordance = 100 - (100 * \frac{(\frac{^{206}Pb}{^{238}U})}{(\frac{^{207}Pb}{^{206}Pb})}) \quad \text{Eq. 4}$$

It is important to note that even if samples are showing a large discordance, it does not mean that the data are poor. But, they can be used as a tool to look more into the data and figure out what is causing the potential high discordance.

3.1.3 Zircon

The main mineral used for geochronology in this study is zircon ($ZrSiO_4$), which is composed of the element zirconium, silicon and oxygen making it a zirconium silicate (orthosilicate group). Zirconium belongs to the fifth period of the periodic table and has an atomic number (Z) of 91. Zircon is a common accessory phase in felsic to intermediate rocks and in some mafic rocks and belongs to the heavy minerals as it has a density of ~ 4.65 g/cm^3. The heavy minerals are defined as minerals with a density >2.9 g/cm^3. Zircon is a favoured mineral for both geochronology and geochemistry as the mineral is highly resistant to both mechanical abrasion and chemical weathering and is stable up to high degrees of metamorphism. These properties, in combination with its affinity to incorporate trace elements and rare-earth-elements (REE), make it perfect for recording magmatic and metamorphic events that the rock has been exposed to since the time of formation. The recording of events is often reflected in the internal textures of the zircon grains: e.g. sector zoning, patchy zoning or skeletal growth. Internal textures, cracks and inclusions can easily be detected using cathodoluminescence images (CL) and backscattered scanning electron images (BSE). Because it has a high resistance to deformation it also preserves a good crystal form (tabular to prismatic) making it easier to pick for geochronological purposes.

3.1.4 U-Th-Pb dating techniques

There are several ways of doing dating analyses, a decision on what analysis to be done is depending on what instruments are available, the number of samples and the purpose. The advantages with the LA-ICP-MS is that it's a less expensive instrument. The disadvantage is that it requires more time to do the measuring. The SHRIMP is a much more expensive instrument, but the number of counts/hours is much larger than for LA-ICP-MS. This study used U-Pb dating performed by the instruments of Laser Ablation Inductively Coupled Plasma Mass Spectrometry (LA-ICP-MS) and sensitive high-resolution ion microprobe (SHRIMP).

LA-ICP-MS

LA-ICP-MS is a dating technique where a sample with a polished surface is inserted into a sample chamber. This chamber is filled with a helium (He) gas. The sample is then ablated with a laser beam. The ablated particles (e.g. U, Pb and Hf) are then transported with the He gas towards the ionized coupled plasma (ICP) where it is mixed with an Argon gas. When the ablated particles enter the ICP it is exposed to a magnetic field set up by a coil

and heated. The heating allows the atoms to be ionized, removal of electrons from the orbital inducing a positive charge of the atom. The positive atoms are then transported into a mass spectrometer (MS) where the atoms are separated based on their mass-to-charge ratio. The separation of the different masses is controlled by the strength of a magnet that based on wanting the low or high mass, bends the elements towards a single or multiple collector that counts the electrons. A single collector has only one collector that counts the electrons, this require an adjustment in the strength set up by the magnet. A multi collector in form of a quadrupole was used for this study. Instead of a magnet, the ion beam travels through four cylindrical rods that set up an electric field which can be adjusted much more efficient than a magnet. Part of the LA-ICP-MS process shown in Figure 3.4.

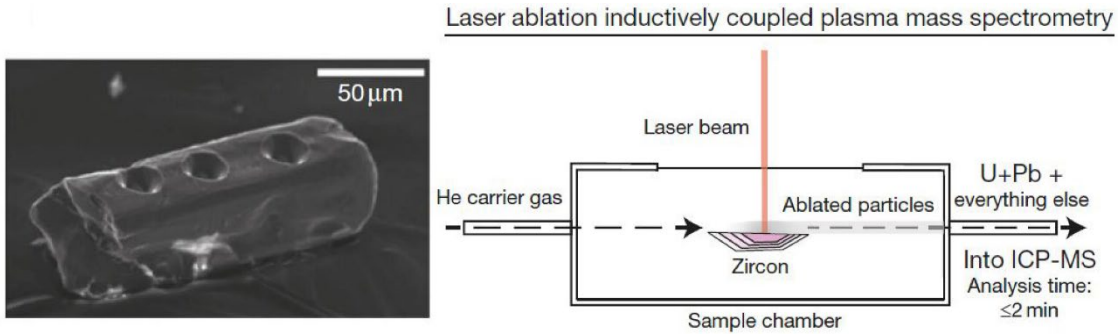

Figure 3.4: *A schematic illustration of how a zircon is treated through LA-ICP-MS analysis Figure from Schoene (2014).*

SHRIMP

SHRIMP is a dating technique where a coated and polished sample is loaded into a sample chamber. The sample is then introduced to the source chamber, where a primary column with associated primary ion beam is sent through a mass filter and an aperture to hit the surface of the sample. The primary ions (O_2^-) are aimed at the sample with an angle of 45° and the resulting secondary ions (e.g. U, Th, Pb) are extracted from the sample at an angle of 90°. The secondary ions are then transported through an electrostatic analyser where the ablated material, with different energies from the emitted secondary ions are aligned. The electrostatic analyser works as the ICP in the LA-ICP-MS, it ionizes the atoms to give them a positive charge. The alignment is based on what elements that are desirable. The secondary ions continue their transport to a magnet, and the objective of the magnet is to form a magnetic field and perform a sorting based on the secondary ion's mass. The ions are then moving into a collector, where the secondary ions are counted. The process is shown in Figure 3.5.

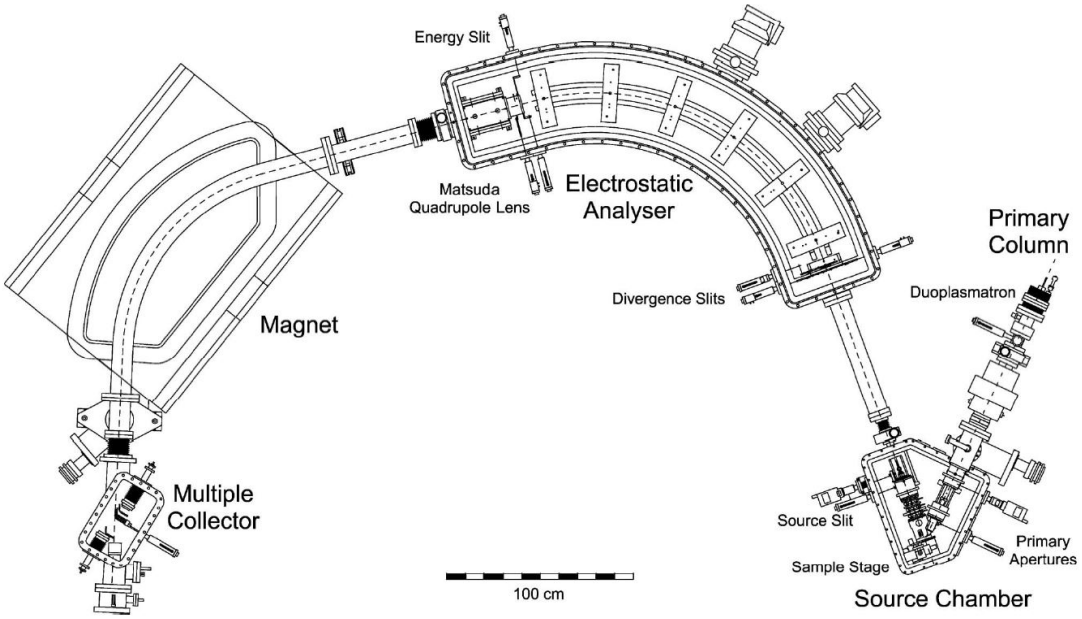

Figure 3.5: *A schematic illustration of the SHRIMP II. Figure from Ireland et al. (2008)*

Alpha dose

A fresh zircon grain consists of among other elements, uranium (U). U is a radioactive element and decays to Pb in a process producing alpha particles. These alpha particles, unlike the Pb is sent out in the zircon crystal with an energy that is capable of destroying the crystal lattice. With time, the zircon will be exposed to a high degree of alpha particles harming the crystal lattice. The destroying of the crystal lattice will allow other elements into the zircon's crystal lattice, especially LREE (this process can be observed in the REE spider plots). The harming of the crystal lattice could also lead to loss of Pb. By calculating the alpha dose, an interpretation of the age and the content of Th and U can be performed. If a U-P concordia plot show very discordant data, the alpha dose together with other data might explain the discordance. The process of alpha decay in zircon is illustrated in Figure 3.6.

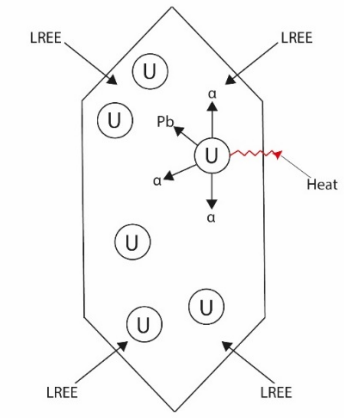

Figure 3.6: *Decay of U in a zircon crystal. The decay of U to Pb results in both alpha particles and heat. The alpha particles are sent out with an energy that bounce into the crystal lattice and cause damage, allowing elements like Pb to leave the crystal lattice and replacement of e.g. LREE.*

3.2 Geochemistry

3.2.1 Whole-rock geochemistry

Geochemical analyses can be performed at different levels, whole-rock geochemistry comprises the chemistry representative for the whole rock and not any specific parts of it. That means, when the rock is crushed the material that is sent to the lab needs to be random and that is why splitting is so important. It provides for a random selection of grain size and mineral proportions. Whole-rock geochemistry is a wide branch of knowledge, but for this thesis the focus has been on major and trace elements, in addition to the Sm-Nd isotope system.

3.2.2 Major elements

The major elements are defined as elements that constitutes >1.0 wt.% of the rock (Winter, 2013) and the most common one being oxides such as SiO_2, Al_2O_3, FeO, MgO, CaO, Na_2O and K_2O. These oxides are put together by the most common elements on the Earth.

Harker Diagram

One of the most common ways to apply major elements is to plot them in variation diagrams, such as the Harker diagram. In this diagram the major elements are plotted against silica dioxide (SiO_2). In that way, variation in major elements concentration relative to changes in the SiO_2 can be studied. Throughout time and large amounts of data, geochemists have found that different magmas display different trends in the Harker diagram. Exceptions exists. One way to use the Harker diagram is to study magmatic processes. It can be used to distinguish between primary magmas and more evolved magmas (a.k.a. derivative magma). Figure 3.7 shows an example of a Harker diagram.

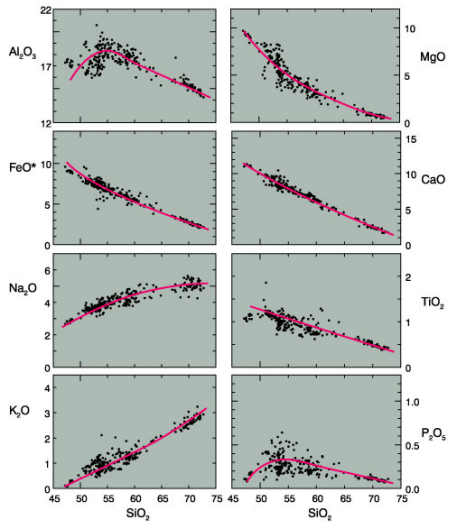

Figure 3.7: *This is a Harker variation diagram that shows 310 analysed volcanic rocks from Crater Lake (Mt.Mazama), Oregon Cascades (data compiled by Rick Conrey). As the purple lines on each diagram shows, there can be interpreted a trend between the different major elements. Since these trends are not linear, the trends are thought to reflect some sort of a chemical differentiation of the magma and thus that the magma the rocks crystallized from were an evolved magma. Caption and figure from (Winter, 2013).*

The Harker diagram is constructed with x-y axes, where it is common to plot various oxides on the y-axes against one determined oxide on the x-axes. In Figure 3.7, SiO_2 is used as the major element on the x-axis plotted against the other major elements. And by this, one can study how the silica dioxide act relatively to the other major elements. The Harker diagram in Figure 3.7 demonstrate data that appear to have a trend, in this case a trend towards an evolved magma. The Harker diagrams can be used to interpret which minerals that might have been crystallized out from the melt.

Alumina Saturation Index (ASI)

Another common characterization diagram used for major elements is the ASI plot. ASI stands for alumina saturation index and is calculated from the equation 5 below:

$$ASI = \frac{\text{molar } Al_2O_3}{\text{molar } (CaO + Na_2O + K_2O)} \qquad \text{Eq. 5}$$

The classification diagram was developed by Shand in 1947 with an aim to distinguish between metaluminous, peraluminous and peralkaline rocks. The diagram differentiates between rock suites instead of one individual rock type. Scientists have attempted to find a better classification scheme (e.g. Frost (2001)) with different approaches, but all of them are constructed based on the alumina saturation index (ASI). If the ASI<1 the rock is said to be metaluminous and has a deficiency of Al_2O_3. If the ASI>1 the rock is said to be peraluminous and has an excess of Al_2O_3. This can be related to information and interpretation of the source rock. Metaluminous rocks are characteristic for basaltic protoliths, whilst peraluminous rocks are most likely derived from a sedimentary rock (read: mudrock). The diagram used for this classification is shown in Figure 3.8. Figure 3.8 shows a rock which plots mostly in the peraluminous field of the A/CNK diagram and has an ASI>1 implying a rock that has an excess of Al_2O_3, interpreted to have a sedimentary protolith.

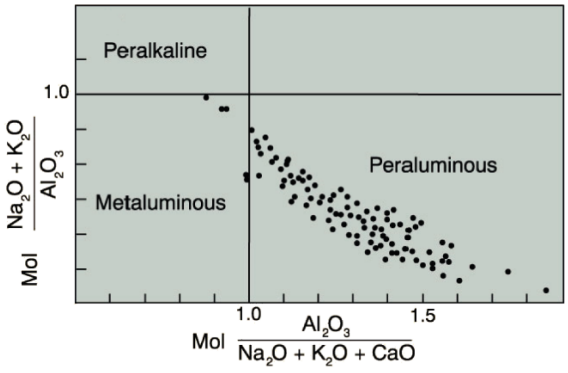

Figure 3.8: *ASI discrimination diagram. Depending on where the data plot the source rock of the sample can be interpreted. Figure from (Winter, 2013).*

Total Alkali versus Silica Index (TSI)

A third discrimination diagram that is often used for major elements is the TSI-diagram, short name for total alkalis versus silica diagram. This diagram aims to distinguish between alkaline and subalkaline magma series. Based on the concentration of $\%SiO_2$ versus $\%(Na_2O+K_2O)$ in the rock, an interpretation of what geological setting the magma was formed in can be done. The strongly alkaline magma suites thought to be low-fraction melts can be formed in continental arcs, continental rifts and ocean island settings, while the subalkaline magma suites are thought to be high-fraction melts than can be formed at mid-ocean ridges, arcs and ocean island settings. The two magma suites can be presented in a TSI-diagram as shown in Figure 3.9. The main difference between these two series are the environment of either silica undersaturation (alkaline) or silica saturation to silica oversaturation (subalkaline).

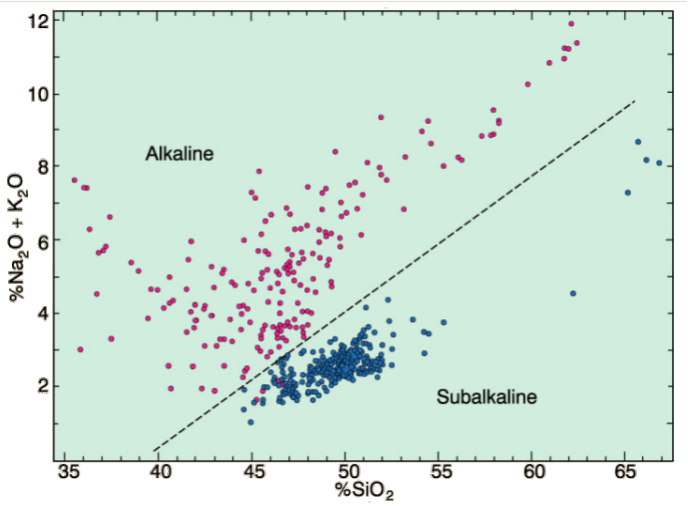

Figure 3.9: *Total alkalis versus silica diagram illustrating the alkaline and subalkaline magma series. Figure from MacDonald (1968), modified by (Winter, 2013).*

3.2.3 Trace elements

Trace elements are those elements that constitute <0.1 wt.% of the rock (Winter, 2013) and some of the most common trace elements used in whole-rock geochemistry are Barium (Ba), Cerium (Ce), Europium (Eu), Gallium (Ga), Lanthanide (La), Niobium (Nb) and Tantalum (Ta). There is also a defined group called minor elements which plots in between those two end-members and constitutes between 0.1 to 1.0 wt.% of the rock.

Element distribution is an important knowledge when it comes to trace elements and Goldschmidt (1937) summarizes this with a rule composed of three bullet points. The first one says *"Two ions with the same valence and radius should exchange easily and enter a solid solution in amounts equal to their overall proportions."* (Winter, 2013). The second rule says *"If two ions have a similar radius and the same valence: the smaller ion is preferentially incorporated into the solid over the liquid."* (Winter, 2013). The third and final rule says that *"If two ions have a similar radius, but different valence: the ion with the higher charge is preferentially incorporated into the solid over the liquid."* (Winter, 2013). This divides the trace elements into incompatible and compatible elements, the latter ones preferring to stay in the solid. The incompatible elements can be subdivided into high field strength elements (HFSE) and large-ion lithophile elements (LILE), the latter ones being more mobile if a fluid phase is present (Winter, 2013). The largest advantage

of trace elements compared to major elements is that they are more sensitive to variation in their crystal lattice, due to the differences in how incompatible they are and therefore tracks magmatic and metamorphic events better than major elements. The most common diagram used with trace elements is the chondrite-normalised spider diagram. This diagram shows the chondrite-normalised values of the rare earth elements (REE) which are all trace elements in most rocks, where the light-REE (less mobile in a hydrous phase: more incompatible) are plotted on the left-hand side with an increasing mobility and higher compatibility towards the heavy-REEs plotted on the right-hand side. An example of such a plot is shown in Figure 3.10. A second plot used for trace element is the primitive mantle spider diagram. And in the same way as the chondrite-normalised diagram, the primitive mantle normalised diagram is used to give an interpretation of what geological processes the rocks were derived from, as they are used to measure deviations from a primitive composition. A typical trend for subduction settings in a REE spider plot would be a high concentration of the LILE, negative Nb and Ta anomalies and low content of the HFSE. An example of a primitive mantle normalised plot is shown in Figure 3.11.

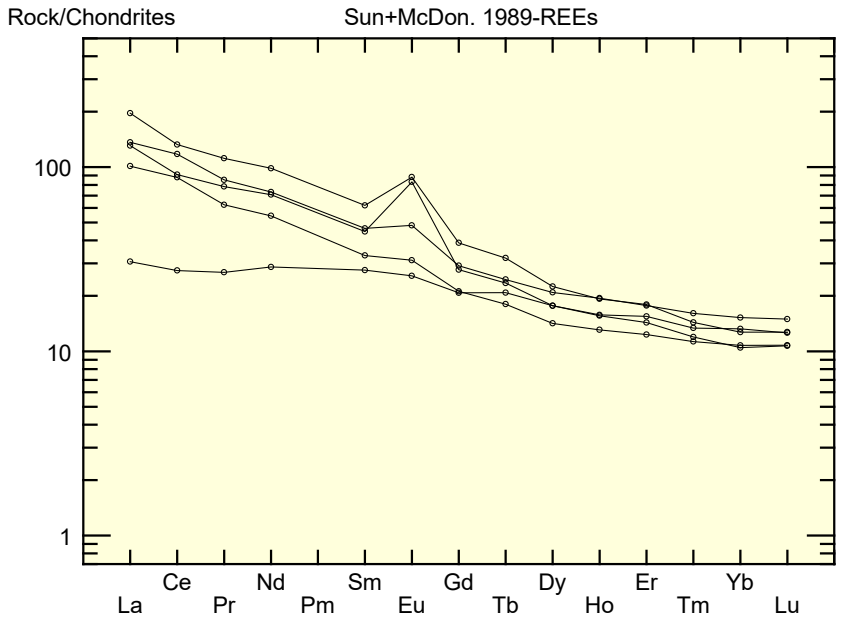

Figure 3.10: *REE-spider plot for geochemical analysis of trace elements. As this figure illustrates, some of the rocks shows a positive Eu anomaly. Meaning that the Eu concentration is enriched compared to other rare-earth elements. Since Eu tend to be incorporated in plagioclase this anomaly reflects crystallization and accumulation of plagioclase.*

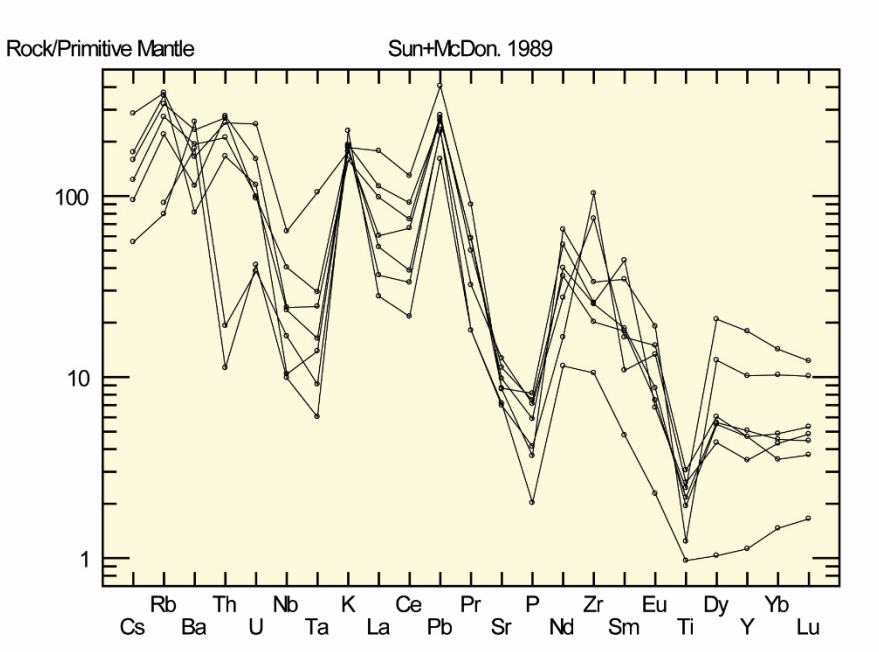

Figure 3.11: *REE-spider plot for geochemical analysis of trace elements. As this figure illustrates, it shows a negative anomaly for Nb-Ta and high values for the LILE and lower values for the HFSE. A typical trend for subduction settings.*

3.2.4 The Sm-Nd system

Sm-Nd isotopic data has been used to establish the magmatic evolution and magma sources in the in the study area. Samarium (Z=62) belongs to the light rare-earth elements (LREE). The LREE are a little larger in size and more incompatible in common silicate minerals than the heavy rare-earth elements (HREE) (Best, 2013). Out of its seven naturally occurring isotopes only the ^{147}Sm isotope has a short enough half-life to make it feasible to measure the variations in the abundance of the daughter isotope ^{143}Nd. The half-life is found to be 1.06x10^^{11} years , which gives a decay constant (λ) of 6.54x10^{-12}yr^{-1} (Faure and Mensing, 2005) and this is the basis of the Sm-Nd method. The decay of ^{147}Sm is shown in the equation 6 below, where $^{4}_{2}He$ is an α-particle and E is the energy released during the decay (Faure and Mensing, 2005).

$$^{147}_{62}Sm \rightarrow {}^{143}_{60}Nd + {}^{4}_{2}He + E \qquad \text{Eq. 6}$$

The composition of the Nd isotopes is expressed with the ^{143}Nd/^{144}Nd ratio (where ^{144}Nd is the non-radiogenic isotope). From equation 7 it is noticeable that the composition is dependent on the ^{147}Sm isotope and the decay constant (Faure and Mensing, 2005).

$$\frac{^{143}Nd}{^{144}Nd} = \left(\frac{^{143}Nd}{^{144}Nd}\right) I + \frac{^{147}Sm}{^{144}Nd}(e^{\lambda t} - 1) \qquad \text{Eq. 7}$$

Neodymium is also a LREE, but it has an atomic number that is lower (Z=60) than for Sm and will therefore tend to be more incompatible than Sm. From this it is found that the Sm/Nd ratio is lower in the continental crust than in the mantle. Even though the chemical properties of the Sm/Nd system are very similar, their benefit versus the rubidium (Rb)/ strontium (Sr) system is that they are more immobile and therefore more resistant to post crystallisation disturbances. The ^{143}Nd/^{144}Nd ratio is often given as an epsilon notation as

the isotope values are very small, this notation was used for this study. The equation for epsilon neodymium is shown below in equation 8, where ($^{143}Nd/^{144}Nd$) sample(t) is the isotope ratio calculated at the time of formation (t), whilst ($^{143}Nd/^{144}Nd$) CHUR(t) is the isotope ratio of the chondritic uniform reservoir at time *t*.

$$\varepsilon_{Nd} = \left[\frac{\left(\frac{^{143}Nd}{^{144}Nd}\right)_{sample(t)}}{\left(\frac{^{143}Nd}{^{144}Nd}\right)_{CHUR(t)}} - 1 \right] x\ 10\,000 \qquad \text{Eq. 8}$$

Based on the dependency of samarium in the neodymium ratio and how the two LREE are fractionated between liquids and solids, an evolution diagram to characterize the involvement of crust and mantle in melts of rocks has been constructed by geochemists. Neodymium is more incompatible than samarium, meaning that it prefers to stay in the melt as it doesn't fit as well as samarium into different crystal lattices. This imply that as the melt moves upwards from the mantle and into the crust the concentration of Nd in the melt will increase relatively to the concentration of Sm (crystallizes out of the melt). This will cause the melt to get a lower Sm/Nd ratio when it reaches the surface. The opposite case applies for the mantle where the mantle gets depleted in Nd and therefore create a higher Sm/Nd ratio. Figure 3.12 shows how the $^{143}Nd/^{144}Nd$ ratio evolves through time. As ^{143}Nd prefer to stay in the melt over crystallization as the melt moves towards the surface, it will result in a higher production of the ^{144}Nd isotope and the evolution line of the Nd ratio in the continental crust will therefore have a slacker line than the depleted mantle. And this is because the concentration of ^{143}Nd in the melt is lower in the mantle resulting in less production of the ^{144}Nd isotope, resulting in a steeper slope as the ratio increases. The depleted mantle melt would be expected to consist of a larger part of mafic to ultramafic, dense minerals. Such a melt should also show a Sm/Nd ratio that is higher than for a crustal melt, as Nd is more incompatible than Sm. This means that a melt that travels from the mantle ascending to form crust will cause the mantle to be depleted in both of these elements, including other incompatible elements. As time goes by the crust will be enriched in the incompatible elements, in particular the more incompatible Nd.

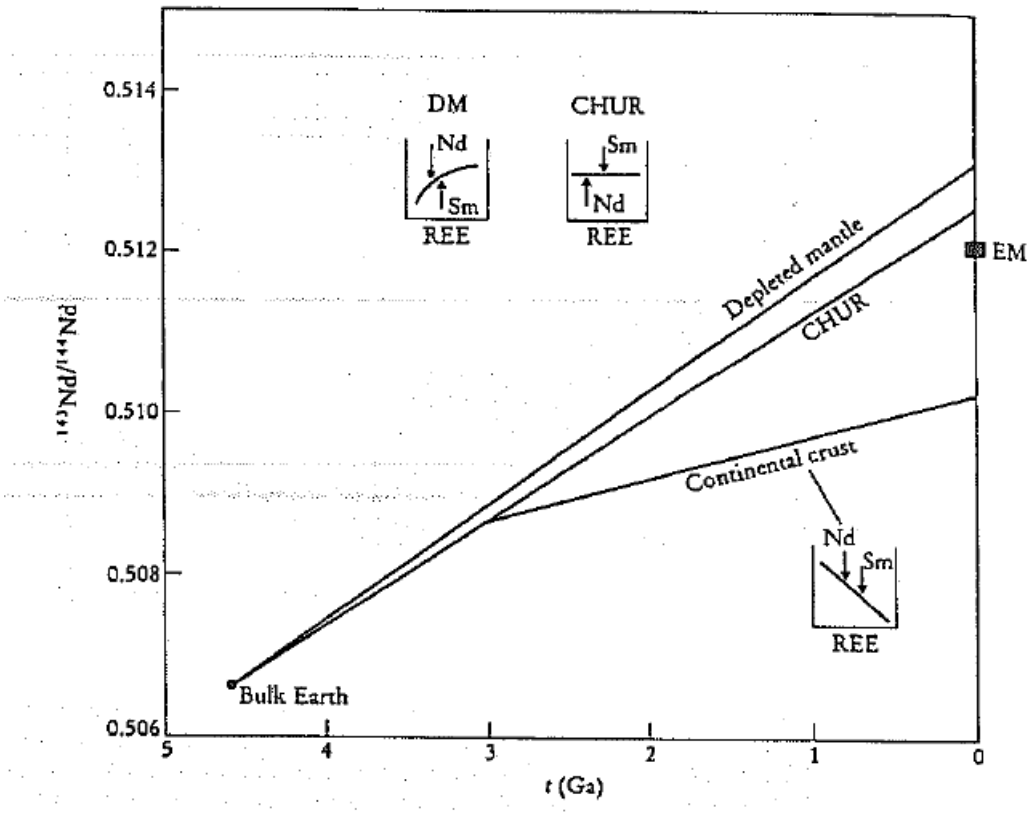

Figure 3.12: *The evolution of 143Nd/144Nd isotopes with time in the mantle, the continental crust and the bulk earth (CHUR). Relative to the bulk Earth in which the fractionation of Sm/Nd is normalized to unity, the depleted mantle (DM) has a high Sm/Nd ratio and shows higher evolution with time. Enriched mantle (EM) shows some affinity with the continental crust in as much as it also has retarded 143Nd/144Nd evolution. After (Rollinson, 2014).*

Sm-Nd data can also be used to model the approximate weighting contribution of depleted mantle and crust in the magma that the rocks crystallized from, if the protolith and the event of the magma formation is known. To do this one has to put in the $^{143}Nd/^{144}Nd$ data for the samples and set an end-member for both crust and mantle and rank them from 0% crust and 100% mantle to 100% crust and 0% mantle. By using the average $^{143}Nd/^{144}Nd$ data from the sample data set and the $^{143}Nd/^{144}Nd$ chondritic value and lambda Sm value, the mixing between the two end-members can be calculated by Equation 9:

$$Nd_{mix} = \frac{X_{DM} \times C_{DM} \times (\frac{^{143}Nd}{^{144}Nd}) + X_C \times C_C \times (\frac{^{143}Nd}{^{144}Nd})}{(X_{DM} \times C_{DM} + X_C \times C_C)} \quad \text{Eq. 9}$$

The ε_{Nd} mixing value is then found by equation 10.

$$\varepsilon_{NdMix} = \left[\frac{Nd_{mix} - (\frac{^{143}Nd}{^{144}Nd})_{CHUR}}{(\frac{^{143}Nd}{^{144}Nd})_{CHUR}} - 1 \right] \times 10^4 \quad \text{Eq. 10}$$

The ε_{Nd} value can then be plotted against the percentage of crust or percentage of mantle to see how large the contribution of the two sources are. This is illustrated in Figure 3.13.

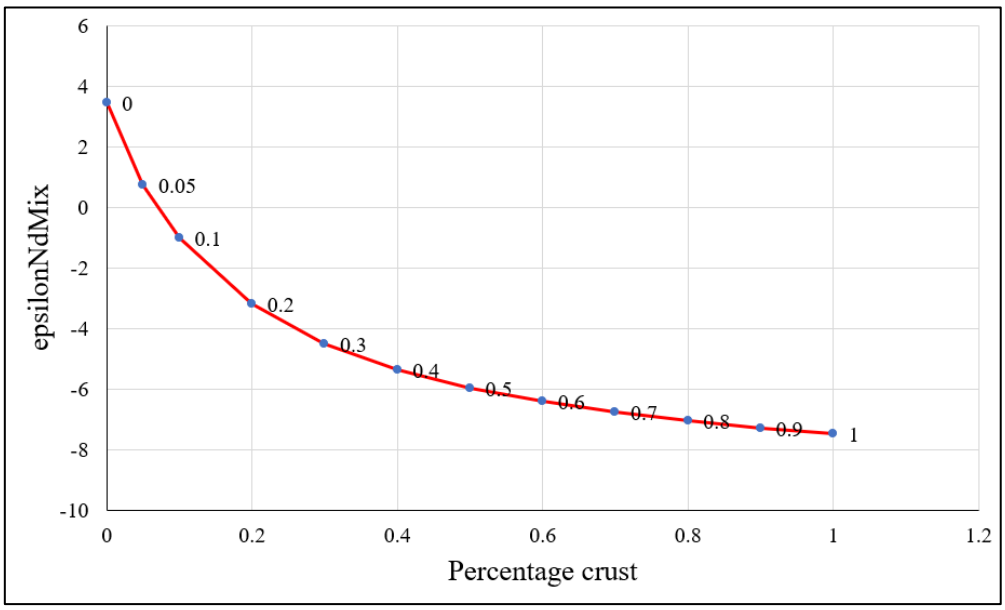

Figure 3.13: *The epsilon Nd-mix diagram is constructed to illustrate the proportion of crust or mantle that is reflected by the epsilon Nd-mix value.*

Figure 3.13 shows that with just 0.05% contamination of crust in the melt the ε_{NdMix} sinks drastically towards the negative epsilon values. This model can therefore be an important tool in the study of melt composition.

3.2.5 The Lu-Hf system

The Lu-Hf isotope system has mostly the same applications as the Sm-Nd system. Lutetium (Lu) is the last element of the rare-earth-element group, belonging to the heavy-rare-earth-elements (HREE) with an atomic number (Z) of 71. Hafnium (Hf) has an atomic number (Z) of 72 and the two elements share a similar electron configuration. Even though the atomic number of Lu is high, its ionic radius of 0.93Å is the smallest in the REE group (Faure and Mensing, 2005). The cation Lu^{3+} has nearly the same ionic radius as the cation Ca^{2+}(0.99Å) and can therefore function as a substitute for its crystal place (Faure and Mensing, 2005). Hf^{4+} has an ionic radius of 0.81Å which is very close to the ionic radius of the cation of zirconium Zr^{4+} (0.80Å), Hf is hence often found in Zr-bearing minerals such as zircon (Faure and Mensing, 2005). Lu has two naturally occurring isotopes, namely ^{175}Lu and ^{176}Lu where the latter is radioactive and decays to either stable ^{176}Hf by beta emission or stable ^{176}Yb by electron capture (Faure and Mensing, 2005). The two possible processes are shown in equations 11-12, where E is the energy released during the decay.

$$^{176}_{71}Lu \rightarrow {}^{176}_{72}Hf + E \qquad \text{Eq. 11}$$

$$^{176}_{71}Lu + E \rightarrow {}^{176}_{70}Yb \qquad \text{Eq. 12}$$

In this study the Lu-Hf system has been used as an application to understand the petrogenesis and source(s) of the rocks, by trying to estimate the influence of continental crust and depleted mantle of the magma that the zircons of the rocks were crystallizing from. Lu can be compared to Sm in the Sm-Nd system as it prefers to fractionate out of a melt and corporate into the solid. Hafnium is enriched in the melt meaning that the Lu/Hf ratio will be highest in a depleted mantle source. Because the ratio between ^{176}Hf and ^{177}Hf is minor, it is preferable to use the epsilon-notation for Hf here as well. As for Nd there has been constructed a Hf evolution plot with ε_{Hf} plotted against the age of the rocks to see what the melt that the rocks crystallized from consisted of. The equation to calculate the ε_{Hf} value is found in equation 13-15 where the ^{176}Hf/^{177}Hf values from the sample are divided with the ^{176}Hf/^{177}Hf CHUR values.

$$\left(\frac{^{176}Hf}{^{177}Hf}\right)i_{CHUR} = \left(\frac{^{176}Lu}{^{177}Hf}\right)_{CHUR} - \left(\frac{^{176}Hf}{^{177}Hf}\right)_{CHUR} \times (e^{\lambda t} - 1) \qquad \text{Eq. 13}$$

$$\left(\frac{^{176}_{72}Hf}{^{177}Hf}\right)i_{sample} = \left(\frac{^{176}_{72}Hf}{^{177}Hf}\right)_{sample} - \left(\frac{^{176}_{71}Lu}{^{177}Hf}\right)_{sample} \times (e^{\lambda t} - 1) \qquad \text{Eq. 14}$$

$$\varepsilon_{Hf_i} = \left[\frac{\left(\frac{^{176}Hf}{^{177}Hf}\right)sample}{\left(\frac{^{176}Hf}{^{177}Hf}\right)CHUR} - 1\right] \times 10^4 \qquad \text{Eq. 15}$$

The values of the epsilon Hf gives an indication of how isotopically evolved the magma that the rocks crystallized from were when the zircons with the Hf formed. Positive epsilon values on the evolution plot would indicate a high content of ^{176}Hf in the sample compared to chondritic conditions, the opposite apply to negative epsilon values. This implies the interpretation that if the magma came directly from the mantle it would give very positive values, whilst if the source was more evolved continental crust it would result in more negative values. The typical ε_{Hf} evolution plot was also used for this study and is shown in Figure 3.14.

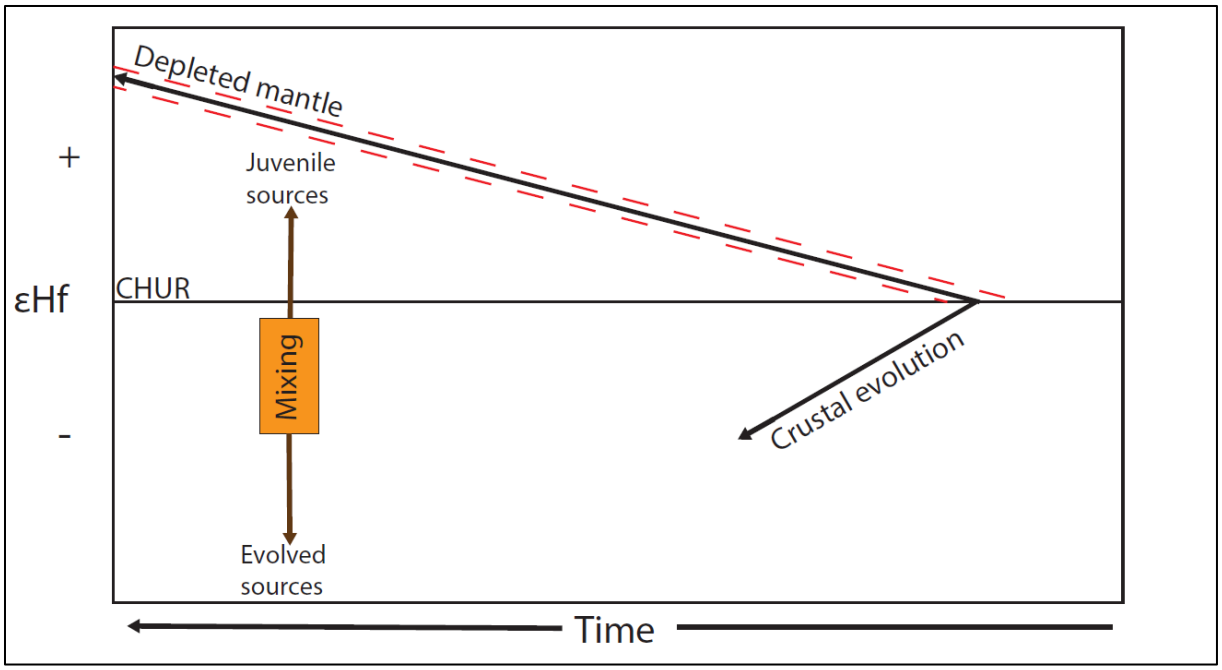

Figure 3.14: *Epsilon Hf evolution plot, illustrating how the $^{176}Hf/^{177}Hf$ ratio evolves over time in a depleted mantle and crustal magma.*

As Figure 3.14 shows, a positive εHf value indicates a melt composition from a juvenile source, whereas a negative εHf value indicates a melt composition from a more evolved source with crustal material. Depending on where the samples plot they are to some degree a mix with magma from both depleted mantle and crust.

4 Methods

The methods that were used for this study are briefly introduced and discussed in this chapter. Mapping of the field area was the first step, where the aim was a study of the geology, record the different geological units and their relationship and collect samples for thin-sections, geochronology and geochemistry.

4.1 Fieldwork preparation and mapping

A total of approximately 60 days were spent in the field mapping out the area of the five islands Grytøya, Sandsøya, Bjarkøya, Krøttøya and Meløyvær. The field area is located within the central to southern part of the West-Troms Basement Complex (WTBC) and covers about 194 km^2 in total. The fieldwork was carried out both digitally and on paper. A larger overview map was printed out, together with several smaller maps (A3 size) giving an appropriate scale of 1:200 000 to carry in the field. The paper maps were provided with a scale, elevation levels and colours to indicate vegetation, outcrops, lakes and settlement. To note down the exact position of the outcrops, a windows tablet with the software ArcPad v.10.2 was used with an integrated map with UTM coordinates. The tablet was also used to register geological measurements such as strike and dip on bedding, foliations, dykes, measured with a handheld compass. In addition, an iPad was carried around to measure the heading of the field photos.

In field, an A3 map with scale, contour lines and colours of vegetation, outcrops, lakes and settlement were carried around together with crayons. The Windows Surface Tablet was used to find the exact position for the drawing of the outcrops and geological measurements on the map. The size of the colouring of the map reflects the size of the outcrop or geological features such as dykes.

4.2 Sampling

A total of 49 samples were collected during the field season of 2016 and 2018. The 17 samples collected during the summer of 2016 were sent to the Geological Survey of Norway's lab, where major- and trace elements and Sm-Nd isotopes were measured. Sm-Nd isotopes were carried out for only 8 of the 17 samples, whilst major- and trace elements were carried out for 16 of the 17 samples. The samples were also used to make 19 thin sections representing five granitic samples, three gabbroic samples, two quartz dioritic samples, two amphibolitic samples, a syenite and monzonite sample taken from Grytøya and Krøttøya. During the field season of 2018 the remaining 31 samples were collected, both from the previous sampled Grytøya and Krøttøya- and from Bjarkøya and Sandsøya. These 31 samples include nine granitic samples, four amphibolitic samples, four quarzitic samples, three gneissic samples, two calc-silicate samples, two aplitic dyke samples, one mafic xenolith, one marble and one meta-gabbro sample. Major- and trace elements were carried out for 27 of 31 samples and thin-sections were made from 21 samples. For a complete list of all samples, see Table 5.1.

4.3 Sample preparation

A major part of the thesis comprises the preparation of the samples that were collected. A schematic overview of the different preparation operations that were performed, together with their purposes are show in Figure 4.1.

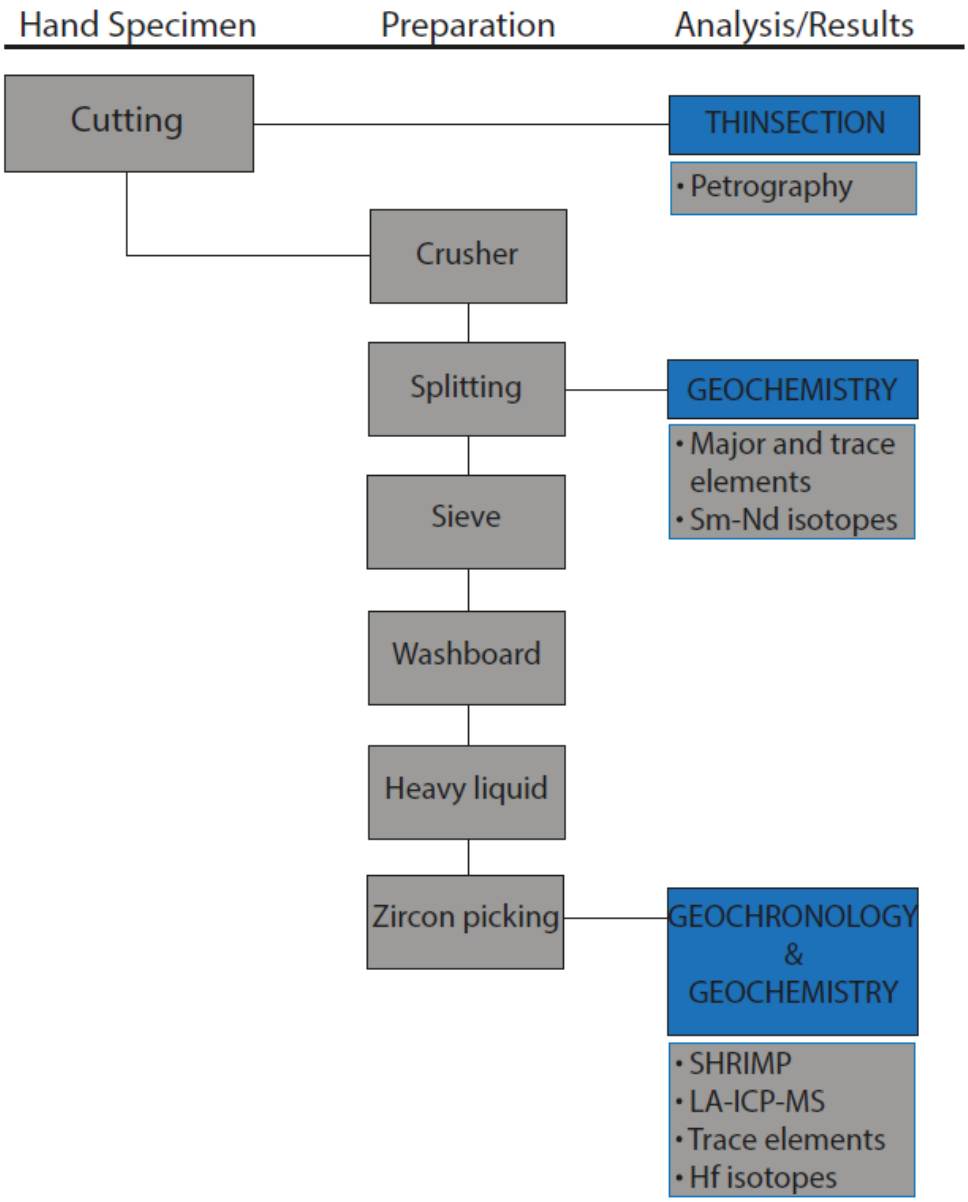

Figure 4.1: *Schematic illustration of the workflow during sample preparation. It starts with a single collected hand specimen that is first cut, then the following procedures branch the sample into two. One part of the sample goes to thin section preparation whilst the other half proceeds to a crusher and splitting for geochemical analyses, and a third part of this sample proceeds through sieving, washboard, heavy liquids to end up at the process of zircon picking to get geochronology of the sample and geochemistry of the zircons.*

4.4 Thin sections

All 17 samples collected during the field season of 2016 were prepared by the thin section laboratory at the Geological Survey of Norway (NGU) into 28x48 mm, 30µm-thick thin sections. 21 samples collected during the field season of 2018 were prepared and polished by the thin section laboratory at the Department of Geology and Mineral Resources Engineering at the Norwegian University of Science and Technology (NTNU) with the same size and thickness. 11 of the thin-sections prepared at NTNU were polished.

Petrography

The thin sections made for this study were examined under a microscope for mineral- and rock texture identification, together with determination of magmatic and metamorphic influence on the rocks. Microphotographs of interesting features found in the thin sections were captured with a Leica binocular polarizing microscope with a built-in camera. All thin section descriptions are found in the Appendix C.

4.5 Geochemical analysis

Mineral chemistry analysis to gain major- and trace elements, and Sm-Nd isotopes were achieved by X-Ray Fluorescence (XRF) by the lab at the Geological Survey of Norway (NGU), Trondheim for the samples collected in 2016. The samples collected in 2018 were sent to ALS Chemex for whole-rock geochemistry including major- and trace elements analysis, the procedure which these analyses are performed with are found in their web brochure that can be downloaded for free at www.alsglobal.com under the code name of ME-MS81d. The samples that were shipped to ALS Chemex for bulk-rock major- and trace element analyses underwent a method noted PREP-31Y and ME-MS81d.

PREP-31Y

According to their brochure this means that the samples are logged and weighed on their entrance to the laboratory before they are crushed with a crusher in combination with a rotary splitter. 70% of the sample is crushed to a size that pass through a 2 mm sieve, then it is split and pulverized until 85% passes through a 75µm sieve and then the samples are forwarded to the next labs to get respectively REE and trace elements, and whole-rock geochemistry.

ME-MS81d

ME-MS81d is described to consist of a combination of Rare-Earth Elements (REE) and Trace Elements from method ME-MS81, in addition to a whole-rock package by the method of ME-ICP06. The process starts with a sample that has been crushed down to a powder that is added to a lithium-borate mixture. This mixture is then heated up until it melts, followed by a cooling of the mixture forming a glass. This glass is then exposed to an acid so that the glass dissolves and leave unattached minerals ready for measuring. This procedure is performed to dissolve minerals that are attached to each other, such that all minerals will be measured.

4.6 Geochronological analysis

Crushing and sieving

The crushing, sieving, washing and heavy liquid separation of the samples were executed at the Mineral Processing Lab at the Geological Survey of Norway, the full process from hand specimen to petrography, geochemistry and geochronology can be viewed in Figure 4.1. The first step was to cut the samples with a diamond saw to make hand specimens that were stored for each sample and then sliced to thinner slabs that could be processed into thin sections at the Department of Geology and Mineral Resources at NTNU. The diamond saw was also used to remove weathered surfaces and to cut the remainder of the samples into pieces that could fit into the crusher. The second step was performed at the crusher, where the size of the samples was reduced from several centimetres to pebbles with a varying grain size <0.5 cm. The two first steps include splitting of the sample, where 175-200g were put in a container for storage at Løkken and 35-40 g were put in a container ready to be shipped to ALS Chemex for whole-rock major- and trace element analysis.

Water table, heavy liquid separation, mounting, mapping and coating

The residual of the samples after splitting went to the process of sieving (see Figure 4.1). The samples, individually, were put in a sieve with three levels of mesh size, at <1000 µm, <500 µm and <250 µm. Only the smallest fraction was pursued to the next step, the water table. The water table works in a way that vibration and continuing water flow provide for a sorting between grains that have a light and heavy density, where the zircons belong in the latter category. That way, the zircons can be extracted from the rest of the minerals in the crushed samples. In the following step the zircons were sorted out from the denser magnetic minerals as iron oxides and garnets. This was done by using a vertical and horizontal Frantz, where in both cases a magnet is used to perform the partition of zircons based on magnetism. After these four steps was performed, the last step of the preparation process was to use a heavy liquid to sort out the zircons from the remaining minerals that have a lower density than 3.3 g/cm^3. The technique required a safe lab where the work was done under fume cupboards. The sample was filtrated through a heavy liquid to split the minerals that are heavier than 3.3 g/cm^3 from the lighter ones and by that get rid of other minerals than zircons in the sample, which makes the zircons easier to pick. The grains extracted from the heavy liquid separation were brought in round plastic cups and transferred into the microscopy lab. Under the microscope the samples were put in alcohol and the zircons were picked out based on their light refraction and shape with a pair of tweezers and placed on a piece of double-sided tape. The samples were put within a circle with a radius of 2 cm, so that a circular plastic mould could be put on to limit and form a block consisting of epoxy and the zircons. This block was then put on a desk overnight to harden and then polished to expose the centres of the zircon grains. This process was executed for both samples going to the LA-ICP-MS and SHRIMP-analysis.

Before the samples were sent into the sensitive high-resolution ion probe (SHRIMP), they were properly cleaned and coated with gold. The cleaning was done to prevent any common lead and other sources of contamination into the chamber of the ion probe. This process included wiping of the samples with petroleum spirit, propanol, soap, with an ultrasonic bath in between each of the baths in the liquids. After this, the samples were put in an oven that held a temperature of 60°C, to dry. For this study, the samples were kept in the

oven for several hours. Then they were taken out and placed into a gold coater for coating to avoid charging during analysis.

Scanning Electron Microscope (SEM)

The SEM work was performed at NGU on a 1450 Variable Pressure (VP)
SEM produced by LEO Electron Microscopy Ltd. The SEM had an X-ray analytical system with an accompanying INCA software (v.4.09). The SEM was used for mapping purposes and to check whether the zircon mounts were successfully polished (meaning that the surface of the zircons were not covered by epoxy). The mapping was performed with an electron beam of 15kV and a working distance of 20 to 22mm. Both backscattered electron (BSE) images and cathodoluminescence (CL) were carried out and stitched together in the INCA software for a complete image of the sample. These images were then investigated as part of the preparation for the geochronological- and geochemical analysis. BSE images were studied with an objective to spot cracks and voids, whilst the CL images were studied with an objective to observe and describe internal textures in the zircons. Both images make it easier to know which grains that should be aimed at in the laser sessions and after the shooting, to orientate where the spot hit. And this is important information when interpreting the results from U-Pb dating, zircon trace elements and isotopes.

SHRIMP

U-Pb zircon geochronology was performed using a Sensitive High-Resolution Ion Microprobe at the University of Curtin, Perth, Australia. The zircons that were picked for this analysis were put on a mount together with two standards, namely 91500 and Temora. The 91500 standard yields an age of 1065 Ma (Wiedenbeck et al., 1995) and the Temora standard yields an $^{238}U/^{206}Pb$ age of 416.8 Ma (Black et al., 2004). After the coating with gold, the mount was loaded into the sample chamber of the SHRIMP II 48 hours before the analytic session. The operational procedure for uranium, thorium and lead for zircons was set by Professor Chris Kirkland, from the setup described by Compston et al. (1984) and Claouè-Long et al. (1995) with modifications by Williams (1998). The zircons were aimed at with a primary beam consisting of O_2^- ions adjusted to form a spot size of 28µm. To get accurate data, the standards were analysed at every 6^{th} grain of the unknown zircons.

LA-ICP-MS

Uranium (U)-, Lead (Pb)-, and Hafnium (Hf) isotopes and trace elements in zircons for geochronological purpose were analysed using a Resonetics Resolution M-50A coupled to a Nu Plasma II multi-collector inductively coupled plasma mass spectrometer (MC-ICPMS) and an Agilent 7700 quadrupole inductively coupled plasma mass spectrometer (Q-ICP-MS) at the University of Curtin, Perth, Australia. The laser ablation split stream was configured and operated by professors Noreen Evans and Bradley McDonald, with the author being responsible for the selection of spots. The standard reference material used for these analyses were 91500 (1062.4 ± 0.4 Ma; Wiedenbeck et al., 1995) and OG1 (3465.4 ± 0.6 Ma; Stern et al., 2009) with Plesovice (337.13 ± 0.37 Ma; Sláma et al., 2008) and GJ-1 (608.53 ± 0.37 Ma; Jackson et al., 2004) analysed as secondary age

standards. $^{206}Pb/^{238}U$ ages and $^{207}Pb/^{206}Pb$ were calculated for zircon age standards by the operators and were found to be within 3% of the accepted value.

4.6.1 Zircon U-Pb dating

As previous described, the zircons were separated by the standard techniques including water table, heavy liquids, magnetic separation and hand picking under a binocular microscope. The zircons were mounted in epoxy and polished to approximately half the thickness. The zircons were mapped with backscattered electrons (BSE) images and cathodoluminescence (CL) images obtained from a scanning electron microscope (SEM) to reveal any voids or internal textures. The U-Pb geochronology analyses were performed on the SHRIMP II at the John de Laeter Centre at Curtin University, Perth. Operating procedures for uranium, thorium, and lead isotopic measurements on zircon are based on those described by Compston et al. (1984) and Claoué-Long et al. (1995), with modifications by Williams (1998). A 30 μm diameter primary beam of O2− ions at 10 keV, purified by means of a Wien filter, was employed to sputter secondary ions from the surface of each target mineral. The net primary ion current was typically between 1.5 and 2.1 nA. Secondary ions were accelerated to 10 keV, energy-filtered by passage through a cylindrical 85° electrostatic analyser with a turning radius of 1.27 m, and mass-filtered using a 72.5° magnet sector with a turning radius of 1 m. Secondary ions were counted by switching the magnetic field to direct the secondary ion beam of interest into an electron multiplier, used in pulse-counting mode. During the analytical session, the secondary ion analyser was set to a mass resolution of ≥5000 (1% peak-height definition), which is sufficient to resolve lead isotopes from most potential molecular interferences. The magnetic field was cycled several times to select isotopic masses in the following sequence: 196 (species [90Zr216O]+), 204 (204Pb+), 204.1 (background), 206 (206Pb+), 207 (207Pb+), 208 (208Pb+), 238 (238U+), 248 ([232Th16O]+), and 254 ([238U16O]+).

LA-ICP-MS analyses were also conducted at the John de Laeter Centre at Curtin University on a Resonetics resolution M-50A incorporating a Compex 102 excimer laser ablation split stream and an Agilent 7700 quadrupole inductively coupled plasma mass spectrometer (Q-ICP-MS). Following two cleaning pulses and a 40s period of background analysis, samples were spot ablated for 40 s at a 10Hz repetition rate using a 50 μm beam and laser energy at the sample surface of 2.2 J cm-2. An additional 15s of baseline was collected after ablation. The sample cell was flushed with ultrahigh purity He (320 mL min-1) and N2 (1.2 mL min-1) and high purity Ar was employed as the plasma carrier gas, split to each mass spectrometer.

4.6.2 Zircon trace elements

For the trace element analyses, the following elements were monitored for 0.01 s each: ^{28}Si, ^{31}P, ^{44}Ca, ^{49}Ti (0.05 s dwell), ^{89}Y, ^{90}Zr, ^{139}La, ^{140}Ce, ^{141}Pr, ^{146}Nd, ^{147}Sm, ^{153}Eu, ^{157}Gd, ^{159}Tb, ^{163}Dy, ^{166}Er, ^{172}Yb, ^{175}Lu, ^{201}Hg, ^{204}Pb, ^{206}Pb, ^{207}Pb, ^{208}Pb (0.1 s dwell time on all Pb isotopes), ^{232}Th (0.025 s dwell time), and ^{238}U (0.025 s dwell time). International glass standard NIST 610 and reference zircon GJ-1 were used as primary standards to calculate elemental concentrations and to correct for instrument drift (using ^{29}Si and ^{90}Zr as the internal standard elements, respectively and assuming 14.26% Si and 43.14% Zr in the zircon unknowns). NIST 610 was the primary reference material for P, Ca, Zr, Pb, Th and U determination, while GJ-1 was the primary reference material for Ti, Y, La, Ce, Pr, Nd, Sm, Eu, Gd, Tb, Dy, Er, Yb and Lu. NIST 614 was treated as a secondary standard for trace

element determination with most elements reproducing within 5% of the recommended value.

4.6.3 Hafnium isotopes

The Hf isotopes were measured in the same operation as the U-Pb age, with a spot size of 50 µm and a laser energy of 2.8-3.0 J/cm^2. In addition to the Resonetics Resolution M-50A, a Nu Plasma II multi-collector inductively coupled plasma mass spectrometer (MU-ICPMS) were used. All isotopes (^{180}Hf, ^{179}Hf, ^{178}Hf, ^{177}Hf, ^{176}Hf, ^{175}Lu, ^{174}Hf, ^{173}Yb, ^{172}Yb and ^{171}Yb) were counted on the Faraday collector array. According to the instruction papers from the lab the time resolved data was baseline subtracted and reduced using Iolite (DRS after (Woodhead et al., 2004)), where ^{176}Yb and ^{176}Lu were removed from the 176-mass signal using ^{176}Yb/^{173}Yb = 0.7962 (Chu et al., 2002) and ^{176}Lu/^{175}Lu = 0.02655 (Chu et al., 2002) with an exponential law mass bias correction assuming ^{172}Yb/^{173}Yb = 1.35274 (Chu et al., 2002). The interference corrected ^{176}Hf/^{177}Hf was normalized to ^{179}Hf/^{177}Hf = 0.7325 (Patchett and Tatsumoto, 1980) for mass bias correction.

4.6.4 Data reduction

The U-Pb data and the Lu-Hf data were reduced with the add-in software Squid.xla and Isoplot.

4.7 Sources of error

Sample preparation

The largest probability of contamination was in the Mineral Processing Lab at the Norwegian Geological Survey. From the crushing sequence all the way through the heavy liquid separation and to the zircon picking under the microscope there exists a danger of contamination of the samples. Therefore, in all the labs, the rooms were cleaned after each sample were prepared. At the crushing room the crusher was stripped down and cleaned with compressed air, a vacuum cleaner and alcohol. The same procedure was used for the splitting and the sieving. In addition to this, the sieves were put in an ultrasonic bath for cleaning. At the water table all the equipment was washed with alcohol and the washboard itself was cleaned with a water hose and scrubbed with a brush to make sure no material from the previous sample was left. When the material for heavy liquid separation was put on the oven to dry, a paper was put on top of the bowl to avoid grains from jumping out or in. At the chemistry lab the lab equipment was cleaned with acetone under fume cupboards and water and alcohol after it was taken out from the fume cupboards. At the microscope lab the work space was cleaned with alcohol every time a new sample was examined under the microscope, and pipettes used for zircon transfer were thrown after use. These safety routines were followed strictly and the results from the analysis performed on the samples used for this study show no indications of contamination.

Samples sent to ALS Chemex

Some of the samples were sent to ALS Chemex, a global company that provides the industry with geochemical data. Their brochures describe the sample preparation methods that they use to ensure the clients that they can be trusted. The lab work is strictly

regulated, they have certifications and requirements of international standards. The results of their analysis also provide the client with a quality control certificate where the results are compared to standards. It would be hard to discover any contamination as there are not many samples from the area that has been studied.

LA-ICP-MS

The laser ablation split stream was used to carry out both U-Pb isotopes, trace elements and Hf-isotopes of the zircons. The strength of the signal that is demanded for these operations are different, with a lower signal required to measure the U-Pb isotopes and trace elements than for the Hf-isotopes. This could have an impact on the signal detection from the laser and result in the finalized data. Some of the trace elements appear as not detectable and this could possibly be due to a too low signal when the trace elements were measured. Another aspect is the aiming of the laser. Some of the ages received from the dating could be disturbed if the laser spot hit outside the grain and into the epoxy. However, this error in the dating would not be caused by contamination from other samples and can in most cases be revealed by studying the zircon grains after the laser analysis.

5 Results

The results from the study area are presented in this section and comprises detailed descriptions of geochronology, geochemistry and petrography of the samples collected at the four islands of Grytøya, Sandsøya, Bjarkøya and Krøttøya. A thorough geological mapping of the field area combined with lab results were performed in order to be able to understand and interpret the field observations. Two samples from Raftsundet were also dated to place the samples from the field area on a regional scale. A geological map with the exact location of the collected samples is provided in Figure 5.1. The geochronological analyses were performed on zircons. Mineral abbreviations used for thin section descriptions are listed in Table 5.1. A map showing all localities and geological measurements are found in Appendix A, together with detailed thin-section descriptions in Appendix D.

Mineral	Abbreviation	Formula
Apatite	Ap	$Ca_5(PO_4)_3(F,Cl,OH)$
Allanite	All	$(Ce,Ca,Y,La)_2(Al,Fe)_3(SiO_4)_3(OH)$
Biotite	Bt	$K(Mg,Fe)_3(AlSi_3O_{10})(F,OH)_2$
Calcite	Cal	$CaCo_3$
Chlorite	Chl	$(Mg,Fe)_5Al[Al,Si_3O_{10}](OH)_8$
Clinopyroxene	Cpx	$XY(Si,Al)_2O_6$
Diopside	Di	$MgCaSi_2O_6$
Epidote	Ep	$Ca_2Al_2Fe[Si_2O_7]O(OH)$
Fayalite	Fay	Fe_2SiO_4
Garnet	Grt	$X_3Y_2(SiO_4)_3$
Hornblende	Hbl	$Ca_2(Mg,Fe,Al)_5(Al,Si)_8O_{22}(OH)_2$
K-feldspar	Kfs	$KAlSi_3O_8$
Muscovite	Ms	$KAl_2(AlSi_3O_{10})(OH)_2$
Olivine	Ol	$(Mg,Fe)_2SiO_4$
Omphacite	Omph	$(Ca,Na)(Mg,Fe_2,Al)Si_2O_6$
Opaque	Opq	
Orthopyroxene	Opx	$XY(Si,Al)_2O_6$
Pigeonite	Pgt	$(Ca,Mg,Fe)(Mg,Fe)Si_2O6$
Plagioclase	Plag	$NaAlSi_3O_8 – CaAl_2Si_2O_8$
Quartz	Qtz	SiO_2
Serpentine	Ser	$(Mg,Fe,Ni)_3Si_2O_5(OH)$
Titanite	Tit	$CaTiSiO_5$
Zircon	Zr	$ZrSiO_4$

Table 5.1: *Minerals found in the samples of the field area, with accompanying abbreviation and chemical formulas.*

A total of 51 samples have been examined for this thesis. 49 of them were collected from the study area, whilst two of the samples were collected at Raftsundet by researcher Peter Ihlen. All the samples from the field area are listed in Table 5.2, with information regarding sample number, locality, map sheet, east and north coordinates and rock type.

Sample nr.	Locality	Map sheet	East	North	Rock type
90328	245	33	560294	7663987	Meta-sediment
90329	245	33	560294	7663987	Skarn
90330	245	33	560294	7663987	Magnetite
90331	249	33	560352	7663246	Gabbro
90332	211	33	560717	7662441	Diorite
90333	211	33	560717	7662441	Mafic dyke
90334	263	33	560817	7660935	Granodiorite
90335	197	33	561365	7660783	Granite/Granodiorite
90336	61	33	564522	7648977	Granite
90337	269	33	564711	7645119	Granite
90338	60	33	563190	7641422	Granite
90339	43	33	559790	7642011	Granite
90340	42	33	559106	7641943	Quartz diorite
90341	41	33	559129	7641938	Granite
90342	38	33	557309	7642999	Granite
90343	53	33	556985	7643896	Mafic xenolith
90344	33	33	554311	7647535	Amphibolite
90345	21	33	550784	7652662	Meta-gabbro
140808	1	33	559084	7653079	Granite
140809	2	33	562561	7655107	Mafic xenolith
140810	2	33	562561	7655107	Granite
140811	3	33	558745	7655904	Calc-silicate
140812	4	33	558741	7655949	Calc-silicate
140813	5	33	558752	7655999	Gneiss
140814	6	33	558776	7655998	Gneiss
140815	8	33	561538	7656825	Granodioritic dyke
140816	9	33	562257	7653504	Granite
140817	10	33	560453	7663241	Meta-sandstone
140818	13	33	567049	7650943	Granite
140819	15	33	567447	7651542	Supracrustal
140820	20	33	551209	7653232	Granite
140821	22	33	550815	7652714	Aplitic dyke
140822	40	33	558261	7642478	Amphibolite
140823	271	33	565074	7644207	Plagioclase vein
140824	180	33	560268	7657316	Amphibolite
140825	176	33	558878	7656243	Gneiss
140826	187	33	560642	7657287	Granodiorite
140827	68	33	556057	7645699	Granite
140828	69	33	555842	7645987	Granite
140829	135	33	560606	7657491	Amphibolite
140830	164	33	564874	7646897	Meta-sandstone
140831	109	33	561497	7656765	Amphibolite
140832	132	33	561558	7657330	Granite
140833	129	33	561315	7657407	Granite
140834	115	33	561731	7657015	Quartzite
140835	247	33	560310	7663641	Amphibolite
140836	218	33	560310	7663641	Quartzite
140837	218	33	560570	7663125	Quartzite
140838	12	33	560538	7661642	Granite

Table 5.2: *A list of all the samples collected from the field area of Grytøya, Bjarkøya, Sandsøya and Krøttøya, with locality, east and north coordinates and rock type.*

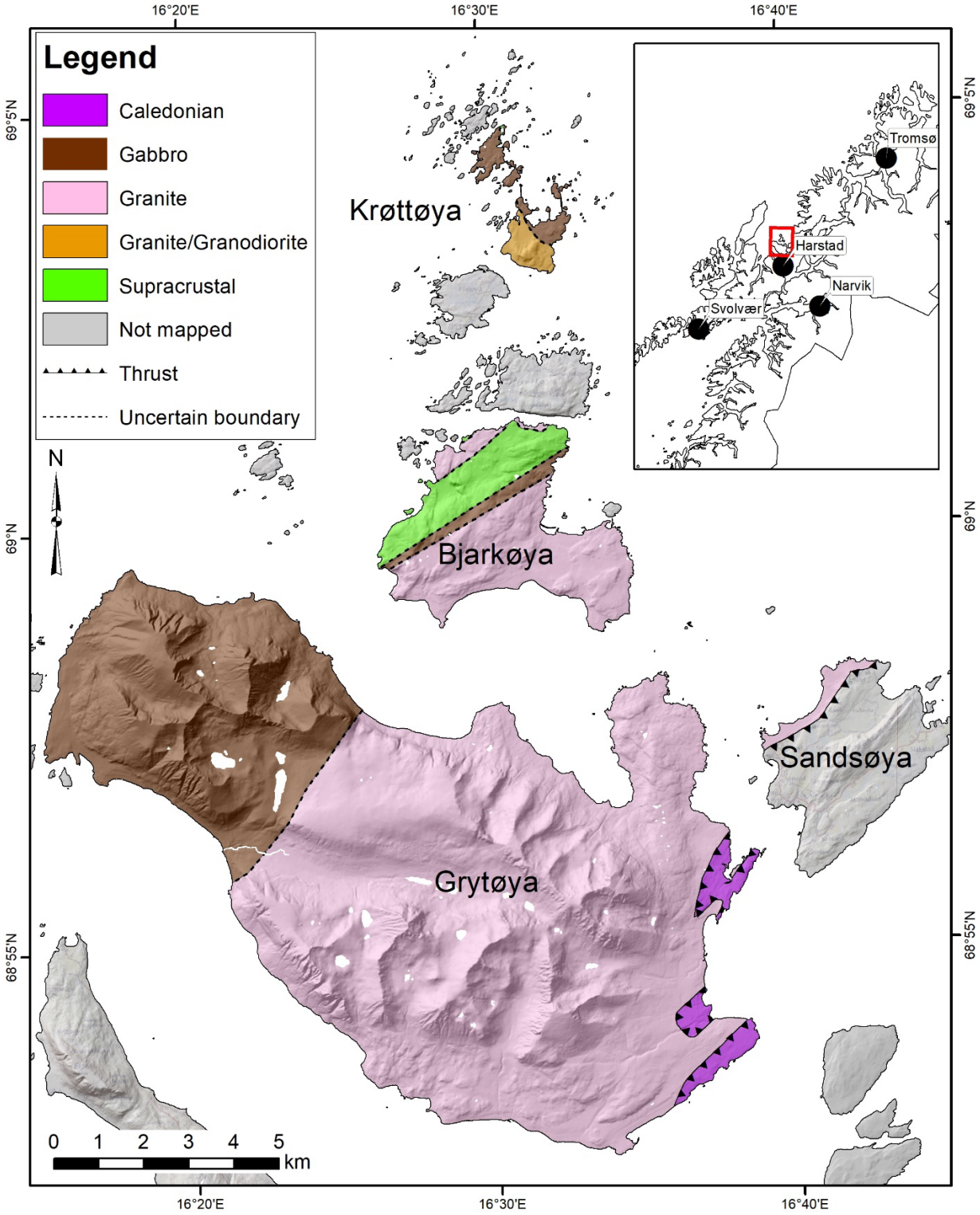

Figure 5.1: *Geological map based on the fieldwork that was done in the summer of 2017 and 2018, with associated legend of the geological units that were examined. Field notes can be provided from the author personally to anyone who would be interested.*

5.1 Field observations and petrographic descriptions

The field area can be divided into four main geological units: a granite, a granodiorite, a meta gabbro and a supracrustal unit. All units show variation in both grain size and texture, and all the different units have been examined by geochronology, petrography and geochemistry. The finalized geological map of Grytøya, Bjarkøya, Sandsøya and Krøttøya is shown in Figure 5.1.

5.1.1 Granite

Granite is the most common rock in the field area (Figure 5.2). The grain size and texture vary from medium-grained to coarse-grained, porphyritic to equigranular, and undeformed to deformed. On Grytøya the granite is found to have three different textures. The one seen closest to the gabbro is a phaneritic rock with a coarse-grained granitic texture. Mafic xenoliths are often observed within it (Figure 5.2A). This westernmost granite on Grytøya shows no distinct foliation. Aplitic, pink, centimetric to decimetric dykes intruding the granite is a common feature (Figure 5.2B). The mineral assemblage in these dykes is mainly feldspar, quartz and amphibole. Further east on Grytøya the same granitic unit can be found with a porphyritic texture (Figure 5.2C). The colour of this outcrop appears darker in colour than the granite both east and west from this porphyritic, more mafic granite. The rock shows spread feldspar phenocrysts in a fine-grained matrix consisting mainly of feldspar, amphibole, biotite and quartz. At the same location the granite is found with a texture consisting of amphibole clusters in a lighter and fine-grained matrix consisting of feldspar and quartz (Figure 5.2D). The texture of this amphibole-rich granite can be described as fine-grained, foliated and gneissic. The granite unit border to the Caledonian nappe stacks that are prominent on the eastern side of Grytøya (Figure 5.2E), and to a meta-gabbro to the west. Close to these contacts the texture of the granite is in various degrees deformed and at the old quay west on the island the granite shows an augen-like texture (Figure 5.2F). Occurrence of purple-coloured fluorite is found at some locations in the granite field, presumably formed by a late hydrothermal phase of the crystallization.

The granite has been studied in microscope and is found to consists of feldspar, biotite, hornblende, quartz and accessory minerals of titanite, apatite, epidote, allanite and iron oxides. The feldspar appears both as phenocrysts and as a constituent in the matrix, together with the biotite, hornblende and quartz. All thin sections from the granite show intermediate to coarse-grained texture. The variation within the unit is observed at microscopic level by some samples showing a clear foliation (Figure 5.2G) formed by biotite and in less degree amphibole. The amphibole is interesting as it appears with a very dark green pleochroism that suggest a composition rich in aluminium. Other interesting features are the common occurrence of accessory titanite and allanite (Figure 5.2F).

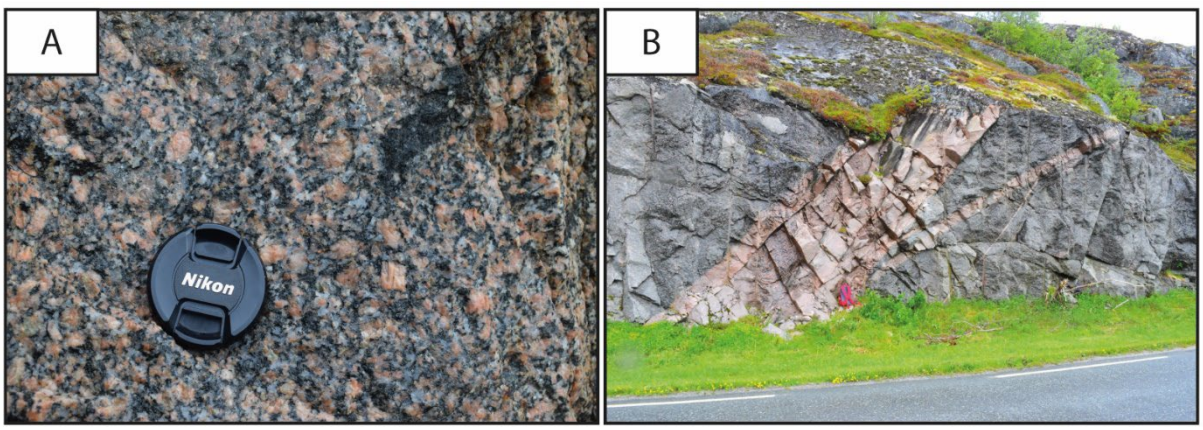

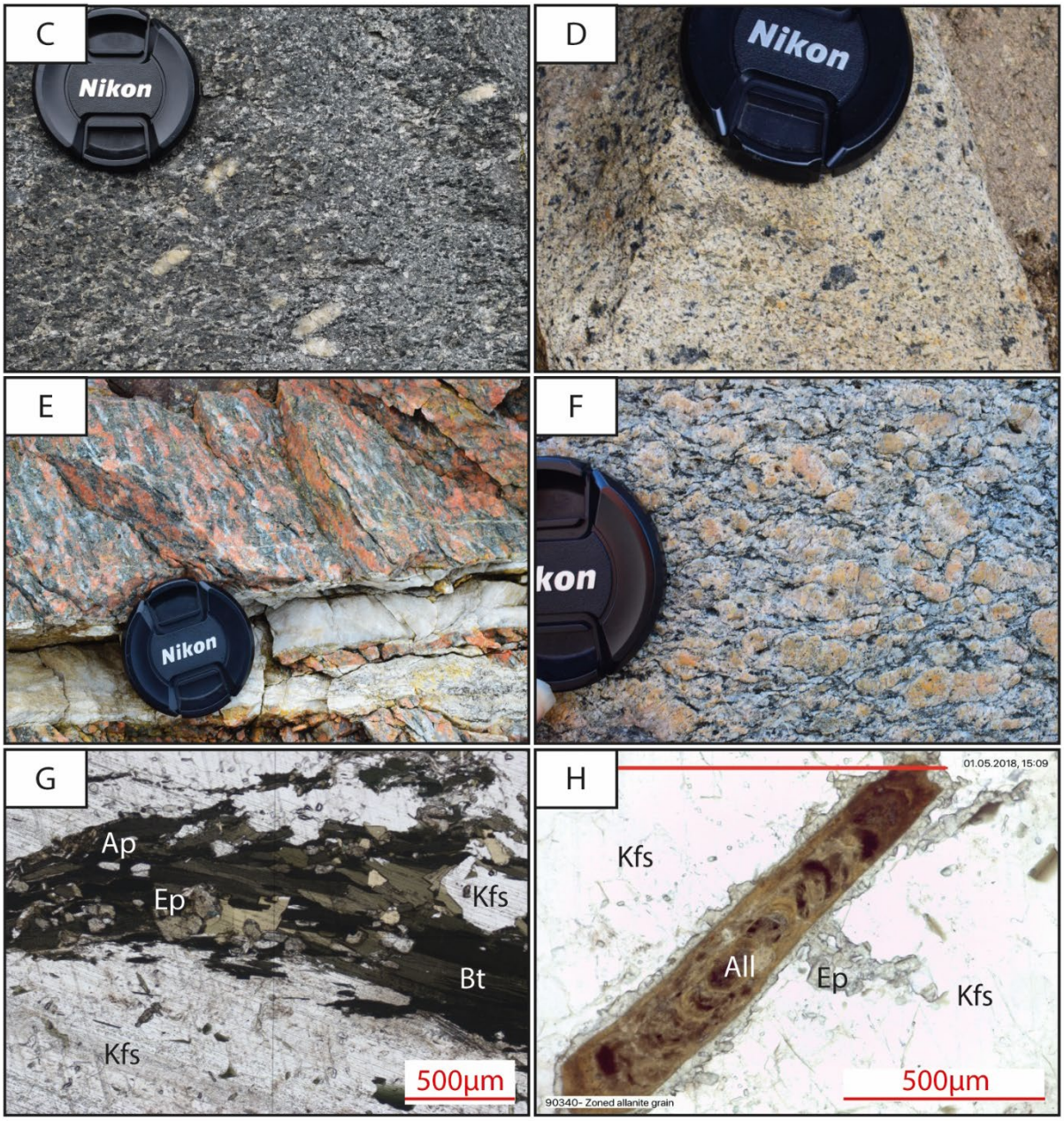

Figure 5.2: *Granite unit. A) Texture of the granite on the northwestern side of Grytøya, shown with a mafic xenolith. B) Large-scale aplitic dyke cutting through the granite at a roadcut further west on Grytøya. C) A porphyritic texture found in the same granitic unit with porphyroclast of feldspar in a finer-grained matrix of amphibole, biotite and quartz. D) Right next to the porphyritic granite shown in photo C is an outcrop of what can be described as a more gneissic textured granite with clusters of amphiboles. E) A more k-feldspar rich type of the granite on the eastern side of Grytøya, with a distinct pink colour in field. F) The more deformed texture of the granite which is found close to the boundaries with the Caledonian rocks and towards east. G) Microphotograph (ppl) of the common coarse-grained display of the granite. Here shown with biotite forming a weakly foliation with inclusions of apatite and epidote, surrounded by coarse grains of k-feldspar. H) Microphotograph (PPL) of a large grain of allanite showing zonation, rimmed by epidote interstitial between large k-feldspar grains.*

5.1.2 Meta-gabbro

The westernmost part of Grytøya, the north to north-eastern part of Krøttøya and the middle part of Bjarkøya is dominated by a meta-gabbro (Figure 5.3A). This unit can be described as heterogenous as it shows variation in grain-size, from fine-grained to coarse-grained (Figure 5.3B). At Grytøya the outcrops of the meta-gabbro are found with two set

of veins perpendicular to one another. These veins appear to be fine-grained and sticks out from the rock surface. Another common feature that is observed in the meta-gabbro are leucocratic and granitic dykes. The leucocratic dykes consist of plagioclase and amphibole. At one locality in the meta-gabbro, the rock shows a schisty foliation which is cut by a decimetric wide leucocratic dyke (Figure 5.3C-D), suggesting that the dyke is younger than the meta-gabbro. A long the coast on the northwestern side of Grytøya, the meta-gabbro is seen with large-scale leucocratic dykes that appear with a deformation structure (Figure 5.3E). Aplitic dykes and pegmatitic granitic dykes are also observed within the meta-gabbro and they vary from centimetric to metric in thickness. The aplitic dykes are pink and are made up of k-feldspar and small amounts of biotite. The granitic dykes show both pink and more white colours and consist of k-feldspar, plagioclase, amphibole and biotite. A contact between the gabbro and the granite on Grytøya is thought to be somewhere between the two entries of the Toppen tunnel. As the gabbro turns into an amphibolite and the amount of intrusive granitic dykes increases towards the western entry, it was unsuccessful to find a sharp contact between these two units. The amphibolite is most likely part of the transition between the two intrusive rocks and is described as fine-grained to very fine-grained. The amphibolite can be described as a dark grey to black rock with no foliation. Like the meta-gabbro, it is cut by aplitic and granitic dykes. The contact between the gabbro and the granite/granodiorite on both Bjarkøya and Krøttøya are observed as intrusive contacts and characterized by an increasing number of mafic xenoliths towards the contact. Deformation zones are also observed close to the intrusive contacts (Figure 5.3F).

In the microscope, the texture can be described as phaneritic and granular, with inequigranular larger subhedral grains of pyroxene in an equigranular matrix of amphibole (hornblende) and feldspar (plagioclase). The rock is presented as equigranular with an ophitic texture in thin section (Figure 5.3G). The mineral assemblage comprises of pyroxene, biotite, feldspar and accessory garnet and apatite. The amphibolite assumed to be part of the meta-gabbro unit is equigranular and consists of 80% amphibole (hornblende), with minor amounts of biotite, and plagioclase (Figure 5.3H).

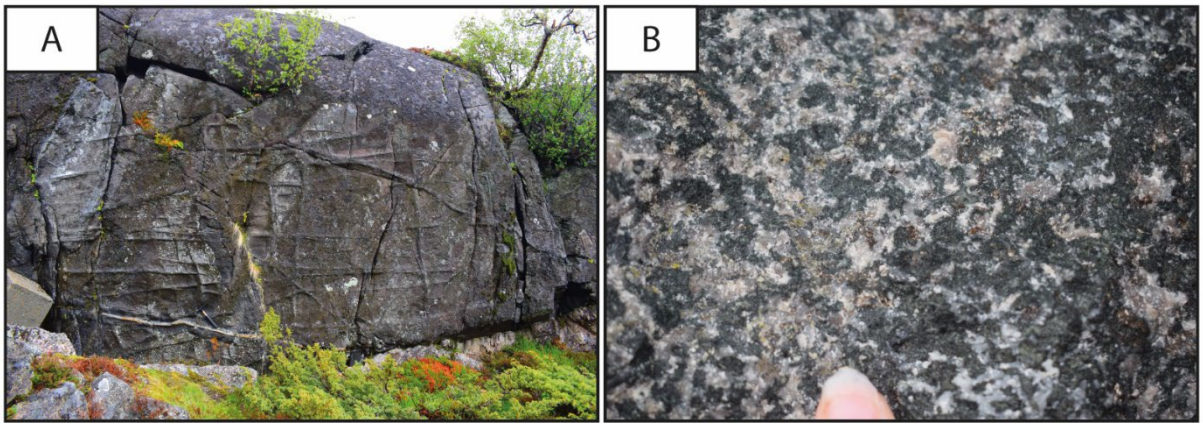

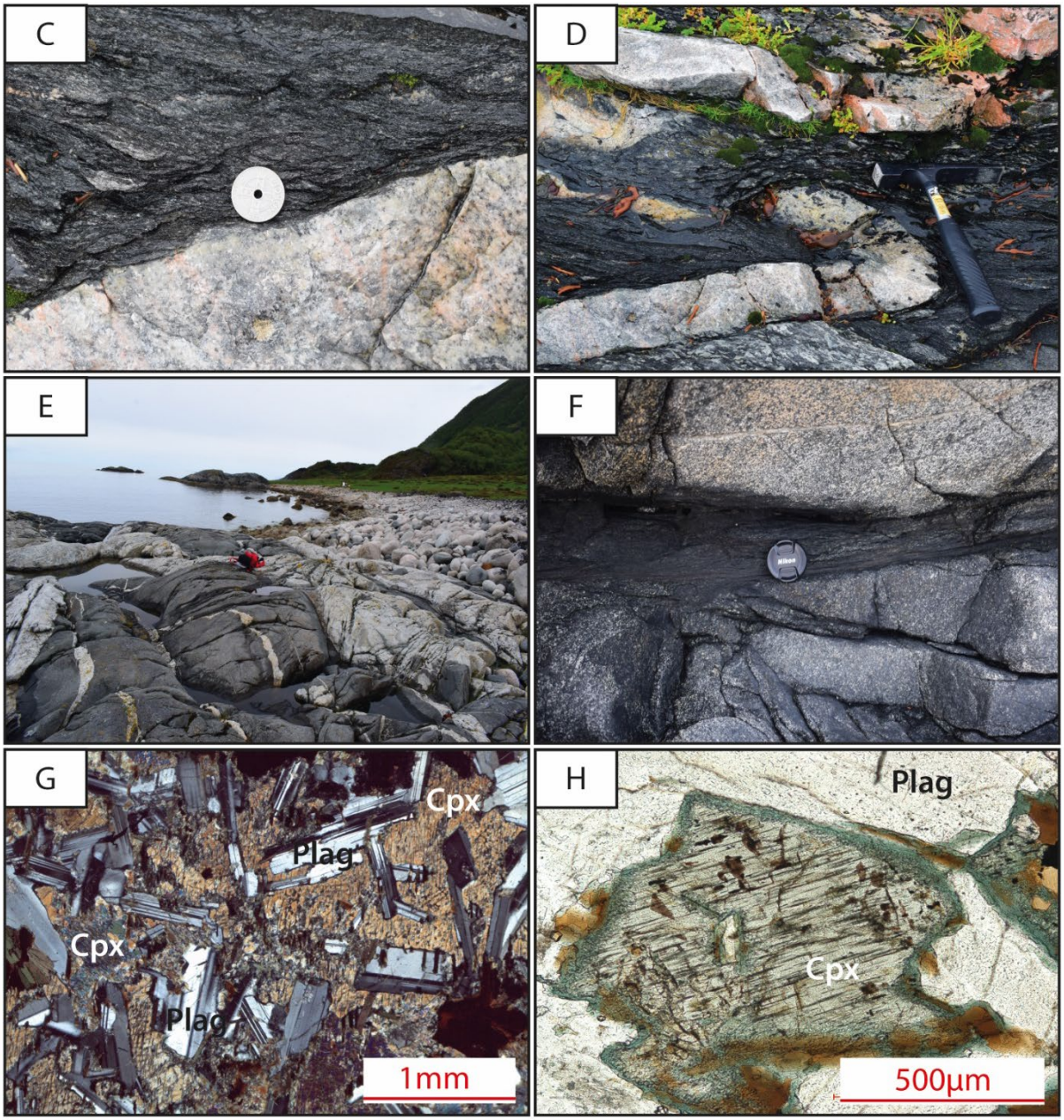

Figure 5.3: *Meta-gabbro unit. A) Field photograph of one of the meta-gabbro outcrops on Grytøya, showing the two set of veins sticking out of the rock surface. B) Texture of the meta-gabbro as it is seen on Krøttøya, a coarse-grained rock with green and brown pyroxene together with white plagioclase. C) Foliated meta-gabbro cut by a leucocratic dyke. D) The same leucocratic dyke as shown in C), highlighting the folding structure. E) Structural photo that shows several leucocratic dykes in the meta-gabbro along the coast of Grøtavær. F) Deformation zone found in the meta-gabbro at Krøttøya. The deformation zone shows a fine-grained fault gouge of mainly amphibolite. G) Microphotograph (XPL) showing the ophitic texture observed in thin section, plagioclase appear as random oriented laths enclosed in larger crystals of pyroxene. H) Microphotograph (PPL) showing a pyroxene grain with exsolution lamellae.*

5.1.3 Supracrustal rocks

The supracrustal rocks are found on Sandsøya, Bjarkøya and Krøttøya. The supracrustal rocks vary in composition (Figure 5.4A-H) from meta-arkose, carbonates, quartzites, amphibolite to amphibolitic gneiss, hornblende slate to mica schist, and they are sulphide and graphite bearing with iron mineralisations. The grain size and textures vary within the different rock types but are in general coarse-grained. On Sandsøya the supracrustal unit is characterized by a very fine-grained amphibolitic rock with centimetric to decimetric calc-silicate lenses in it. The amphibolite is observed to alternate within the granites. The supracrustal unit is intruded by granitic and granodioritic dykes on all the three islands; these dykes vary in thickness and orientation. On Bjarkøya the supracrustal unit is exposed as a belt stretching from the east/north-eastern side to the north/northwestern side. On the northwestern side the unit is found to consist of mostly biotite mica schist with calc-silicate of diopside, sulphides and graphite (Figure 5.4B-D). Small-scale plagioclase veins are also observed in the supracrustal rocks. The supracrustal unit varies from fine to intermediate-grained quartzite, to coarser grained carbonates and meta-sandstones (Figure 5.4E). On the east side of Bjarkøya the unit consists mostly of amphibolite to amphibolitic gneisses with common appearance of iron precipitation veins (5.4F-H). Apart from the gneisses and slates, the rocks of the supracrustal unit show little foliation and are often difficult to do measurements on, as the outcrops are mostly evident close to the shore.

Thin section from the gneiss from Bjarkøya show an intermediate- to coarse grained rock (Figure 5.4I-J). The mineral assemblage consists of k-feldspar and plagioclase, foliated hornblende lenses enclosing coarse-grained diopside (Figure 5.4I). There is also biotite present in the gneissic rocks, and they are often seen together with fine-grained epidote (Figure 5.4J).

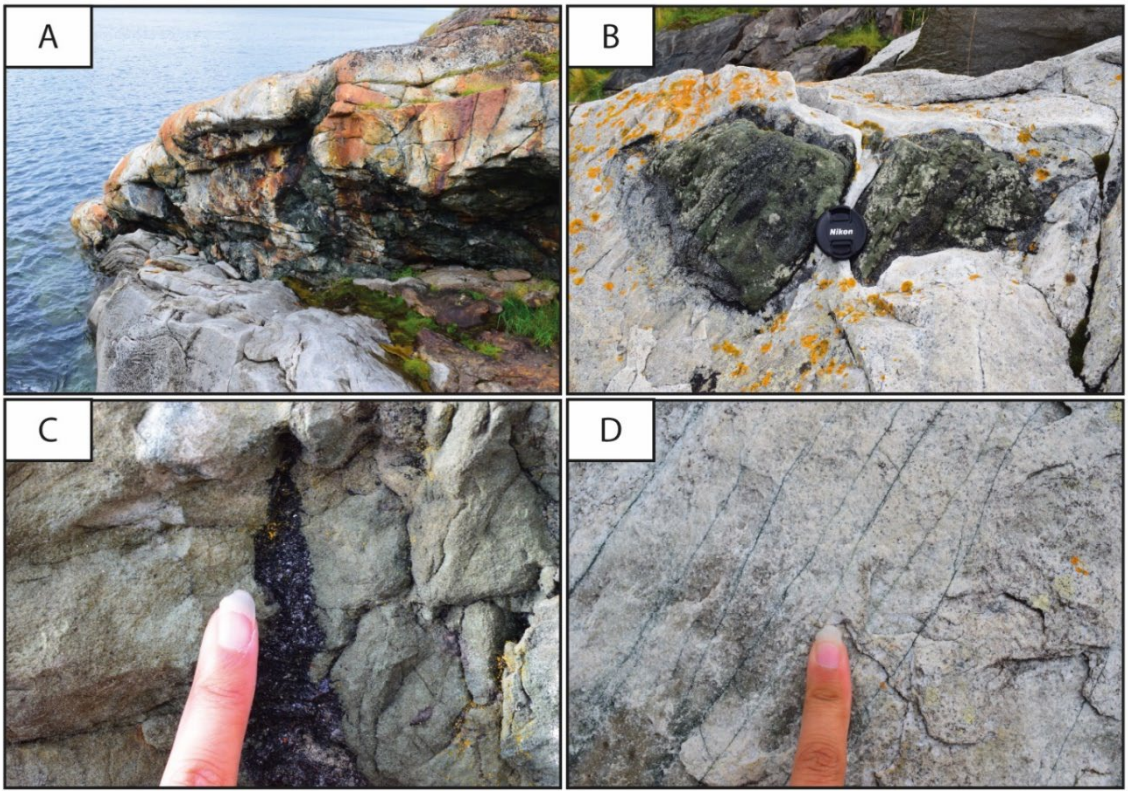

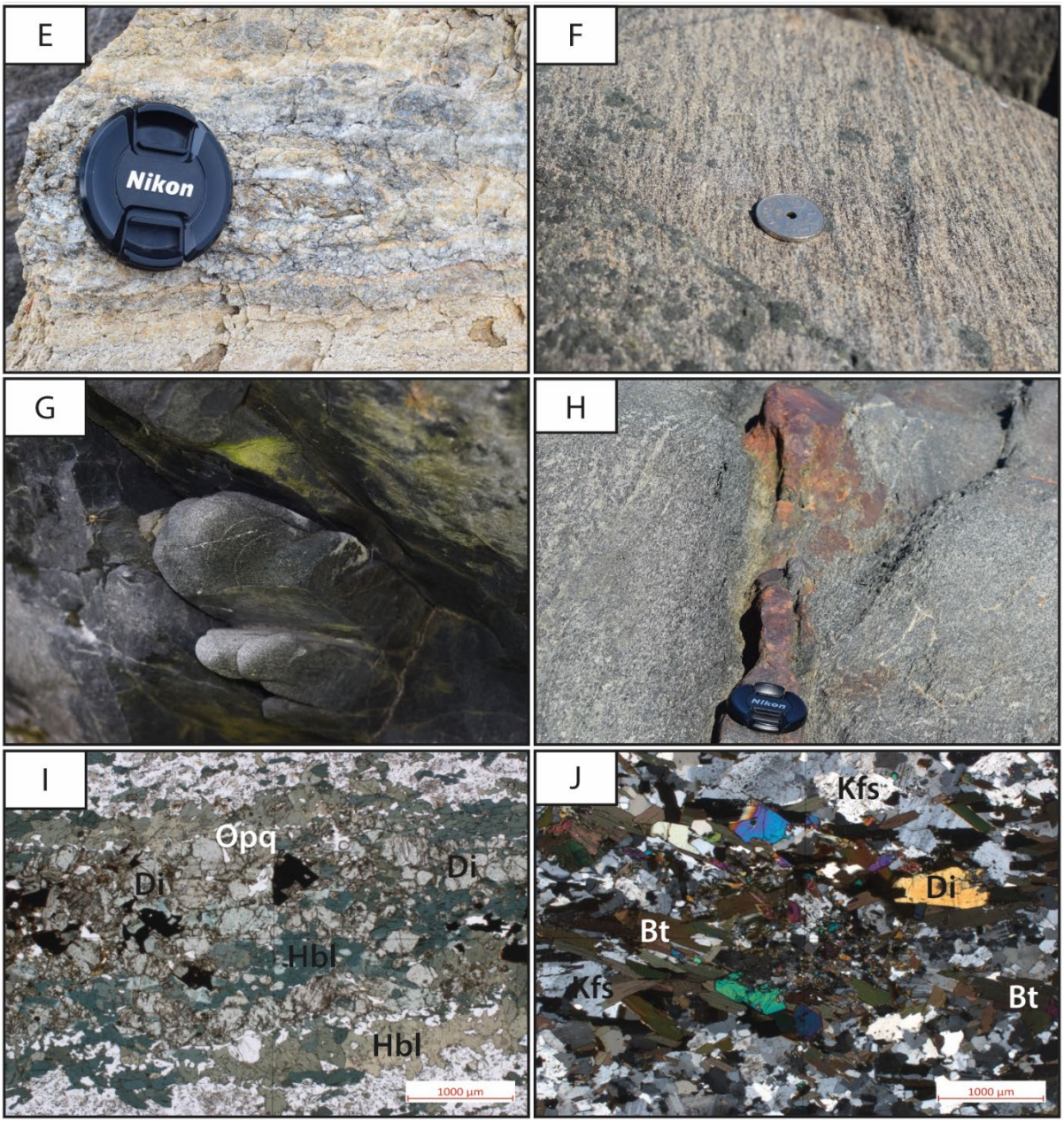

Figure 5.4: Supracrustal unit*. A) A large-scale outcrop of the supracrustal unit at Bjarkøya. The photo shows a quartzite with associated diopside (green colour) and iron precipitation veins (rusty colour). B) A smaller outcrop of the quartzite with small lenses of diopside. C) The supracrustal unit can also be found with sulphide-rich layers. D) The quartzite is some places found with a network of thin diopside veins. E) A layer of coarse-grained carbonate found in association with a meta-arkose layer. F) The supracrustal unit also shows layers of gneissic rocks, with the mafic dark mineral of amphibole creating a foliation. G) Amphibolite with a pillow structure found at the boundary with the granitic unit on the north side of Bjarkøya. H) A typical observation of the supracrustal unit are the many iron precipitation veins. I) Microphotograph (PPL) of a gneiss showing a lens of diopside that is surrounded by amphibole, both minerals oriented the same direction. Opaque grains interpreted to be iron oxides are found in this hydrous mineral company. J) Microphotograph (XPL) of the second sample of gneiss with a mineral assemblage mainly composed of k-feldspar, biotite, diopside and quartz.*

5.1.4 Granite/Granodiorite

This granite/granodiorite unit is only present at Bjarkøya, where it makes up half of the island of Krøttøya. The granodioritic unit is a compositional variation between granite and a diorite. In field it appears heterogenous, coarse-grained and light in colour. It consists of feldspar (plagioclase), quartz and small proportions, almost accessory biotite. On Bjarkøya the unit is observed close to the boundary of the meta-gabbro. The granodiorite is also present as dykes in the amphibolite and meta-gabbro at Bjarkøya and Krøttøya. The dykes vary in size and thickness, but the composition is largely homogenous with feldspar and pyroxene being the main mineral present. One of the very interesting features in the field observations are found in a 20-30 cm thick granodioritic dyke that intrudes the amphibolite on the north-eastern side of Bjarkøya (Figure 5.5A-B). The dyke shows pink, fine-grained crystals of garnet in addition to a mineral that is thought to be the pyroxene, omphacite. This suggestion is based on the findings in thin section. The mineral shows a pale-green colour, undulose extinction and the cleavage (Figure 5.5C-D). Omphacite is commonly formed in a high-pressure environment and is often related metamorphism in eclogite facies.

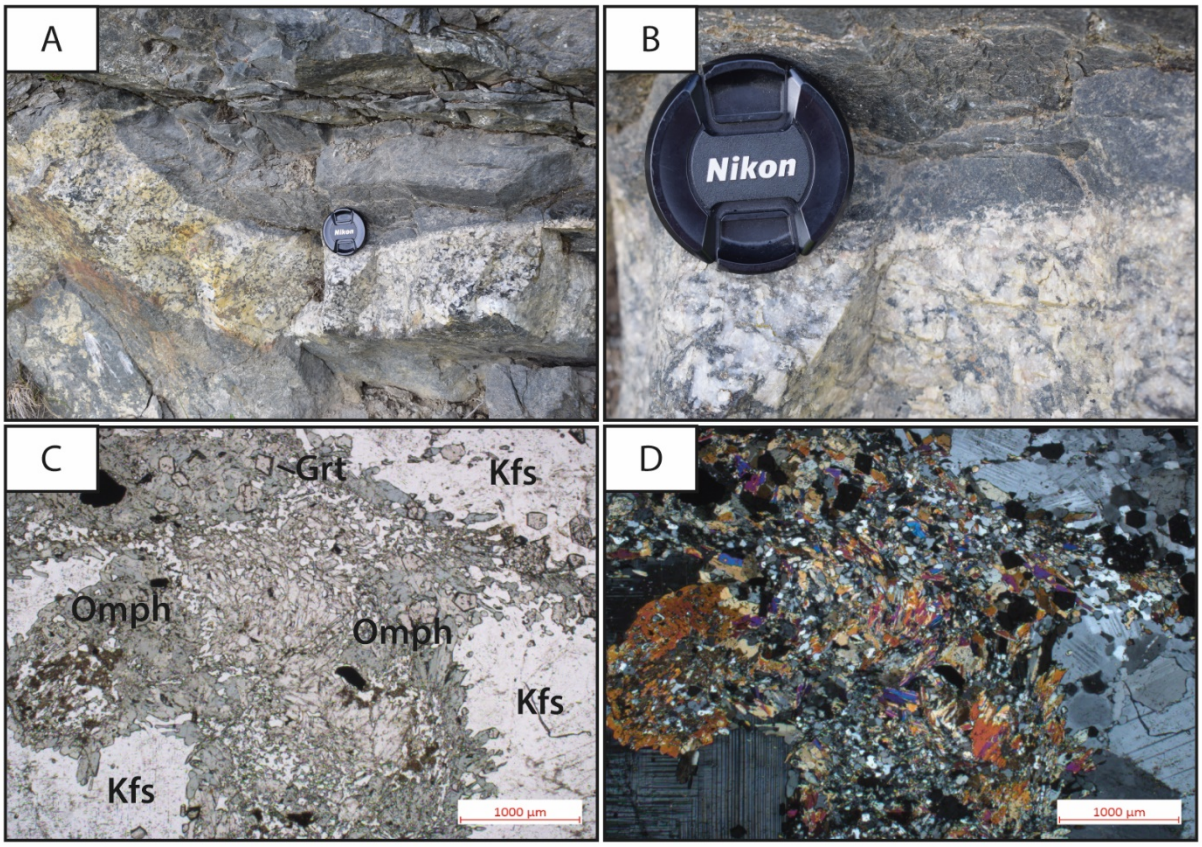

Figure 5.5: *Granodioritic unit. A) Granodioritic dyke found at Bjarkøya B) Close-up picture of the same dyke, showing the coarse-grained texture. C) Microphotograph in PPL showing the green mineral believed to be omphacite. D) Microphotograph in XPL showing the same grain as shown in C), highlighting the interference colours.*

5.1.5 Caledonian rocks

Caledonian rocks are observed at Grytøya and Sandsøya where they form tectonic shear zone contacts with the granitic unit. These rocks were mentioned in the description of the granite unit, as the Caledonian rocks are shown to be associated with deformation textures in the granites. The Caledonian rocks are associated with the Caledonian orogeny event that took place at Late Silurian-Early Devonian time, making them younger than the surrounding igneous units at Grytøya and Sandsøya. The rock types found in the Caledonian unit include mica-schists, meta-sandstones, marble and amphibolite (Figure 5.6A-D). The Caledonian rocks have been variably metamorphosed and deformed and shows textures and structures as a result of these processes. The rock types are mainly homogenous and fine-grained. The mica-schist is fine-grained, dark and shiny in colour- with garnet indicating the high temperature and pressure that the rock has been exposed to. The meta-sandstone is exposed in the mid-part of the Caledonian unit on Grytøya and in the Caledonian unit close to the boundary with the granite on Sandsøya. The meta-sandstone is fine- to intermediate-grained and appear with a light grey colour in field, with Z-folds (Figure 5.6B). Associated with the meta-sandstone are thin layers of fine-grained marble with dark layering within it (Figure 5.6C). The amphibolite appears with a dark (black) colour in field and consists of mainly amphibole and plagioclase, the plagioclase appearing as porphyritic foliated minerals giving the amphibolite a gneissic texture (Figure 5.6D). As the meta-sandstone, the amphibolite contains z-folds (Figure 5.6E).

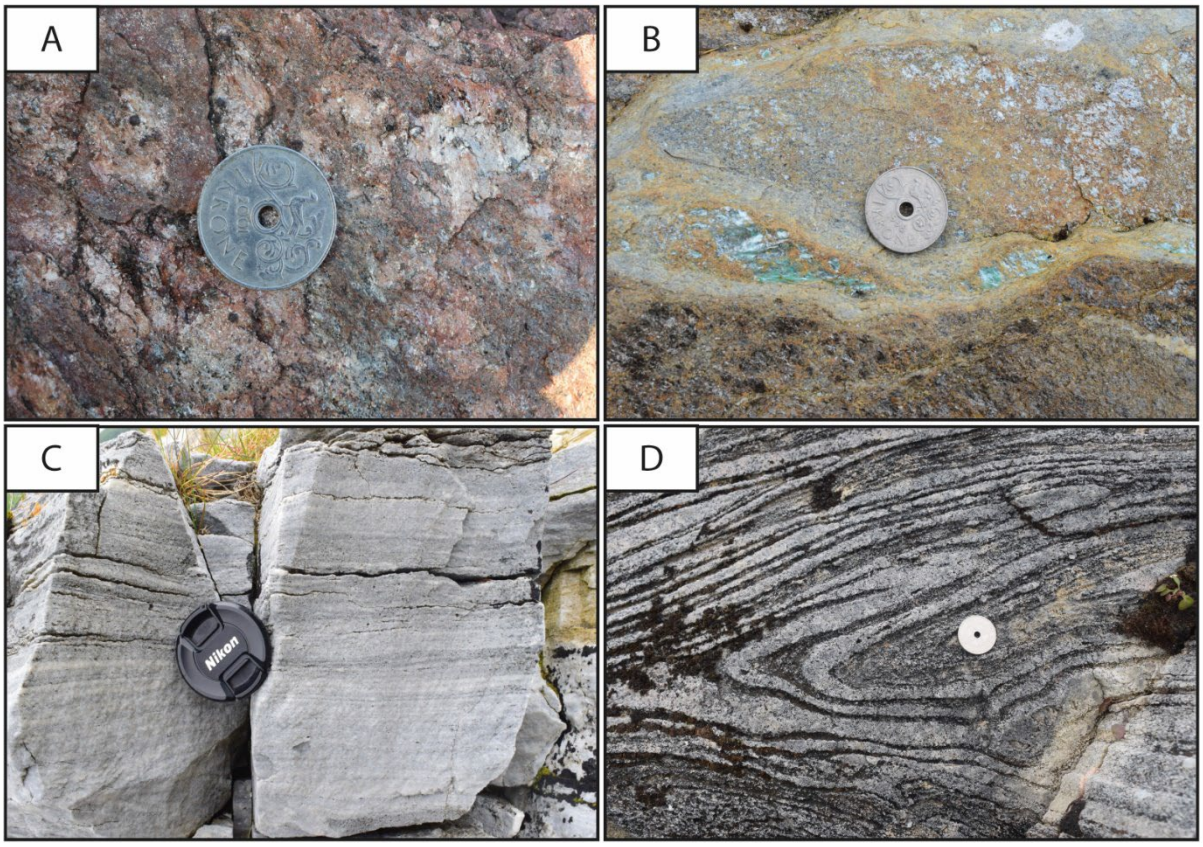

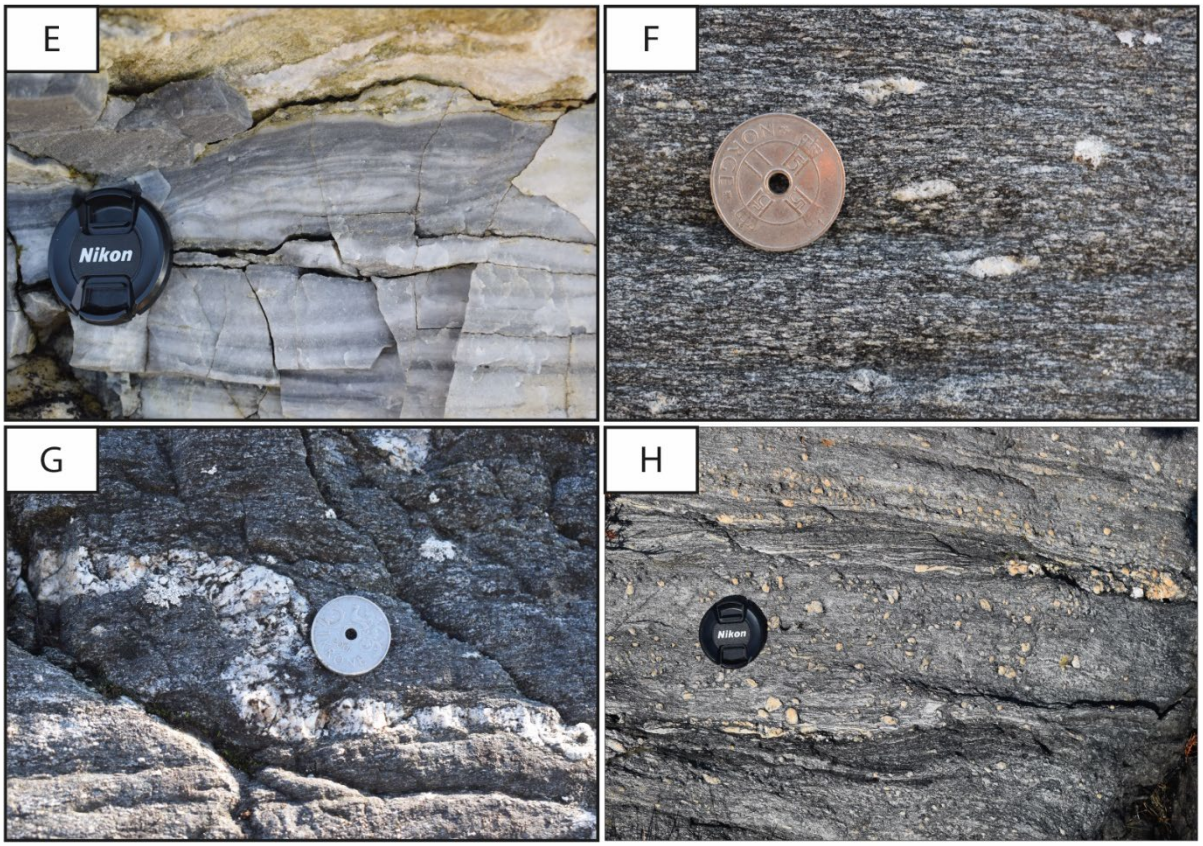

Figure 5.6: *A) Photo showing the texture of the garnet-mica schist. B) Malachite found in the mica-schist. C) A layer of marble showing a block of the carbonate layer found between the schist and meta-sandstone. D) Folding in the meta-sandstone. E) Close-up photo of the layered marble. F) Gneissic texture of the amphibolite G) Z-fold found in the amphibolite. H) A conglomeratic texture found in the amphibolite, close to the boundary of the granite.*

5.2 Zircon geochronology

A total of 14 samples from the study area were analysed using laser-ablation inductively coupled plasma mass spectrometry (LA-ICP-MS) for zircon U-Pb geochronology, trace element concentrations and Hf isotopic composition. In addition, two samples from the Lofoten-Vesterålen area were analysed with sensitive high-resolution ion microprobe (SHRIMP). The 14 samples from the field area are distributed between the four islands of Grytøya, Sandsøya, Bjarkøya and Krøttøya. This chapter presents the results from the geochronology analyses with U-Pb ages, trace element geochemistry and Lu-Hf isotopes of the zircons. A map with the sample localities of the samples analysed for U-Pb ages, zircon trace elements and zircon Lu-Hf isotopes is shown in Figure 5.7. U-Pb data, zircon trace elements and isotope data are listed in Appendix B.

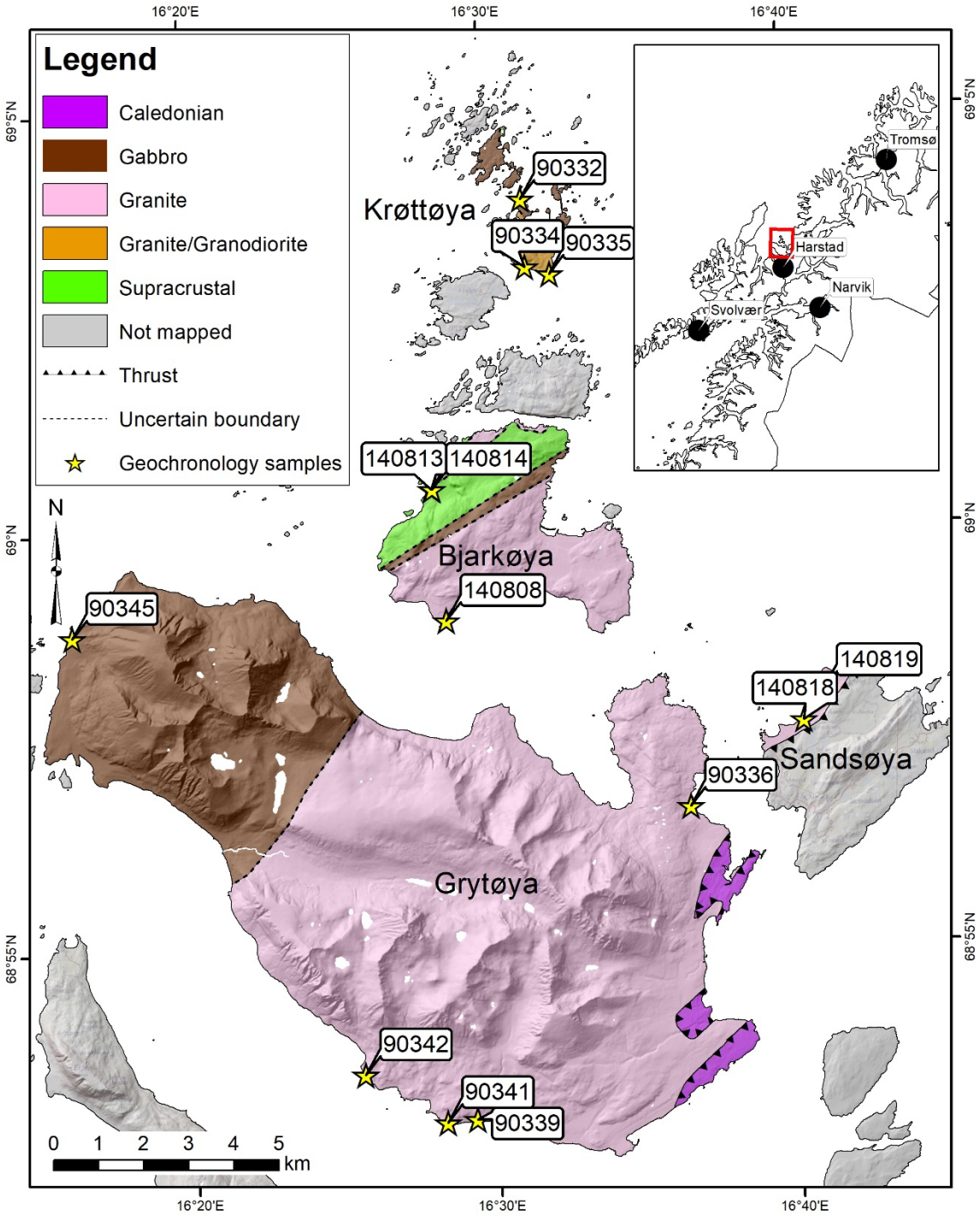

Figure 5.7: *Geological map based on the fieldwork that was done in the summer of 2017 and 2018, with associated legend of the geological units that were examined. The yellow stars indicate the sample localities for the sample that were analysed for U-Pb dating, zircon trace elements and zircon Lu-Hf isotopes.*

To get the best U-Pb ages a numerous of examination of the U-Pb data was performed. The images from the laser were used to check if the spots could be divided into core and rim data and whether the spots hit only the grain or outside in the epoxy. The trace element data was used to see if any of the data showed anomalous patterns that could be related to open system behaviour. Alpha dose was also calculated for the data in the search for an explanation of outliers or very discordant data.

5.2.1 Meta gabbro

Sample 90345

This is a sample collected from the meta-gabbro on Grytøya (Figure 5.8A-E). It is a coarse-grained, heterogenous rock composed of mainly plagioclase and pyroxene forming an ophitic texture (Figure 5.8C). Hornblende and biotite, together with accessory zircon and garnet makes up the rest of the rock. The texture and the inclusion relationship suggest that the plagioclase crystallized before the pyroxenes. Another feature that can be observed in the microscope is that in the case where plagioclase appears as cumulus and pyroxene as intercumulus- the pyroxene shows exsolution lamellae.

The zircon crystals are transparent and pale-brown in colour. The shape of the zircons is subhedral fragments, some rounder than others, and they vary from 100 to 200 µm in size. The CL images show weak zoning in one of the zircon grains, whilst the other four zircons show a less clear internal texture with some areas of the grain being lighter or darker than the rest of the grain (Figure 5.8B). The Th/U ratio was found to be in the range of (1.62-2.42). One grain was removed from the U-Pb data as a discordant outlier with a high alpha dose. This grain also shows a highly elevated LREE pattern on the REE spider plot (Figure 5.8D), interpreted to be the result of an opening of the crystal structure of this zircon. The remaining four grains yield a Concordia age of 1785±11 Ma (Figure 5.8E). This age is interpreted to be the crystallization age of the gabbro. The Hf evolution plot shows epsilon values in the range (-2.9 to -6.6), more radiogenic than the granites found on Grytøya. The ε_{Nd} value of -5.85 is also higher than the surrounding granite.

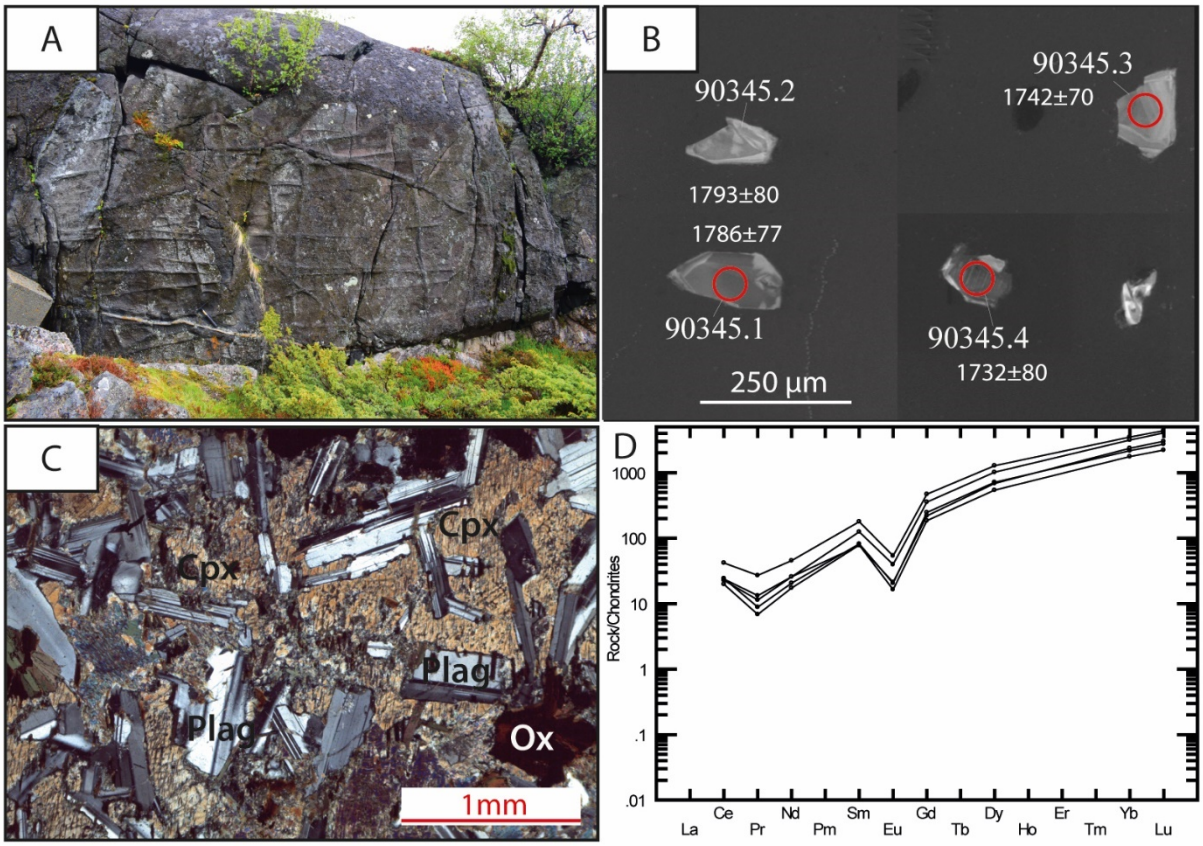

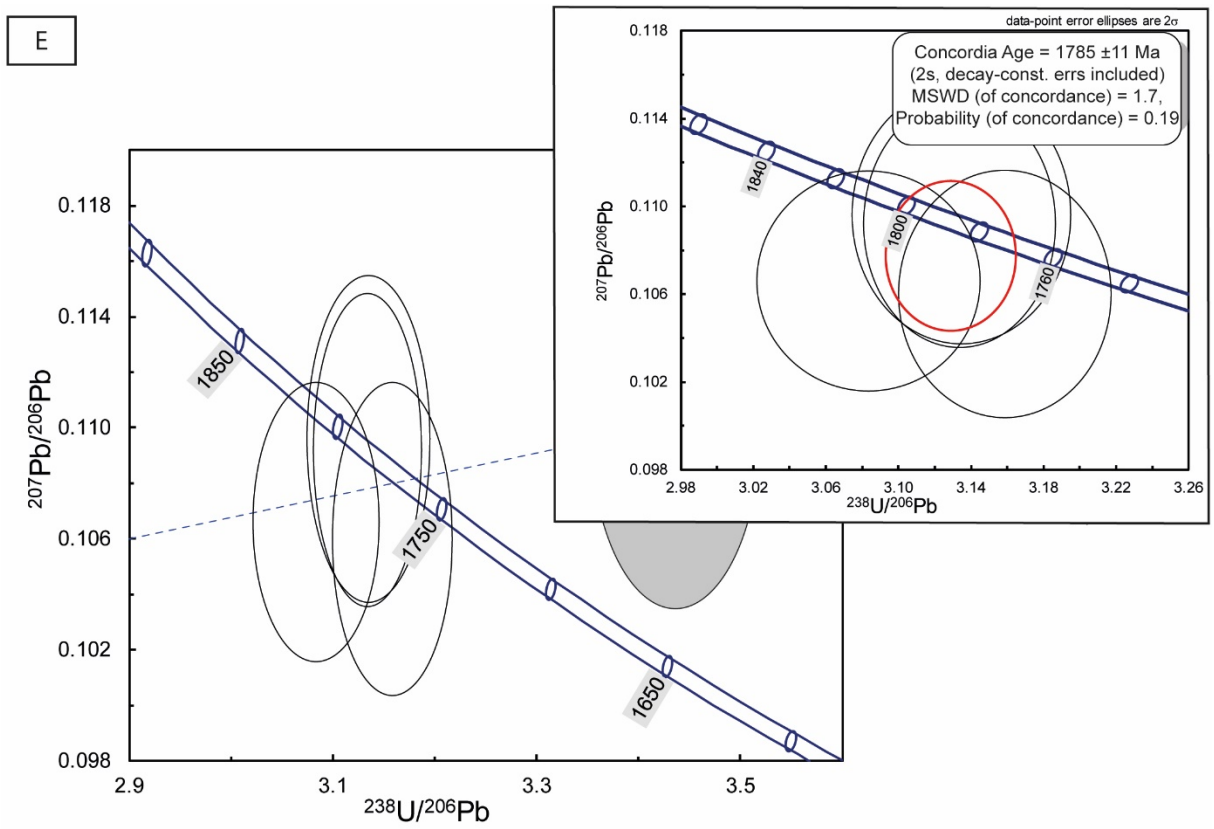

Figure 5.8: *Sample 90345. A) Photo of the locality where the sample was taken. B) CL-images showing internal textures of three zircon grains that were analysed by LA-ICP-MS together with the U-Pb age (red circle indicates where the laser spot was aimed). C) Microphotograph (XPL) of the subophitic texture in the rock, with plagioclase enclosed in larger pyroxene grains. D) Chondrite-normalised REE spider plot showing an increase from the LREE to the HREE and a negative Eu anomaly. E) Tera-Wasserburg plot with all the grains that was analysed for the sample (grey ellipses are grains that were removed from the final calculation). The diagram in the upper right corner shows the calculated concordia age.*

5.2.2 Diorite/Granodiorite

Sample 90332 (diorite)

This sample was collected at Meløyvær (Krøttøya) at the intrusive contact between the meta-gabbro and the granodioritic unit shown in Figure 5.7. The sample location is close to the sea where a fine-grained amphibolitic rock alternates with a coarse-grained quartzdiorittic rock. This quartzdiorittic rock was sampled and appears coarse-grained with plagioclase and quartz making up approximately 70% of the rock. The plagioclase is present with saussuritization resulting in very fine-grained grains of epidote. The remaining 30% of the rock consists of a mush consisting of biotite and hornblende (Figure 5.9C) Accessory minerals are titanite, quartz and iron oxides.

The zircon crystals are transparent to pale brown in colour, with mostly anhedral to subhedral shapes. The size ranges from 50 to 200 µm. In CL images they lack distinct internal textures, but some of them show what could be interpreted as a core and rim internal texture (Figure 5.9B). One of the grains that were picked for laser seem to show magmatic, oscillatory zoning, but the grain was too small to be analysed with a 50µm laser spot. The Th/U ratio for the zircons are all >0.5 suggesting a magmatic origin. The zircon grains are enriched in the HREE and show a negative Eu-anomaly (Figure 5.9D). All the U-Pb data (9 of 9 samples) are concordant and yield a concordia age of 1809±20 Ma. The age is interpreted to reflect crystallization age of the quartz-diorite. The zircon ε_{Hf} isotopes

measured for this sample are in the range of (-5.45 to -7.17) and yields a whole-rock ε_{Nd} value of -7.3.

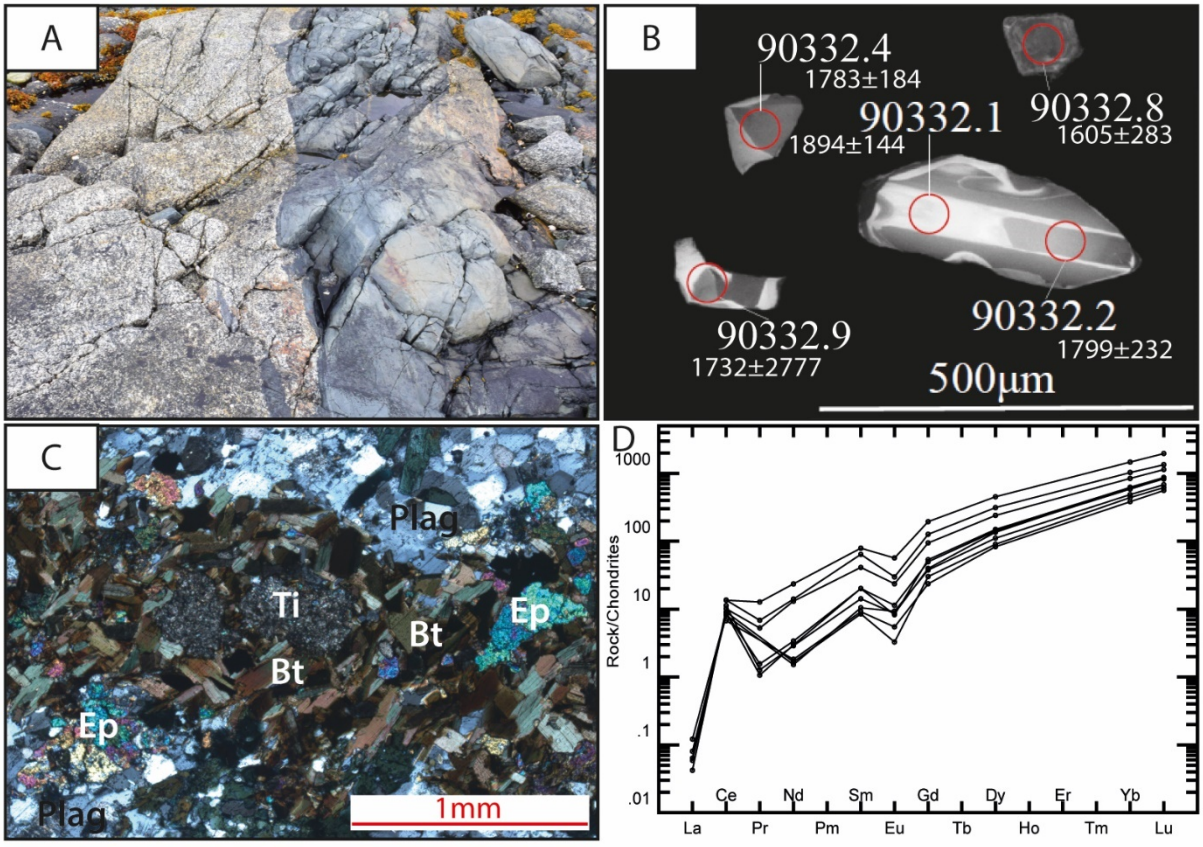

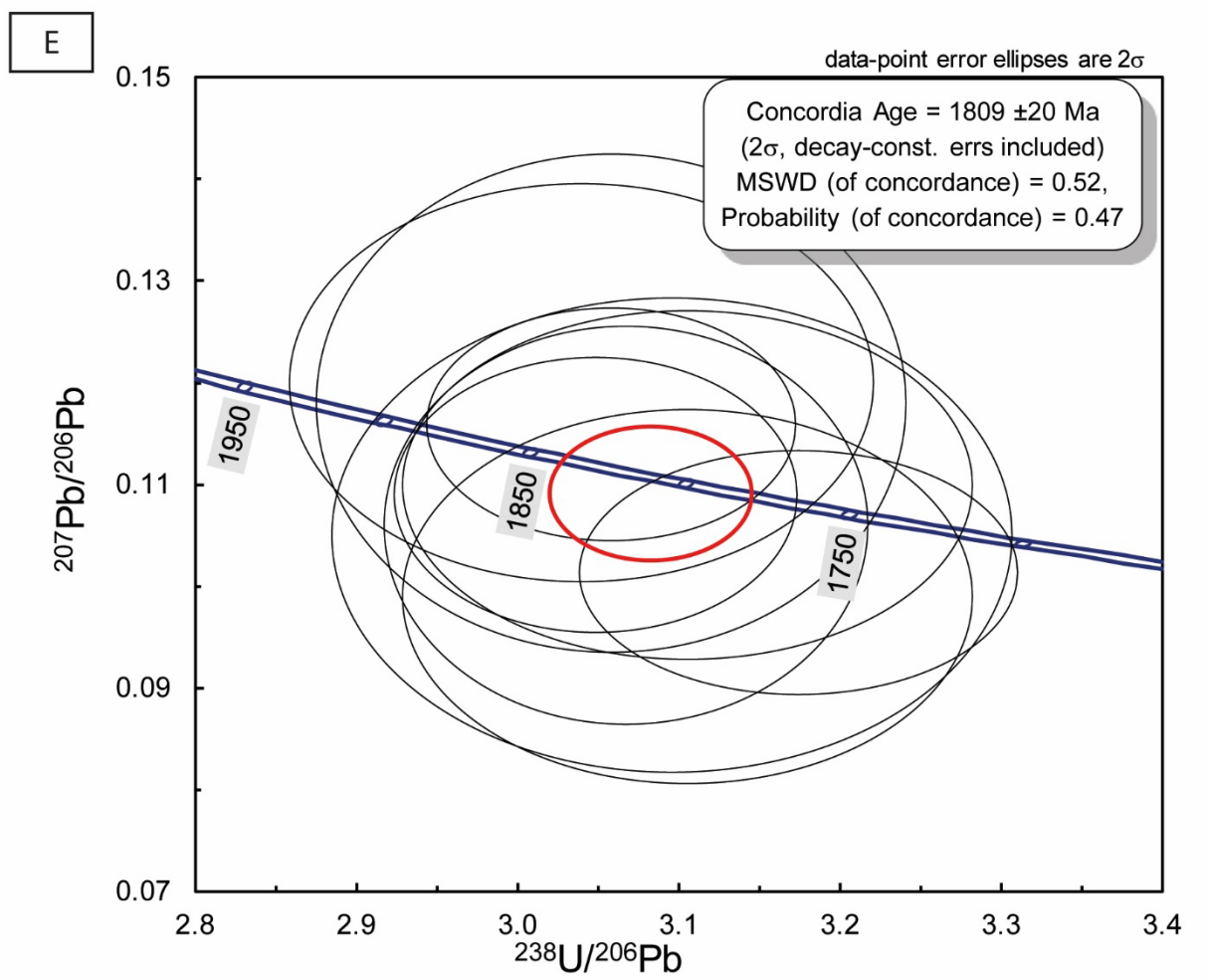

Figure 5.9: *Sample 90332. A) Photo of the outcrop were the sample was collected. B) CL-images showing internal textures of four of the zircon grains that were analysed by LA-ICP-MS (red circle indicates where the laser spot was aimed). C) Microphotograph of the alteration textures than can be found in the rock. Shown is an altered grain of titanite with a rimming texture consisting of mainly biotite grains. D) Chondrite-normalised REE spider plot showing an increase from the LREE to the HREE and a negative Eu anomaly. E) Tera-Wasserburg plot showing the calculated concordia age from the U-Pb data. Black ellipses are all the grains (9) analysed, whilst the red ellipse is the calculated concordia age.*

Sample 90334 (granodiorite)

This sample was collected in the granite/granodioritic unit on Krøttøya and is an intermediate to coarse-grained granite (Figure 5.10A-E). The mineral assemblage consists of phenocrysts of k-feldspar in a matrix of hornblende, plagioclase and quartz. Oxides, epidote, titanite and garnet occur as accessory minerals. The grains are anhedral to subhedral, except from some of the titanite grains. The amphibole is weakly oriented and shows a dark green colour, suggesting a high content of Al in the crystal structure. The feldspar grains, especially the plagioclase grains have been partly altered to epidote through the hydrothermal alteration process of saussuritization (Figure 5.10C).

The zircons from this sample are mostly pale brown in colour and show a subhedral to euhedral prismatic shape. The size varies from 150 to 300 µm. The zircons have complex internal textures, with CL dark oscillatory-zoned cores transacted by CL-lighter, weakly

oscillatory-zoned rims. Spots of inclusions are also visible in some of the cores, which appear darker than the rest of the core. The zircons have Th/U ratios between (0.41 to 0.54). U-Pb data was obtained from 14 of the best-looking zircons. Despite five grains having a discordance higher than 10% only two grains were considered removed from the calculation, one because of high alpha dose and one for showing an extremely elevated LREE value (Figure 5.10D). In general, the REE spider plot show that the grains have a clear negative Eu anomaly. A weighted average was calculated and gave a U-Pb age of 1794±22 (Figure 5.10E). The ε_{Hf} values for these zircons lay in the range from (-4.1 to -9).

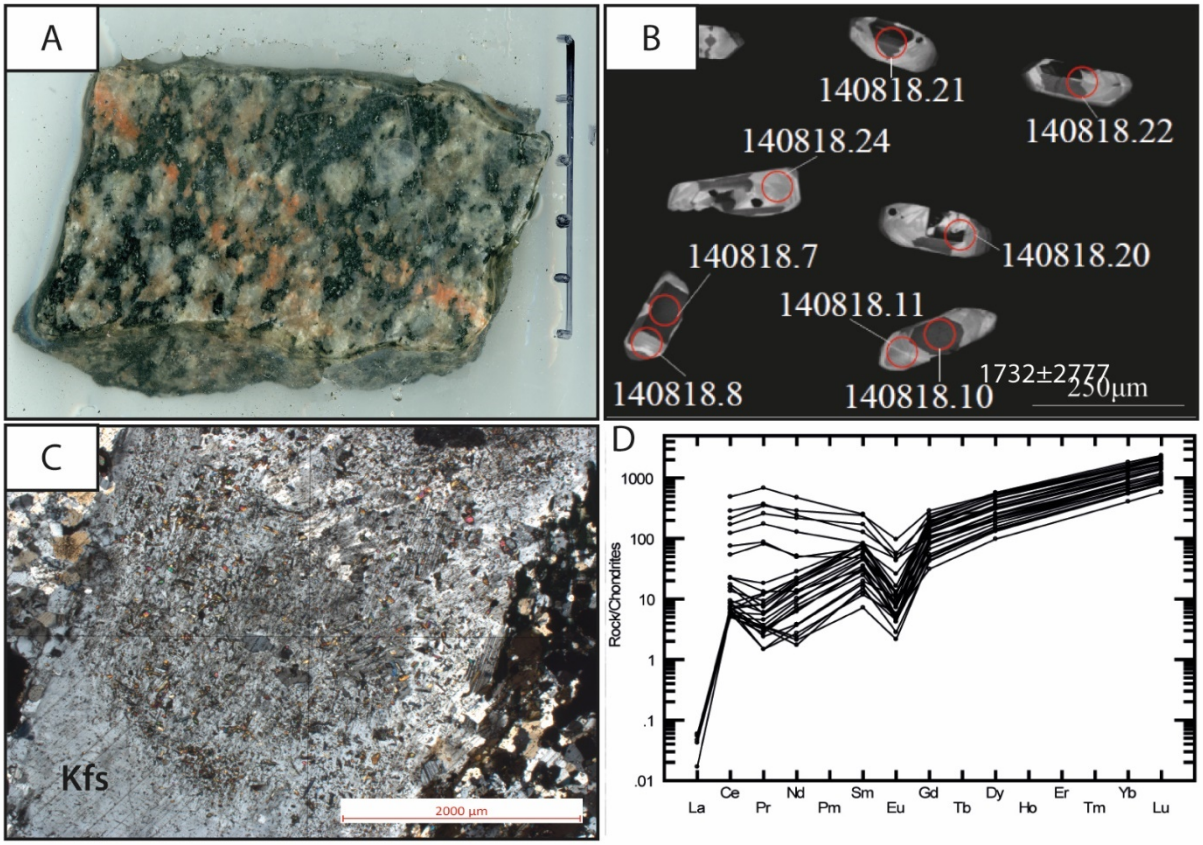

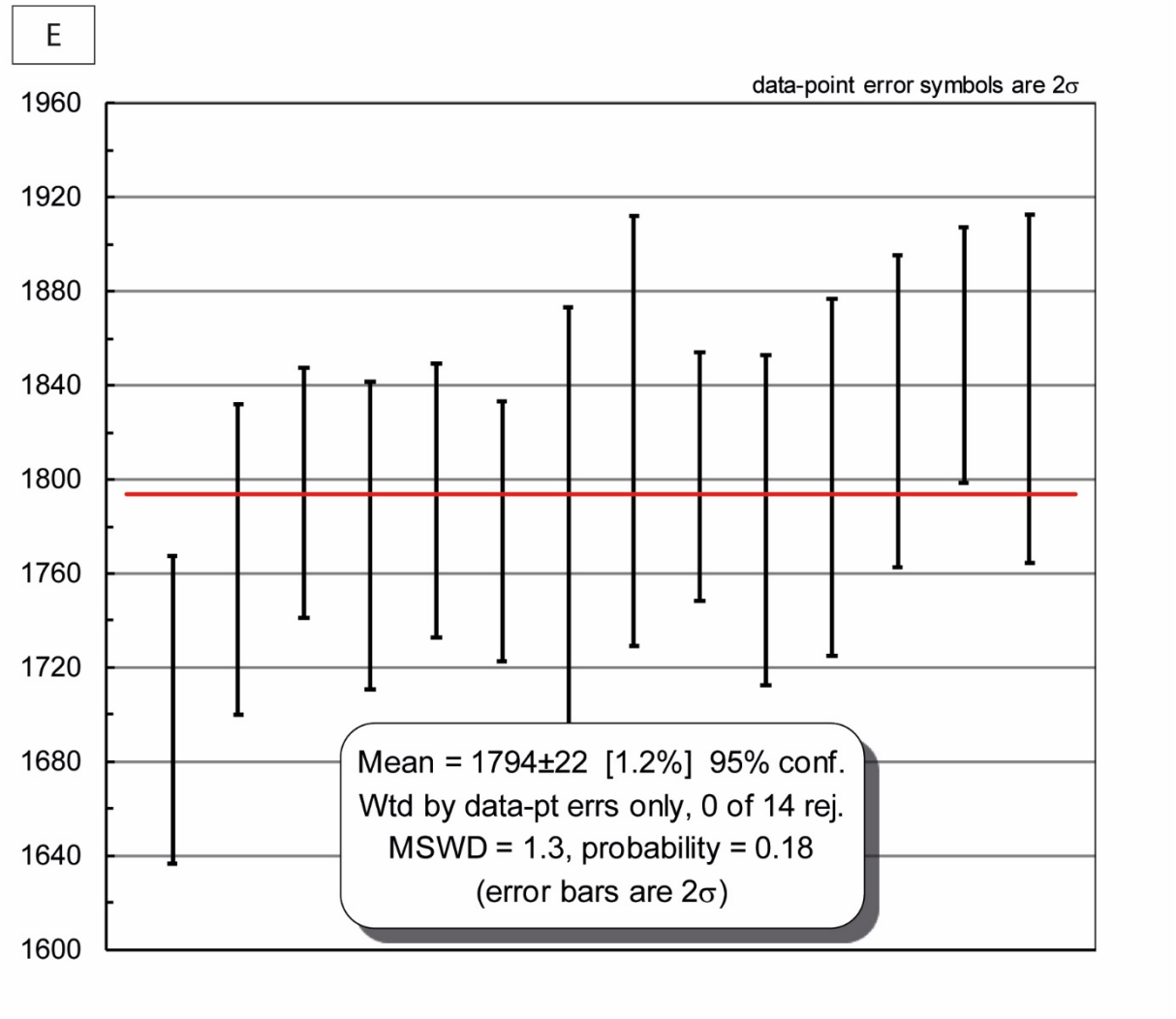

Figure 5.10: *Sample 90334. A) Photo of a hand specimen of the rock. B) CL-images showing internal textures of six of the zircon grains that were analysed by LA-ICP-MS (red circle indicates where the laser spot was aimed). C) Microphotograph (PPL) of a feldspar grain with a dusty appearance, a typical indication of alteration processes. D) Chondrite-normalised REE spider plot showing an increase from the LREE to the HREE and a negative Eu anomaly. Note how three of the grains from the sample have a detectable concentration of La, these three grains are the ones that appear concordant in the concordia plot. E) A diagram showing the weighted average of the sample, giving the U-Pb age. The red line corresponds to the mean (calculated age), with the black columns illustrating the uncertainty.*

Sample 90335 (granite)

This sample is also taken from Krøttøya, a rock that appear to have a more granitic composition than sample 90332 and 90334. It is coarse-grained with phenocrysts of feldspar in a matrix consisting of mainly hornblende, plagioclase and quartz (Figure 5.11A). Accessory minerals are epidote, titanite and garnet. The texture of the rock is weakly foliated, showing a redder/pinker colour in field than the whiter/greyer granodioritic rocks from sample 90332. In the microscope, the large randomly oriented grains of hornblende are interpreted to indicate more hydrous conditions (Figure 5.11C).

This sample contains transparent to pale brown crystals of zircon, with mostly euhedral prismatic shapes. The zircons vary in size from 200 to 400 µm. The CL images show

inclusions in some of the grains (Figure 5.11B) and only a few of the grains show oscillatory zoning. The Th/U ratios for the zircons range from (0.34 to 0.61). REE data has been studied and show that some of the zircons have elevated LREE concentrations (Figure 5.11D), interpreted as reflecting incorporation of non-lattice-bound elements. The U-Pb age was therefore calculated from the three zircons that did not show elevation in the LREE. This calculation resulted in a Concordia age of 1794±31 Ma, interpreted to be the crystallization age of the rock. The U-Pb age of all the grains were found to be 1756±19 Ma which is likely to be the age of a later hydrothermal event. The ε_{Hf} values are in the range of (-6.3 to -10.8) and the sample yields a whole-rock ε_{Nd} value of -7.68 indicating a rock that crystallized from a crustal melt.

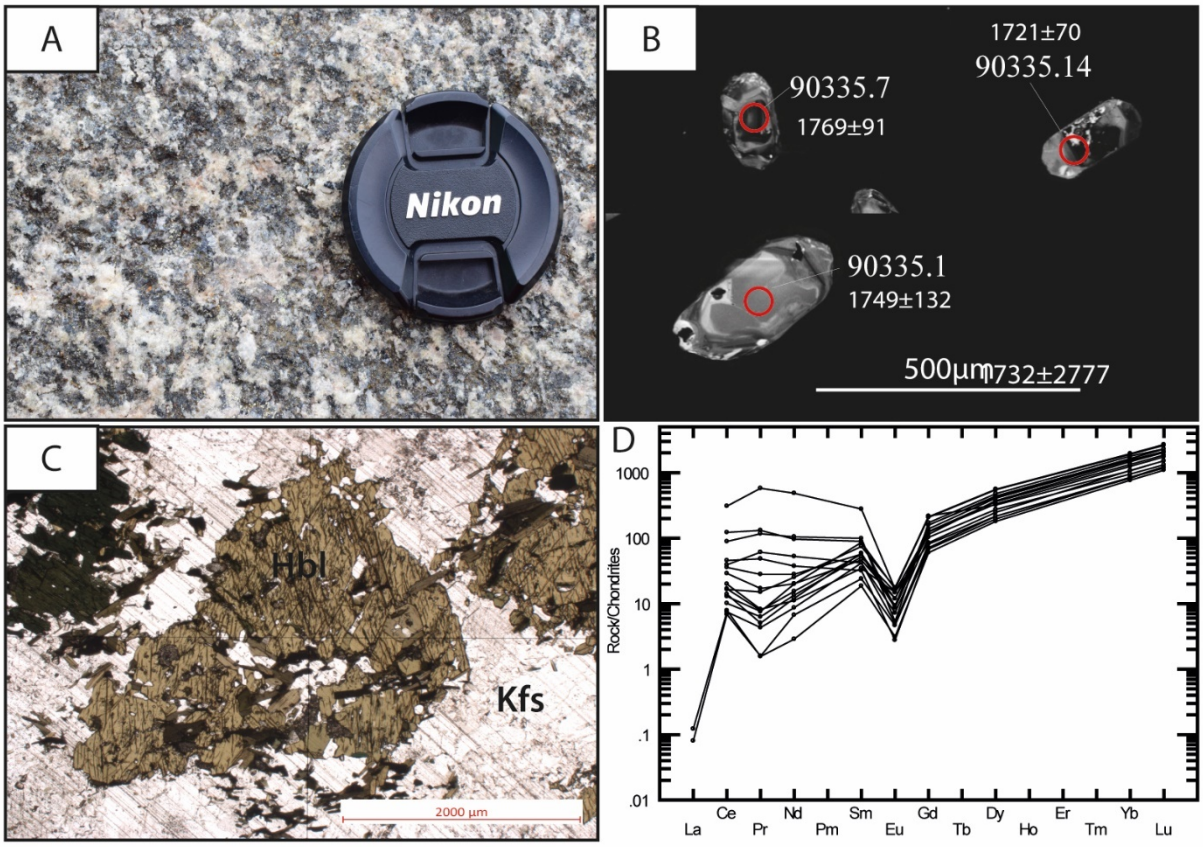

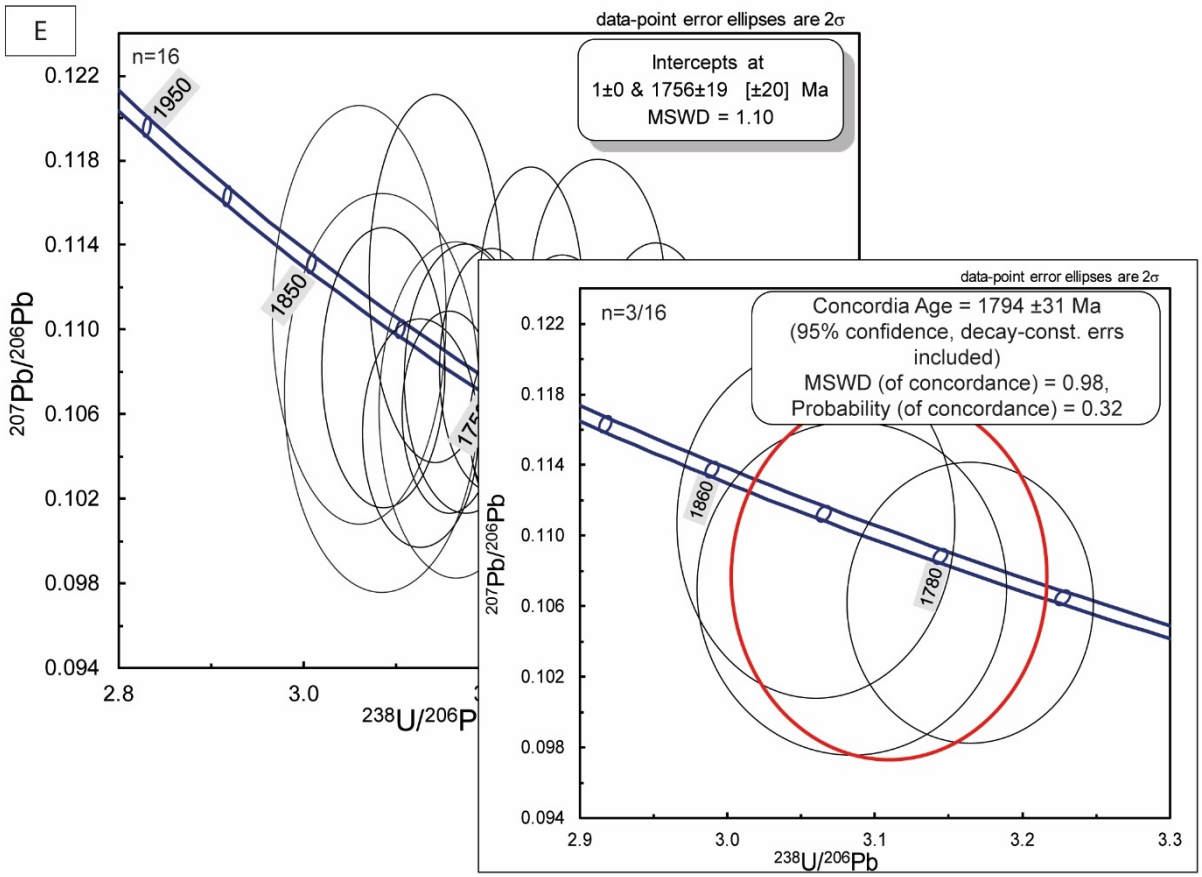

Figure 5.11: *Sample 90335. A) Photo of the texture of the rock, as it appears in the field. B) CL-images showing internal textures of three of the zircon grains that were analysed by LA-ICP-MS together with the U-Pb age (red circle indicates where the laser spot was aimed). C) Microphotograph (PPL) showing large grains of hornblende in a feldspar grain with strong pleochroism changing from a dark to a light green colour. D) Chondrite-normalised REE spider plot showing an increase from the LREE to the HREE and a negative Eu anomaly. Note how three of the grains from the sample have a detectable concentration of La, these three grains are the ones that are considered to reflect the crystallization age. E) A Tera-Wasserburg plot with all the grains that were analysed. The diagram in the lower right corner shows the Concordia age that was calculate from three of the grains.*

5.2.3 Granite

Sample 90336

This is a granitic sample taken from the eastern side of Grytøya. The rock is coarse-grained and appears with a slightly deformed texture in field (Figure5.12A). Phenocrysts of feldspar gives the rock a pink colour in field, with the more mafic minerals giving it a darker shade. The rock is made up of mainly k-feldspar, biotite and quartz. Accessory minerals are epidote, muscovite and allanite. A microphotograph of the sample shows that there is a clear magmatic foliation formed by the biotite (Figure 5.12C).

This sample from a porphyritic, foliated granite on Grytøya shows transparent to brown coloured zircons. The grains show a subrounded shape and vary in size from 200 to 600 µm, a wide range that caused a loss of some of the zircons during the polishing of the zircon mount. The CL-pictures show grains that are not fresh and most of the internal texture is patchy zoning with CL-bright spots (Figure 5.12B). Only two of the 15 grains show growth zoning. Four of the zircons show a dark (black) core with a lighter rim and

each and all of them were removed from the U-Pb age calculation due to high alpha dose, together with two other grains that also showed a high alpha dose and highly elevated LREE values (Figure 5.12D). The Th/U ratio is very clear, no grains plot lower than 0.53 and the highest ratio is found to be 1.79 indicating magmatic zircons. The U-Pb data give an age of 1784±38 Ma based on 9 of the 15 grains (Figure 5.12E). The Hf evolution plot shows a similar trend as for the two granitic/granodioritic samples from Krøttøya with ε_{Hf} values in the range of (-6.7 to -12.6) giving an accumulation of grains plotting closer to the Archean crustal evolution line. The sample has a ε_{Nd} value of -7.85.

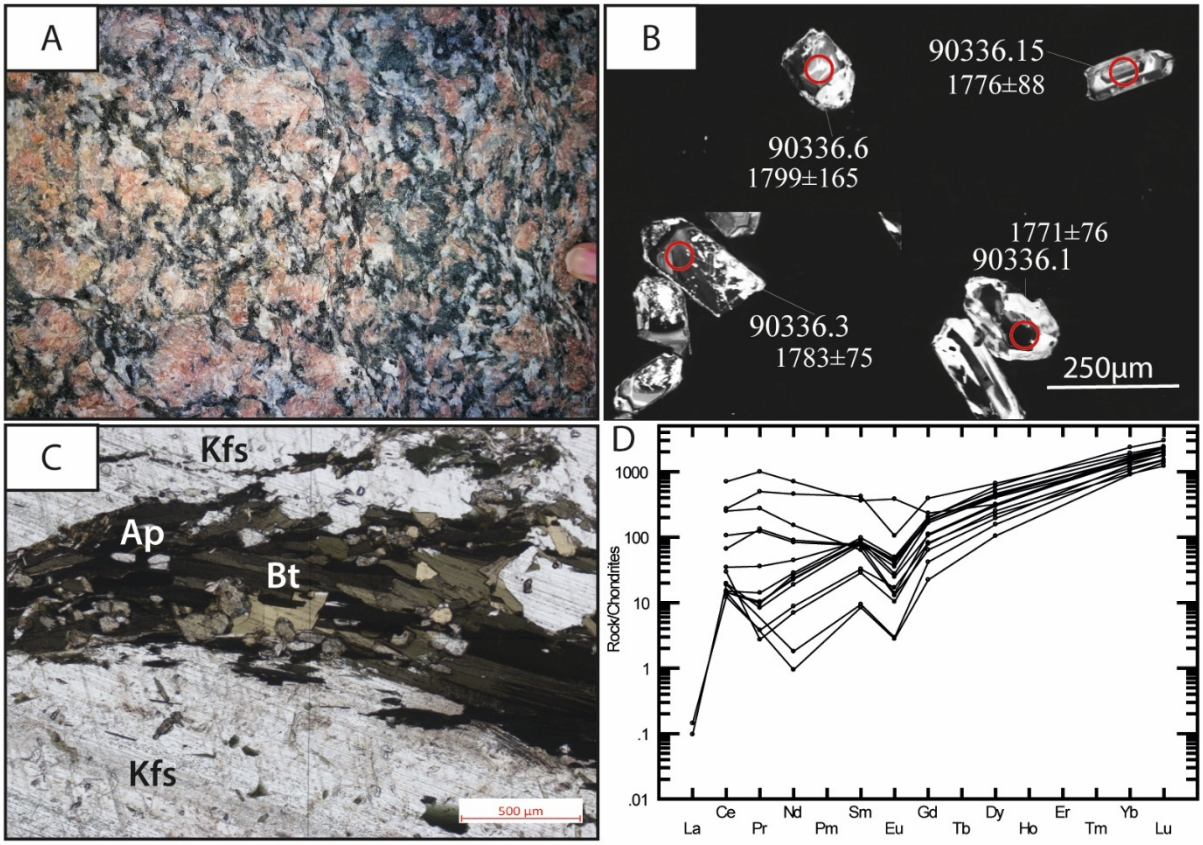

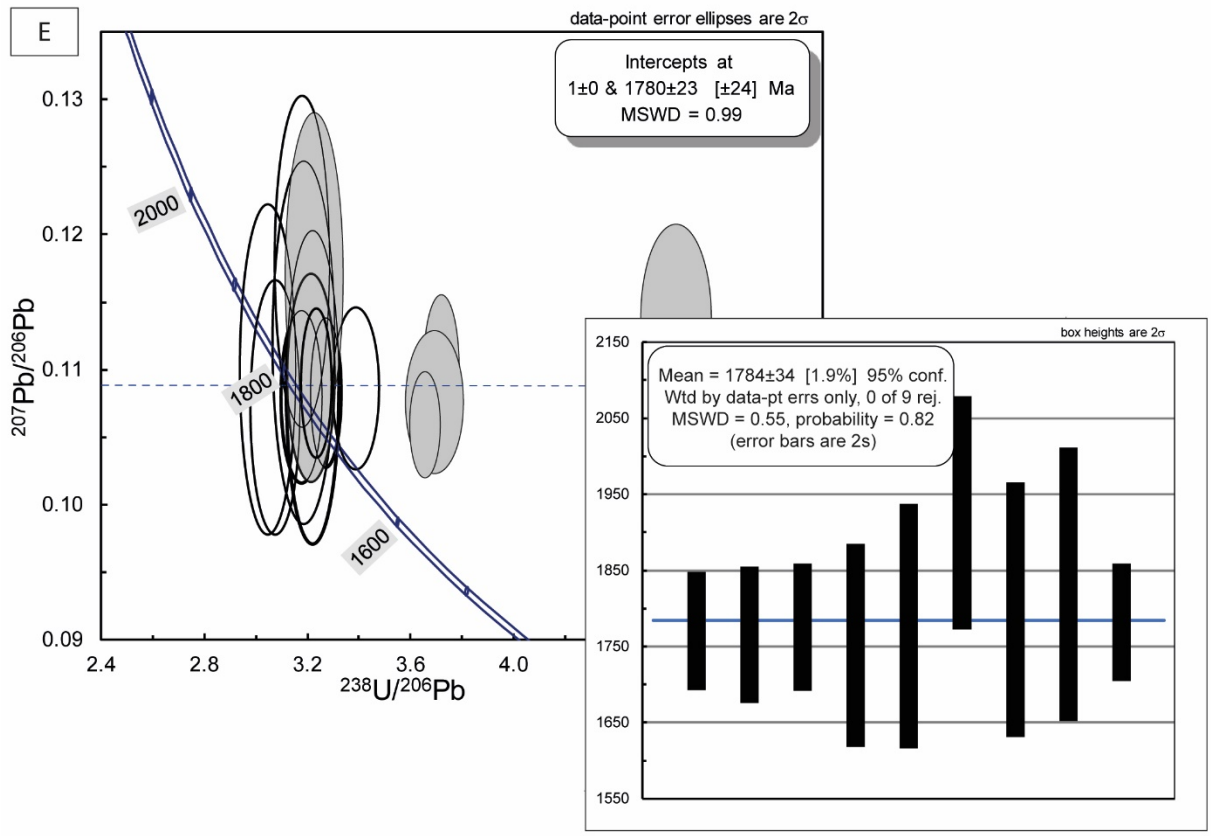

Figure 5.12: *Sample 90336. A) Photo of the texture of the rock, as it appears in the field. B) CL-images showing internal textures of seven of the zircon grains that were analysed by LA-ICP-MS together with the U-Pb age for four of them (red circle indicates where the laser spot was aimed). C) Microphotograph (PPL) showing a clear magmatic foliation of biotite grains with inclusions of apatite. D) Chondrite-normalised REE spider plot showing an increase from the LREE to the HREE and a negative Eu anomaly. The grains that were removed are shown with elevated LREE values. E) A Tera-Wasserburg plot with all the grains that were analysed, assuming recent lead loss (grey ellipses are grains that were removed from the calculation). The diagram in the lower right corner shows a weighted average for 9 of the 14 grains that had a low alpha dose and normal LREE values. (Blue line indicates the mean (calculated age), and the columns illustrate the range of uncertainty).*

Sample 90339 (granite)

This sample was collected in an outcrop on the southwestern side of Grytøya. The sample is a coarse-grained granite, with phenocrysts of k-feldspar (Figure 5.13A). The rock is seen with a pink colour in field, surrounded by white to black crystals of quartz and plagioclase. Grains of biotite gives the rock a darker colour. Accessory minerals are epidote, iron oxide and zircon. The rock shows no distinct foliation and appears homogenous in the sampled outcrop. In the microscope, coarse-grained biotite can be observed with fine-grained zircons appearing as inclusions, surrounded by halos (Figure 5.13C).

The zircons are pale-brown to brown coloured, with subhedral to euhedral prismatic shape. The size varies from 100 to 200 µm, the largest grains being fragments of larger zircons. The crystals show oscillatory zoning and core and rim textures in the CL images (Figure 5.13B). The majority of the grains have a Th/U ratio close to or larger than 0.5, with the concordant grains showing the highest Th/U values. Two grains were removed from the age calculation being interpreted as outliers. One grain was removed due to high alpha dose and highly elevated LREE found from the REE plot (Figure 5.13D). 7 grains lay higher

up on the Tera-Wasserburg concordia plot and could reflect zircon grains with common lead or lead loss. This was examined by a calculation of the $^{207}Pb/^{206}Pb$ ratio anchored in 1.8 Ga (blue, vertical line in Figure 5.13E). The remaining 6 grains forms the basis of the U-Pb age found to be 1811±52 Ma (Figure 5.13E). The ε_{Hf} values are in the range of (-2.1 to -12). The whole-rock ε_{Nd} value is -8.74, the most negative ε_{Nd} value found in the study area.

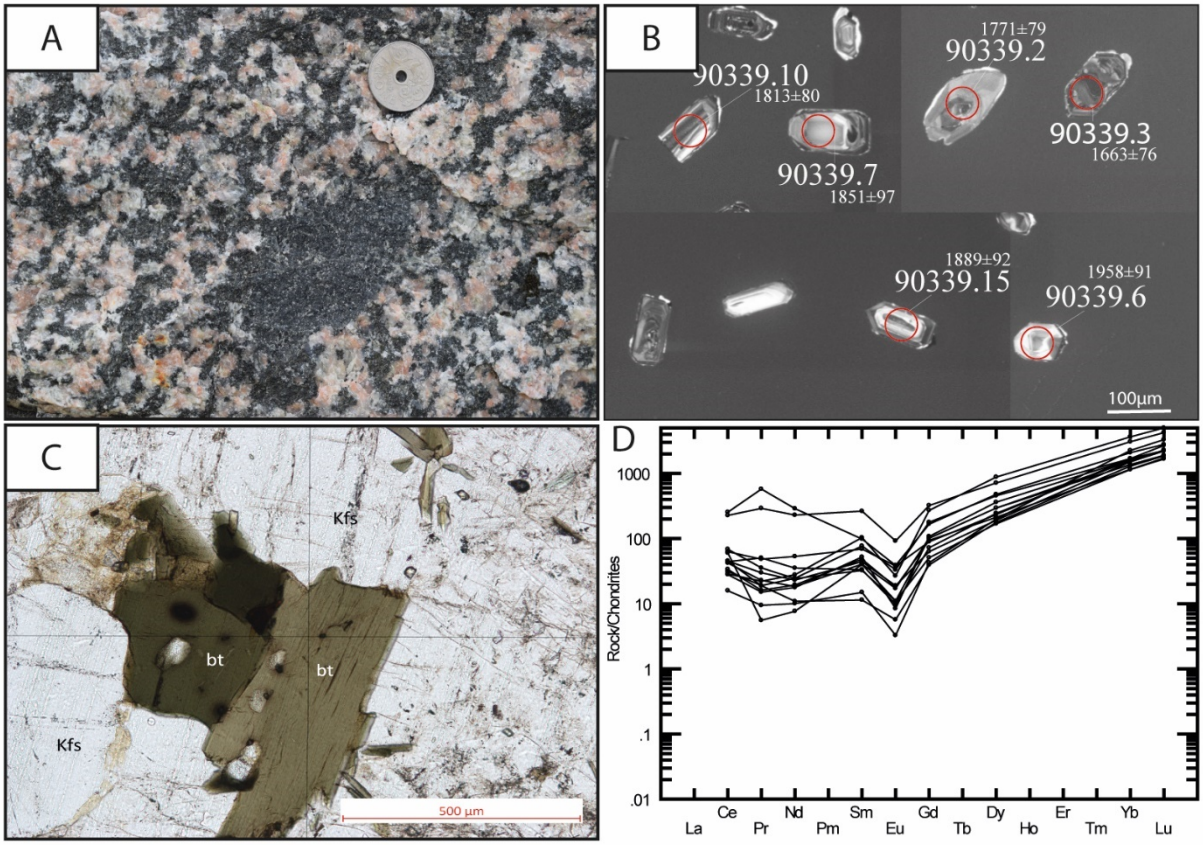

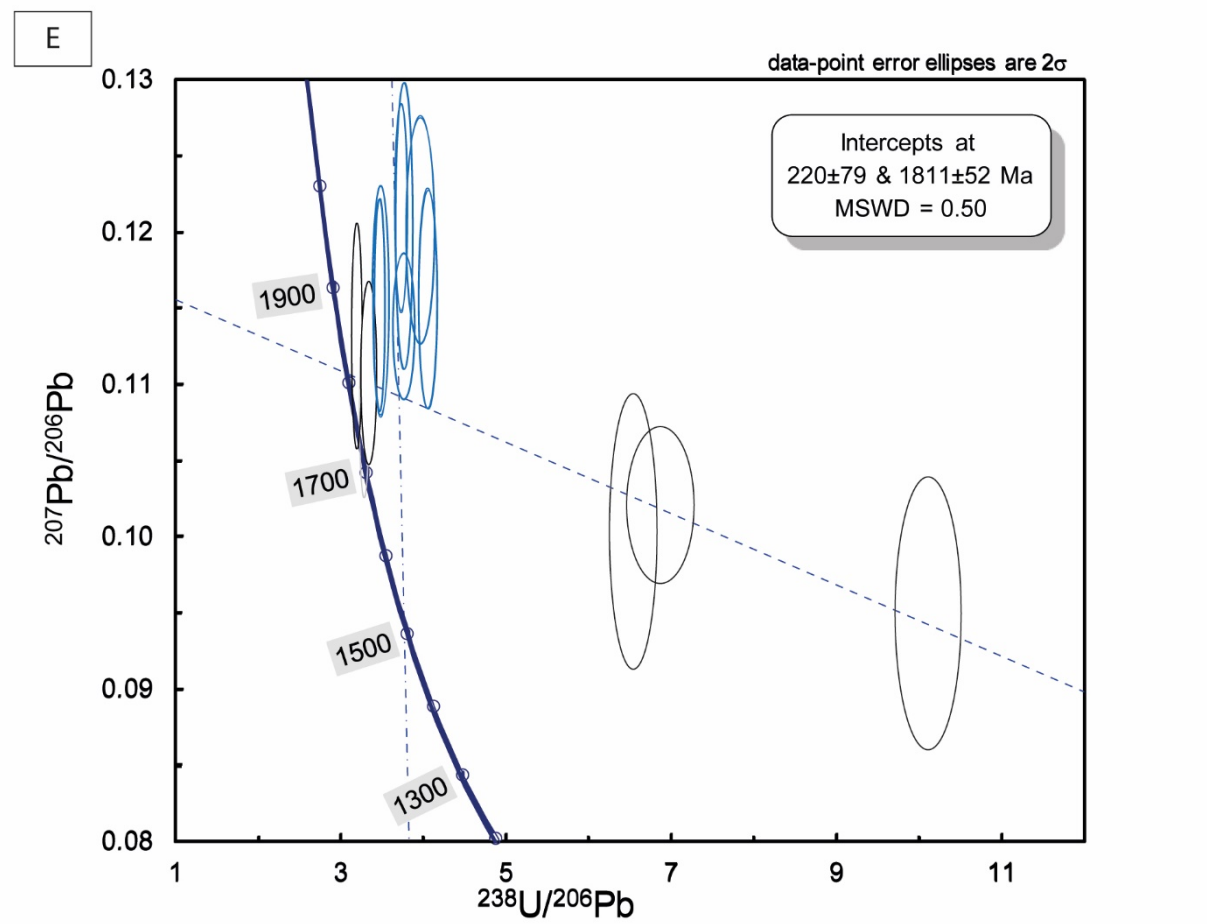

Figure 5.13: *Sample 90339. A) Photo of the texture of the rock, as it appears in the field. B) CL-images showing internal textures of six of the zircon grains that were analysed by LA-ICP-MS together with the U-Pb age (red circle indicates where the laser spot was aimed). C) Microphotograph (PPL) showing interstitial biotite grains and k-feldspar, with inclusions of zircon. D) Chondrite-normalised REE spider plot showing an increase from the LREE to the HREE and a negative Eu anomaly. As can be seen from the spider plot, some of the grains have an elevated value for La. This is reflected in E) A Terra-Wasserburg plot with all the grains that were analysed. The vertical blue line that intercepts the concordia at 1500 Ma is a modelling of the $^{207}Pb/^{206}Pb$ ratio anchored in 1.8 Ga. The purpose of this modelling was an attempt to explain why some of the grains plots further up than the other and whether this could be a common lead feature. It is not found to be that and could just be a result of inheritance. The numbers used to calculate the $^{207}Pb/^{206}Pb$ ratio at 1.8 were; $^{207}Pb/^{204}Pb$=15.303 divided by $^{206}Pb/^{204}Pb$=15.664, which gives a $^{207}Pb/^{206}Pb\approx0.98$ at t=1.8 Ga (Faure and Mensing, 2005).*

Sample 90341 (granite)

This sample was collected from the southwestern side on Grytøya, in an outcrop of porphyritic granite. The texture consists of large (up to 5cm) phenocrysts of feldspar, in a matrix consisting of amphibole and quartz (Figure 5.14A). Accessory minerals are epidote, apatite, titanite and allanite. The microphotographs show a porphyritic texture with some of the coarse feldspar grains showing replacement textures (Figure 5.14C).

The zircons are brown in colour and do not look very fresh. The shape varies from subhedral to anhedral prisms, where some of the anhedral grains are just fragments of a larger grain.

A few grains can be described as more rounded. The size of the crystals is in the range of 100 to 250 µm. The CL-images shows oscillatory growth zoning (Figure 5.14B) in most of the zircons, with some grains having a patchier zoning pattern. The Th/U ratio was found to be in the range of (0.31 to 0.72). The REE were plotted on a spider plot (Figure 5.14D) and three grains were removed based on highly elevated LREE concentrations, another two grains were removed due to very high alpha dose, whilst two grains were removed due to both elevated LREE and high alpha dose. Three grains appeared as discordant outliers, while three grains were classified as discordant. The remaining 17 grains gave a U-Pb age of 1770±16 Ma (Figure 5.14E). The ε_{Hf} values were found to be in the range (-5 to -12), possible slightly more mafic than the granitic sample 90339. The whole-rock ε_{Nd} value of this sample was found to be -7.58.

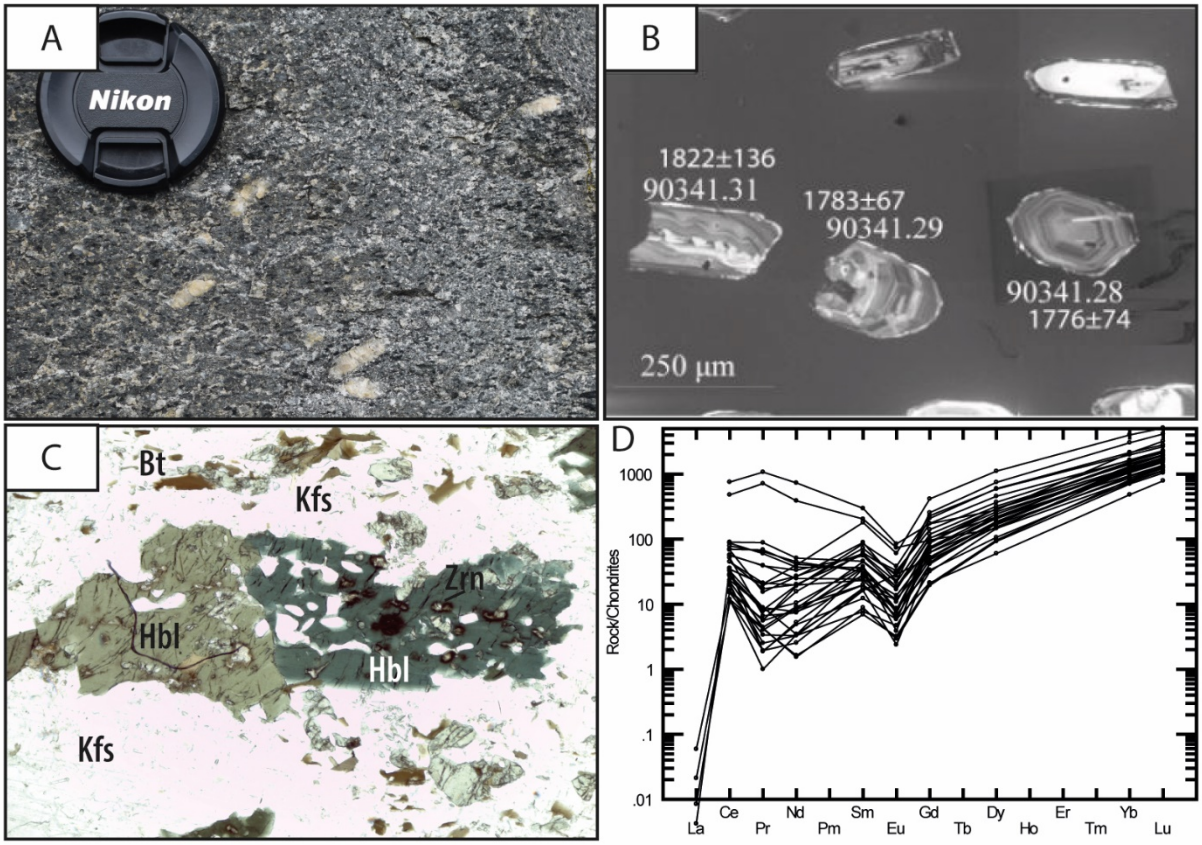

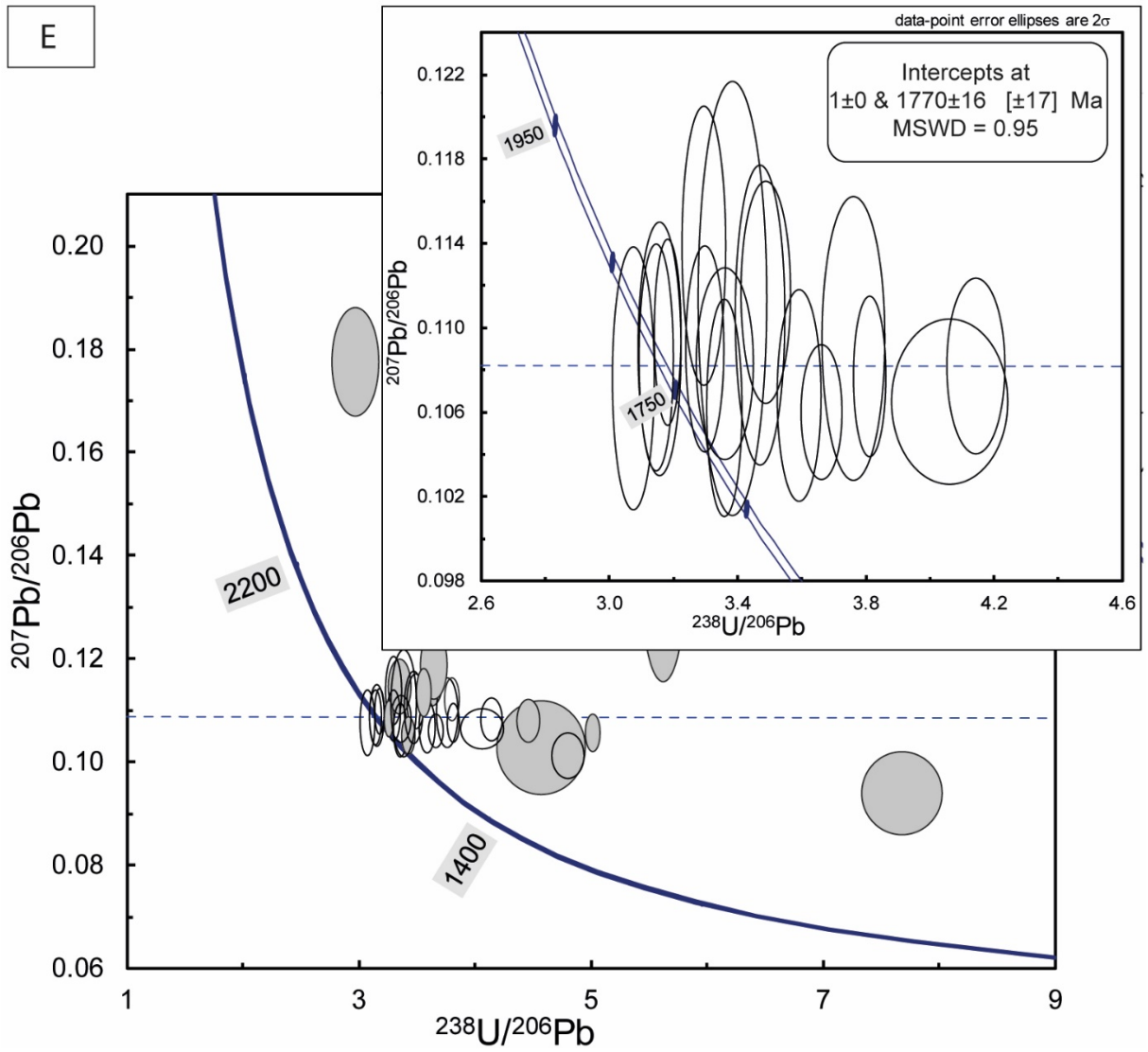

Figure 5.14: *Sample 90341. A) Photo of the texture of the rock, as it appears in the field. B) CL-images showing internal textures of three zircon grains that were analysed by LA-ICP-MS together with the U-Pb age (red circle indicates where the laser spot was aimed). C) Microphotograph (PPL) showing replacement processes of a larger feldspar grain, surrounded by fine-grained quartz and feldspar grains. D) Chondrite-normalised REE spider plot showing an increase from the LREE to the HREE and a negative Eu anomaly. As can be seen from the spider plot, some of the grains have a very elevated value for La, whilst four grains have a very low La concentration. E) A Tera-Wasserburg plot with all the grains that were analysed for the sample, assuming recent lead loss (grey ellipses are grains that were removed from the calculation). The diagram in the upper right corner shows the calculated U-Pb age.*

Sample 90342 (granite)

This sample was collected on the western side of Grytøya. The outcrop where the sample was taken shows a coarse-grained granitic rock with a mineral assemblage of feldspar, plagioclase, quartz, biotite and epidote. It also shows mafic xenoliths (Figure 5.15A). The study of the rock in thin section show phenocrysts of orthoclase surrounded by coarse-grained quartz, biotite, microcline and epidote (Figure 5.15C).

The zircon crystals of this sample are all prismatic, subhedral to euhedral in shape and vary in size from 150 to 300 µm. The majority of the zircons have small cracks or voids within them and imply that the grains are not very fresh, supported by their brown colour. The CL-images show very poor zircons that has a patchy texture, only a few grains showing something that might look like a core and rim texture (Figure 5.15B). Trace element geochemistry of the sample shows that the Th/U ratio of the grains are close to 1.0 indicating a magmatic origin. Three discordant outliers were removed from the U-Pb data. Eight other analyses were removed based on their REE data (Figure 5.15D). The remaining 9 analyses were found to have a regression line cutting the discordia curve at 1764±20 Ma, assuming recent Pb loss (anchored in 1 ± 0 Ma). The εHf values are found to be in the range -7.9 to -11.3, whilst the εNd value is found to be -7.3.

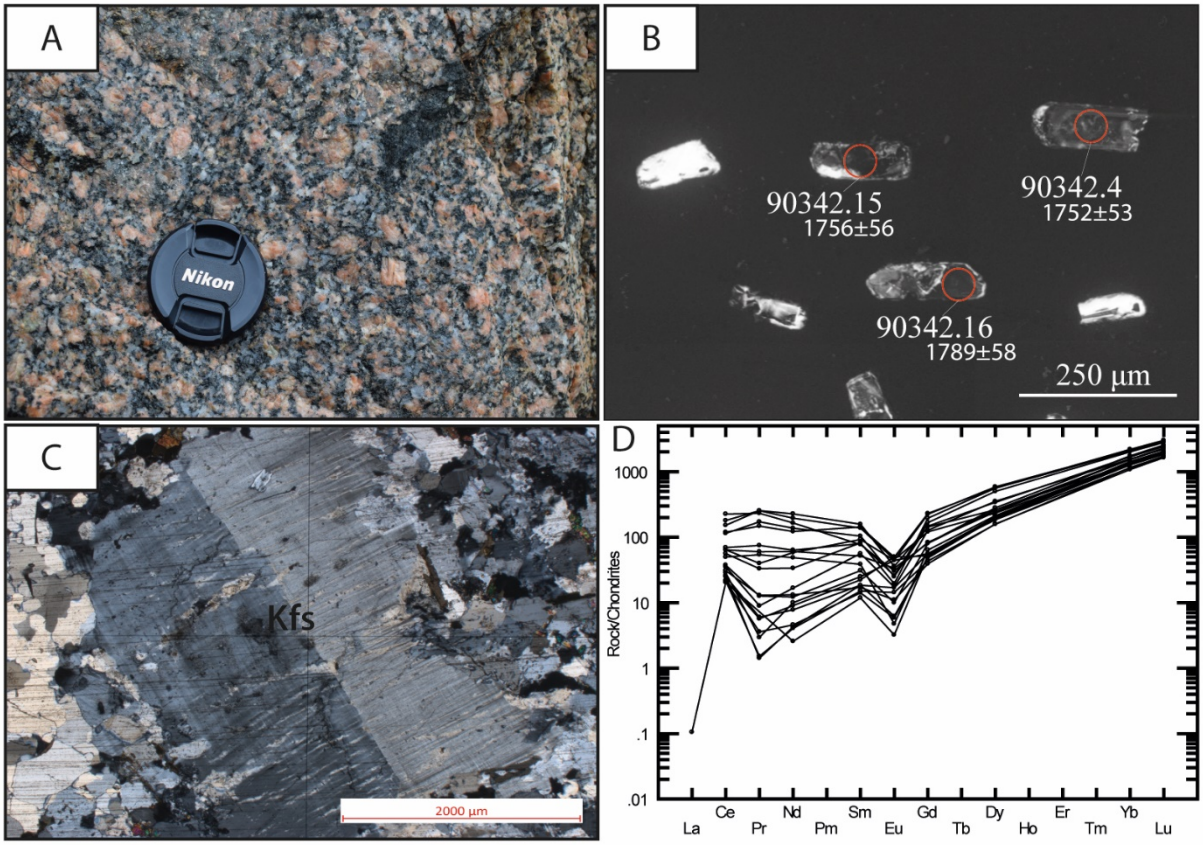

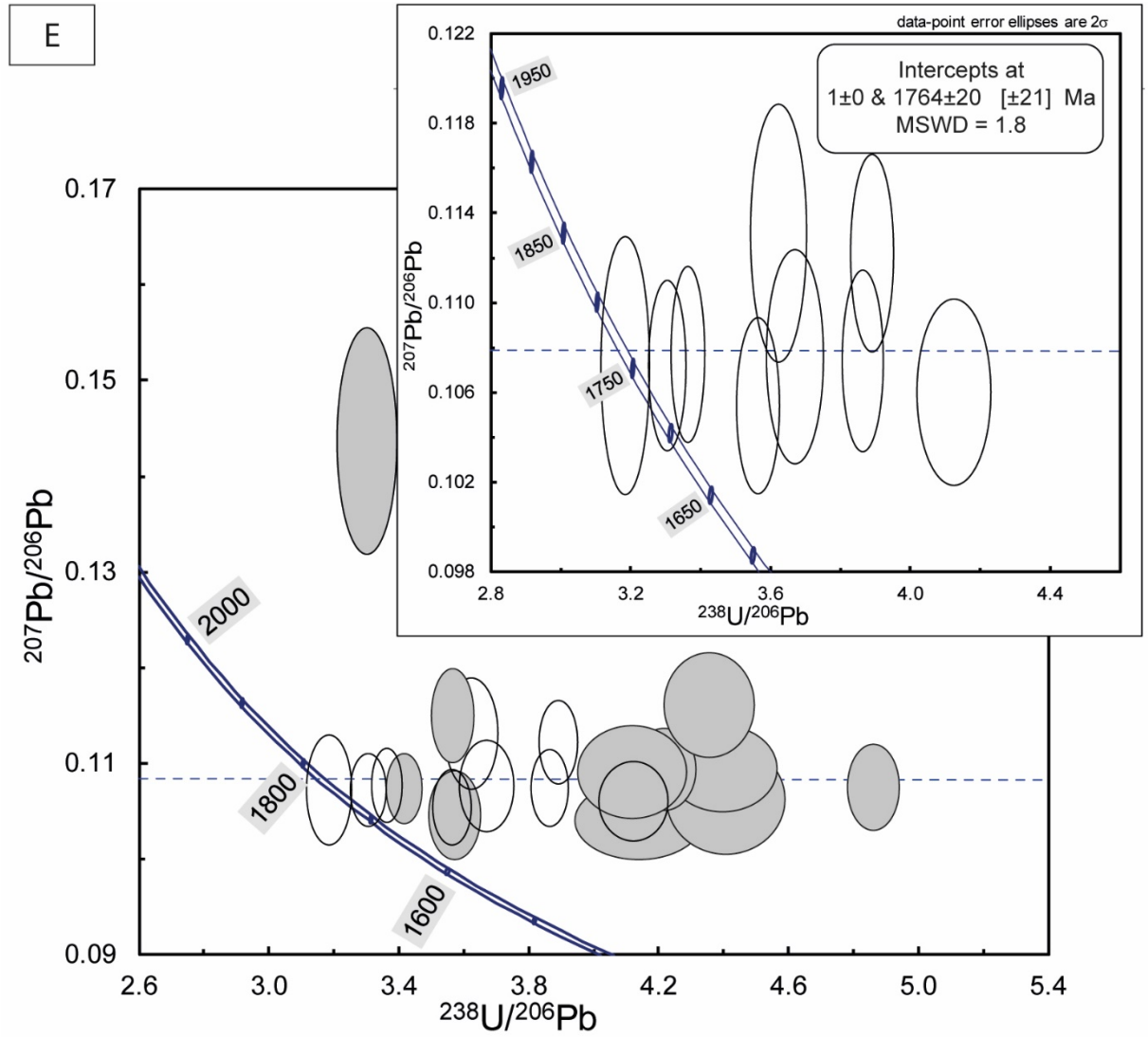

Figure 5.15: *Sample 90342. A) Photo of the texture of the rock, as it appears in the field. B) CL-images showing internal textures of three zircon grains that were analysed by LA-ICP-MS together with the U-Pb age (red circle indicates where the laser spot was aimed). C) Microphotograph (PPL) that shows a porphyritic texture, with phenocrysts of perthitic orthoclase surrounded by intermediate to coarse-grained quartz and biotite. D) Chondrite-normalised REE spider plot showing an increase from the LREE to the HREE and a negative Eu anomaly, with one grain plotting at a very at a low La concentration. E) A Tera-Wasserburg plot with all the grains that were analysed for the sample (grey ellipses are grains that were removed from the final calculation). The diagram in the upper right corner shows the calculated U-Pb age.*

Sample 140808 (granite)

This sample was collected on the southwestern side of Bjarkøya and is a granitic rock similar to the ones found on Grytøya and Sandsøya. It appears coarse-grained with a pink colour in the field. The mineral assemblage that can be observed by the naked eye is feldspar, quartz, amphibole and biotite (Figure 5.16A). In thin section the mineral allanite can be observed, together with the accessory minerals of epidote, titanite and apatite. The allanite is presented with a zoning, most certainly caused by radioactive decay of Th and U (Figure 5.16C)

The rock is rich in zircon and they appear mostly pale-brown coloured. The zircons are prismatic, subhedral and the size is in the range of 150 to 250 µm. Most of the crystals show oscillatory zoning or a clear core and rim internal texture in the CL-images (Figure 5.16B). The Th/U ratio for the zircons are close to or larger than 1, indicating a magmatic origin. Out of 36 grains six zircons were discordant outliers and removed from the U-Pb data set. REE spider plots (Figure 5.16C) were used to study the geochemistry of the zircons and seven grains were found to have a highly elevated LREE pattern, these were removed from the data set. The remaining 23 zircon analyses gave a concordia age of 1767.6±9.3 Ma (Figure 5.16E). This age is interpreted to be the crystallization age of the rock. The young age resemble the U-Pb age found for the granite on Sandsøya. The Hf data gives ε_{Hf} values in the range -6.5 to -18.7.

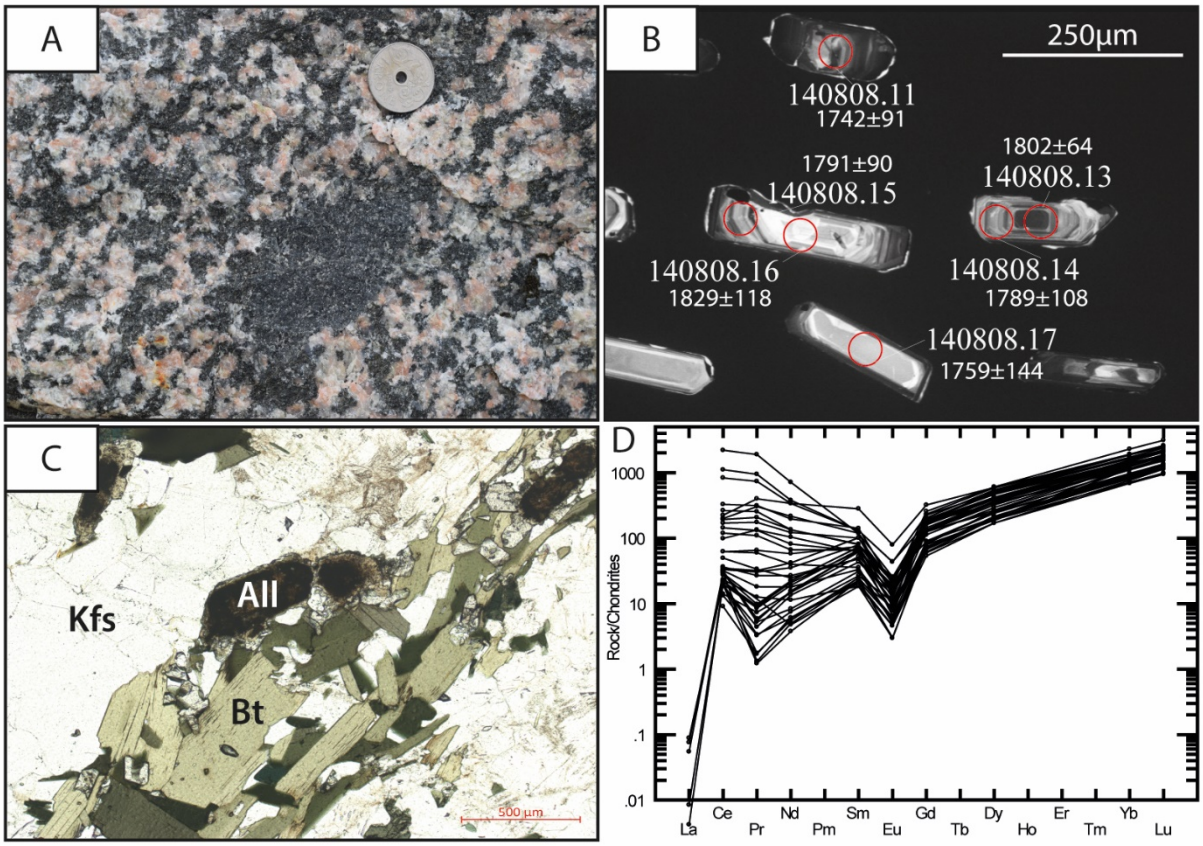

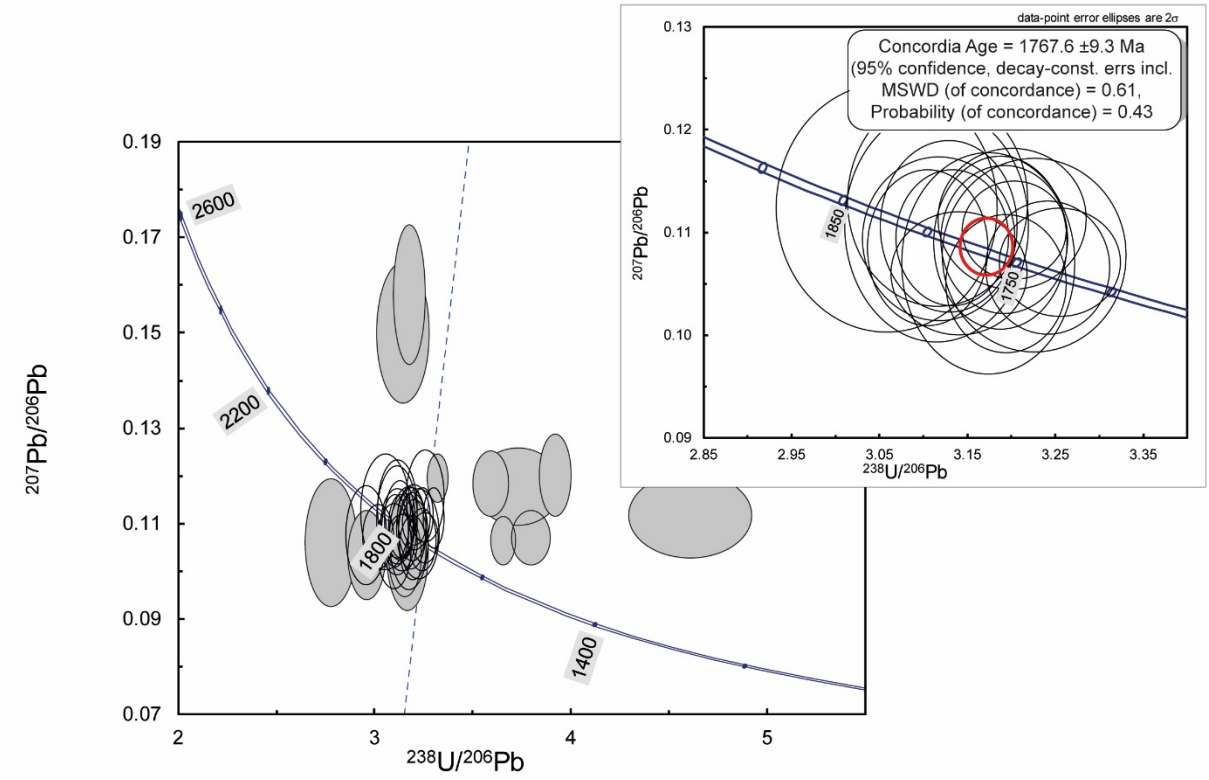

Figure 5.16: *Sample 140808. A) Photo of the texture of the rock, as it appears in field. B) CL-images showing internal textures of four zircon grains that were analysed by LA-ICP-MS together with the U-Pb age (red circle indicates where the laser spot was aimed). C) Microphotograph (PPL) of a zoned allanite grain. D) Chondrite-normalised REE spider plot showing an increase from the LREE to the HREE and a negative Eu anomaly. E) Tera-Wasserburg plot with all the grains that were analysed from the sample, assuming recent lead loss (grey ellipses are grains that were removed from the final calculation). The diagram in the upper right corner shows the calculated concordia age.*

5.2.4 Gneiss

Sample 140813 (gneiss)

This sample was taken from the northwest side of Bjarkøya, in the supracrustal unit. It is a fine-grained gneissic, migmatitic rock with a mineral assemblage of feldspars, amphibole, pyroxene and quartz. The amphibole is concentrated in melanosomes, whilst the quartz and feldspars form leucosomes. The pyroxene forms the green nuggets (Figure 5.17A-B).

The zircons are all subhedral in shape and more rounded than prismatic. The grains have a pale-brown colour and show small cracks within them. The size varies in the range of 150 to 200 µm, with a few grains being larger. The CL images of the zircon grains show internal core and rim textures and some grains with oscillatory zoning patterns (Figure 5.17B). The Th/U ratio range from 0.12 to 0.54, generally much lower values than for the granites. Five discordant grains were excluded from the age calculation, and three grains were removed due to elevated LREE values (Figure 5.17D). The remaining 9 grains were found to have a U-Pb age of 1882±47 Ma (Figure 45E). The ε_{Hf} values vary from -6.1 to -18.2.

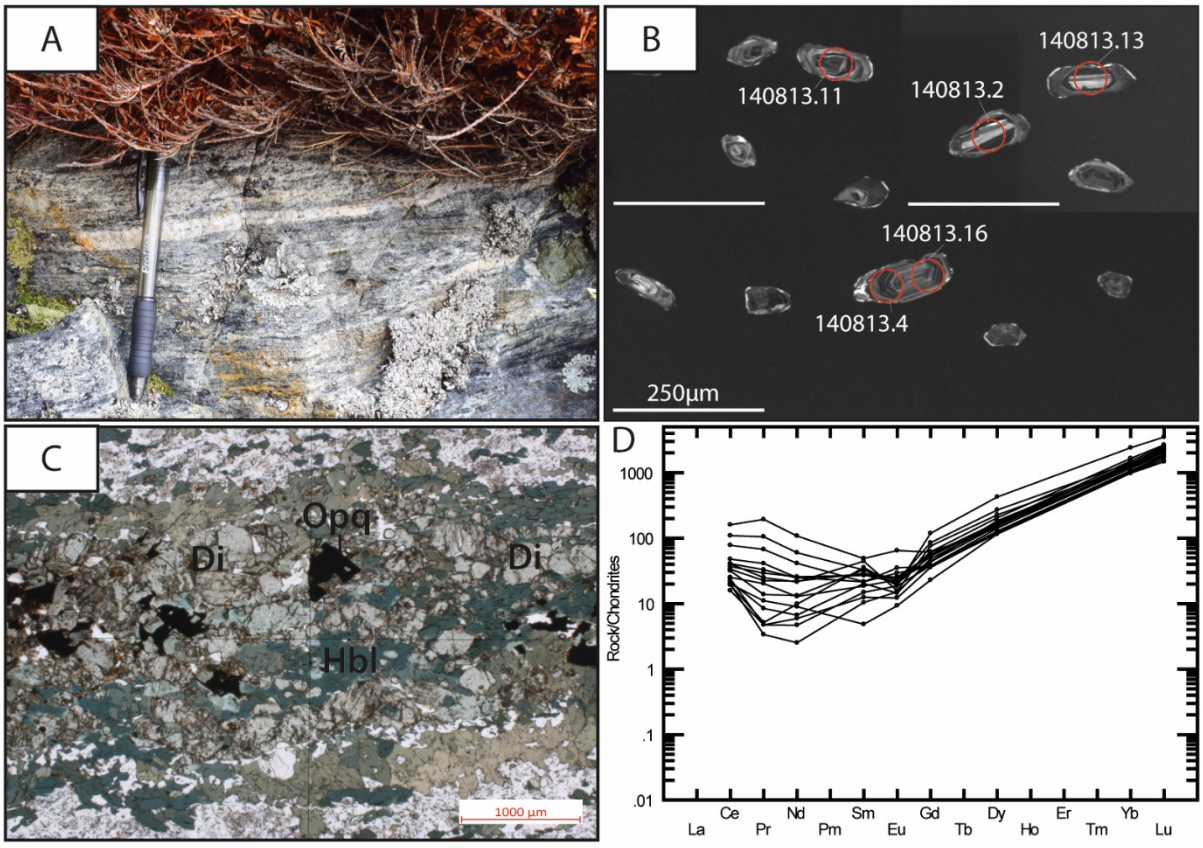
A
B
140813.13
140813.11
140813.2
140813.16
140813.4
250µm
C
Opq
Di
Di
Hbl
1000 µm
D
1000
100
10
1
.1
.01
Rock/Chondrites
La
Ce
Pr
Nd
Pm
Sm
Eu
Gd
Tb
Dy
Ho
Er
Tm
Yb
Lu

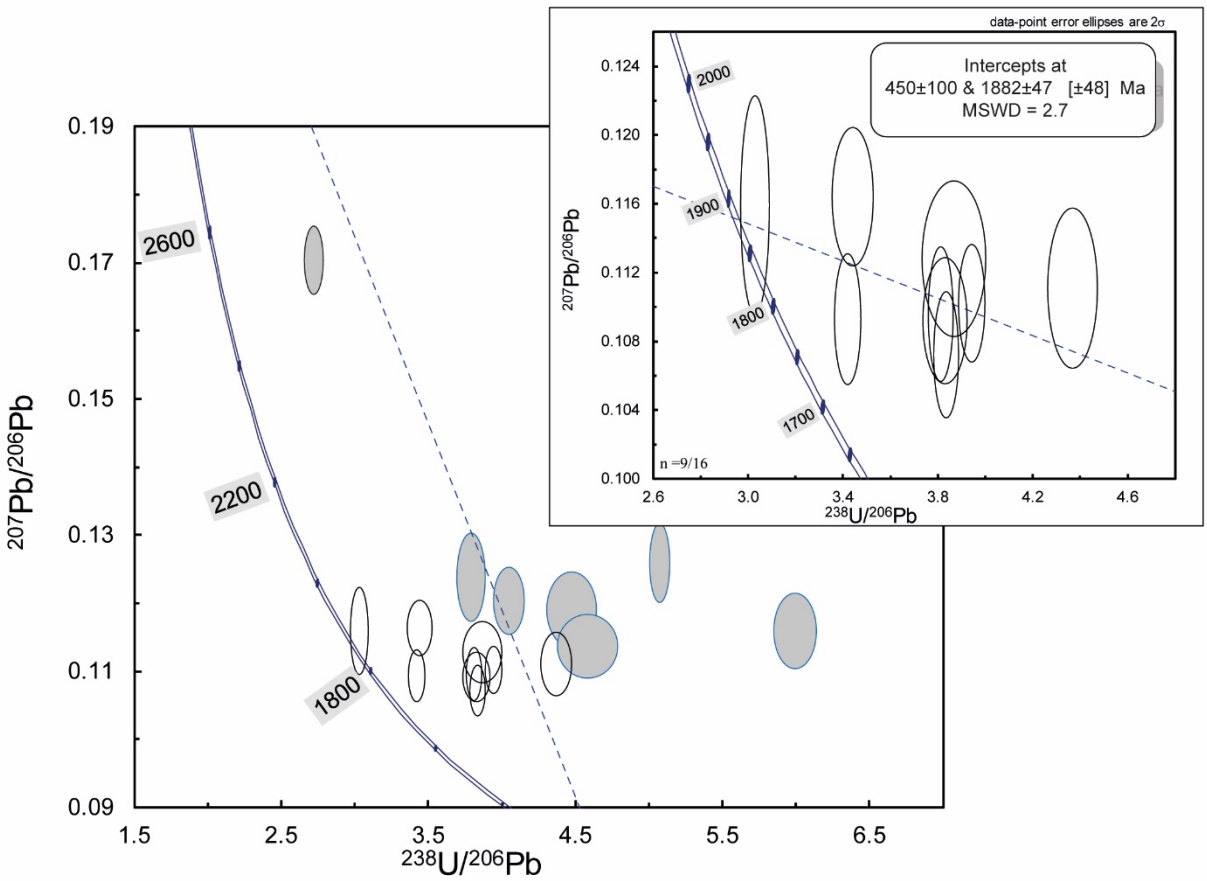

Figure 5.17:*Sample 140813. A) Photo of the outcrop. B) CL-images showing internal textures of four zircon grains that were analysed by LA-ICP-MS together with the U-Pb age (red circle indicates where the laser spot was aimed). C) Microphotograph (PPL) of one of the diopside pebbles, in the middle of a melanosome formed by hornblende. D) Chondrite-normalised REE spider plot showing an increase from the LREE to the HREE and a negative Eu anomaly for all grains except two. The La concentration is very high for most of the grains. E) Tera-Wasserburg plot with all the grains that were analysed for the sample (grey ellipses are grains that were removed from the final calculation, grey ellipses with blue outlines are grains that might be affected by common lead and lead loss). The diagram in the upper right corner shows the calculated U-Pb age.*

Sample 140814 (gneiss)

This sample was collected from a gneiss on Bjarkøya. It is a fine-grained, gneissic rock where the migmatitic texture only seen in the microscope (Figure 5.18A and C). The mineral assemblage is of plagioclase, quartz, diopside, and contrary to the 140813 sample it contains biotite and not hornblende.

The zircons are transparent to pale-brown in colour. The smallest zircons are more prismatic than the larger ones that are rounder grain, and in general they all show a subhedral shape. The size varies in the range of 150 to 250 µm. The CL-images show grains with an internal texture of growth zoning and distinct boundaries between core and rim (Figure 5.18B). U-Pb data plotted on a concordia plot show two discordant zircon populations with one analysis that cannot be assigned to either of the two populations. These two populations are also seen in the REE plot, where the youngest population plots higher on the HREE side of the spider plot (Figure 5.18D). The oldest population is found to have a U-Pb age of 2656±50 Ma. The younger population have a U-Pb age of 1946±93

Ma and unlike the older population these zircons shows differences in the REE plot in positive and negative europium anomalies (Figure 46D). The interpretation of the sample is that the oldest population reflect the supracrustal rocks, and that the youngest zircons reflect rocks that were formed around 1.9 Ga. The ε_{Hf} values for the oldest population are in the range of -0.8 to -8.9, and a range of (-5.2 to -10.6) for the younger population. The Th/U ratio were calculated for both populations and shows that the older population has a slightly higher range (0.15 to 0.73) than the younger ones (0.11 to 0.17).

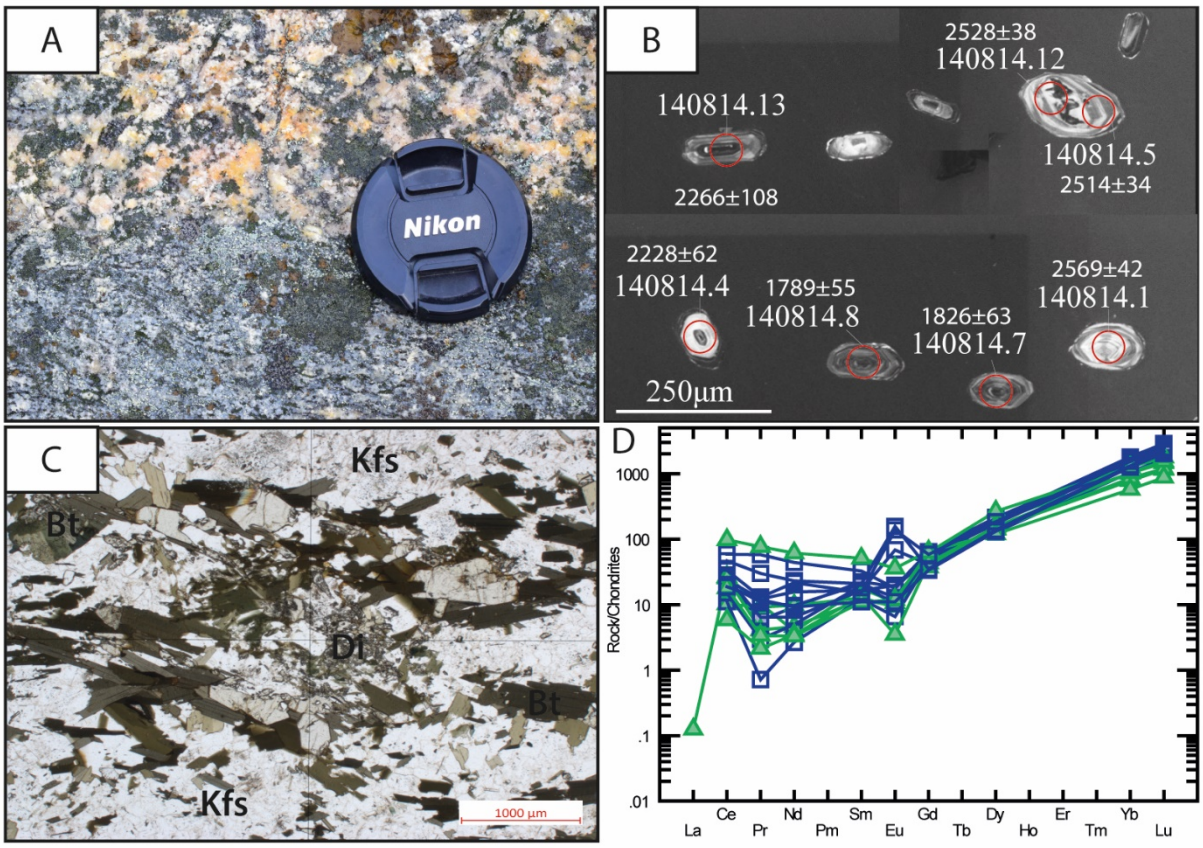

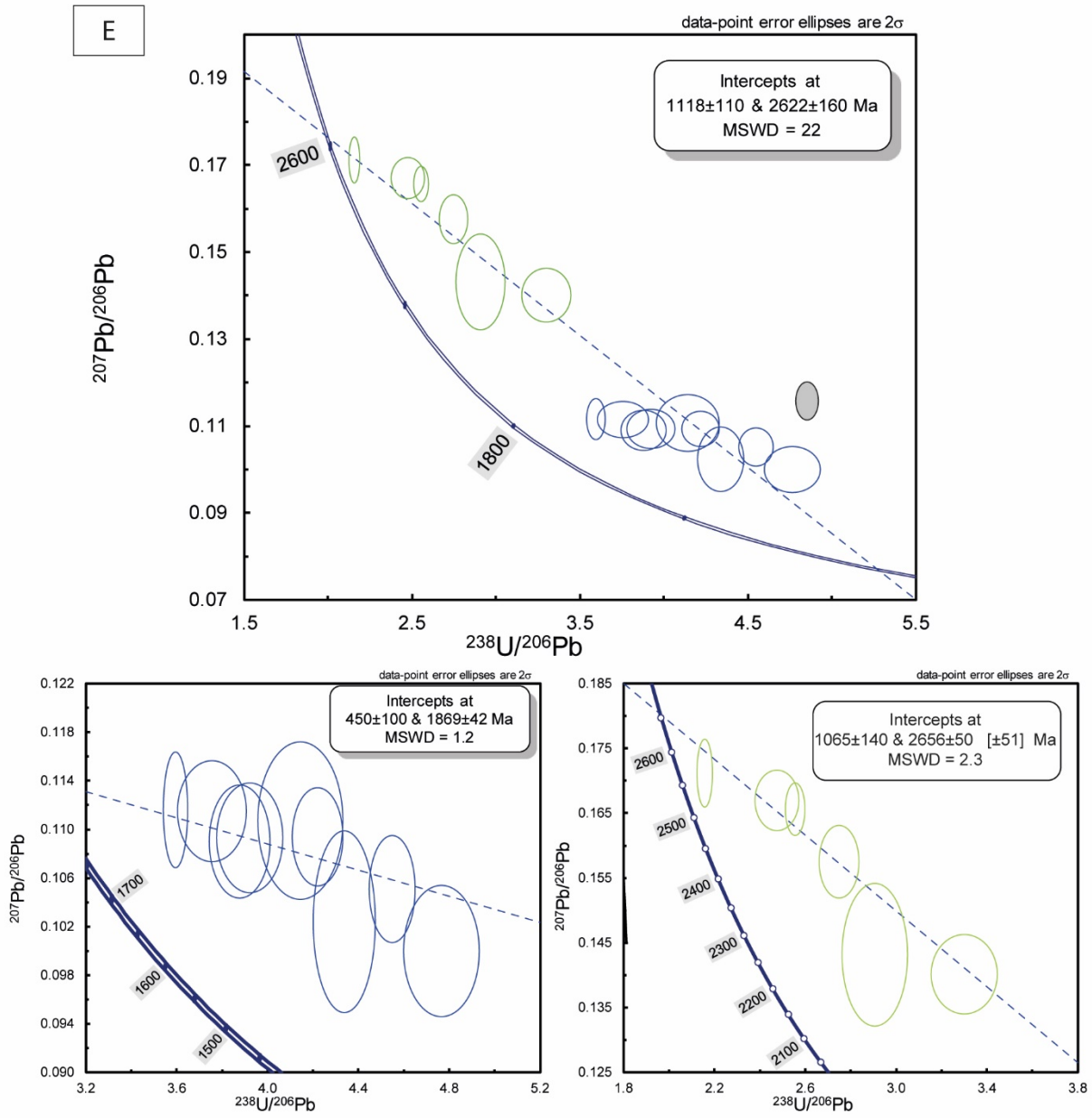

Figure 5.18: *Sample 140814.* A) Photo of the outcrop. B) *CL-images showing internal textures of six zircon grains that were analysed by LA-ICP-MS together with the U-Pb age (red circle indicates where the laser spot was aimed)*. C) Microphotograph (PPL) showing the foliation of biotite in a groundmass of euhedral diopside, quartz and k-feldspar grains. D) *Chondrite-normalised REE spider plot showing an increase from the LREE to the HREE, with a clear visualization of the two zircon populations (green indicates the oldest population, blue indicates the youngest population). There is a negative Eu anomaly* for most of the grains, except some of the grains belonging to the youngest zircon population. E) *Tera-Wasserburg plot with all the grains that were analysed for the sample (the grey ellipse is a grain that was removed from the final calculation). The diagram in the lower left corner shows the U-Pb age calculated for the youngest zircon population, the lower right corner shows the U-Pb age calculated for the oldest zircon population.*

Sample 140818

This sample was the only sample collected from Sandsøya. It is a coarse-grained to medium-grained, non-foliated granitic rock. The mineral assemblage consists of k-feldspar, plagioclase, amphibole, biotite and quartz. It appears with a light grey to pink colour in field (Figure 5.19A). Epidote appears as an accessory mineral. The sample shows a coarse-grained, non-foliated rock in the microscope, with replacive textures of the feldspar grains giving it a dusty look in PPL (Figure 5.19C).

This sample consists of transparent zircon with subhedral prismatic shapes. The size varies from 200 to 400 µm. Some of the grains are rounder, they all show cracks and inclusions. The CL images show internal textures of core and rim, with most of them being rugged (Figure 5.19B). The Th/U ratio were calculated for the 30 grains and shows a value close to 0.5, indicating a magmatic origin of the zircons. Three of the 30 analyses have been were excluded as discordant outliers. Seven other grains were removed based on their elevated LREE pattern in the REE spider plot (Figure 5.19D). The remaining 14 zircons were calculated to give a concordia age of 1768 ± 14 Ma (Figure 5.19E). This young age bears a close resemblance to the granite on Bjarkøya, implying a younger magmatic event than the known 1.8 Ga magmatic event of the region. The ε_{Hf} evolution plot give values in the range of (3.9 to -14.8).

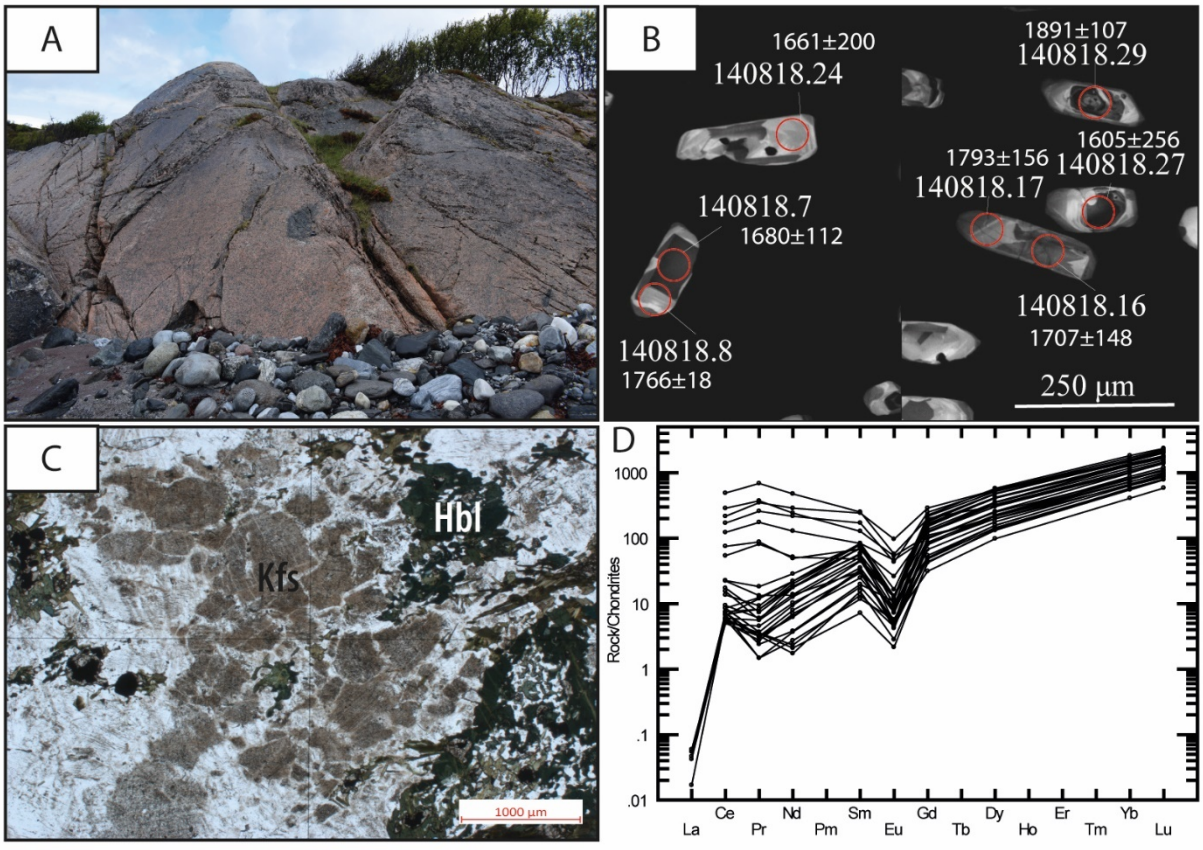

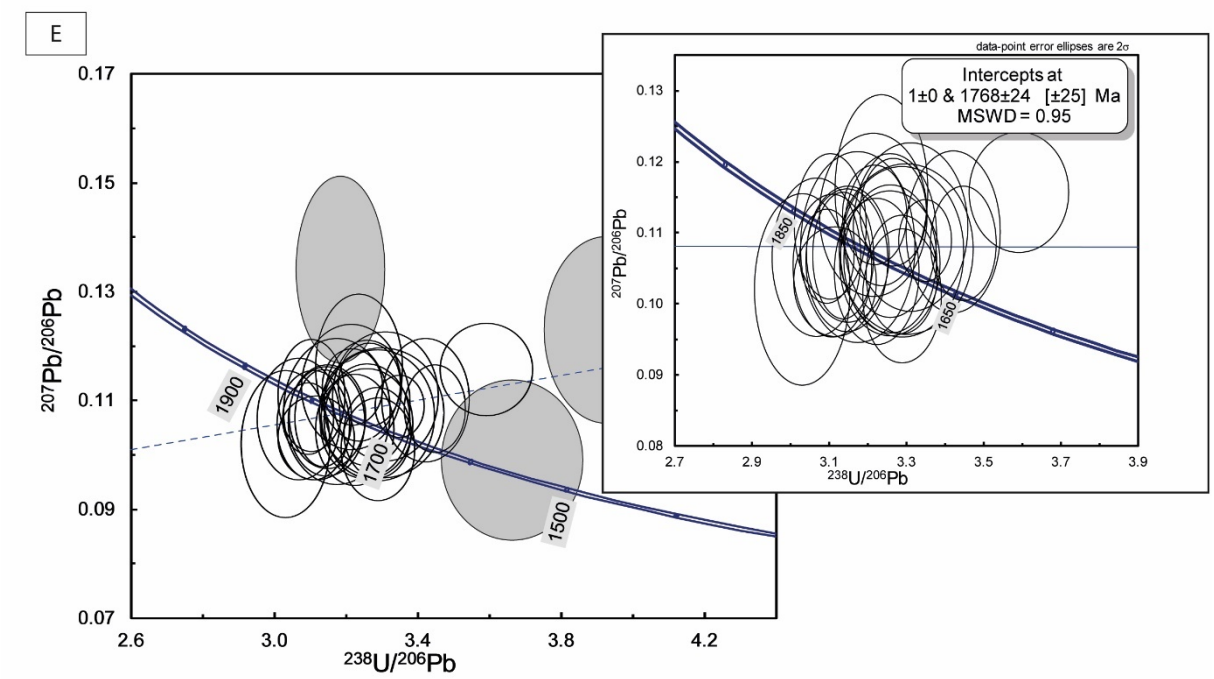

Figure 5.19: *Sample 140818.* A) Photo of the outcrop. B) *CL-images showing internal textures of five zircon grains that were analysed by LA-ICP-MS together with the U-Pb age (red circle indicates where the laser spot was aimed)*. C) Microphotograph (PPL) showing a large k-feldspar being replaced by alteration processes, surrounded by hornblende, biotite and smaller grains of feldspar. D) *REE spider plot showing that the concentration increases from the LREE to the HREE*. E) *Tera-Wasserburg plot with all the grains that was analysed for the sample (grey ellipses are grains that were removed from the final calculation). The diagram in the upper right corner shows the calculated U-Pb age after removing the discordant grains, assuming recent lead loss.*

5.2.5 Syenite and monzonite

Sample RAF131505

This sample was collected along the northern part of the Raftsund. In field, the rock can be characterized as a medium-grained, equigranular pigeonite-clinopyroxene syenite (Figure5.20A). A fresh surface shows a dark-grey to brown rock (Coint, personal communication).

The CL images show zircon grains with a size in the range of 150-250 µm, with varying degrees of internal textures (Figure 5.20B). The microphotographs (Figure 5.20C-D) show a mineral assemblage of inverted pigeonite and clinopyroxene are subhedral and rimmed locally by late hornblende. Minor subhedral biotite. Subhedral mesoperthitic alkali feldspar and plagioclase, anhedral K-feldspar, anhedral magnetite and ilmenite, euhedral apatite and rare zircon (Coint, personal communication). The zircons were analysed with SHRIMP for U-Pb ages. None of the grains were removed from the calculation, giving a U-Pb age of 1790±9 Ma (Figure 5.20E).

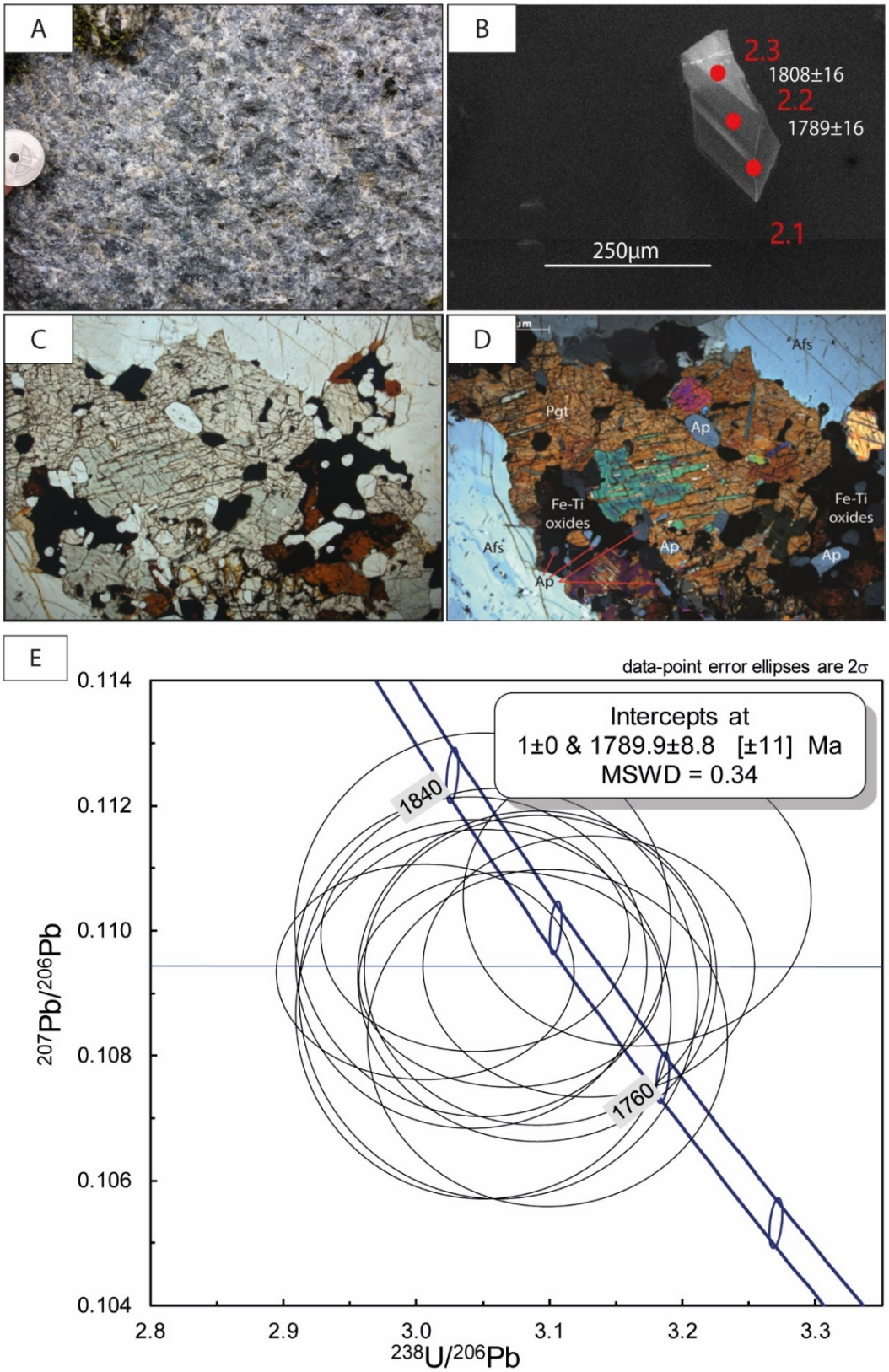

Figure 5.20: *Sample RAF131505. A) Photo of the rock as it appears in the field. B) CL-image showing internal textures of one of the zircon grains that were analysed by SHRIMP, together with the U-Pb age (red circle indicates where the laser spot was aimed). C) Microphotograph (PPL) showing the complex texture of the rock. D) Microphotograph (XPL) showing the same texture with assigned mineral assemblage. E) Tera-Wasserburg plot with all the grains plotted and the calculated U-Pb age. Microphotographs by Nolwenn Coint, field photo from Peter Ihlen.*

RAF106465 (Fayalite-clinopyroxene monzonite)

This sample is collected from the north-eastern part of Årsteinen island. The rock appears medium-grained and equigranular in field. The mineral assemblage is Clusters of subhedral clinopyroxene, fayalite, ilmenite associated with anhedral allanite and ilmenite forming a fayalite-clinopyroxene monzonite (Figure 5.21A). Hornblende is late and anhedral. Figure 5.21C shows a microphotograph of this complex mineral assemblage in PPL, the same texture is shown in XPL in Figure 5.21D. Zircon and apatite are euhedral, but zircon is much more abundant than apatite. Coronas of orthopyroxene and garnet at the border between alkali feldspar and fayalite resulting from granulite facies metamorphism of unknown age (Coint, personal communication).

The zircon that was shot with SHRIMP is in the size of 250 to 400 µm and show growth zoning (Figure 5.21B). The U-Pb age is found to be 1790.5 ± 7 Ma (Figure 5.21E).

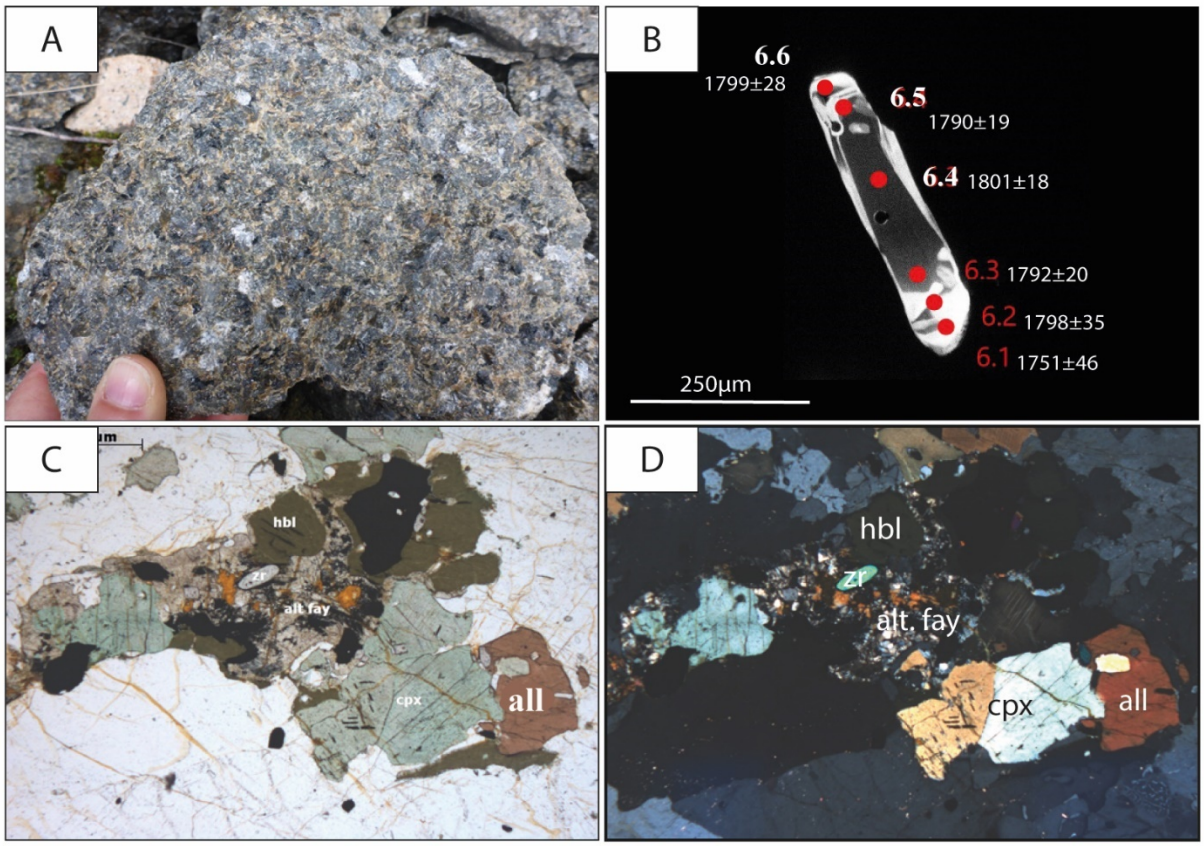

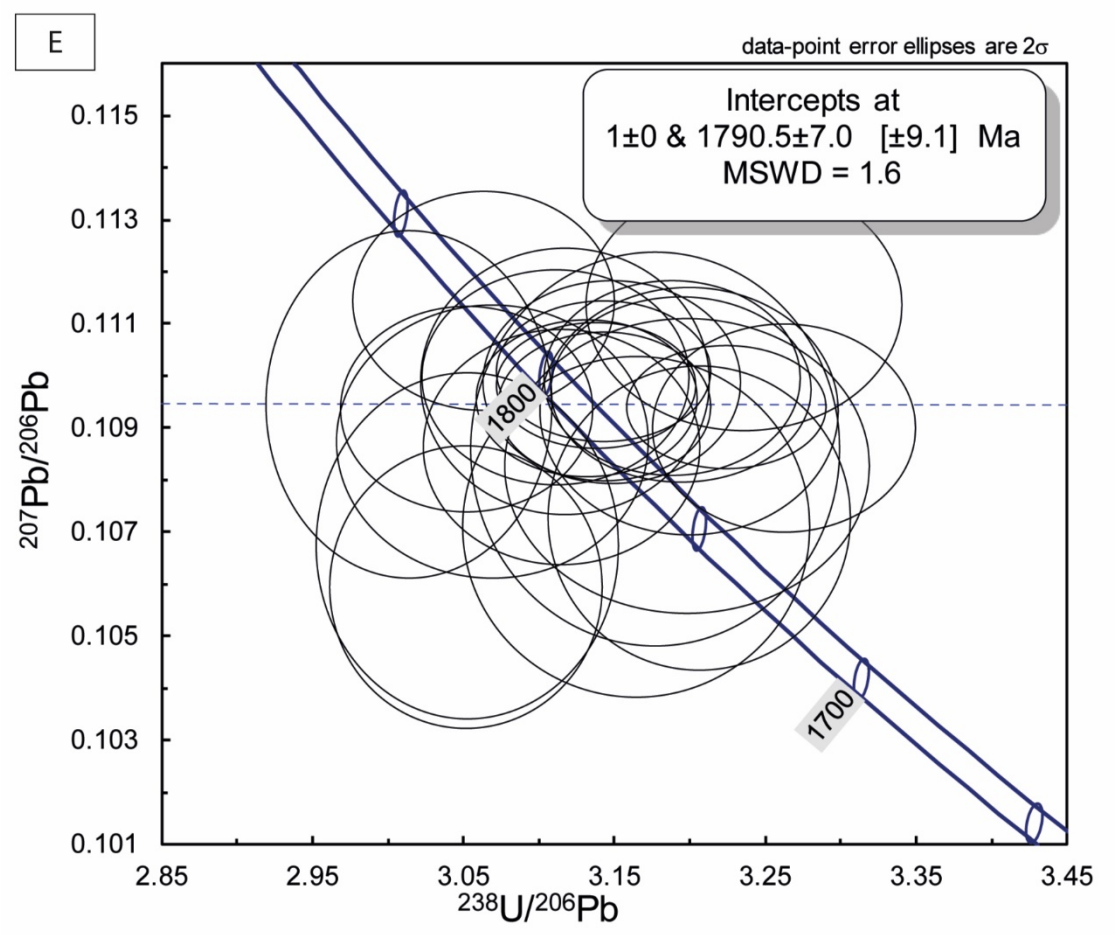

Figure 5.21: *Sample RAF 106465. A) Photo of the rock as it appears in the field. B) CL-image showing internal textures of one zircon grain that was analysed by SHRIMP, together with the U-Pb age (red circle indicates where the laser spot was aimed). C) Microphotograph (PPL) showing the complex textures with assigned mineral assemblage. D) Tera-Wasserburg plot with all the grains plotted and the calculated U-Pb age. Microphotographs by Nolwenn Coint. Field photo from Peter Ihlen.*

5.2.6 Lu-Hf isotopes

All the 14 samples from the study area ran through the LA-ICP-MS for U-Pb geochronology were also analysed for Lu-Hf isotope compositions. 12 of these samples gave results and are shown in Figure 5.22. The oldest rock that was dated is a gneiss which shows two populations of zircons (sample 140814), the oldest one being 2.65 Ga plotting at a ε_{Hf} value between +1.46 and -5.46. The youngest population of zircon from this sample is dated to 1.9 Ga and has a ε_{Hf} value with a wider range of -3.12. to -10.46. Sample 140813 has a similar age as the youngest population in sample 140814 and a ε_{Hf} value in the range of -4.1 to -8.3. Most of the rock samples plot around 1.8 Ga where the mafic rocks typically fall at a more positive ε_{Hf} value. Lu-Hf-data can be read in Appendix B.

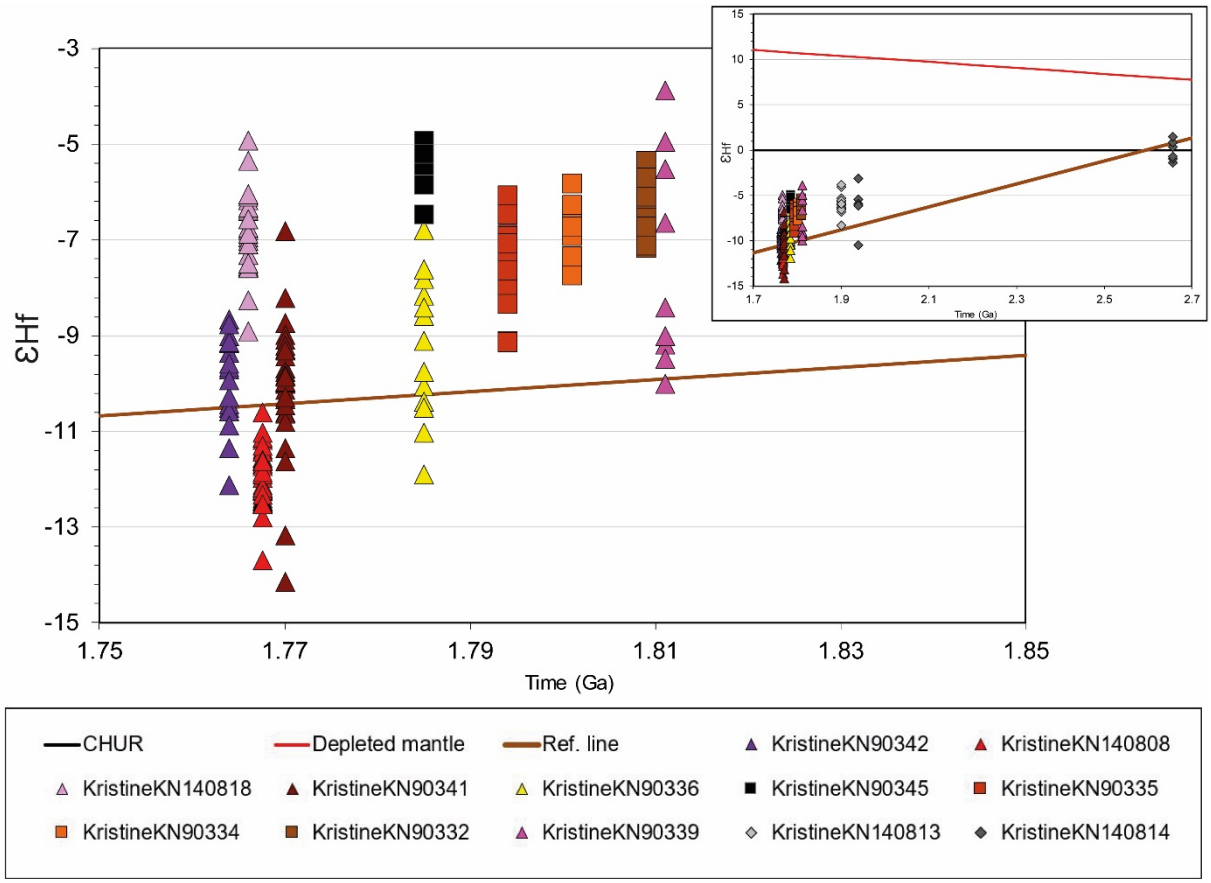

Figure 5.22: *ε_{Hf} vs time evolution plot constructed with an Excel add-in from Tom Andersen. The modelled line for the evolution of the Hf-ratio is used with a T_{DM}=3.1 Ga and a crustal $^{176}Hf/^{177}Hf$ = 0.015. The samples with a square symbol are gabbro/dioritic rocks, the samples with oblique squares are gneisses and the samples with a triangle symbol are granitic rocks. The diagram in the upper right corner shows the same evolution plot with a timeline from 1.7 to 2.7 Ga, this is to include the oldest population of zircon found from sample 140814.*

5.3 Whole-rock geochemistry and Sm-Nd isotopes

The results from the whole-rock geochemistry analyses are presented in this chapter. The data has been divided into three different units based on their major element composition and how they appear in field. The supplementary data from the major- and trace elements, plus Sm-Nd data are provided in Appendix C. The sample localities for the whole-rock geochemistry samples are shown in Figure 5.23.

The major elements present variation and differentiation between the rocks found in the study area. The meta-gabbros show a SiO_2-content vary from 49 to 51 wt.%, and the FeO and MgO are found with respectively values of 4 to 6 and 13 wt.%. The contrasting granitic rocks show SiO_2-content in the range of 60 to 75 wt.%, with FeO and MgO wt.% values of respectively 1.7 to 5.3 and 0.3 to 3. These numbers are similar to a discrimination between mafic and intermediate to felsic rocks.

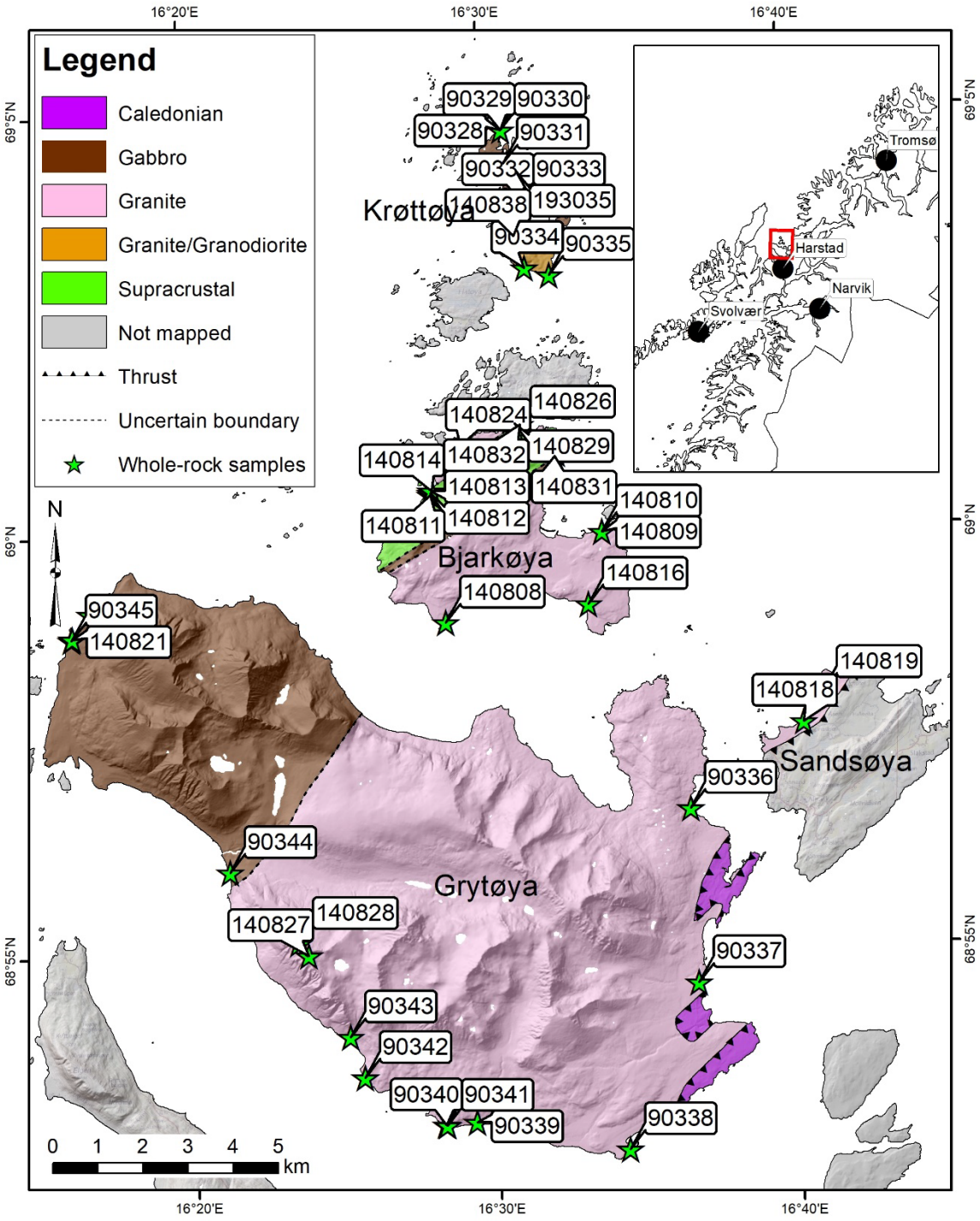

Figure 5.23: *Geological map based on the fieldwork that was done in the summer of 2017 and 2018, with associated legend of the geological units that were examined. The sample localities for the samples that were analysed for whole-rock analyses are indicated with green star symbols, together with a label of the sample number.*

5.3.1 Major elements

Harker diagram

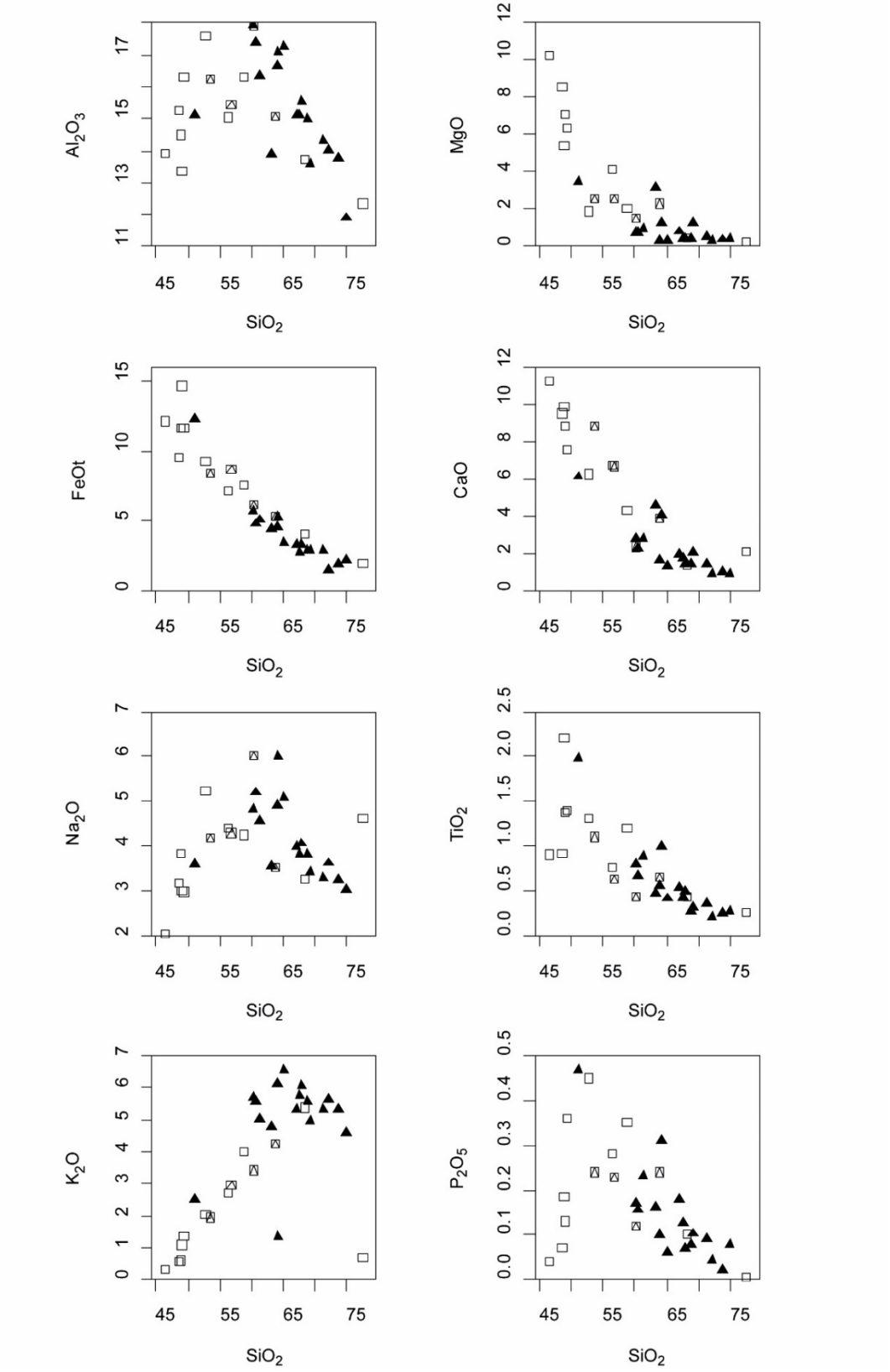

Figure 5.24: *Selected Harker diagrams for the major elements of meta-gabbro/granodiorite (squares), the granites (triangles) and gneissic rocks (squares with built-in triangles).*

The Harker diagrams display mostly negative trends for the major elements of the granites, the exception is for K_2O (Figure 5.24). The gneissic rocks follow the same trends. The negative trends for the major elements are also displayed for the mafic rocks, with the same positive trend for K_2O. The mafic rocks are scattered for Al_2O_3, Na_2O and P_2O_5.

ASI Diagram

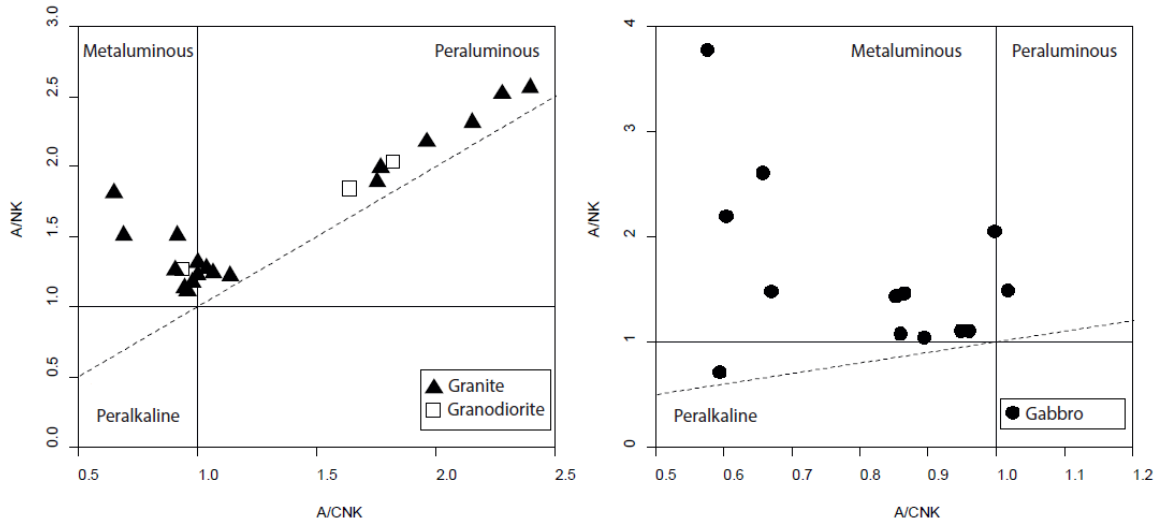

Figure 5.25: *Shand (1943) ASI classification scheme used to classify the granite, granodiorite and gabbro unit. Abbreviation: ASI=Alumina Saturation Index, A=Al_2O_3, N=Na_2O, K=K_2O, C=CaO. Diagrams made with the software RStudio complemented with GCDkit.*

Figure 5.25 shows that the granites are showing two trends, 6 of the samples plot high up in the peraluminous field and the other samples plot close to, or within the metaluminous field. The granodioritic rocks show two samples in the peraluminous field and one in the metaluminous field. The gabbroic/amphibolitic samples are mainly plotting in the metaluminous field and show one outlier in the peralkaline field. A few samples are plotting in the peraluminous field. The samples from the granite unit that plots within the peraluminous field are mainly from Grytøya and the eastern side of Bjarkøya. This means that the granite found on these locations have an excess of Al_2O_3 and that they probably had a higher contamination from continental crust in the magma which they crystallized from. The other half of the granite group collected from Sandsøya and on the north/northwestern part Bjarkøya plots within the metaluminous field reflecting a deficiency of Al_2O_3. This is thought to indicate a more mafic magma than the peraluminous rocks. The three granodioritic samples from Sandsøya shows a spreading between the metaluminous and peraluminous field, with the one collected closest to the intrusive contact with the gabbro being metaluminous. The gabbroic to amphibolitic samples shown on the right-hand side of Figure 5.25 are even more widely spread. There is one sample plotting in the peralkaline field, this is a sample collected from an amphibolitic dyke on Sandsøya. The two samples plotting in the peraluminous field are from dykes on the central and northern part of Bjarkøya. The outliers plotting in the metaluminous field are all dykes. Dykes are more prone to contamination as they travel through the crust compared to a large intrusion, as the magma travels with a smaller distance to the surrounding rocks.

5.3.2 Trace elements

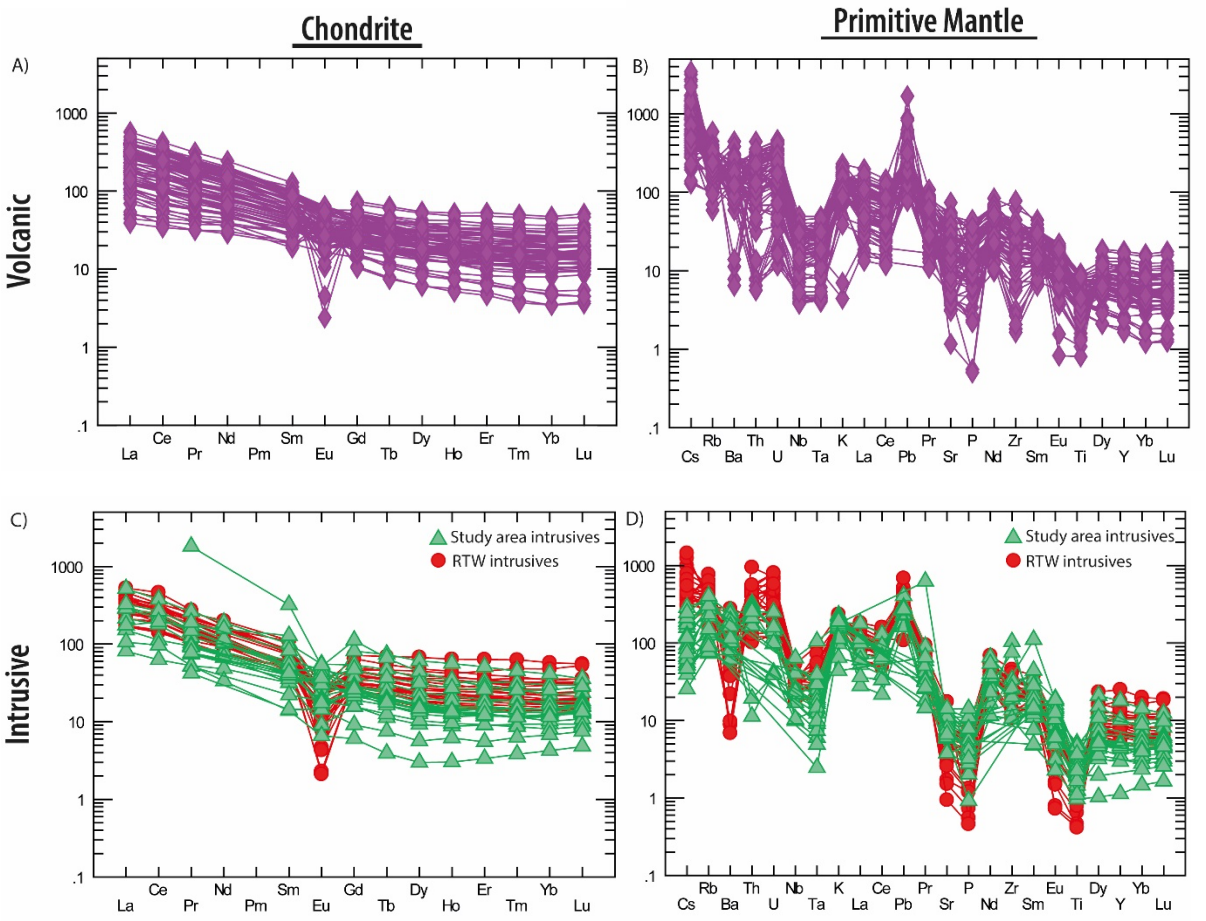

Figure 5.26: *The volcanic- and intrusive rocks from the RTW and the study area normalized to chondrite and primitive mantle, after Sun and McDonough (1989). Purple diamonds represent the 1.8 Ga volcanic rocks of the RTW, the filled green triangles represent the 1.8 Ga intrusive granitic samples from the study area and the filled red circles represents the 1.8 Ga intrusive rocks of the RTW. A) Chondrite-normalized arc volcanites. B) Primitive mantle-normalized arc volcanites. C) Chondrite-normalized intrusive rocks. D) Primitive mantle-normalized intrusive rocks.*

The volcanic rocks from the RTW show an enrichment of 40 up to 500 ppm for the LREE with a steep decrease from La to Sm and a negative Eu anomaly on the chondritic REE plot. Most of the samples show this negative Eu anomaly apart from a couple of samples that have a positive anomaly. From Gd the slope flattens out towards the HREE (Figure 5.26A). In the primitive mantle plot the volcanic rocks have a high enrichment of La (up to 4000 ppm), negative anomalies for Nb-Ta, P and Ti, and a positive anomaly for Pb (Figure 5.26B).

The intrusive rocks have a REE pattern similar to the volcanic rocks on the chondritic plot. The enrichment of LREE is 90 to 500 ppm with a steep decrease towards Sm, and all the samples have a negative Eu anomaly before the slope flattens out towards the HREE (Figure 5.26C). The primitive mantle plot show that the intrusives from the RTW are in general enriched on Cs and have a larger negative anomaly for Ba. Other than that, the two intrusive populations have negative anomalies for Nb-Ta, P and Ti (Figure 5.26D). The

variation for REE within the intrusive rocks from RTW seems to be slightly smaller than for the samples collected in the study area.

Discrimination diagrams

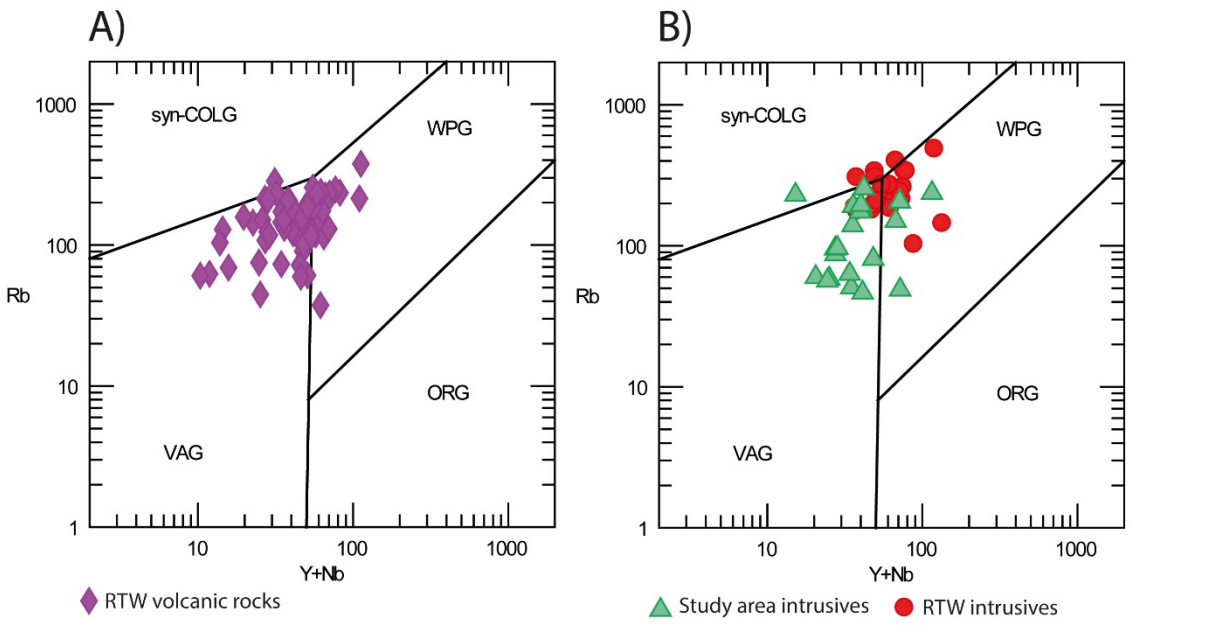

Figure 5.27: *Granitoid discrimination diagrams after (Pearce et al., 1984). Abbreviations: syn-COLG = syn-collisional granitoid, VAG= volcanic arc granitoid, WPG= within plate granitoid and ORG= ocean ridge granitoid. A) The 1.8 Ga arc volcanites from the RTW. B) The 1.8 intrusive rocks from the RTW and study area.*

The results from plotting Rb vs (Y+Nb) is shown in Figure 5.27. The 1.8 Ga arc volcanites in the RTW plot as a cluster in the VAG-field, with some of the samples plotting in the WPG-field. The 1.8 intrusive rocks in the RTW and the granitic samples collected from the study area overlaps in the discrimination diagram. However, the samples from the study area seem to plot further into the VAG field than the rocks from the RTW. The intrusive rocks from the RTW has a higher density of samples plotting in the WPG field.

5.3.3 Sm-Nd isotopes

Sm-Nd isotope analyses were carried out at the British Geological Survey in Nottingham for seven of the samples from the study area. Two samples from Krøttøya and five samples from Grytøya. The purpose of these analyses was to compare the samples with other magmatic rocks crystallized at approximately the same time and see if they had a signature from a primitive magma or a more evolved magma. A map with the sample locations for the samples that were carried out Sm-Nd for are shown in Figure 5.28.

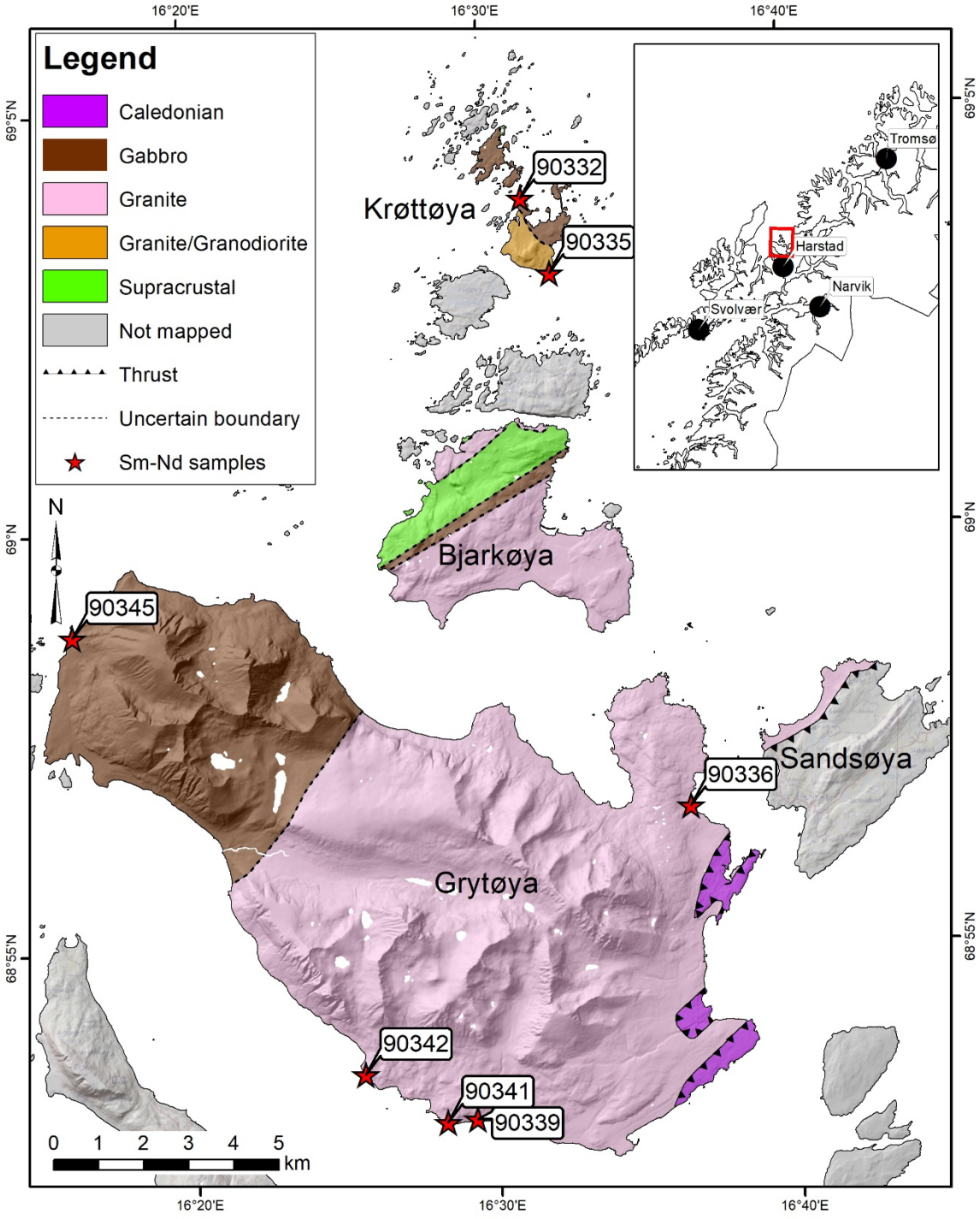

Figure 5.28: *Geological map based on the fieldwork that was done in the summer of 2017 and 2018, with associated legend of the geological units that were examined. The red star symbol indicates the sample locations with associated label showing the sample name.*

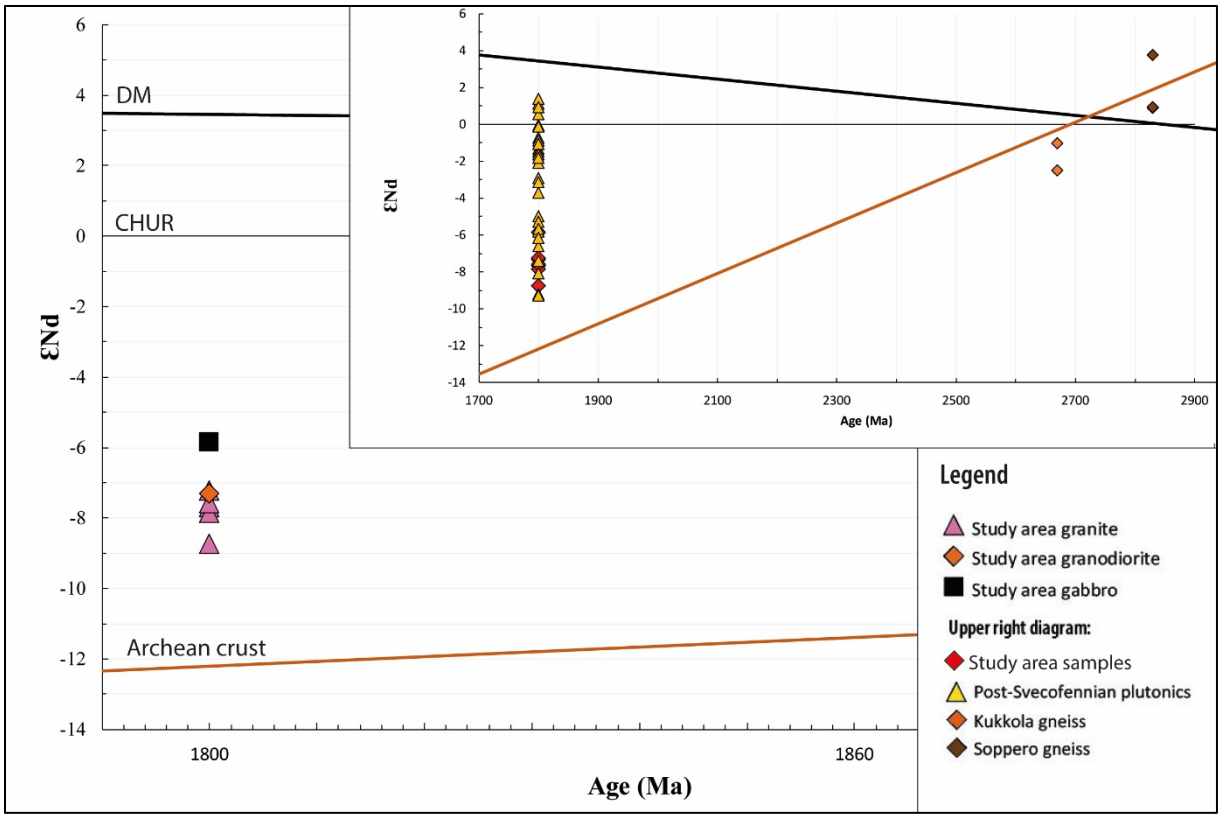

Figure 5.29: *Sm-Nd evolution plot with Depleted Mantle line modelled after DePaolo (1981), the Archean crust line modelled after (Öhlander and Skiöld, 1994, Öhlander et al., 1987) together with the rocks from the study area. The upper right diagram shows the samples which the evolution plot was modelled after.*

As Figure 5.29 shows, the 1.8 Ga samples plots in a range of (-5.85 to –8.74) for the ε_{Nd} whole-rock value. The most mafic rock, the gabbro has the less negative Nd value. The more felsic granites plot closer to the Archean crustal evolution line. Figure 5.29 shows that the 1.8 Ga samples collected for this study plots in a range of -6 to -9, indicating a mix between a crustal- and depleted mantle melt.

6 Discussion

The new observations and data presented in this study (i) gives new information about the Paleoproterozoic magmatic and tectonic evolution, (ii) together with previously published data they can be used to say something about the extent of Archean crust, and (iii) the extent of ca. 1.9 Ga, locally mineralised volcanic rocks (intruded by younger granites) and why they are not found in a greater amount in Norway.

6.1 Magmatic and tectonic evolution of the SW margin of the Fennoscandian Shield

6.1.1 Arc volcanic rocks in Rombak Tectonic Window

The Rombak Tectonic Window (RTW) is located on the Paleoproterozoic southwestern margin of the Fennoscandian Shield. The rocks found in this area are of both Archean and Proterozoic ages, surrounded by Caledonian nappe complexes (Gustavson, 1974, Tull et al., 1985). The Proterozoic rocks are mainly supracrustal belts constituting both turbidites and felsic to mafic volcanic rocks (Korneliussen and Sawyer, 1989). As for the study area, these older rocks have been intruded by younger intrusive granitic rocks. The volcanic rocks were for a long period thought to be 1.91 to 1.88 Ga, determined by their similar composition and texture to the supracrustal sequences found in northern Sweden (Frietsch and Perdahl, 1987). Slagstad et. al (unpublished data,2019) have dated these volcanic rocks to be 1.78 to 1.80 Ga, together with an age of 1.79 to 1.80 Ga for the intrusive rocks. The supracrustal rocks of Rombak Basement Window have been exposed to metamorphism in the lower amphibolite facies, with a following retrograde metamorphism during the Caledonian orogeny (Korneliussen and Sawyer, 1989). The supracrustal belts vary in rock types and composition (Korneliussen and Sawyer, 1989). In Sørdalen the supracrustal belt consists of porphyritic, intermediate to felsic volcanic rocks with interbedded debris flows, whilst at Stasjonsholmen-Rombak the supracrustal belt consists of pelite-greywacke turbidites with tuffitic layers (Korneliussen and Sawyer, 1989). The tectonic setting at which these volcanic rocks formed is interesting and important for the interpretation of the geological history of the region.

Korneliussen & Sawyer (1989) have used geochemistry for both the extrusive and the intrusive rocks of Rombak to present the idea of a magmatic arc located above a subduction zone responsible for the formation of the volcanic rocks. Based on whole-rock major element geochemistry plotted in SiO_2 vs. (Na_2O+K_2O) and Na_2O vs. K_2O diagram, the volcanic rocks of Rombak can be divided into three groups. 1) Low-K_2O mafic to ultramafic subalkaline extrusives, 2) low-K_2O, high Na_2O rhyodacitic to rhyolitic volcanites, and 3) K_2O-rich mafic to felsic extrusives (Korneliussen and Sawyer, 1989). Whole-rock trace element geochemistry of the felsic to mafic volcanic rocks in the Rombak Tectonic Window shows a primitive mantle plot with a typical subduction zone related pattern: high concentration of large ion lithophile elements (LILE) and a negative Ta-Nb anomaly. This enrichment of the LILE in subduction-related rocks is interpreted to be a result of dehydration, or incipient melting of subducted lithosphere enriching the overlying mantle wedge (Best, 1975, Gustavson, 1974, Hawkesworth et al., 1977b). The intrusive rocks of Rombak show a REE-pattern with negative Ta-Nb and Ti anomalies, which can be interpreted as subduction-related magmas (Korneliussen and Sawyer, 1989). Several discrimination diagrams have been developed for modern arc systems. One of them is the Th-Hf-Ta diagram by Wood (1980). When plotting the volcanic rocks of Rombak in this diagram, all samples plot within the D-field which corresponds to magma series at

destructive plate margins. The TiO_2 vs. Zr diagram after Pearce (1980) and the Rb vs. (Y+Nb) diagram after Pearce et al. (1984) shows that the sample plots respectively within the arc- to within-plate lavas and the volcanic arc- and within-plate granite fields. Based on these findings, Korneliussen & Sawyer (1989) suggest three stages of the evolution of the volcanic rocks in Rombak: Stage (1) include a parental magma supposedly originating from the mantle wedge above a subducting plate, followed by stage (2) where Fe and Mg-rich silicates formed by fractional crystallization generates a more silica-rich, intermediate magma, leading to stage (3) which is assumed to be a late stage of magma evolution, comprising of more felsic magma, mainly controlled by fractional crystallization of plagioclase at a relatively shallow level in the crust.

New data from Slagstad et al. (unpublished data, 2019) shows that the 1800 Ma volcanic rocks of Rombak have ε_{Nd} values in the range of -2.8 to -6.4, and a SiO_2 content that vary from 46.6 to 76.4. The Fe_2O_3 and MgO content of the volcanic rocks are distinctly higher than for the intrusive, granitic rocks and vary respectively in the range of 2.04 to 13.6 and 0.165 to 20.5.

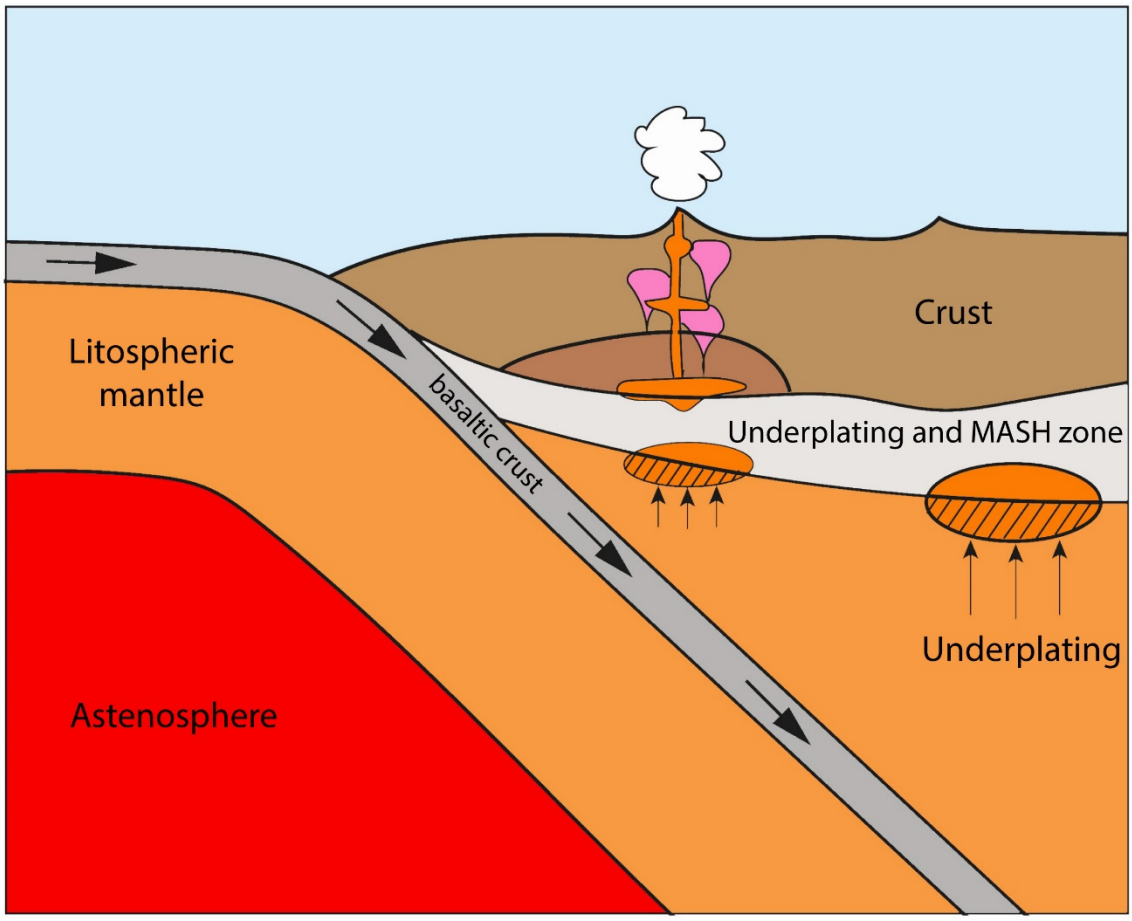

Figure 6.1: *Simplified schematic overview of a continental arc subduction zone showing the typical melting processes in the crust and mantle. The subducting plate sinks under the overlying crust, bringing hydrous sediments to the depth making it a possible catalysator for generating hot magma ascending toward the overlying crust where it heats the crust in the process of underplating.*

A rock that shows highly positive ε_{Nd} values is interpreted to be more juvenile than a rock that shows highly negative ε_{Nd} values, and this follows from the properties of the

incompatible elements. The highly compatible elements are accumulating in the melt, and when this melt is removed from the mantle and move upwards to the crust it will be enriched in the incompatible elements (e.g. Nd) compared to the residue in the mantle. The varying geochemical data and the varying negative ε_{Nd} values in the volcanic rocks of Rombak could therefore represent a source with mixing of depleted-mantle material and continental crust material. The ε_{Nd} values would plot between the depleted mantle evolution line and the Archean crustal evolution line on a ε_{Nd} evolution plot. Whether the variation in the geochemical and isotopic data reflects a process of mixing or assimilation is impossible to conclude without modelling the mixing/assimilation ratio. The volcanic rocks of Rombak could reflect a depleted mantle magma ascending toward crust, that assimilated some of the crustal magma it passed in a magma chamber. Or it could reflect a depleted-mantle magma that crystallized in a magma chamber with crustal material and over time got mixed and more homogenised. The differences in the ε_{Nd}- and the major element values can be explained by the processes of mixing, assimilation, storage and homogenisation (MASH) taking place on the border between mantle and crust. The MASH-zone in a continental arc setting is shown in Figure 6.1.

6.1.2 The Svecofennian deformation in Rombak

The Svecofennian orogeny took place around 2.0-1.8 Ga (Roberts and Slagstad, 2014) at the southwestern margin of Fennoscandia and is said to be the main contributor for deformation of the rocks in Rombak. This deformation in Rombak caused ductile folding, thrusting and anastomosing shear zones in the metasupracrustal belts and volcanic rocks in this area (Angvik, 2014). The Rombak-Skjomen shear zone (RSSZ) is described as a major crustal scale Paleoproterozoic ductile structure that cuts the Paleoproterozoic metasupracrustal and felsic igneous rocks of the RTW (Angvik, 2014). This deformation event can be divided into four phases of deformation (D_1-D_4), where the two first phases are very interesting for this study. D_1 and D_2 represent the formation of a N-S striking and east verging fold- and thrust belts and, whilst the D_3 and D_4 represent two oblique-slip events with steep ductile N-S striking and NE-SW striking shear zones (Angvik, 2014). The D_1 and D_2 observed in the volcanic rocks are cut by intrusive rocks dated to be between 1.80 and 1.79 Ga (Slagstad et al., unpublished data,2019), implying that the volcanic rocks are older than these intrusives. Both D_1 and D_2 belongs to the initiation of the Svecofennian deformation in the RTW, where the D_1 structures are characterized by pure-shear folding with isoclinal, N-S-striking and east-verging folds (Angvik, 2014). The D_2 phase is a refolding of the D_1 structures from a pure-shear fold-thrust belt event, resulting in a dominant S-striking, upright east verging and open folds (Angvik, 2014). The two first phases can therefore be categorized as structures formed in a compressional environment.

6.1.3 Voluminous granitic magmatism

At 1.8 Ga a major magmatic event happened at the southwestern margin of the Fennoscandian Shield, as a large volume of granitic melt intruded a large area. The 1.8 Ga granites can be found as far as the WTBC to the north (1.80-1.77 Ga; Bergh et al., 2007), in the RTW to the east (1.80-1.79 Ga:Angvik, 2014 Slagstad et al. (unpublished data,2019)), in the study area, the Lofoten-Vesterålen area to the west (1.80-1.79 Ga; Corfu, 2004) and southernmost in the CNBW (1.80-1.79 Ga; Skår, 2002). The dating of these areas testifies to the emplacement of a large pulse of granitic melt over a relatively short period of time. These granitic intrusive rocks cut the D_1 and D_2 structures found in

the RTW volcanic rocks and show that the intrusive granites are younger than the arc volcanic rocks and thereby, D_1+D_2. The granites found in the study area have been dated and shows U-Pb ages of 1809 ± 20 Ma to 1764 ± 20 Ma. The time span could be interpreted as reflecting the 1.8 Ga, short-time voluminous granitic magmatism, followed by a later event of magmatism.

The whole-rock geochemistry of the intrusives of the RTW show clear differences compared to both the intrusive rocks in the study area and the volcanic rocks of RTW. The volcanic rocks have been described with variation from felsic to mafic rocks, reflected in the whole-rock SiO_2 content which varies from 46.6 to 76.4 wt.%. In comparison, the intrusive rocks from the study area show a SiO_2 content between 46.5 to 77.5 wt.%, and the intrusive rocks of RTW having a SiO_2 content in the range of 66.0 to 77.3 wt.%. The respective Fe_2O_3 and MgO contents are in the range of 2.04 to 13.6 and 0.165 to 20.5 wt.% for the volcanic rocks, 1.43 to 13.7 and 0.23 to 14.65 wt.% for the intrusive rocks in the study area, and 1.27 to 4.58 and 0.109 to 0.616 wt.% for the intrusive rocks in RTW. The isotopic data from the same rocks show some interesting variation in the ε_{Nd} values. The volcanic rocks of the RTW have ε_{Nd} values in the range of -2.8 to -6.4, overlapping with the intrusives of the same area that have values from -3.4 to -6.9. The intrusive rocks from the study area have a more consistent ε_{Nd} value varying from -7.2 to 8.7. These ranges can be tracked on the ε_{Nd} evolution plot and imply that all three rock types have a larger or smaller degree of mixing between depleted mantle and evolved continental crust. The intrusive rocks from the study area have the most negative ε_{Nd} values. Both the intrusive rocks from the study area and the volcanic- and intrusive rocks from Rombak are assumed to be result of crustal melt. However, the difference in geochemistry and isotope composition could be explained by the rocks from the study area being a pure Archean crustal melt, whilst the volcanic and intrusive rocks of Rombak could be a crustal melt generated from a 2.1-1.9 Ga crust that was generated with different depleted mantle input than the Archean crust had when it was formed at 3.0 Ga.

Magma mixing and magma assimilation

As it is highly uncommon to find 100% primitive magmas, different theories have been suggested to explain the diverse geochemistry and isotopic data that are found for the rocks on Earth's surface. The two end-members in such a case would be a primitive mantle melt that is generated directly from the depleted mantle, and a pure crustal melt. These end-members would show differences in both mineral assemblage, geochemistry and isotopic data. Most magmas lay in between these two end-members and the degree of mixing varies from magma to magma. Two generally accepted cases for magma mixing is the "fountain" and the "ponding" models. The first one is thought to be driven by a pressure change where the incoming magma can be compared to a fountain where the injected magma is flowing around, mixing with the magma that's already present in the magma chamber. The second case of magma mixing is when a denser magma is introduced from outside the magma chamber and immediately ponds on the floor of the magma. This latter case would probably result in a less mixing than the first case. However, either of these processes of mixing would change the properties of the magma. If a depleted mantle melt is mixed with a crustal melt, the resulting geochemistry and isotopic properties of this magma should be something intermediate depending on the concentration of each of the two end-members.

Another process to generate a magma with different properties is assimilation. Magma assimilation happens when a heated magma incorporates chemical constituents from the host rock in the walls or the roof of a magma chamber, a process that requires heat. This

heat must be produced by the magma itself and that happens when the magma crystallizes out various minerals when it encounters the colder walls or roofs of the chamber. This crystallization releases energy that is transformed into heat (latent heat of crystallization). Assimilation is detectable isotopically in the same way as for magma mixing. The Sm/Nd is low in the crust, meaning that if a primitive magma (e.g. a very mafic rock) show high numbers of this ratio, it might reflect contamination from a crustal source.

A modelling of ε_{Nd} and ε_{Hf} mixing has been done in an attempt to visualize the degree of assimilation or magma mixing. The result is shown in Figure 6.2 and Figure 6.3. For this study the modelling was based on an assumed two-component system, the end-members being an Archean crustal source (3.0 Ga) and a 1.8 Ga magmatic source. This assumption is made on the basis of it being impossible to differentiate between a source at 1.8 Ga and 1.9 Ga. The geochemical differences would not be possible to track as both magmatic events would include a crustal melt component of the 3.1 Ga crust. It is therefore reasonable to treat it as a two-component system.

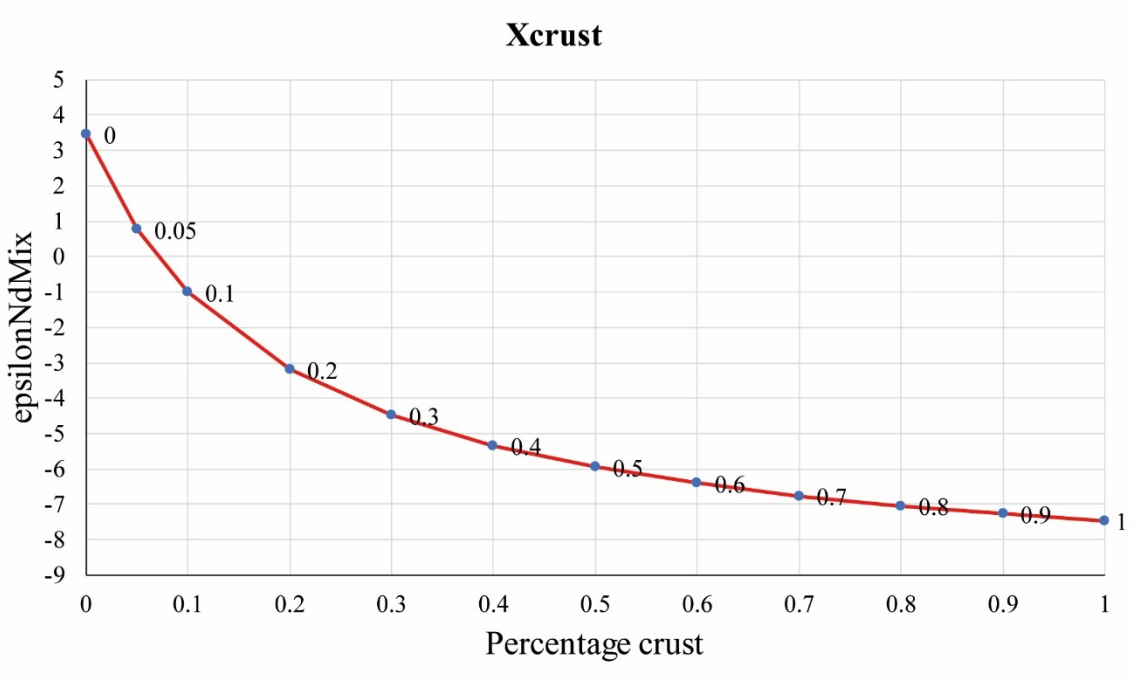

Figure 6.2: *A diagram showing the a ε_{Nd} mixing model. As shown from the diagram, the ε_{NdMix} value sinks drastically with a concentration of only 0.05 crustal material.*

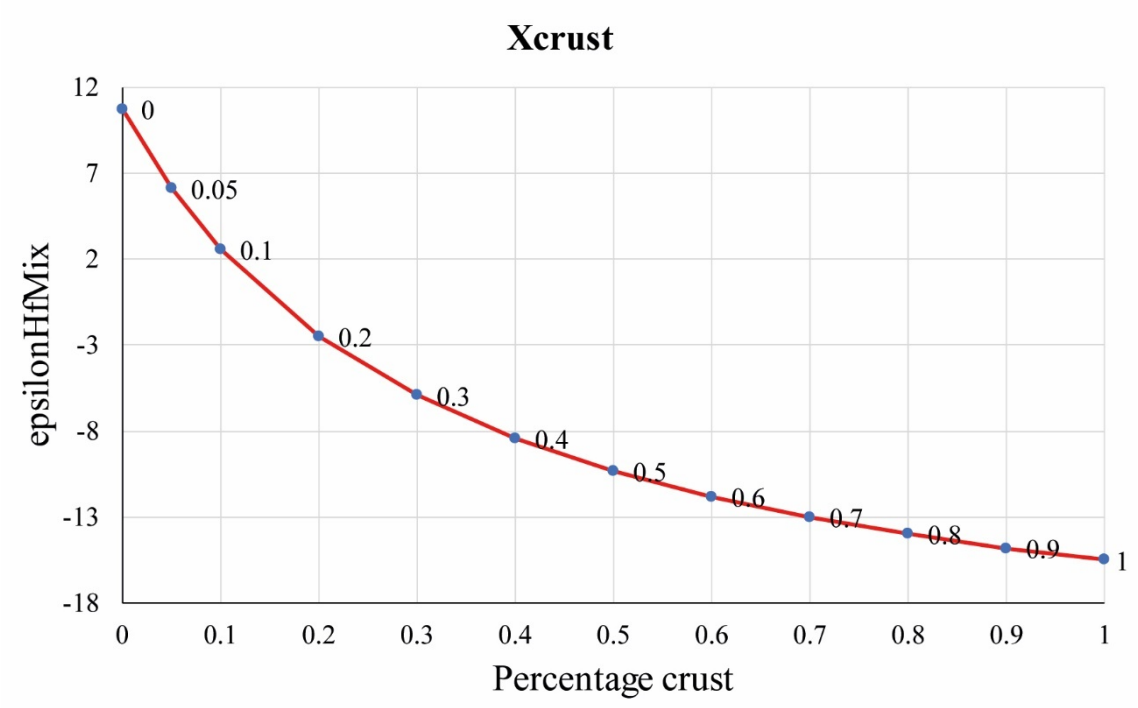

Figure 6.3: *A diagram showing the* ε_{Hf} mixing model.

From Figure 6.2 an estimate of the degree of mixing based on ε_{Nd} of the volcanic rocks and intrusive rocks can be done. The volcanic rocks have a ε_{Nd} in the range of -2.8 to -6.4, corresponding to a mix of 20-50% crust and 80-50% depleted mantle according to this model. For the intrusive rocks of the RTW the same method gives proportions varying from 20-30% depleted mantle and 70-80%. For the intrusives in the study area the values vary from 85-100% crust and 0-15% depleted mantle. Another interesting comparison can be done on a sample of gabbro found in both the study area and the RTW. The gabbro in the study area has a ε_{Nd} value of -5.8, the gabbro of the RTW has a value of -5.4. These values give a percentage of crust between 35 to 45. Figure 6.3 gives an estimate of the degree of mixing based on the ε_{Hf} values. The intrusive rocks from the study area have ε_{Hf} values in the range of 1.47 to -21.2, 193 of the 204 data points lay in a range between -3 to -13. That range give an assumed mixing of 20-70% crust and 30-80% depleted mantle. The mixing ranges found for the volcanic-and intrusive rocks of Rombak and the intrusive rocks of the study area are highly variable and can only be used as an indicator of mixing to be present-not to find accurate values of how much mixing that is present.

The geochemistry of the three rock populations imply that none of them reflect a completely juvenile source and that the 1.8 Ga magmatism forming the intrusive rocks of RTW and the study area were dominated by a larger proportion of crustal melt. The data collected in the study area and from studies done in the WTBC, Altevatn, the RTW, the Lofoten-Vesterålen area and the CNBW all agree that the tectonic setting has shifted from a volcanic arc/active margin with more juvenile magmatism to a tectonic setting dominated by crustal melt in a short span of time. As previously said, the geographical extent of the 1.8 Ga magmatism is huge, and it is therefore interesting to investigate possible tectonic settings at which this voluminous melt formed. The volcanic rocks and the intrusive rocks from the RTW are dated to be 1.79-1.80 Ga (Slagstad et al., unpublished data, 2019). In a geological perspective the time between the formation of the different rocks is very short (ca. 10 Ma). Angvik (2014) has done comprehensive structural studies of the RTW and the

two deformation phases recorded in the volcanites (D_1+D_2) show indications of a compressional geological environment.

Korneliussen & Sawyer (1989) have suggested that the previous tectonic setting of Rombak was an evolving magmatic arc overlying a subduction zone that resulted in formation of the 1.8 Ga volcanic rocks that are found in the area. The interpretation is based on both geochemistry- and isotope data. Angvik (2014) has studied the same volcanic rocks and found that they show compressional structures , and that these volcanic rocks are intruded by the younger granitic rocks. This imply that the tectonic setting at which the 1.8 voluminous granitic formed at, must have happened in a compressional environment. How to generate such a large volume of granitic melt at a time-span found to be ca. 10 My in a compressional tectonic setting has left an unresolved question.

This study suggests a tectonic model for the tectonic setting at which the granitic intrusive rocks of both Rombak and the intrusive rocks from the study area may have formed. Based on the findings of Angvik (2014), the magmatic arc described by Korneliussen & Sawyer (1989) underwent compression and a possible thickening of the crust. The subduction zone with the associated subducting plate could initiate melting of the overlying lithospheric mantle wedge by migration of melt formed by dehydration of basaltic crust and sediments. The partial melted mantle rocks would then ascend towards the Moho and accumulate beneath the crust, and gradually generate a heating of the lower crust. This would result in a melting of the crust and a generation of magma rising upwards in the crust driven by density differences between the lighter melt and the surrounding solid crustal rocks. These processes could apply to the formation of the 1.8 Ga volcanic rocks found in RTW. However, this partial melting of the crust would not generate enough melt of the voluminous granitic melt that formed the intrusive rocks of RTW and the study area at 1.8 Ga. To generate this enormous volume of granitic melt in a compressional environment, a model of delamination is suggested. Delamination is a process where cold and dense lithosphere is sinking into a less dense hot asthenosphere, caused by thermal-, compositional- and phase changes (Kay and Kay, 1993). In Rombak, this process is believed to have formed by a compressional environment resulting in a crustal shortening, followed by a thickening of the continental crust. The crustal thickening caused an exposure of the lower crust to higher temperature and pressure as it is pushed further down. The lower crust exposed to this increased temperature and pressure would gradually form eclogite at both crustal and lithospheric levels (rocks with a density >3.0g/cm^3). This significant higher density of the eclogites, in combination with a heating leading to partial melt of the deeper crust/lithosphere would then make it possible for delamination to happen. The cold denser lower crust/lithosphere consisting of eclogite would due to density differences sink into the hot asthenosphere. This process would create space for hot asthenosphere to move upwards in the crust and trigger a melting of the lower crust. This melting of the lower crust could possibly give rise to the 1.8 Ga intrusive granitic rocks that are found in both Rombak and the study area, Altevatn, WTBC, Lofoten-Vesterålen and CNBW. The suggested tectonic setting is illustrated in Figure 6.4.

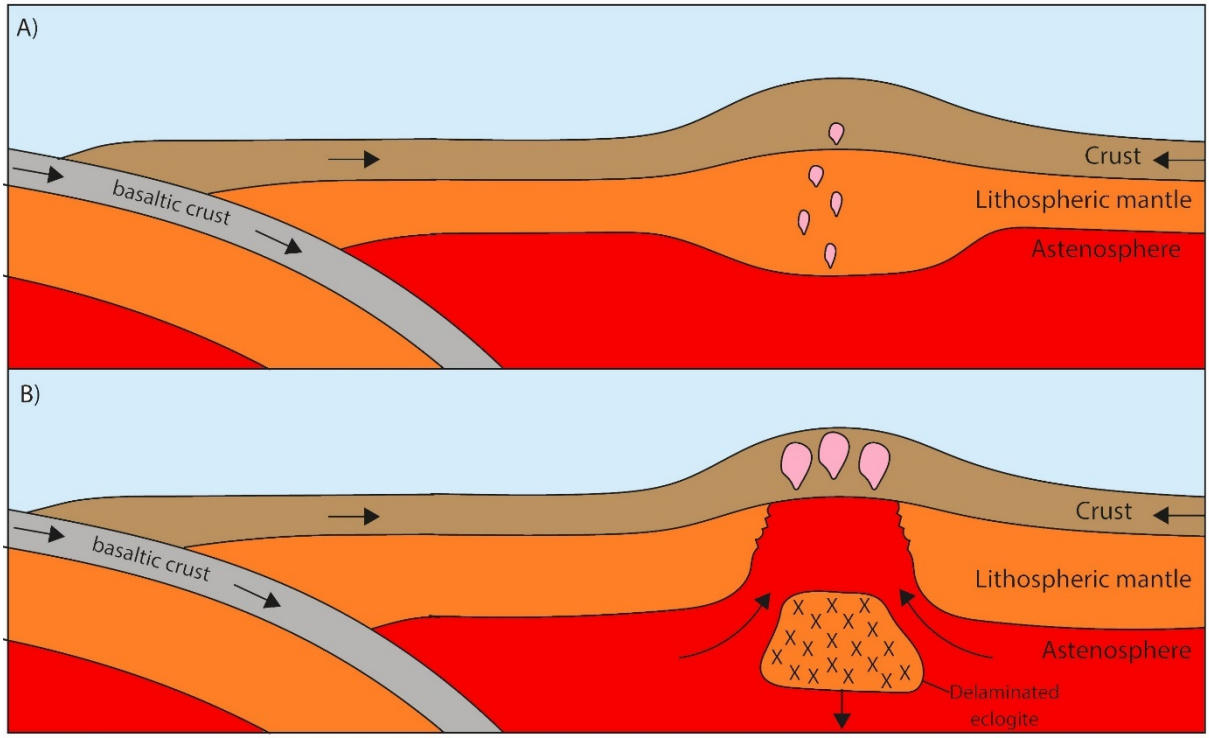

Figure 6.4: *The suggested tectonic setting responsible for the voluminous 1.8 Ga intrusive magmatism. A) A compressional environment causes a shortening and a corresponding thickening of the continental crust. B) The thickening of the continental crust exposes the rocks of the crustal lithospheric mantle to higher temperature and pressure resulting in formation of eclogite that due to density differences result in a delamination, opening space for hot astenospheric material to replace the cold, denser eclogite. The result is a voluminous granitic melt ascending the surface.*

Alternative tectonic models for this voluminous magmatic event include e.g. rifting. Rifting would indisputably be able to produce the amount of magmatism that this area has been exposed to, but there is no evidence of an extensional tectonic setting in the time before the intrusions and the time span expected for a rifting event would be much longer than the 10 Myr that are found between the metavolcanic rocks and the intrusives. Another alternative tectonic setting would be a slab-rollback trench retreat. However, this tectonic setting would also have left traces from an extensional environment- which are not evident in Rombak.

6.2 Archean-Paleoproterozoic Boundary

The Fennoscandian Shield underwent a concentric growth during Palaeozoic time, as new crust was added to the craton related to several orogenies (Bogdanova et al., 2008, Gaál and Gorbatschev, 1987). The West-Troms Basement Complex (WTBC), Lofoten-Vesterålen area, Rombak Tectonic Window (RTW), Altevatn area, the Central Nordland Basement Window (CNBW) are all tectonic basement windows that sit under the Caledonian nappes, such that the basement rocks are still exposed and can be studied. One of the interesting problems that have been approached is where the Archean-Palaeoproterozoic boundary is located. Gaàl and Gorbatschev (1987) are two of the many researchers that have tried to locate this boundary. They drew the boundary between the Archean and Svecofennian Domain in Norway based on data from Öhlander and Skiöld (1994) and the boundary in Sweden with data from Pharaoh and Pearce (1984). These data are Nd-isotope signatures

of the granitoid rocks that are found in a large area in both Troms and Nordland (Figure 6.5).

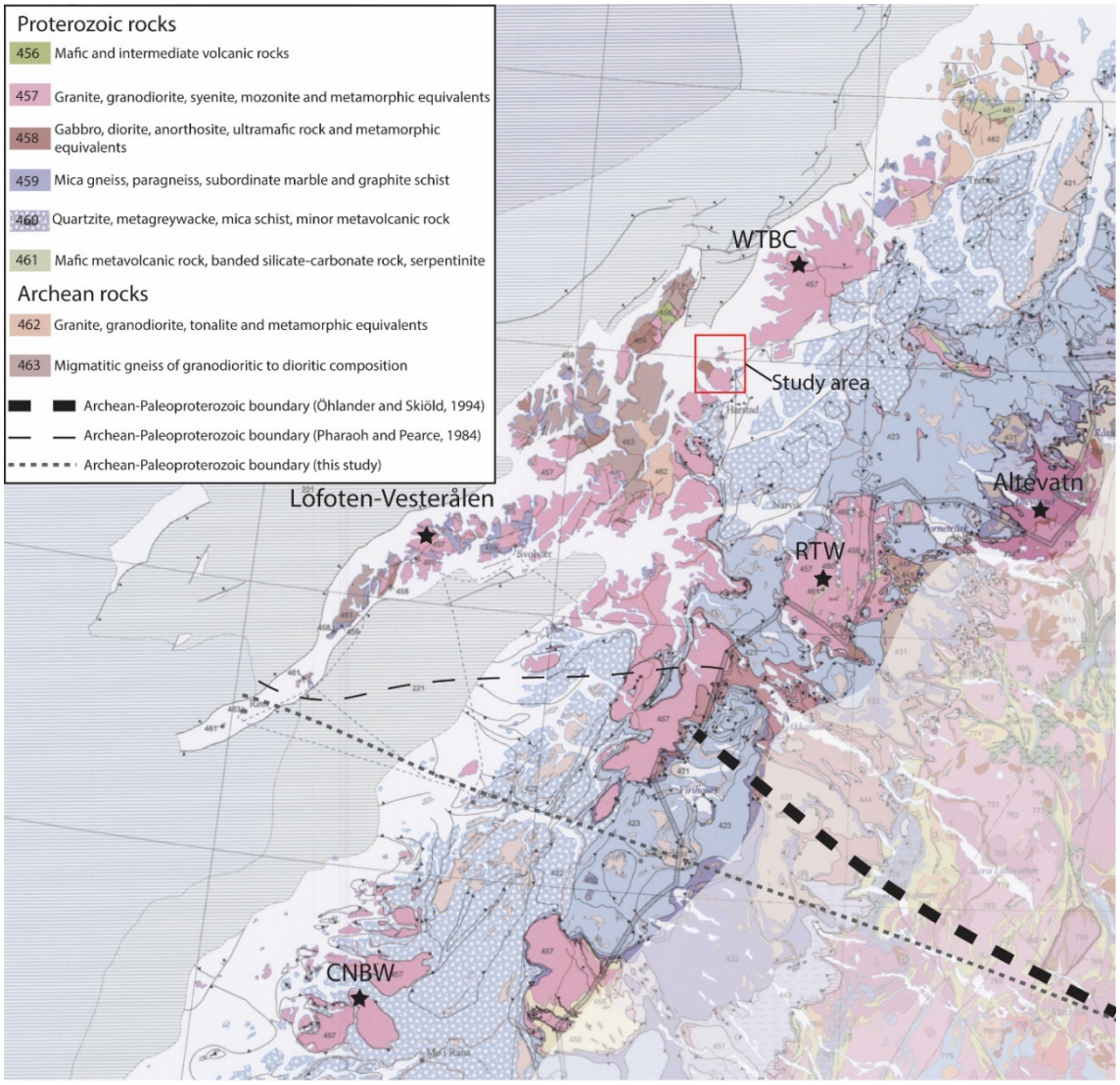

Figure 6.5: *Geological map including the regional geology of this study and the study area (ref). Archean-Paleoproterozoic boundary are drawn in from Öhlander and Skiöld (1994) and Pharaoh and Pearce (1984), in addition to a boundary suggested from this study. Map from Koistinen (2001).*

Before Skår's (2002) most recent work in the CNBW, the only age determinations were based on the older techniques of Rb-Sr, Sm-Nd and Pb-Pb whole-rock analyses which, for variably metamorphosed rocks, are considered inaccurate compared to today's dating methods. Rb-Sr whole-rock ages for Nordland indicated a continuous emplacement of intrusive rocks in the time between 1800-1700 Ma (Griffin et al., 1978). With Skår's (2002) new data this time span is limited to 1800-1795 Ma. These dates are equal to the ages found in Rombak (Angvik, 2014). However, the Archean-Palaeoproterozoic boundary remains unchanged as there has been little or no work to update it. Epsilon Hf data from Lofoten-Vesterålen, the study area and WTBC have been calculated and are shown in Figure 6.6.

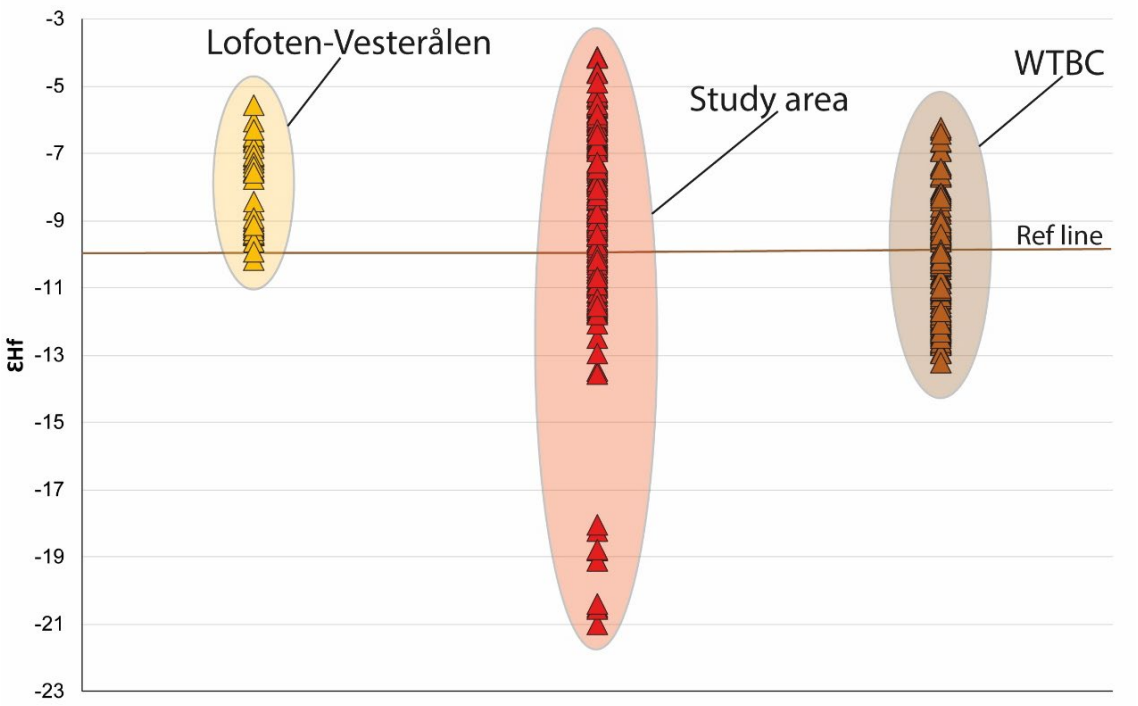

Figure 6.6: *Epsilon-Hf evolution plot for 1.8 Ga volcanic and intrusive rocks from Lofoten-Vesterålen (Laurent et al., 2019), the study area and WTBC (Slagstad et al., unpublished data 2019). The reference line is modelled in an excel sheet from Tom Andersen with a crustal component with a T_{DM} of 3.1 Ga and a $^{176}Lu/^{177}Hf$ value of 0.015.*

The epsilon-Hf evolution plot show that the Lofoten-Vesterålen area seem to have slightly more juvenile compositions than further to the north in WTBC, this is possibly because the WTBC is, based on estimates, lying further away from the Archean-Paleoproterozoic boundary. The study area with over 200 data points show a wider range, with 6 data points forming a cluster at much more negative values than the rest. Epsilon Nd data from CNBW, Lofoten-Vesterålen area, RTW and study area have also been calculated with the same purpose as for the epsilon Hf data. The results are shown in Figure 6.7.

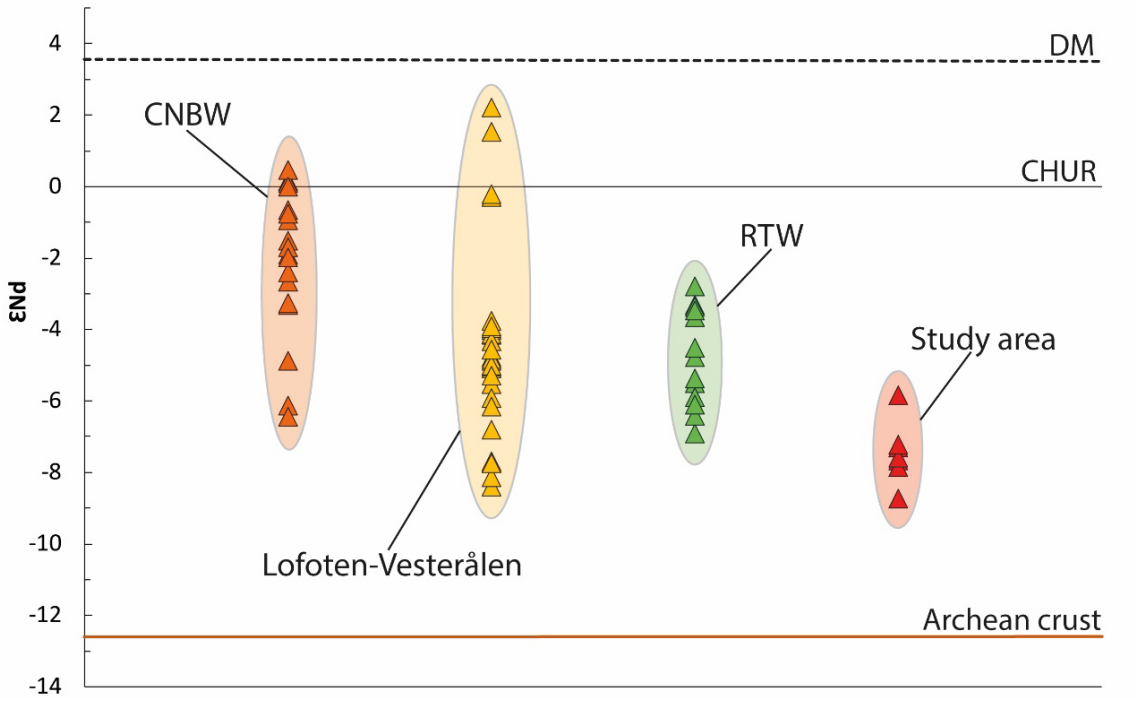

Figure 6.7: *Epsilon-Nd evolution plot for 1.8 Ga volcanic and intrusive rocks from CNBW (Skår, 2002), Lofoten-Vesterålen (Markl and Höhndorf, 2003b), RTW (Romer et al., 1992) and the study area. The depleted mantle evolution line is modelled after DePaolo (1981) and the Archean crust evolution line is estimated after Archean sample data after Öhlander et al. (1987).*

The epsilon-Nd plot shows an even clearer trend from the southernmost most area (CNBW) towards the northernmost area, including the study area. The proportion of more juvenile samples increases further away from the previously estimated Archean-Paleoproterozoic boundary to the southwest, with an opposite trend northwest from the boundary. Samples used for the epsilon-Hf plot and the epsilon-Nd plot are a mix between felsic and more mafic rocks, the mafic rocks could therefore be the reason for the values dragging towards the depleted mantle evolution line and a more juvenile source. Therefore, the rock types have been plotted with different colours in Figure 6.8 and Figure 6.9. In this way, it will be easier to see if the intrusive rocks tend to plot towards a more juvenile source towards southwest, or of it's just a result from the more mafic rocks found in the different areas.

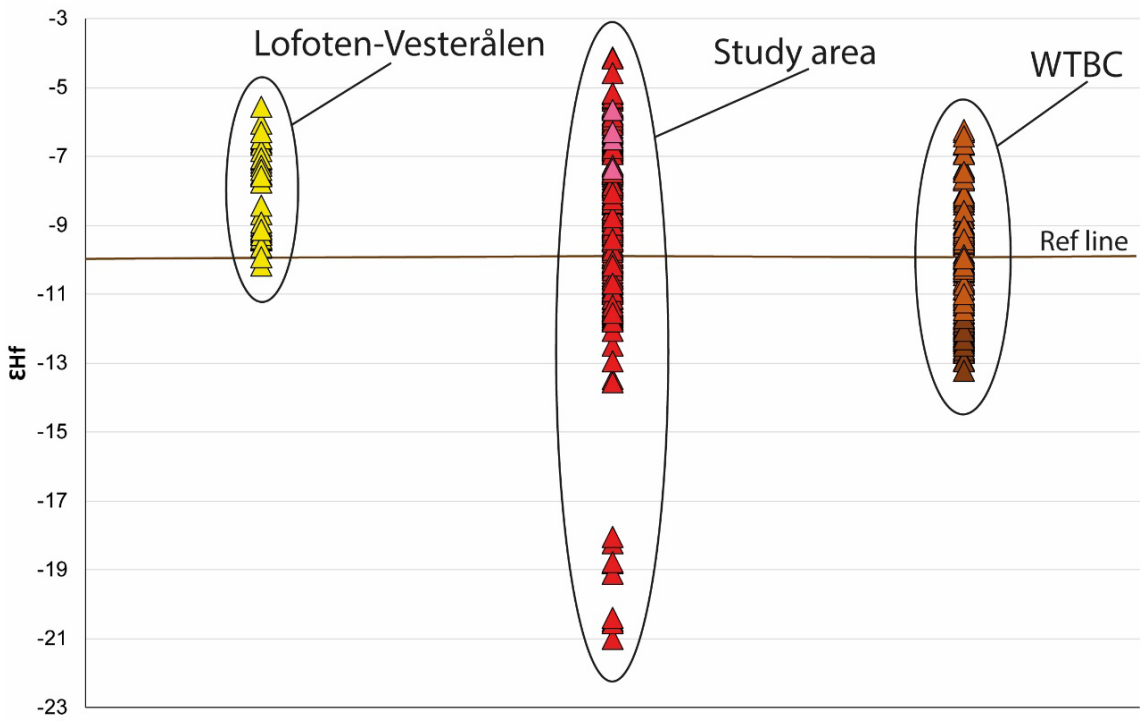

Figure 6.8: *Epsilon-Hf evolution plot for 1.8 Ga rocks from Lofoten-Vesterålen (Laurent et al., 2019), the study area and WTBC (Slagstad et al., unpublished data 2019). The reference line is modelled in an excel sheet from Tom Andersen with a crustal component with a T_{DM} of 3.1 Ga and a $^{176}Lu/^{177}Hf$ value of 0.015. For the study area and WTBC the lightest colour indicates the mafic samples and the darkest colour indicate the granitic rocks.*

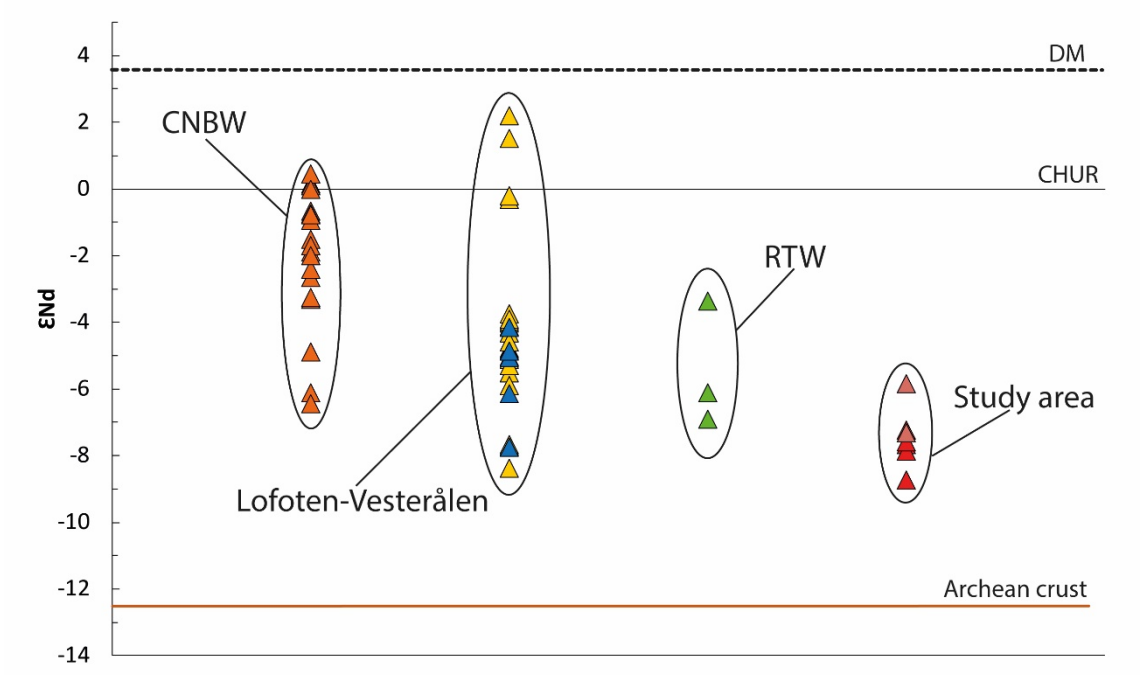

Figure 6.9: *Epsilon-Nd evolution plot for 1.8 Ga rocks from CNBW, Lofoten-Vesterålen, RTW and the study area. The depleted mantle evolution line is modelled after DePaolo (1981) and the Archean crust evolution line is estimated based on Öhlander et al. (1987). For the study area, the RTW and Lofoten-Vesterålen the lightest colour indicates the mafic samples and the darkest colour indicate the more felsic to intermediate rocks.*

Figure 6.8 shows that the two samples from the Lofoten-Vesterålen area and the intrusive rocks from the study area show some samples that plot towards a more juvenile composition than the granitic rocks from further north in the WTBC. However, Figure 6.9 shows that the samples from Lofoten-Vesterålen and the study area did have a bias in the first epsilon-Nd evolution plot and were dragged towards a more juvenile source due to more mafic samples. The samples from the study area plots far down on the diagram, whilst the ε_{Nd} value increases for the RTW, both areas showing rocks that must have been formed from a source with a considerable component of isotopically evolved crust. The granitic samples from CNBW show a clear trend towards a more juvenile source. These findings do not confirm the exact position of the Archean-Paleoproterozoic boundary, but they might give an idea of how the Archean crust might lay at depth in the crust- tapering out towards southwest (see Figure 6.10).

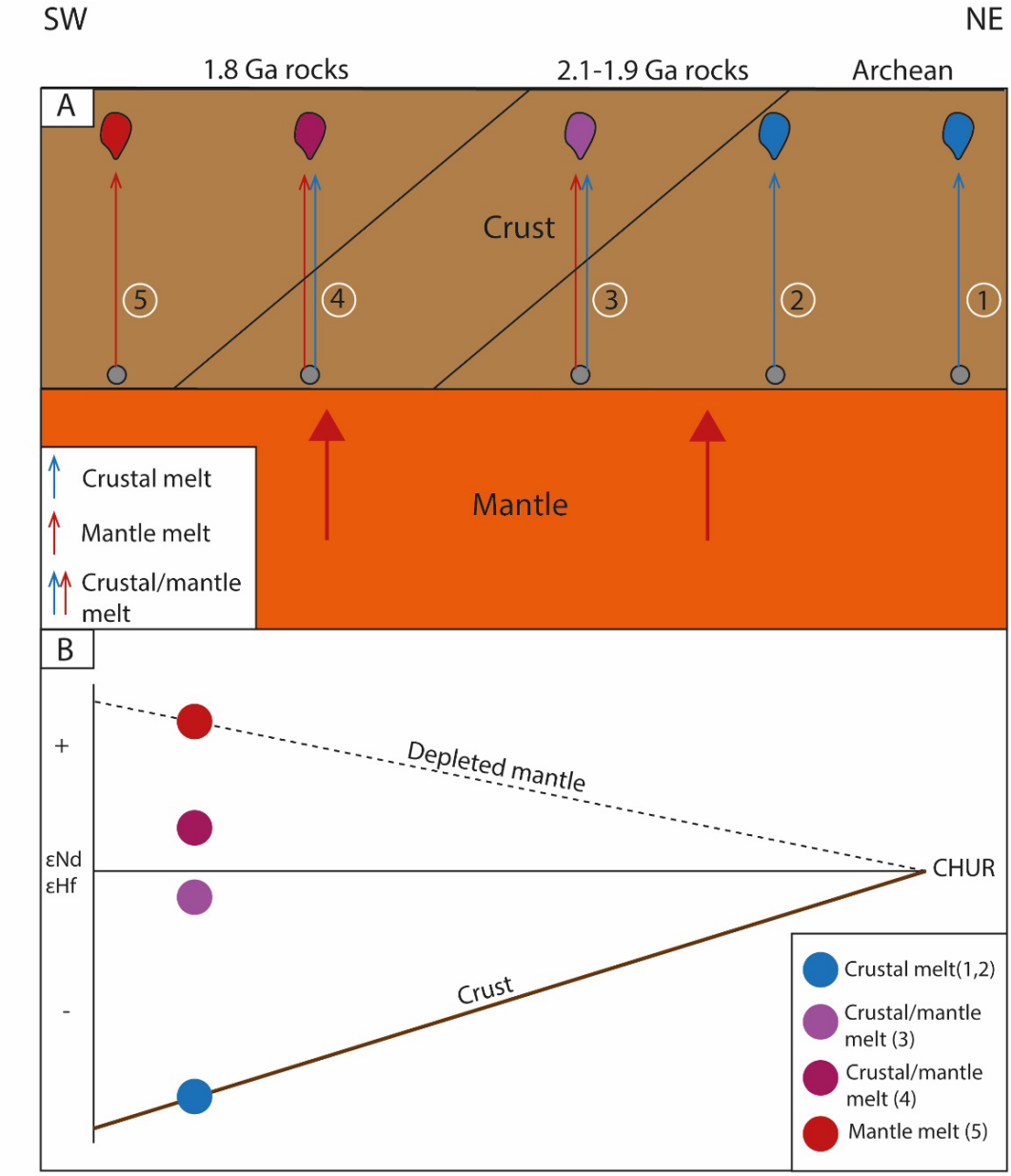

Figure 6.10: *An illustration of how the Archean crust may look underneath the surface dipping towards SW. The numbers from 1 to 5 show how different melts can be composited by only Archean crust (1)(2), a mix between Archean crustal melt and mantle melt (3), a mix between 2.1-1.9 Ga crustal melt and 1.8 Ga mantle melt (4) or only 1.8 Ga mantle melt (5).*

ε_{Nd} values and ε_{Hf} values differ from the Archean rocks and the younger intrusive rocks. However, the boundary between the Archean and Paleoproterozoic rocks is most certainly not very sharp and due to e.g. the 2.1 to 1.9 Ga rocks found in the RTW it is reasonable to believe that the isotopic values reflect more than just the end-members, and this is attempted to be illustrated in Figure 6.10A-B. If a model based on mixing and assimilation were constructed it would be possible to find ε_{Nd} and ε_{Hf} values that are reasonable for rocks crystallized from a pure Archean crustal melt (1)(2), and for a pure 1.8 Ga depleted mantle melt (5). This would then enable a construction of a gradient from the Archean to the Paleoproterozoic boundary. Pure Archean crustal melt would give a highly negative ε_{Nd} and ε_{Hf} value as both elements are highly incompatible, they would be enriched in the crust and therefore have a larger proportion of decay to the respectively two daughter isotopes of ^{144}Nd and ^{177}Hf. These isotopic data can be used to understand the expected ε-values when crustal melt and mantle melt is mixed, as in the case of (3) and (4) in Figure 6.10B. A depleted mantle melt mixed with a crustal melt component would change the properties of the magma, and the resulting ε_{Nd} and ε_{Hf} values would be moved in a direction towards the middle of the evolution plot (Figure 6.10B).

6.3 Extent of the 1.9-1.88 Ga Supracrustals

Supracrustal belts are found several places at the southwestern margin of the Fennoscandian Shield. They are observed in the WTBC, Altevatn and in the RTW. These supracrustal rocks have been dated to an age in the range of 2.85 to 1.97 Ga (Bergh et al., 2010). The supracrustal rocks found in the study area show an age of 1.9 Ga, the same age as found for the supracrustal rocks in Kiruna (Westhues et al., 2017). The rock types found within the supracrustal unit found at Bjarkøya and Meløyvær in the study area varies from carbonates, meta-arkosic rocks, quartzites, mica-schists, amphibolite and gneiss. At Meløyvær there is a skarn deposit with an iron-mineralisation in the supracrustal rocks, that earlier settlement mined for.

6.3.1 Mineralisation in the supracrustal belts

The geology of Norway and Sweden are often said to be the same, the rocks found on the Norwegian side of the border are similar to the rocks found on the Swedish side. It would therefore be tempting to argue that if there is a mineralisation in the supracrustal rocks found in e.g. Kiruna-Gällivare, Skellefte and Bergslagen, these should exist also in the Norwegian supracrustal rocks. As previously mentioned, the supracrustal rocks found in the study area show the same age as the supracrustal rocks in Kiruna. By comparing the isotopic data from the 1.9 Ga rocks from the study area and the 1.9 Ga rocks from Kiruna, it would be easier to make a suggestion if the same mineralisation should be present also on the Norwegian side. The ε_{Hf} values from the study area and from Kiruna are plotted in the squared box in Figure 6.11.

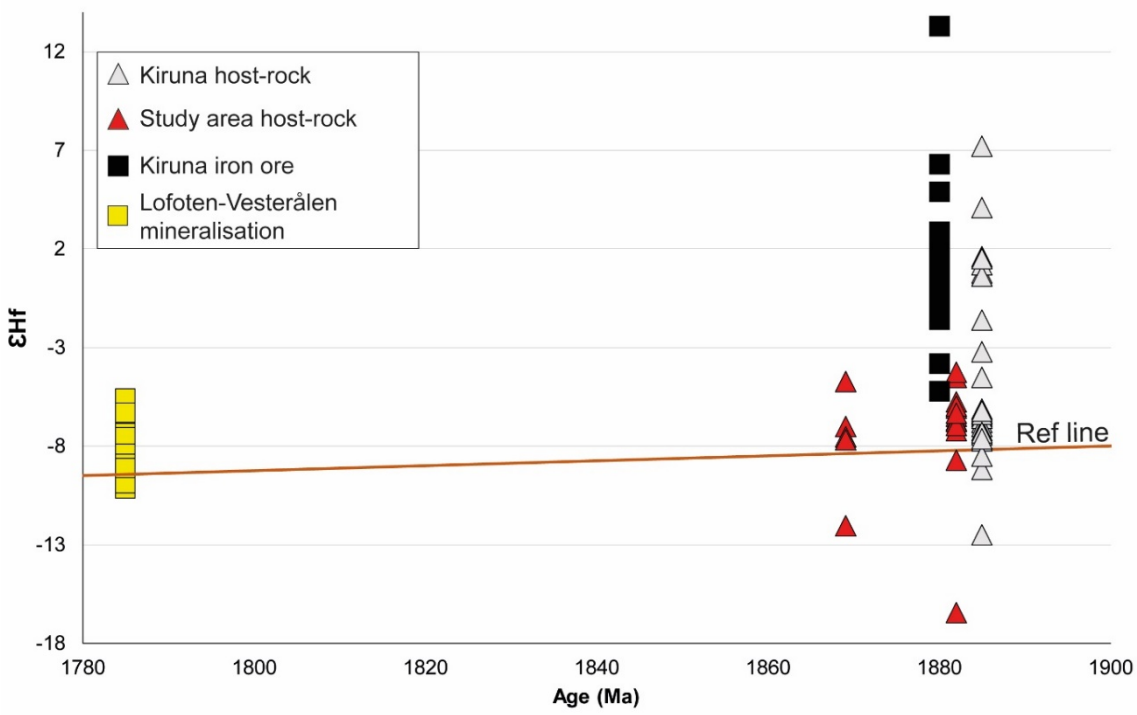

Figure 6.11: *Comparison of ε_{Hf} values from the supracrustal host rock in the study area and Kiruna, together with the mineralisation in Kiruna and from two samples collected in the Lofoten-Vesterålen area.*

The results from Figure 6.11 shows that the supracrustal rocks found in the study area are comparable to the supracrustal rocks of Kiruna. The mineralisations seem to be less correlated, even though some of them have ε_{Hf} values in a slightly similar range. However, it is interesting to investigate possible processes that could be the reason for these differences. A hypothetic idea to explain how the mineralisations in Lofoten-Vesterålen still can be related to the mineralisations in Kiruna would be if a magmatic event with a highly crustal melt intruded a supracrustal rock which had a much lower ε_{Hf} value. The result would be that the newly formed rock would have a ε_{Hf} value dragged towards more negative values.

Based on the data that have been analysed for ε_{Hf} the supracrustal rocks found at Bjarkøya show that the isotopic composition is not similar to the mineralisations of Kiruna. However, the supracrustal rocks show similarities to the host rock of the mineralisations in Kiruna suggesting that the supracrustal rocks found at Bjarkøya could be the host rock.

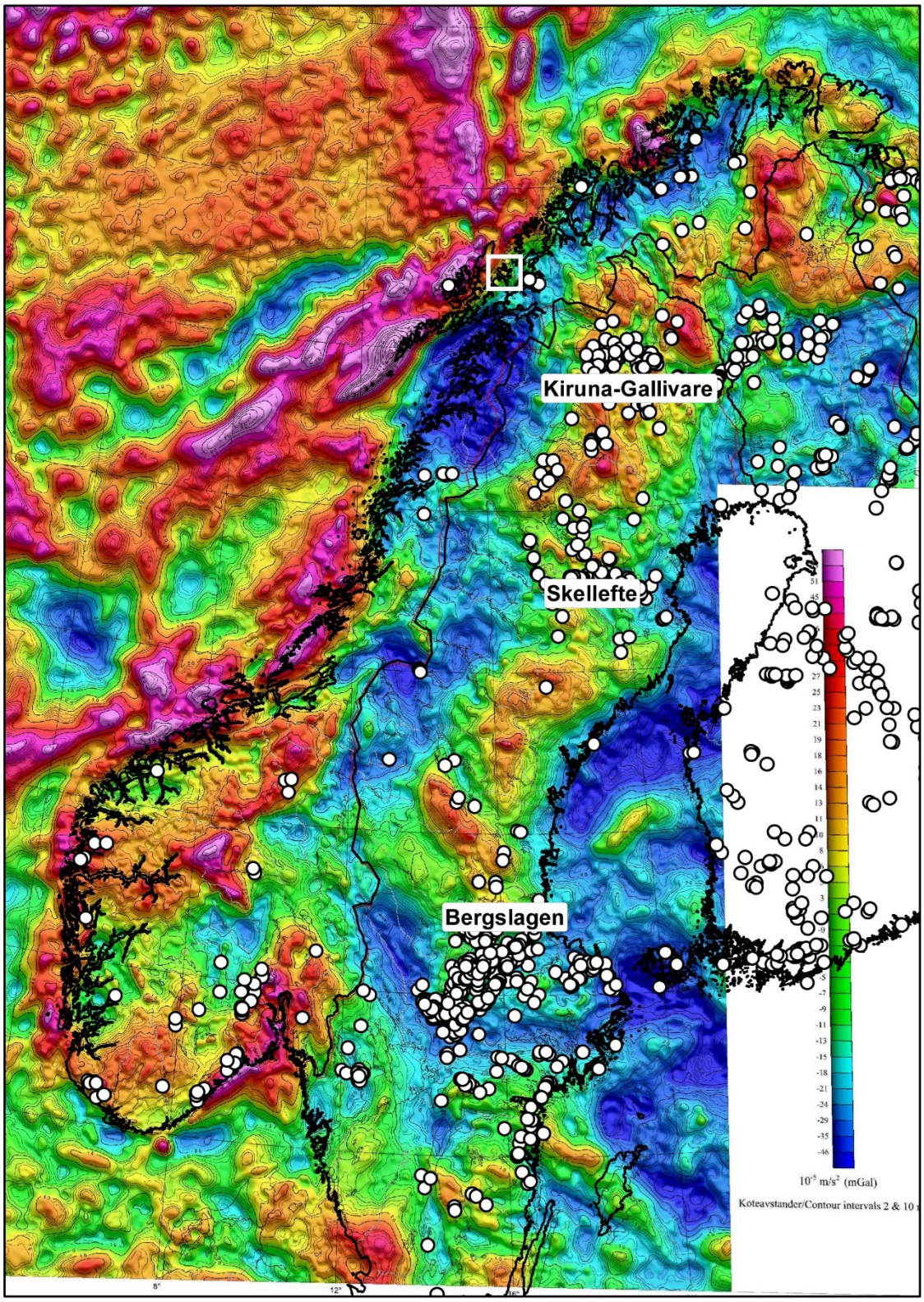

Figure 6.12: *Density map for Norway, Sweden and part of Finland. The largest known ore-deposits in Sweden are marked on the map, together with a white box showing the location of the study area where 1.9 Ga supracrustal rocks are found. Density map from Olesen, O., Ebbing, J., Gellein, J., Kihle, O., Myklebust, R., Sand, M., Skilbrei, J.R., Solheim, D. & Usov, S. 2010. Gravity anomaly map, Norway and adjacent area. Scale 1:3 million. Geological Survey of Norway.*

A close study of Figure 6.12 shows that through Sweden there is a high gravity anomaly, marked with warmer colours on the map. This indicates that Sweden has denser rocks than Norway, and the mining activity on ores are found in exactly these denser rocks (Kiruna-Gällivare, Skellefte, Bergslagen). The same is not evident for Norway, a belt of less dense rocks can be followed from the north of Norway to the central southern part of Norway. This belt is correlative to the TIB, which caused a large magmatic event in large parts of Norway around 1.86 to 1.66 (Roberts and Slagstad, 2014). This magmatic event intruded the supracrustal belts that are found in the northern part of Norway. The interpretation is therefore that there might have been supracrustal rocks with the same mineralisation as those found in Sweden, but because of the intrusions related to the TIB and the 1.8 Ga magmatism- these rocks have largely been replaced.

7 Conclusions

- Geochronological data obtained from this study concludes that the intrusive rocks at Grytøya, Bjarkøya, Sandsøya and Krøttøya were formed by a magmatic event at ca. 1.8 Ga. External geochronological data from Rombak Tectonic Window, West-Troms Basement Complex, Lofoten-Vesterålen area and Central Nordland Basement Window suggest that the 1.8 Ga magmatism was a regional magmatic event.

- Field observations, together with petrographic studies show that the same rocks have been exposed to various degrees of deformation and metamorphism. Mineral assemblages suggest metamorphism mainly in greenschist-facies, with a few exceptions laying in amphibolite-facies.

- Lu-Hf isotope data from zircons and Sm-Nd isotope data from whole-rock geochemistry agrees that the rocks of the study area originated from a crustal melt, with uncertain input of depleted mantle material. Modelling of the Archean crustal ε_{Hf} evolution line of the region, shows that all the rocks plots within a small range close to the evolution line at 1.8 Ga – supporting the idea of a crustal melt.

- The REE spider plots show a typical trend of rocks formed in relation to a subduction zone. They show high concentrations of LILE, with sinking concentrations towards the HFSE, in addition to a negative Nb and Ta anomaly. Furthermore, it follows that Rb vs. (Y-Nb) discrimination diagrams show that the samples from the study area plot within the fields of volcanic-arc granites and within-plate granites. These findings conclude that a comparison with the tectonic setting found for RTW is reasonable.

- A compressional tectonic setting with delamination as a possible driving force is suggested to explain the voluminous granitic magmatism at 1.8 Ga, with an extent from WTBC in the north, Rombak to the east, through the study area and Lofoten-Vesterålen to the west and CNBW in the south. This suggestion is supported by geochemistry, geochronology and structural data from the respective areas.

- Isotope data supports the idea of an Archean-Paleoproterozoic boundary south of the study area but gives no further constraint regarding its exact position.

- This study also concludes that the potential of finding economically commercial mineralisation in the 1.9 Ga supracrustal rocks of Norway, similar to the mineralisation found in 1.9 Ga supracrustal rocks are low. The potential mineralisation is believed to have been destroyed by magmatism related to 1.8 Ga. granitic melts. However, the supracrustal from Bjarkøya do show similarities with the host-rock from Kiruna in ε_{Hf} values, suggesting that the host-rock is the same on both sides of the border between Norway and Sweden.

8 References

ANGVIK, T. L. 2014. Structural development and metallogenesis of Paleoproterozoic volcano-sedimentary rocks of the Rombak Tectonic Window.

BERGH, S. G., KULLERUD, K., ARMITAGE, P. E., BOUKE ZWAAN, K., CORFU, F., RAVNA, E. J. & INGE MYHRE, P. 2010. Neoarchaean to Svecofennian tectono-magmatic evolution of the West Troms Basement Complex, North Norway. *Norwegian Journal of Geology,* 90**,** 21-48.

BERGH, S. G., KULLERUD, K., CORFU, F., ARMITAGE, P. E., DAVIDSEN, B., JOHANSEN, H. W., PETTERSEN, T. & KNUDSEN, S. 2007. Low-grade sedimentary rocks on Vanna, North Norway: a new occurrence of a Palaeoproterozoic (2.4-2.2 Ga) cover succession in northern Fennoscandia. *Norwegian Journal of Geology/Norsk Geologisk Forening,* 87.

BERGH, S. G., KULLERUD, K., MYHRE, P. I., CORFU, F., ARMITAGE, P., ZWAAN, K. & RAVNA, E. 2014. Archaean elements of the basement outliers west of the Scandinavian Caledonides in Northern Norway: architecture, evolution and possible correlation with Fennoscandia. *Evolution of Archean Crust and Early Life.* Springer.

BERGMAN, S., KÜBLER, L. & MARTINSSON, O. 2001. *Description of regional geological and geophysical maps of northern Norrbotten county (east of the Caledonian orogen)*, SGU.

BEST, M. 1975. Migration of hydrous fluids in the upper mantle and potassium variation in calc-alkalic rocks. *Geology,* 3**,** 429-432.

BEST, M. G. 2013. *Igneous and metamorphic petrology*, John Wiley & Sons.

BLACK, L. P., KAMO, S. L., ALLEN, C. M., DAVIS, D. W., ALEINIKOFF, J. N., VALLEY, J. W., MUNDIL, R., CAMPBELL, I. H., KORSCH, R. J. & WILLIAMS, I. S. 2004. Improved 206Pb/238U microprobe geochronology by the monitoring of a trace-element-related matrix effect; SHRIMP, ID–TIMS, ELA–ICP–MS and oxygen isotope documentation for a series of zircon standards. *Chemical Geology,* 205**,** 115-140.

BLYSTAD, P. 1995. Structural elements of the Norwegian continental shelf. Part 2: The Norwegian Sea region. *NPD Bull.,* 8.

BOGDANOVA, S., BINGEN, B., GORBATSCHEV, R., KHERASKOVA, T., KOZLOV, V., PUCHKOV, V. & VOLOZH, Y. A. 2008. The East European Craton (Baltica) before and during the assembly of Rodinia. *Precambrian Research,* 160**,** 23-45.

BREWER, T. S., DALY, J. S. & ÅHÄLL, K.-I. 1998. Contrasting magmatic arcs in the Palaeoproterozoic of the south-western Baltic Shield. *Precambrian Research,* 92**,** 297-315.

CHU, N.-C., TAYLOR, R. N., CHAVAGNAC, V., NESBITT, R. W., BOELLA, R. M., MILTON, J. A., GERMAN, C. R., BAYON, G. & BURTON, K. 2002. Hf isotope ratio analysis using multi-collector inductively coupled plasma mass spectrometry: an evaluation of isobaric interference corrections. *Journal of Analytical Atomic Spectrometry,* 17**,** 1567-1574.

CLAOUÉ-LONG, J. C., COMPSTON, W., ROBERTS, J. & FANNING, C. M. 1995. Two Carboniferous ages: a comparison of SHRIMP zircon dating with conventional zircon ages and 40Ar/39Ar analysis. *Society for Sedimentary Geology (SEPM),* Special Publication No. 54**,** 3-21.

COMPSTON, W., WILLIAMS, I. & MEYER, C. 1984. U-Pb geochronology of zircons from lunar breccia 73217 using a sensitive high mass-resolution ion microprobe. *Journal of Geophysical Research: Solid Earth*

89**,** B525-B534.

CORFU, F. 2004. U–Pb age, setting and tectonic significance of the anorthosite–mangerite–charnockite–granite suite, Lofoten–Vesterålen, Norway. *Journal of Petrology,* 45**,** 1799-1819.

CORFU, F. 2007. Multistage metamorphic evolution and nature of the amphibolite–granulite facies transition in Lofoten–Vesterålen, Norway, revealed by U–Pb in accessory minerals. *Chemical Geology,* 241**,** 108-128.

CORFU, F., ARMITAGE, P. E., KULLERUD, K. & BERGH, S. G. 2003. Preliminary U-Pb geochronology in the West Troms Basement Complex, North Norway: Archaean and Palaeoproterozoic events and younger overprints. *Norges geologiske undersøkelse Bulletin,* 441**,** 61-72.

CRIBB, S. J. 1981. Rb-Sr geochronological evidence suggesting a reinterpretation of part of the North Norwegian Caledonides. *Norsk Geologisk Tidsskrift,* 61**,** 97-110.

FAURE, G. & MENSING, T. M. 2005. *Isotopes: principles and applications*, Wiley-Blackwell.

FRIETSCH, R. & PERDAHL, J.-A. On the nature of the lower Proterozoic volcanic rocks in southern Norrbotten, northern Sweden. Proterozoic Geochemistry: 03/06/1987-06/06/1987, 1987.

GAÁL, G. & GORBATSCHEV, R. 1987. An outline of the Precambrian evolution of the Baltic Shield. *Precambrian research,* 35**,** 15-52.

GRIFFIN, W., TAYLOR, P., HAKKINEN, J., HEIER, K., IDEN, I., KROGH, E., MALM, O., OLSEN, K., ORMAASEN, D. & TVETEN, E. 1978. Archaean and proterozoic crustal evolution in Lofoten–Vesterålen, N Norway. *Journal of the Geological Society,* 135**,** 629-647.

GUSTAVSON, M. 1974. a. Narvik. Beskrivelse til det berggrunnsgeologiske gradteigskart N9–1: 100000. *Nor. Geol. Unders,* 308.

HAWKESWORTH, C., O'NIONS, R., PANKHURST, R., HAMILTON, P. & EVENSEN, N. 1977a. A geochemical study of island-arc and back-arc tholeiites from the Scotia Sea. *Earth Planetary Science Letters,* 36**,** 253-262.

HAWKESWORTH, C., O'NIONS, R., PANKHURST, R., HAMILTON, P. & EVENSEN, N. 1977b. A geochemical study of island-arc and back-arc tholeiites from the Scotia Sea. *Earth and Planetary Science Letters,* 36**,** 253-262.

HUHMA, H. 1986. Sm-Nd, U-Pb and Pb-Pb isotopic evidence for the origin of the Early Proterozoic Svecokarelian crust in Finland. *Geol. Surv. Finland Bull.,* 337.

HÖGDAHL, K., ANDERSSON, U. B. & EKLUND, O. 2004. *The Transscandinavian Igneous Belt (TIB) in Sweden: a review of its character and evolution*, Geological survey of Finland Espoo.

IRELAND*, T., CLEMENT, S., COMPSTON, W., FOSTER, J., HOLDEN, P., JENKINS, B., LANC, P., SCHRAM, N. & WILLIAMS, I. 2008. Development of SHRIMP. *Australian Journal of Earth Sciences,* 55**,** 937-954.

JACKSON, S. E., PEARSON, N. J., GRIFFIN, W. L. & BELOUSOVA, E. A. 2004. The application of laser ablation-inductively coupled plasma-mass spectrometry to in situ U–Pb zircon geochronology. *Chemical Geology,* 211**,** 47-69.

KAY, R. W. & KAY, S. M. 1993. Delamination and delamination magmatism. *Tectonophysics,* 219**,** 177-189.

KOISTINEN, T., STEPHENS, M.B., BOGATCHEV, V., NORDGULEN, Ø., WENNERSTRÖM, M. AND KORHONEN, J. 2001. *Geological Map of The Fennoscandian Shield (Scale 1: 2 000 000)*. Geological Survey of Finland, Norway and Sweden and the North-West Department of Natural Resources of Russia.

KORNELIUSSEN, A. & SAWYER, E. W. 1989. The geochemistry of Lower Proterozoic mafic to felsic igneous rocks, Rombak Window, North Norway. *Nor. geol. unders. Bull. ,* 415**,** 23-38.

KULLERUD, K., CORFU, F. & BERGH, S. G. 2006a. U-Pb constraints on the late Palaeoproterozoic evolution of the West Troms Basement Complex, northern Norway. *Geological Society of Finland Bulletin,* 1**,** 23.

KULLERUD, K., SKJERLIE, K. P., CORFU, F. & JESÚS, D. 2006b. The 2.40 Ga Ringvassøy mafic dykes, West Troms Basement Complex, Norway: the concluding act of early Palaeoproterozoic continental breakup. *Precambrian Research,* 150**,** 183-200.

LAURENT, O., VANDER AUWERA, J., BINGEN, B., BOLLE, O. & GERDES, A. 2019. Building up the first continents: Mesoarchean to Paleoproterozoic crustal evolution in West Troms, Norway, inferred from granitoid petrology, geochemistry and zircon U-Pb/Lu-Hf isotopes. *Precambrian Research,* 321**,** 303-327.

MARKL, G. & HÖHNDORF, A. 2003a. Isotopic constraints on the origin of AMCG-suite rocks on the Lofoten Islands, N Norway. *Mineralogy*

Petrology, 78**,** 149-171.
MARKL, G. & HÖHNDORF, A. 2003b. Isotopic constraints on the origin of AMCG-suite rocks on the Lofoten Islands, N Norway. *Mineralogy and Petrology,* 78**,** 149-171.
MOTUZA, G., MOTUZA, V., BELIATSKY, B. & SAVVA, E. Volcanic rocks of the Ringvassøya Greenstone Belt (North Norway): implication for the stratigraphy and tectonic setting. Journal of Conference, 2001. 577-578.
MYHRE, P. I., CORFU, F. & BERGH, S. 2011. Palaeoproterozoic (2.0–1.95 Ga) pre-orogenic supracrustal sequences in the West Troms Basement Complex, North Norway. *Precambrian Research,* 186**,** 89-100.
MYHRE, P. I., CORFU, F., BERGH, S. G. & KULLERUD, K. 2013. U-Pb geochronology along an Archaean geotransect in the West Troms Basement Complex, North Norway. *Norwegian Journal of Geology/Norsk Geologisk Forening,* 93.
NORDGULEN, Ø. & ANDRESEN, A. 2008. The Precambrian. *The Making of a Land—Geology of Norway***,** 62-119.
PATCHETT, P. & TATSUMOTO, M. 1980. Hafnium isotope variations in oceanic basalts. *Geophysical Research Letters,* 7**,** 1077-1080.
PEARCE, J. A. Geochemical evidence for the genesis and eruptive setting of lavas from Tethyan ophiolites. Proceedings of the International Ophiolite Symposium, Cyprus 1979, 1980. Ministry of Agriculture and Natural Resources, Cyprus, 261-272.
PEARCE, J. A., HARRIS, N. B. & TINDLE, A. G. 1984. Trace element discrimination diagrams for the tectonic interpretation of granitic rocks. *Journal of petrology,* 25**,** 956-983.
PHARAOH, T. C. & PEARCE, J. A. 1984. Geochemical evidence for the geotectonic setting of early Proterozoic metavolcanic sequences in Lapland. *Precambrian Research,* 25**,** 283-308.
ROBERTS, N. M. W. & SLAGSTAD, T. 2014. Continental growth and reworking on the edge of the Columbia and Rodinia supercontinents; 1.86–0.9 Ga accretionary orogeny in southwest Fennoscandia. *International Geology Review,* 57**,** 1582-1606.
ROLLINSON, H. R. 2014. *Using geochemical data: evaluation, presentation, interpretation*, Routledge.
ROMER, R., KJØSNES, B., KORNELIUSSEN, A., LINDAHL, I., SKYSETH, T., STENDAL, M. & SUNDVOLL, B. 1992. The Archaean–Proterozoic boundary beneath the Caledonides of northern Norway and Sweden: U–Pb, Rb–Sr and Nd isotopic data from the Rombak–Tysfjord area. *NGU report,* 91**,** 67.
SCHOENE, B. 2014. 4.10-U–Th–Pb Geochronology. *Treatise on geochemistry,* 4**,** 341-378.
SKIÖLD, T. 1988. Implications of new U□ Pb zircon chronology to early Proterozoic crustal accretion in northern Sweden. *Precambrian Research,* 38**,** 147-164.
SKÅR, Ø. 2002. U–Pb geochronology and geochemistry of early Proterozoic rocks of the tectonic basement windows in central Nordland, Caledonides of north-central Norway. *Precambrian Research,* 116**,** 265-283.
SLAGSTAD, T., DAVIDSEN, B. & DALY, J. S. 2011. Age and composition of crystalline basement rocks on the Norwegian continental margin: offshore extension and continuity of the Caledonian–Appalachian orogenic belt. *Journal of the Geological Society,* 168**,** 1167-1185.
SLAGSTAD, T., WILLEMOES-WISSING, B., COINT, N., STAMPOLIDIS, A., GANERØD, M. & OFSTAD, F. 2015. Geology and metallogenic potential of the northwesternmost Norrbotten Province around Altevatn in Troms, northern Norway. *Norwegian Journal of Geology,* 95**,** 445-466.
SLÁMA, J., KOŠLER, J., CONDON, D. J., CROWLEY, J. L., GERDES, A., HANCHAR, J. M., HORSTWOOD, M. S., MORRIS, G. A., NASDALA, L. & NORBERG, N. 2008. Plešovice zircon—a new natural reference material for U–Pb and Hf isotopic microanalysis. *Chemical Geology,* 249**,** 1-35.
SOLLI, A. & NORDGULEN, Ø. 2006. Berggrunnskart over Norge og kaledonidene i Sverige og Finland. *Norges Geologiske Undersøkelse, Trondheim*.

STEIGER, R. H. & JÄGER, E. 1977. Subcommission on geochronology: convention on the use of decay constants in geo-and cosmochronology. *Earth*

planetary science letters, 36**,** 359-362.
STERN, R. A., BODORKOS, S., KAMO, S. L., HICKMAN, A. H. & CORFU, F. 2009. Measurement of SIMS instrumental mass fractionation of Pb isotopes during zircon dating. *Chemical Geology Geostandards*

Geoanalytical Research, 33**,** 145-168.
SUN, S.-S. & MCDONOUGH, W. F. 1989. Chemical and isotopic systematics of oceanic basalts: implications for mantle composition and processes. *Geological Society, London, Special Publications,* 42**,** 313-345.
SUN, S.-S. & NESBITT, R. W. 1978. Petrogenesis of Archaean ultrabasic and basic volcanics: evidence from rare earth elements. *Contributions to Mineralogy*

Petrology, 65**,** 301-325.
TULL, J., BARTLEY, J., HODGES, K., ANDRESEN, A., STELTENPOHL, M. & WHITE, J. 1985. The Caledonides in the Ofoten region (68–69N), north Norway: Key aspects of tectonic evolution. *The Caledonide Orogen: Scandinavia and Related Areas. Wiley, Chichester,* 553**,** 569.
WESTHUES, A., HANCHAR, J. M., LEMESSURIER, M. J. & WHITEHOUSE, M. J. 2017. Evidence for hydrothermal alteration and source regions for the Kiruna iron oxide–apatite ore (northern Sweden) from zircon Hf and O isotopes. *Geology,* 45**,** 571-574.
WIEDENBECK, M., ALLE, P., CORFU, F., GRIFFIN, W., MEIER, M., OBERLI, F., QUADT, A. V., RODDICK, J. & SPIEGEL, W. 1995. Three natural zircon standards for U-Th-Pb, Lu-Hf, trace element and REE analyses. *Geostandards newsletter,* 19**,** 1-23.
WILBERG, R. 1987. Rekognoserende Rb-Sr aldersbestemmelser av gra nitisk gneiser fra grunnfjellsvinduene Høgtuva og Sjona I Nord land. *Norges Geologiske Undersøkelse Rapport,* 87**,** 21.
WILLIAMS, I. S. 1998. U-Th-Pb geochronology by ion microprobe. *Reviews in Economic Geology,* 7**,** 1-35.
WILSON, M. R. & NICHOLSON, R. 1973. The structural setting and geochronology of basal granitic gneisses in the Caledonides of part of Nordland, Norway. *Journal of the Geological Society,* 129**,** 365-386.
WINTER, J. D. 2013. *Principles of igneous and metamorphic petrology*, Pearson education.
WOOD, D. A. 1980. The application of a ThHfTa diagram to problems of tectonomagmatic classification and to establishing the nature of crustal contamination of basaltic lavas of the British Tertiary Volcanic Province. *Earth and planetary science letters,* 50**,** 11-30.
WOODHEAD, J., HERGT, J., SHELLEY, M., EGGINS, S. & KEMP, R. 2004. Zircon Hf-isotope analysis with an excimer laser, depth profiling, ablation of complex geometries, and concomitant age estimation. *Chemical Geology,* 209**,** 121-135.
ZHANG, S., LI, Z.-X., EVANS, D. A., WU, H., LI, H. & DONG, J. 2012. Pre-Rodinia supercontinent Nuna shaping up: a global synthesis with new paleomagnetic results from North China. *Earth*

Planetary Science Letters, 353**,** 145-155.
ZHAO, G., CAWOOD, P. A., WILDE, S. A. & SUN, M. 2002. Review of global 2.1–1.8 Ga orogens: implications for a pre-Rodinia supercontinent. *Earth-Science Reviews,* 59**,** 125-162.
ZWAAN, K. & TUCKER, R. Absolute and relative age relationships in the Precambrian West Troms Basement Complex, northern Norway. 22nd Nordic Geological Winter Meeting, Åbo, Finland, 1996. 237.
ÖHLANDER, B. & SKIÖLD, T. 1994. Diversity of 1.8 Ga potassic granitoids along the edge of the Archaean craton in northern Scandinavia: a result of melt formation at various depths and from various sources. *Lithos,* 33**,** 265-283.

ÖHLANDER, B., SKIÖLD, T., HAMILTON, P. J. & CLAESSON, L.-Å. 1987. The western border of the Archaean province of the Baltic Shield: evidence from northern Sweden. *Contributions to Mineralogy*

Petrology, 95**,** 437-450.
ÅHÄLL, K.-I. & CONNELLY, J. N. 2008. Long-term convergence along SW Fennoscandia: 330 my of Proterozoic crustal growth. *Precambrian Research,* 161**,** 452-474.
ÅHÄLL, K.-I., PERSSON, P.-O. & SKIÖLD, T. 1995. Westward accretion of the Baltic Shield: implications from the 1.6 GaÅmål-Horred Belt, SW Sweden. *Precambrian Research,* 70**,** 235-251.
ÅHÄLL, K. & DALY, J. 1989. Age, tectonic setting and provenance of Østfold-Marstrand Belt supracrustals: Westward crustal growth of the Baltic Shield at 1760 Ma. *Precambrian Research,* 45**,** 45-61.
ÅHÄLL, K. I. 1984. Pillow lava in the Stora Le-Marstrand formation, south-western Sweden. *Geologiska Föreningen i Stockholm Förhandlingar,* 106**,** 105-107.

9 Appendix

Appendix A – Field map with localities and geological measurements

Appendix B – Zircon geochronology

- Appendix B1 – Zircons in alcohol
- Appendix B2 – CL-images with laser spots
- Appendix B3 – U-Pb data
- Appendix B4 - Zircon Trace Elements
- Appendix B5 – Lu-Hf isotope data

Appendix C – Whole-rock geochemistry

- Appendix C1 – Whole-rock major- and trace elements
- Appendix C2 – Sm-Nd isotope data

Appendix D – Thin section descriptions

9.1 Appendix A- Field map

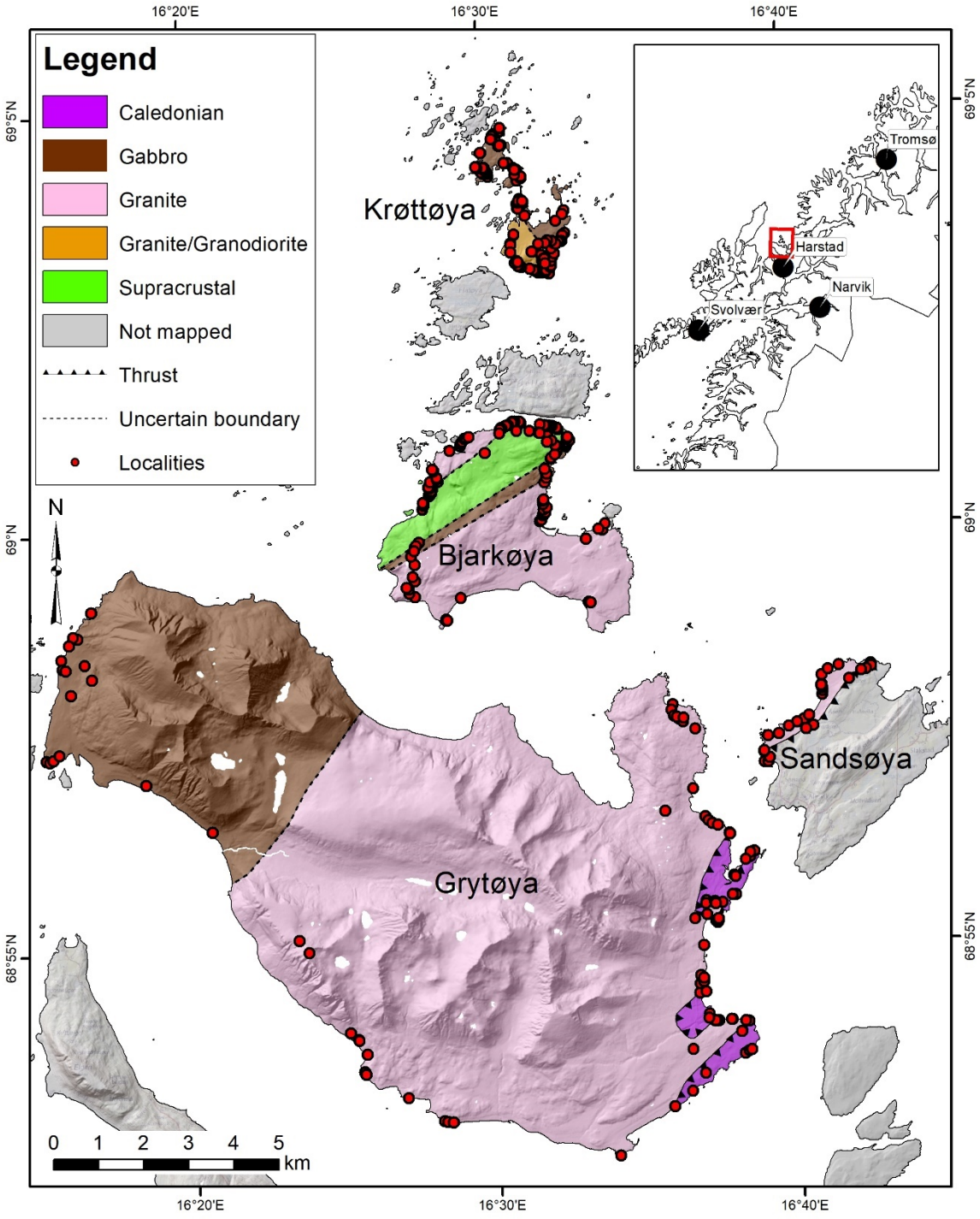

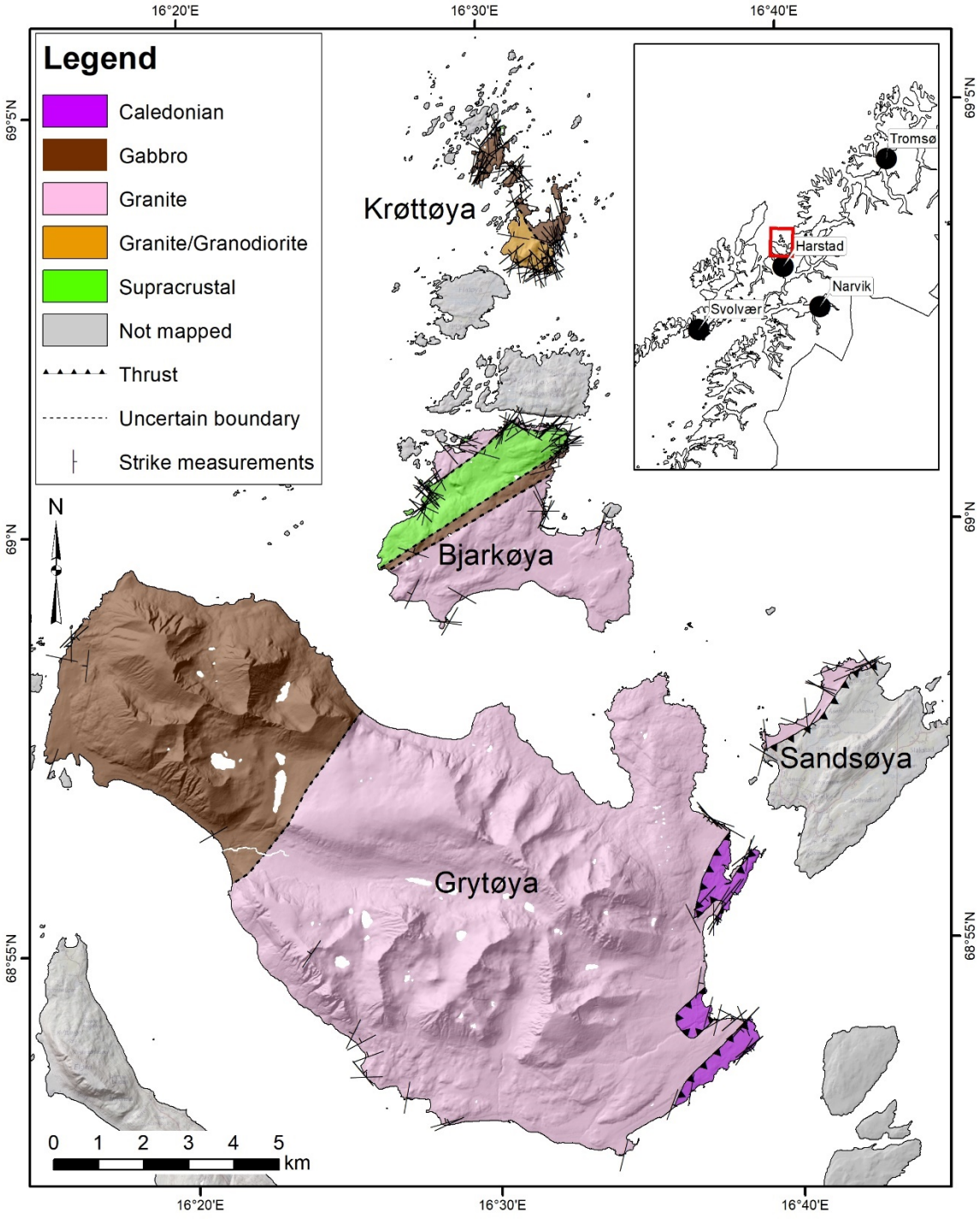
16°20'E
16°30'E
16°40'E
69°5'N
69°N
68°55'N
Legend
Caledonian
Gabbro
Granite
Granite/Granodiorite
Supracrustal
Not mapped
Thrust
Uncertain boundary
Strike measurements
N
Krøttøya
Bjarkøya
Grytøya
Sandsøya
Tromsø
Harstad
Narvik
Svolvær
0 1 2 3 4 5
km

9.2 Appendix B – Zircon geochronology

Appendix B1 – Zircon in alcohol

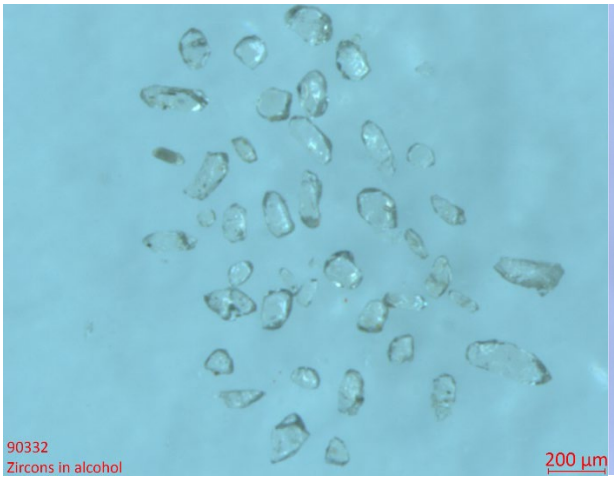

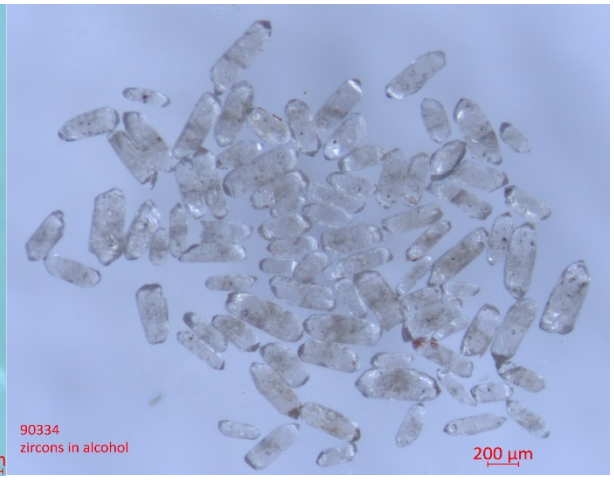

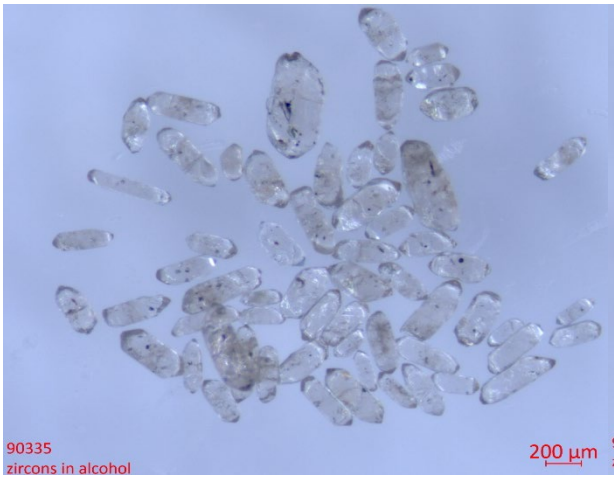

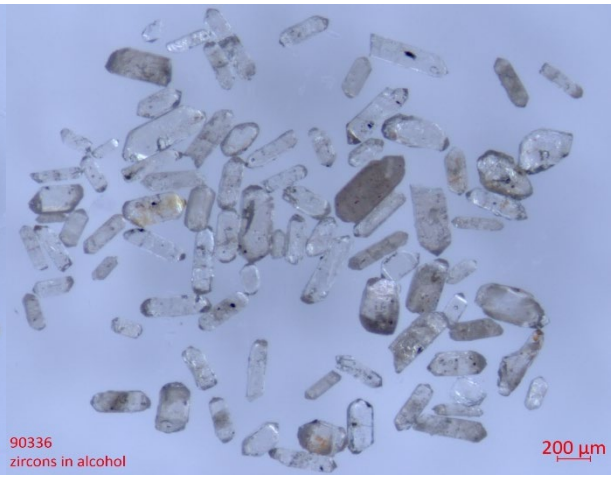

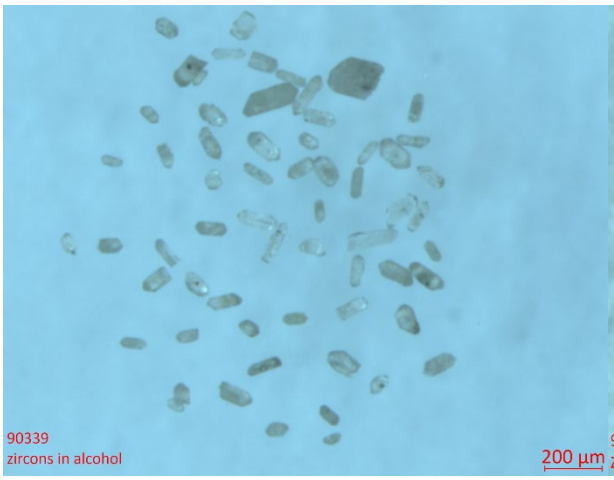

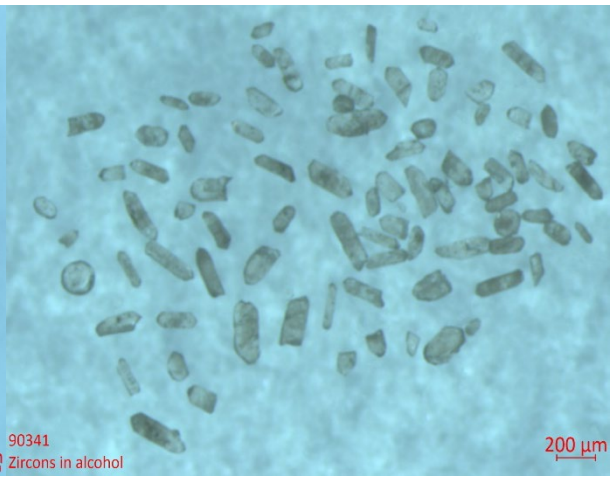

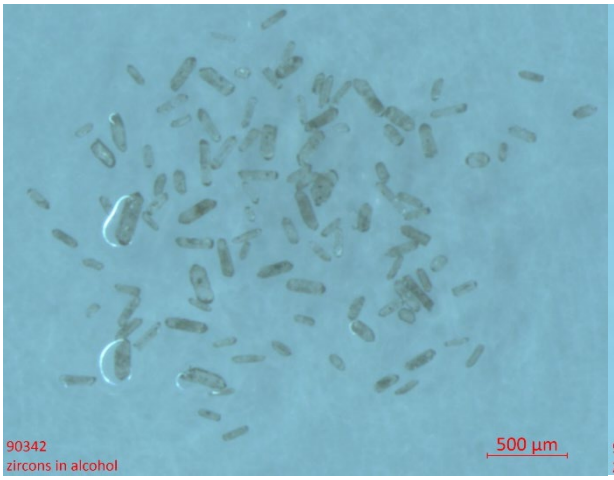
90342
zircons in alcohol
500 µm

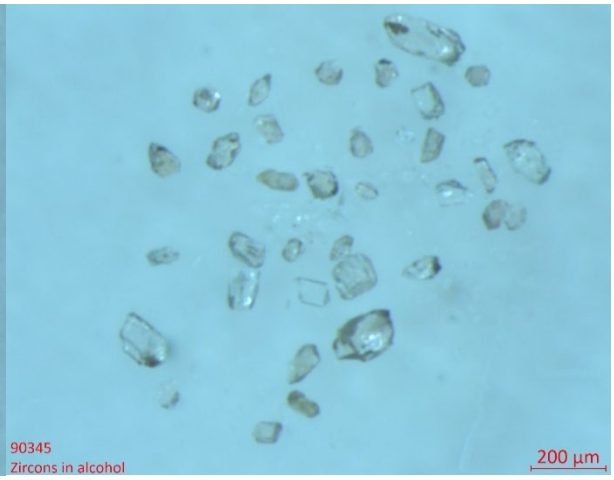
90345
Zircons in alcohol
200 µm

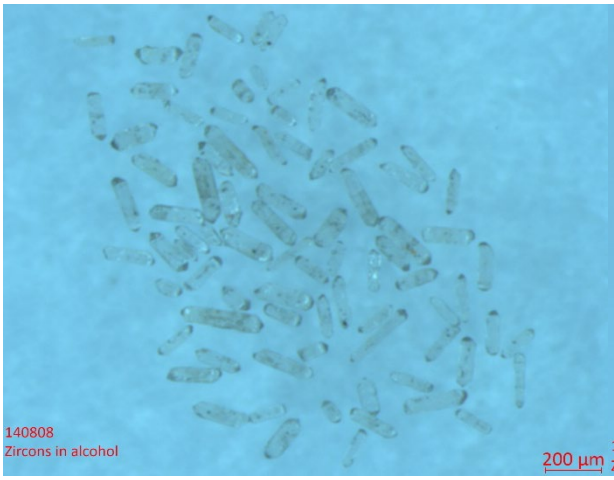
140808
Zircons in alcohol
200 µm

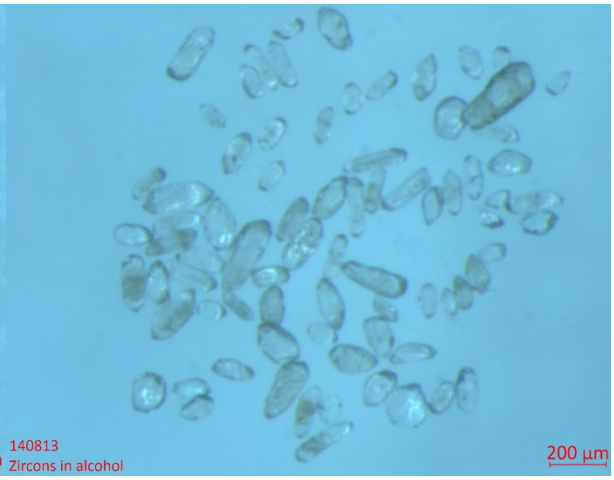
140813
Zircons in alcohol
200 µm

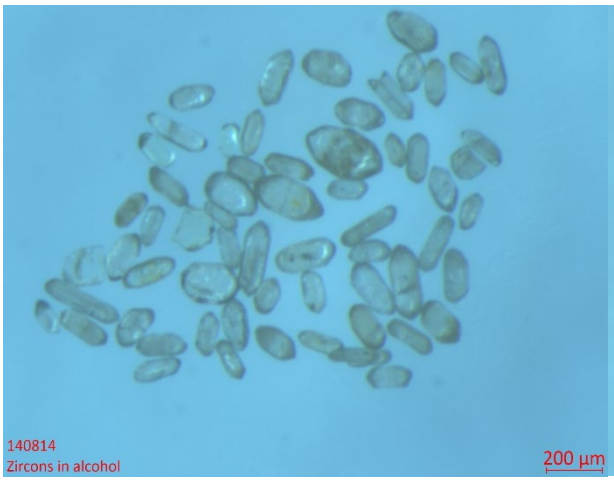
140814
Zircons in alcohol
200 µm

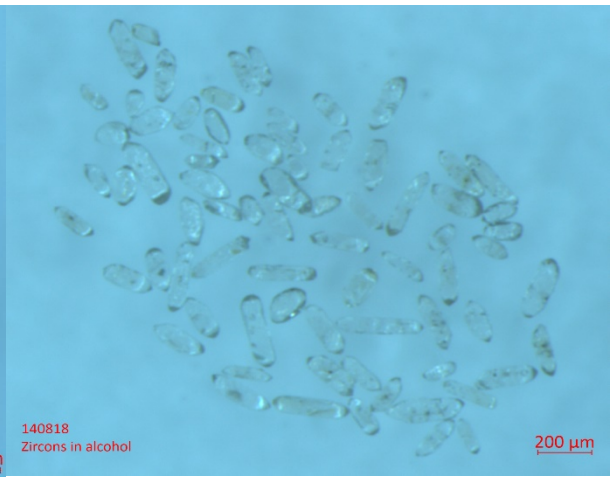
140818
Zircons in alcohol
200 µm

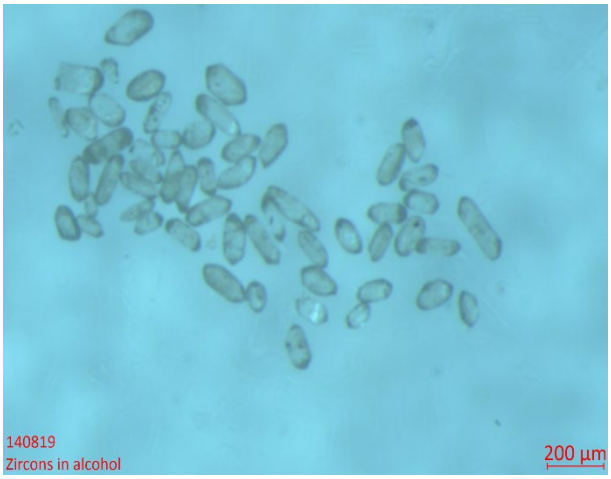
140819
Zircons in alcohol
200 µm

Appendix B2- CL-images with laser spots

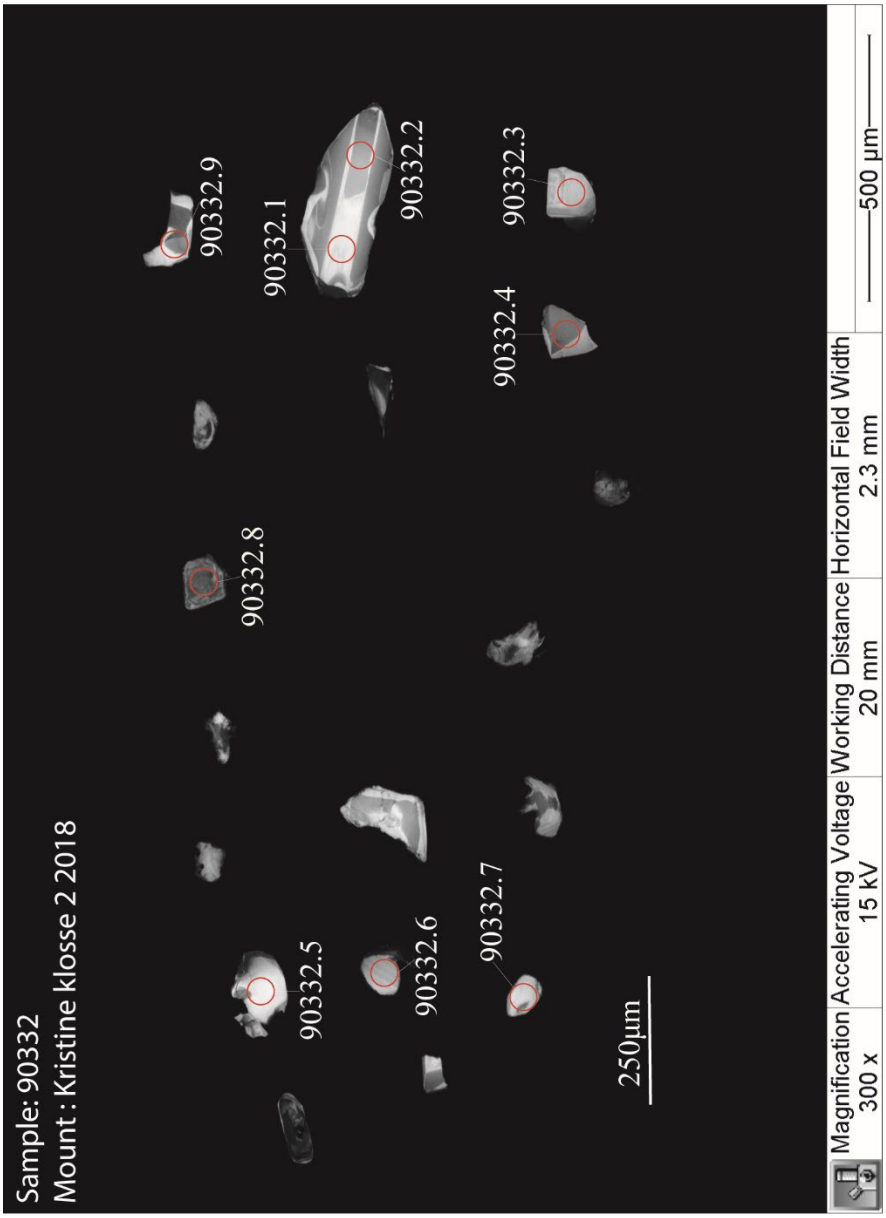

Sample: 90334
Mount : 2018 KristineGN_A

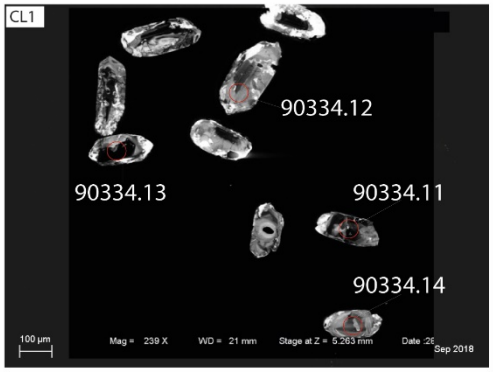

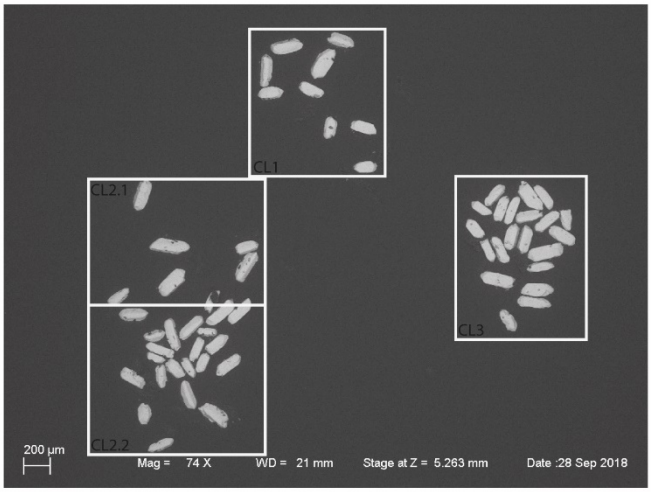

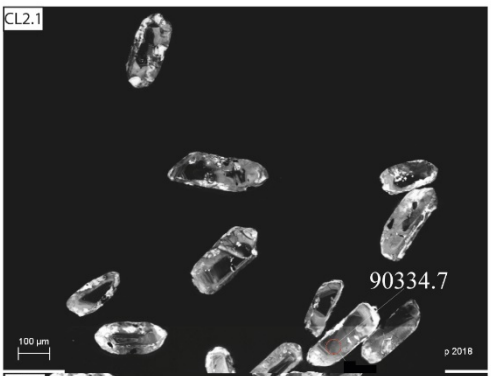

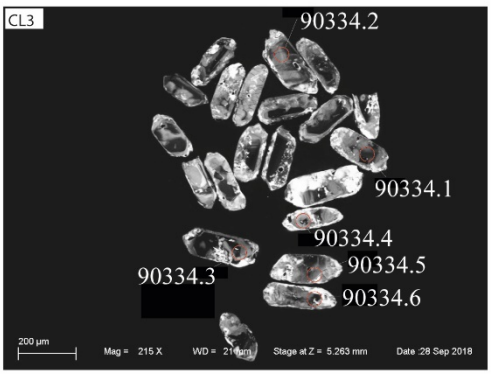

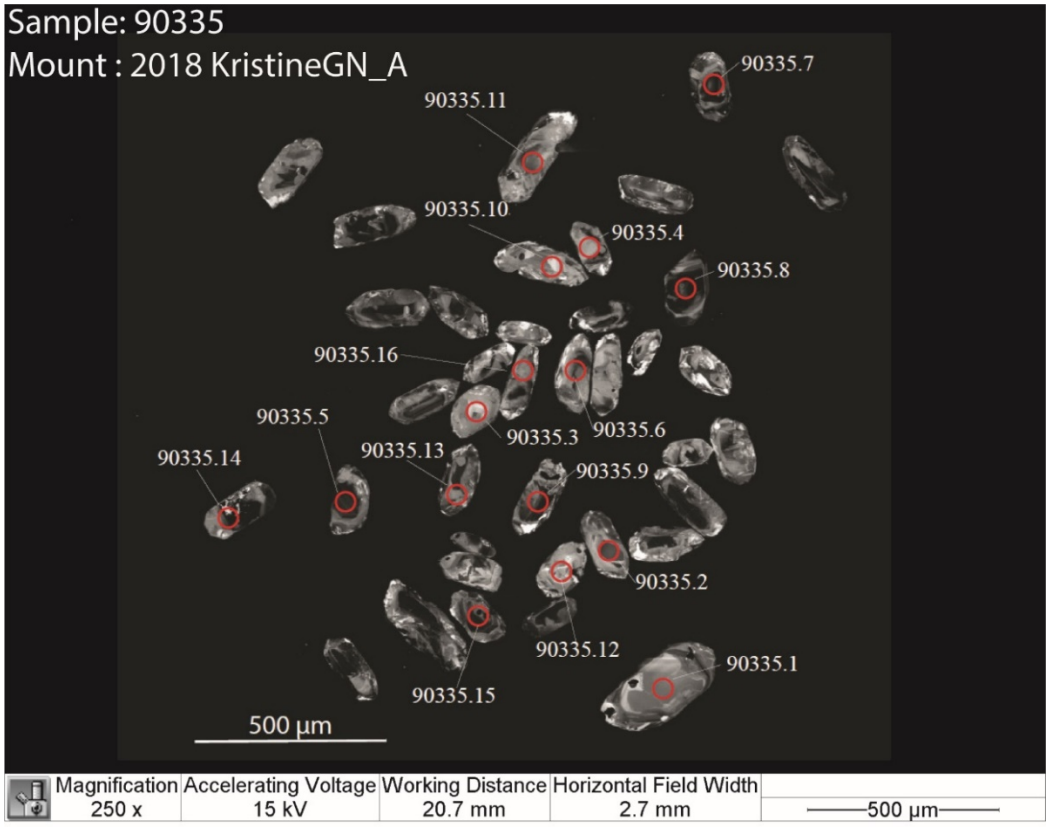
Sample: 90335
Mount : 2018 KristineGN_A
90335.7
90335.11
90335.10
90335.4
90335.8
90335.16
90335.5
90335.3
90335.6
90335.14
90335.13
90335.9
90335.2
90335.12
90335.1
90335.15
500 µm
Magnification
250 x
Accelerating Voltage
15 kV
Working Distance
20.7 mm
Horizontal Field Width
2.7 mm
500 µm


Sample: 90336
Mount : 2018 KristineGN_A
90336.14
90336.8
90336.1
90336.15
90336.11
90336.4
90336.9
90336.10
90336.3
90336.2
90336.13
90336.5
90336.7
90336.12
90336.6
500µm
Magnification
250 x
Accelerating Voltage
15 kV
Working Distance
20.7 mm
500 µm

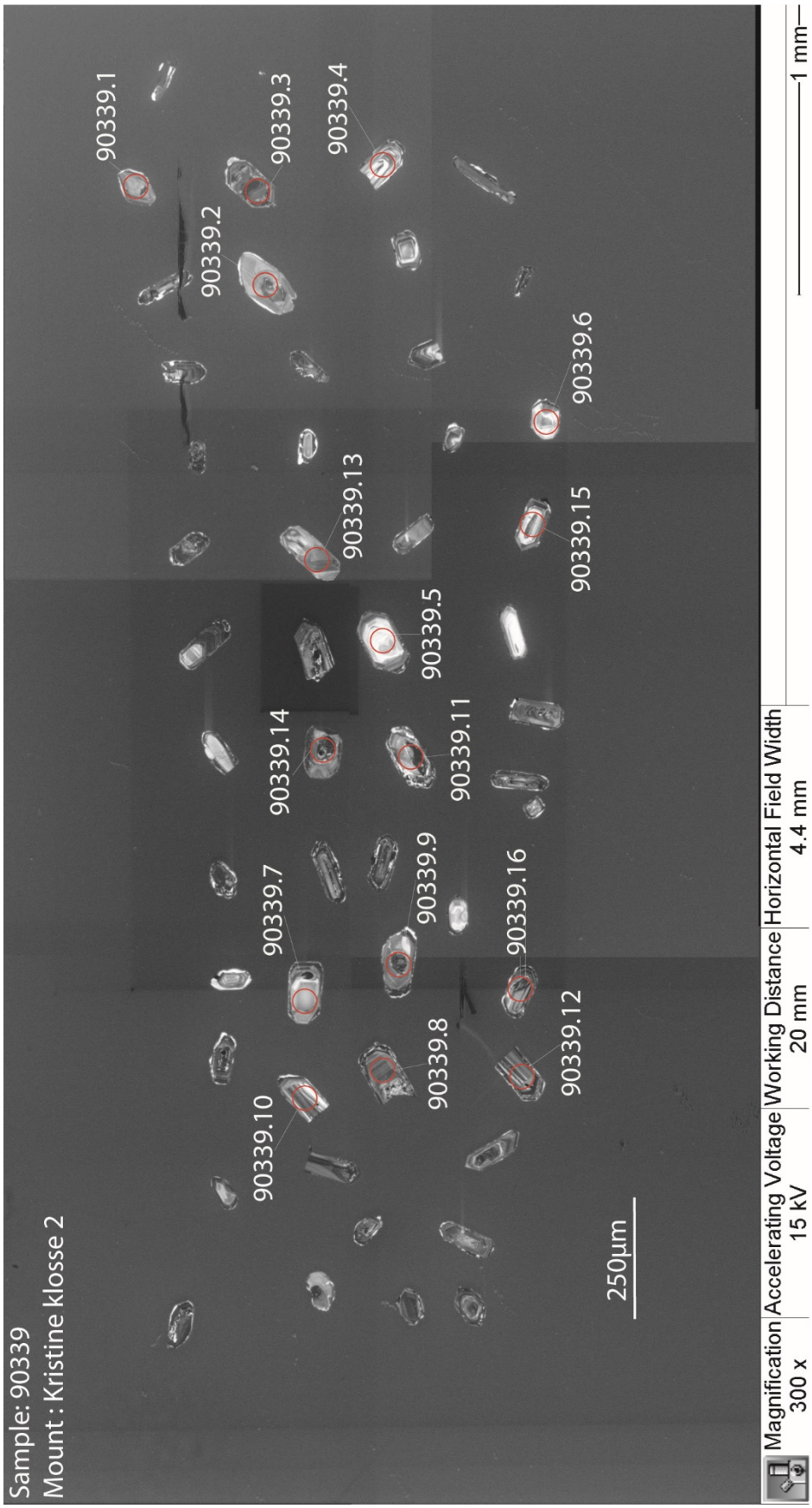
Sample: 90339
Mount : Kristine klosse 2
90339.1
90339.2
90339.3
90339.4
90339.5
90339.6
90339.7
90339.8
90339.9
90339.10
90339.11
90339.12
90339.13
90339.14
90339.15
90339.16
250µm
Magnification
300 x
Accelerating Voltage
15 kV
Working Distance
20 mm
Horizontal Field Width
4.4 mm
1 mm

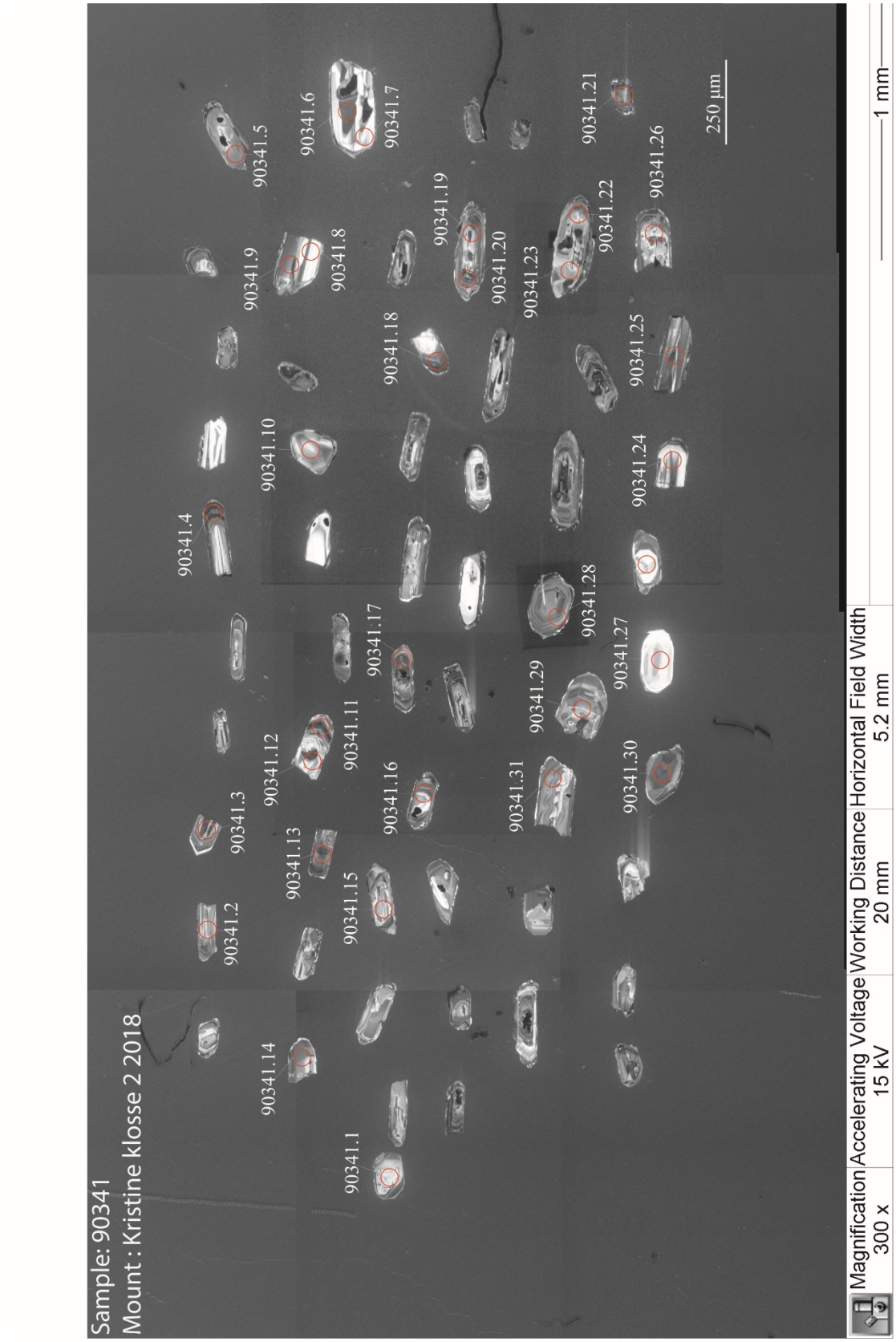
Sample: 90341
Mount : Kristine klosse 2 2018
90341.1
90341.2
90341.3
90341.4
90341.5
90341.6
90341.7
90341.8
90341.9
90341.10
90341.11
90341.12
90341.13
90341.14
90341.15
90341.16
90341.17
90341.18
90341.19
90341.20
90341.21
90341.22
90341.23
90341.24
90341.25
90341.26
90341.27
90341.28
90341.29
90341.30
90341.31
250 µm
Magnification
300 x
Accelerating Voltage
15 kV
Working Distance
20 mm
Horizontal Field Width
5.2 mm
1 mm

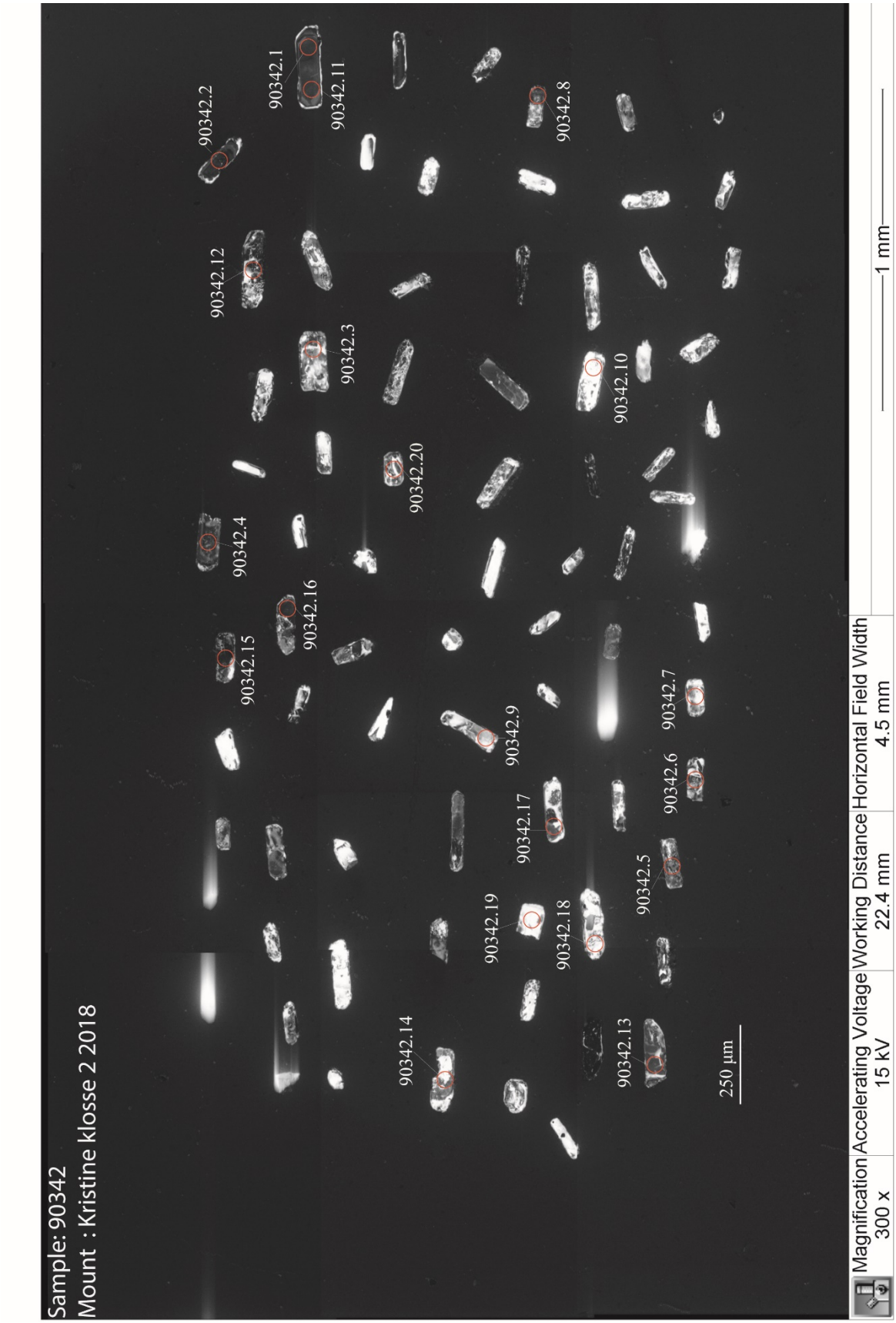
Sample: 90342
Mount : Kristine klosse 2 2018
90342.1
90342.2
90342.3
90342.4
90342.5
90342.6
90342.7
90342.8
90342.9
90342.10
90342.11
90342.12
90342.13
90342.14
90342.15
90342.16
90342.17
90342.18
90342.19
90342.20
250 µm
Magnification 300 x
Accelerating Voltage 15 kV
Working Distance 22.4 mm
Horizontal Field Width 4.5 mm
1 mm

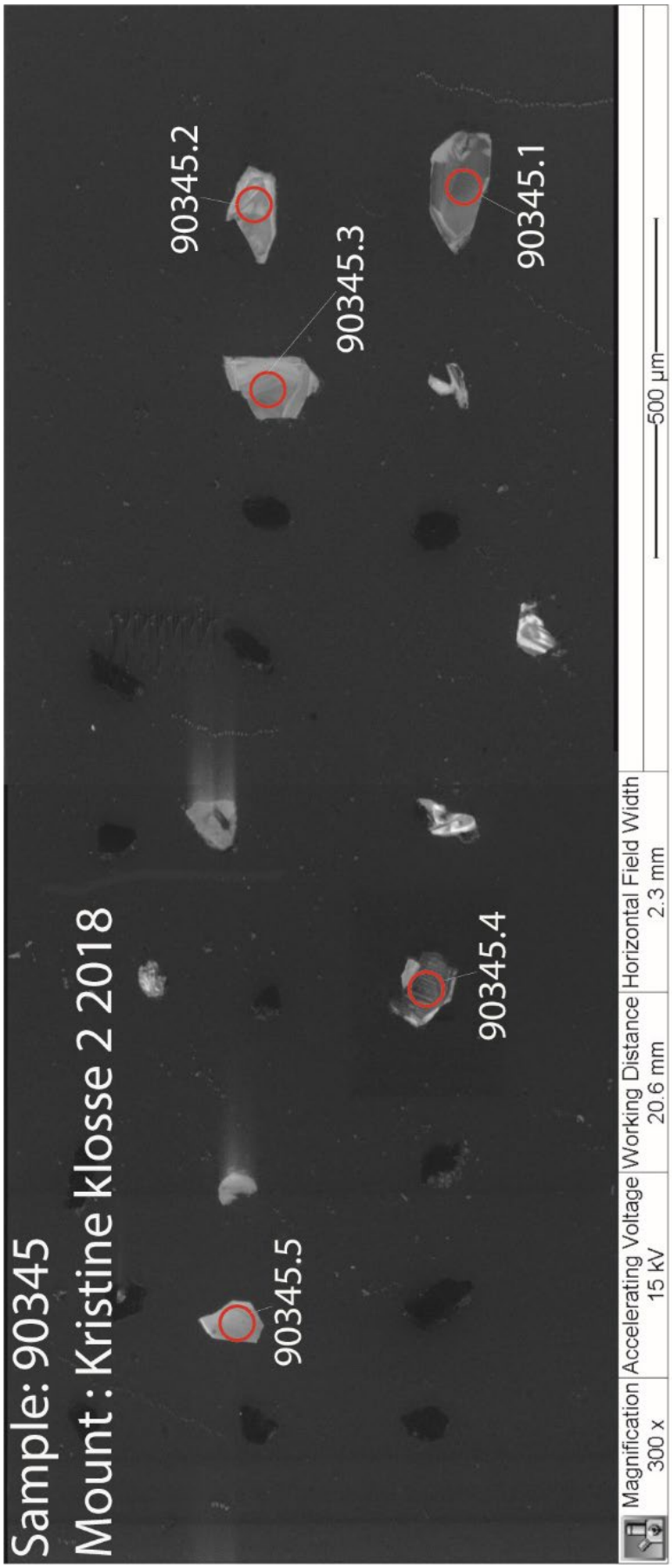
Sample: 90345
Mount : Kristine klosse 2 2018
90345.1
90345.2
90345.3
90345.4
90345.5
500 µm
Magnification
300 x
Accelerating Voltage
15 kV
Working Distance
20.6 mm
Horizontal Field Width
2.3 mm

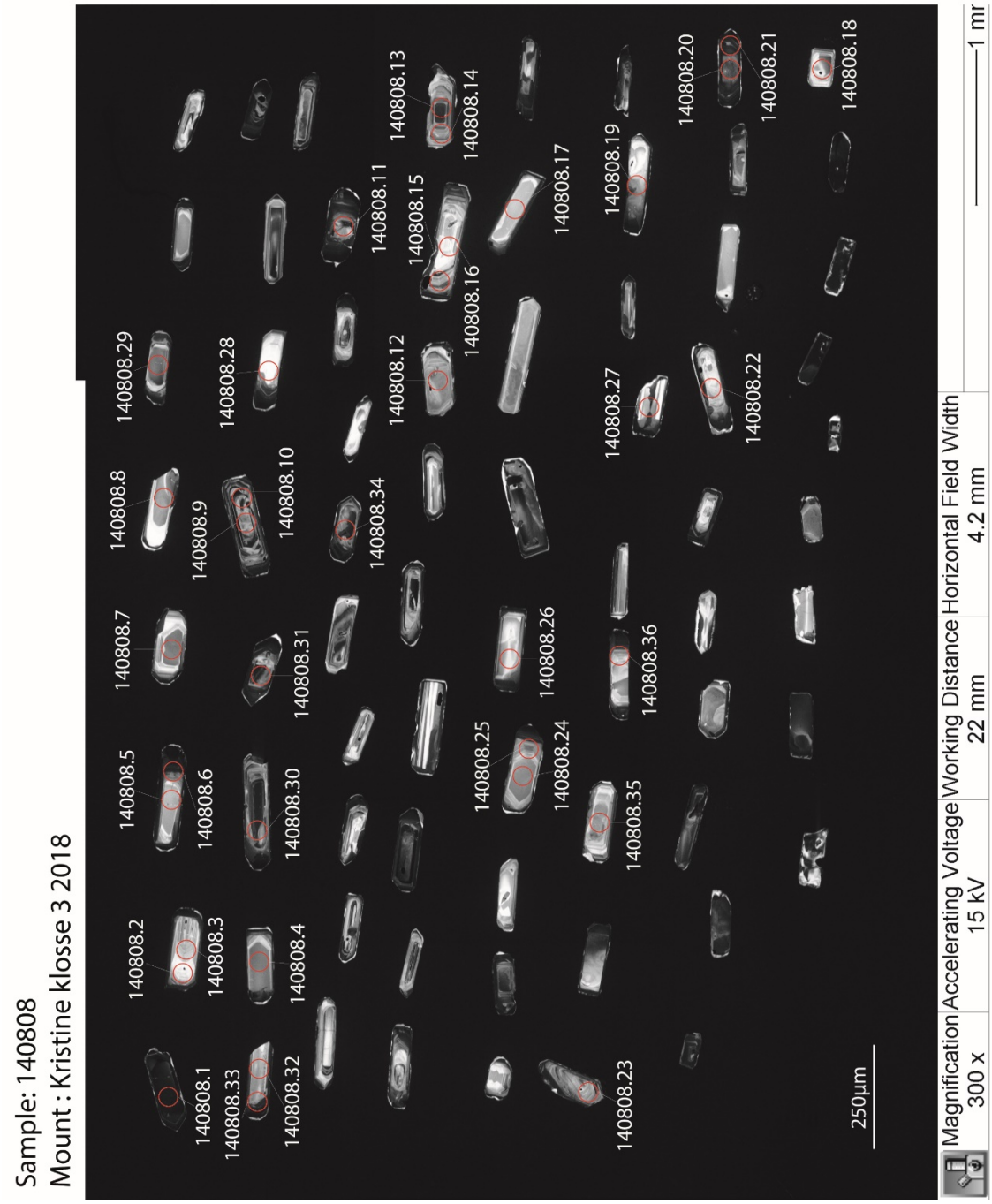
Sample: 140808
Mount : Kristine klosse 3 2018
140808.1
140808.2
140808.3
140808.4
140808.5
140808.6
140808.7
140808.8
140808.9
140808.10
140808.11
140808.12
140808.13
140808.14
140808.15
140808.16
140808.17
140808.18
140808.19
140808.20
140808.21
140808.22
140808.23
140808.24
140808.25
140808.26
140808.27
140808.28
140808.29
140808.30
140808.31
140808.32
140808.33
140808.34
140808.35
140808.36
250µm
Magnification
300 x
Accelerating Voltage
15 kV
Working Distance
22 mm
Horizontal Field Width
4.2 mm
1 mr

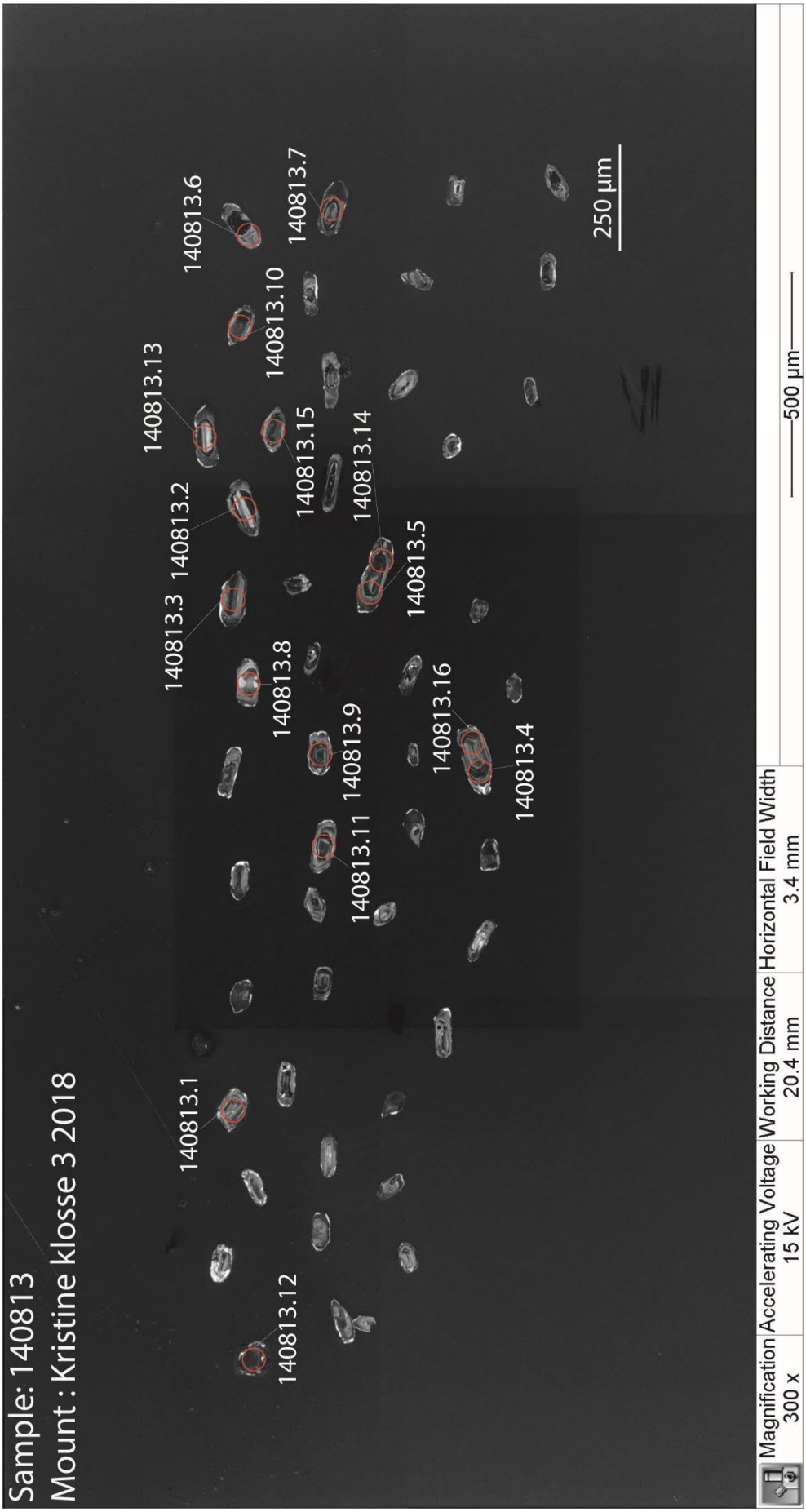
Sample: 140813
Mount : Kristine klosse 3 2018
140813.1
140813.12
140813.11
140813.9
140813.8
140813.3
140813.2
140813.13
140813.15
140813.14
140813.5
140813.16
140813.4
140813.10
140813.6
140813.7
250 µm
500 µm
Magnification
300 x
Accelerating Voltage
15 kV
Working Distance
20.4 mm
Horizontal Field Width
3.4 mm


Sample: 140814
Mount : Kristine klosse 3 2018
140814.13
140814.4
140814.8
140814.7
140814.1
140814.11
140814.2
140814.12
140814.5
140814.16
140814.10
140814.3
140814.9
140814.15
140814.14
140814.6
500 µm
Magnification 300 x
Accelerating Voltage 15 kV
Working Distance 20.6 mm
Horizontal Field Width 3.4 mm

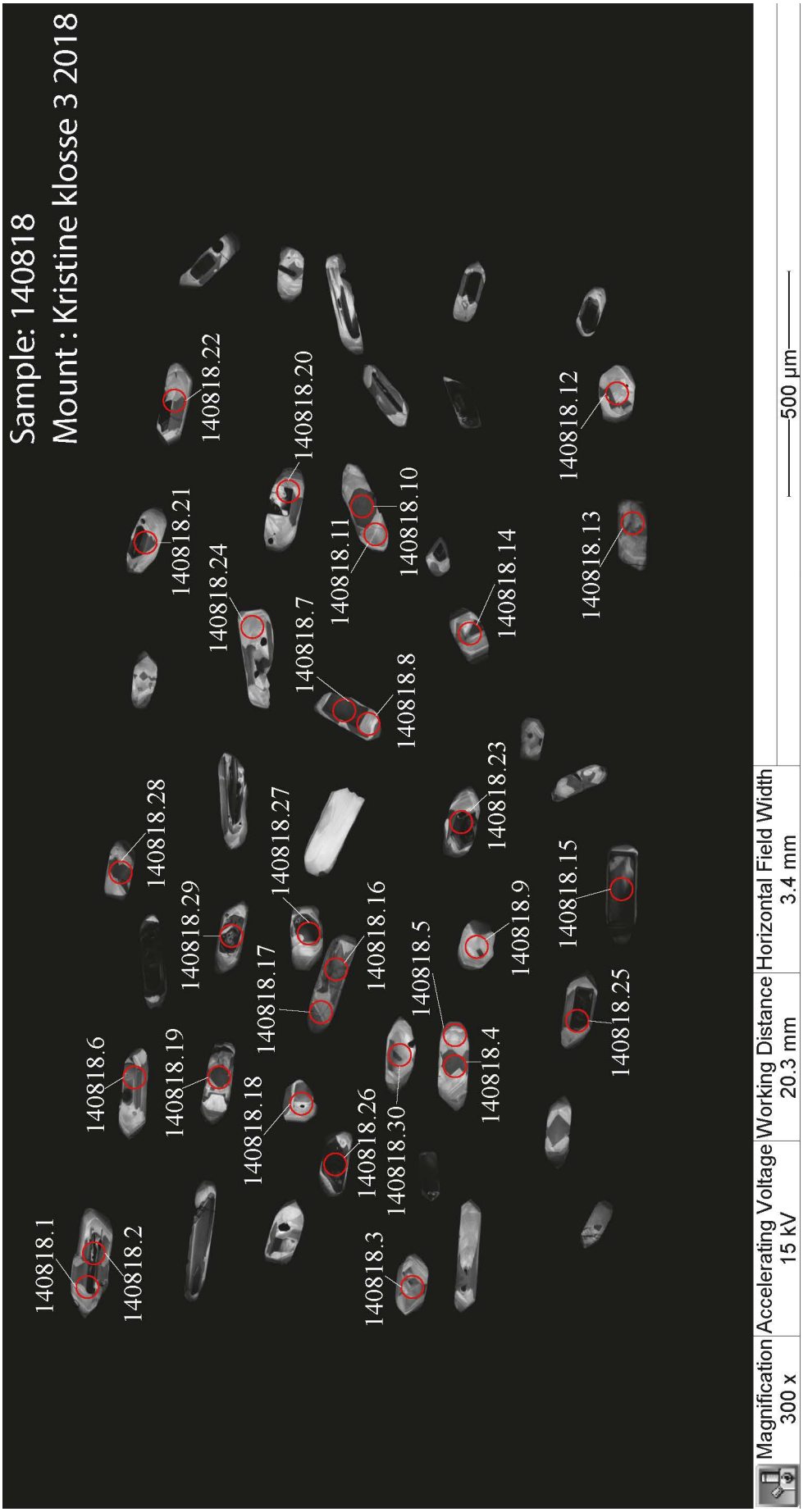
Sample: 140818
Mount : Kristine klosse 3 2018
140818.1
140818.2
140818.3
140818.4
140818.5
140818.6
140818.7
140818.8
140818.9
140818.10
140818.11
140818.12
140818.13
140818.14
140818.15
140818.16
140818.17
140818.18
140818.19
140818.20
140818.21
140818.22
140818.23
140818.24
140818.25
140818.26
140818.27
140818.28
140818.29
140818.30
500 µm
Magnification
300 x
Accelerating Voltage
15 kV
Working Distance
20.3 mm
Horizontal Field Width
3.4 mm


140819.2
140819.1
140819.3
140819.4
140819.5
Sample: 140819
Mount : Kristine klosse 3 2018
Magnification
300 x
Accelerating Voltage
15 kV
Working Distance
20.4 mm
Horizontal Field Width
2.3 mm
500 µm

Appendix B3 – U-Pb data

Sample 90332		Isotope ratios								Age estimates (Ma)						
		Concordia output					Tera-Wasserburg output									
Analysis #	Comments	Pb207/U235	2σ	Pb206/U238	2σ	roh	238/206	2σ	207/206	2σ	Pb207/Pb206	2s	Pb207 U235	2σ	Pb206 U238	2σ	Disc.
90332 - 1		5.09	0.39	0.327	0.01	0.36	3.058104	0.09352	0.1159	0.0093	1894	144	1834	67	1824	50	3.70
90332 - 2		4.87	0.54	0.322	0.015	0.34	3.10559	0.14467	0.11	0.014	1799	232	1797	98	1799	76	0.00
90332 - 3		5.25	0.66	0.329	0.016	0.34	3.039514	0.147818	0.12	0.016	1956	238	1861	113	1834	81	6.27
90332 - 4		4.82	0.46	0.328	0.011	0.32	3.04878	0.102246	0.109	0.011	1783	184	1788	84	1829	55	-2.58
90332 - 5		5.33	0.88	0.327	0.016	0.28	3.058104	0.149632	0.118	0.02	1926	304	1874	152	1824	81	5.31
90332 - 6		4.4	0.45	0.315	0.011	0.34	3.174603	0.110859	0.1014	0.0098	1650	179	1712	88	1765	56	-6.99
90332 - 7		4.23	0.71	0.323	0.018	0.29	3.095975	0.172531	0.105	0.019	1714	333	1680	148	1804	92	-5.25
90332 - 8		4.27	0.58	0.322	0.015	0.29	3.10559	0.14467	0.099	0.015	1605	283	1688	118	1799	76	-12.09
90332 - 9		4.73	0.69	0.326	0.013	0.26	3.067485	0.122323	0.106	0.016	1732	277	1773	130	1819	65	-5.04

Sample 90334		Isotope ratios									Age estimates (Ma)						
		Concordia output					Tera-Wasserburg output										
Analysis #	Comments	Pb207/U235	2σ	Pb206/U238	2σ	roh	238/206	2σ	207/206	2σ	Pb207/Pb206	2s	Pb207 U235	2σ	Pb206 U238	2σ	Disc.
90334 - 1		4.56	0.11	0.2999	0.0041	0.410609	3.334445	0.045586	0.1087	0.0033	1778	55	1742	20	1691	20	4.89
90334 - 2		4.17	0.16	0.2712	0.0051	0.438596	3.687316	0.069341	0.109	0.0042	1783	70	1668	32	1547	26	13.23
90334 - 3		4.65	0.14	0.3051	0.0037	0.354733	3.277614	0.039748	0.1095	0.0035	1791	58	1758	25	1717	18	4.16
90334 - 4		4.13	0.18	0.2673	0.0051	0.415403	3.741115	0.071379	0.1101	0.0046	1801	76	1660	36	1527	26	15.21
90334 - 5		4.02	0.17	0.2532	0.0033	0.303447	3.949447	0.051474	0.1124	0.0046	1839	74	1638	35	1455	17	20.87
90334 - 6	Alpha dose	4.76	0.14	0.3099	0.0031	0.32438	3.226847	0.032279	0.1097	0.0032	1794	53	1778	25	1740	15	3.02
90334 - 7		4.63	0.17	0.306	0.004	0.342046	3.267974	0.042719	0.1086	0.0039	1776	66	1755	31	1721	20	3.10
90334 - 8		4.72	0.17	0.3138	0.0038	0.317942	3.186743	0.03859	0.108	0.0039	1766	66	1771	31	1759	19	0.37
90334 - 9		4.21	0.17	0.2655	0.0067	0.643611	3.766478	0.095049	0.1133	0.0034	1853	54	1676	34	1518	34	18.08
90334 - 10	REE	4.42	0.14	0.3047	0.004	0.347057	3.281917	0.043084	0.1043	0.0037	1702	65	1716	27	1715	20	-0.74
90334 - 11		4.15	0.15	0.2674	0.0036	0.344623	3.739716	0.050348	0.1118	0.0041	1829	66	1664	30	1528	18	16.47
90334 - 12		4.63	0.24	0.2992	0.0058	0.359517	3.342246	0.06479	0.1113	0.0056	1821	91	1755	44	1687	29	7.33
90334 - 13		4.48	0.13	0.2914	0.0032	0.353444	3.431709	0.037685	0.1101	0.0032	1801	53	1727	24	1649	16	8.47
90334 - 14		4.33	0.27	0.29	0.0062	0.324737	3.448276	0.073722	0.1076	0.0067	1759	114	1699	53	1642	31	6.69

Sample 90335		Isotope ratios									Age estimates (Ma)						
		Concordia output					Tera-Wasserburg output										
Analysis_#	Comments	Pb207 U235	2σ	Pb206 U238	2σ	roh	238/206	2σ	207/206	2σ	Pb207 Pb206	2σ	Pb207 U235	2σ	Pb206 U238	2σ	Disc.
90335 - 1	REE (CA)	4.83	0.34	0.3242	0.009	18.89244	3.084516	0.085628	0.107	0.0077	1749	132	1790	61	1810	44	-3.50
90335 - 2		4.62	0.17	0.3122	0.0045	18.88769	3.203075	0.046169	0.1081	0.0047	1768	79	1753	31	1752	22	0.91
90335 - 3		4.96	0.3	0.3182	0.0059	25.41932	3.142678	0.058271	0.1124	0.0071	1839	114	1813	52	1781	29	3.14
90335 - 4		4.61	0.16	0.3049	0.0043	18.60759	3.279764	0.046254	0.1089	0.0038	1781	64	1751	29	1716	21	3.68
90335 - 5		4.65	0.18	0.3199	0.0052	17.31179	3.125977	0.050813	0.1051	0.0044	1716	77	1758	33	1789	25	-4.26
90335 - 6		4.78	0.2	0.3081	0.0043	23.2526	3.245699	0.045299	0.1117	0.0049	1827	80	1781	36	1731	21	5.25
90335 - 7		4.86	0.22	0.324	0.0057	19.29957	3.08642	0.054298	0.1082	0.0054	1769	91	1795	39	1809	28	-2.26
90335 - 8		4.7	0.17	0.3167	0.0042	20.2398	3.157562	0.041875	0.1061	0.0039	1733	67	1767	31	1774	21	-2.32
90335 - 9		4.6	0.14	0.3089	0.0032	21.87427	3.237294	0.033536	0.1074	0.0033	1756	56	1749	26	1735	16	1.17
90335 - 10	REE (CA)	4.97	0.33	0.3268	0.0082	20.12225	3.059976	0.07678	0.1107	0.0081	1811	133	1814	58	1823	40	-0.66
90335 - 11		4.68	0.21	0.3014	0.0054	19.44583	3.31785	0.059444	0.1118	0.0051	1829	83	1764	38	1698	27	7.14
90335 - 12	REE (CA)	4.7	0.28	0.316	0.0068	20.58928	3.164557	0.068098	0.1062	0.0065	1735	112	1767	51	1770	33	-2.02
90335 - 13		4.67	0.21	0.3149	0.0054	19.44538	3.175611	0.054456	0.1077	0.0052	1761	88	1762	38	1765	27	-0.22
90335 - 14		4.52	0.16	0.3087	0.0047	17.02533	3.239391	0.04932	0.1054	0.004	1721	70	1735	30	1734	23	-0.76
90335 - 15		4.56	0.13	0.3094	0.0041	15.86259	3.232062	0.04283	0.1047	0.0027	1709	47	1742	24	1738	20	-1.68
90335 - 16		4.46	0.18	0.2958	0.0044	20.45398	3.380663	0.050287	0.1086	0.0045	1776	76	1724	34	1670	22	5.95

Sample 90336		Isotope ratios									Age estimates (Ma)						
		Concordia output					Tera-Wasserburg output										
Analysis_#	Comments	Pb207 U235	2σ	Pb206 U238	2σ	roh	238/206	2σ	207/206	2σ	Pb207 Pb206	2σ	Pb207 U235	2σ	Pb206 U238	2σ	Disc.
90336 - 1		4.6	0.18	0.3058	0.0045	0.333836	3.270111	0.048121	0.1083	0.0045	1771	76	1749	33	1720	22	2.88
90336 - 2	REE + alpha	4.09	0.18	0.2707	0.0067	0.526535	3.694126	0.091432	0.1076	0.0043	1759	73	1652	37	1544	34	12.21
90336 - 3		4.68	0.18	0.3092	0.0047	0.345515	3.234153	0.049161	0.109	0.0045	1783	75	1764	33	1737	23	2.58
90336 - 4		4.59	0.36	0.3105	0.0082	0.289257	3.220612	0.085053	0.1087	0.0095	1778	159	1747	68	1743	40	1.94
90336 - 5		5.16	0.41	0.3144	0.0086	0.307169	3.180662	0.087003	0.118	0.01	1926	152	1846	70	1762	42	8.51
90336 - 6		4.88	0.41	0.3284	0.0096	0.306122	3.045067	0.089015	0.11	0.01	1799	165	1799	73	1831	47	-1.73
90336 - 7	REE + alpha	3.4	0.16	0.2159	0.0052	0.43336	4.631774	0.111557	0.1138	0.0057	1861	90	1504	38	1260	28	32.28
90336 - 8	REE	4.67	0.25	0.3112	0.0073	0.377246	3.213368	0.075378	0.1094	0.0063	1789	105	1762	46	1747	36	2.39
90336 - 9		4.79	0.33	0.3252	0.0082	0.331232	3.075031	0.077538	0.1072	0.0077	1752	131	1783	60	1815	40	-3.58
90336 - 10		4.44	0.2	0.2952	0.0064	0.433101	3.387534	0.073442	0.1086	0.0049	1776	82	1720	38	1667	32	6.11
90336 - 11		4.83	0.42	0.3138	0.0097	0.300216	3.186743	0.098507	0.112	0.011	1832	178	1790	76	1759	48	3.97
90336 - 12	REE+ alpha	4.03	0.12	0.2735	0.0036	0.399359	3.656307	0.048127	0.1059	0.0032	1730	55	1640	25	1559	18	9.91
90336 - 13	REE + alpha	4.13	0.17	0.2689	0.0041	0.349243	3.718855	0.056703	0.11	0.0045	1799	74	1660	34	1535	21	14.68
90336 - 14	REE	4.87	0.38	0.3098	0.0088	0.318002	3.227889	0.09169	0.1169	0.0099	1909	152	1797	68	1740	43	8.88
90336 - 15		4.7	0.22	0.3146	0.0065	0.394342	3.17864	0.065674	0.108	0.0052	1766	88	1767	40	1763	32	0.15

Sample 90339		Isotope ratios									Age estimates (Ma)						
		Concordia output					Tera-Wasserburg output										
Analysis_#	Comments	Pb207 U235	2σ	Pb206 U238	2σ	roh	238/206	2σ	207/206	2σ	Pb207 Pb206	2σ	Pb207 U235	2σ	Pb206 U238	2σ	Disc.
90339 - 1		4.4	0.27	0.2655	0.0058	0.323247	3.766478	0.082281	0.1204	0.0077	1962	114	1712	52	1518	30	22.64
90339 - 2	Concordant	4.56	0.18	0.3047	0.0047	0.334906	3.281917	0.050624	0.1083	0.0047	1771	79	1742	33	1715	23	3.19
90339 - 3	Disc.	2.07	0.12	0.1456	0.0071	0.764355	6.868132	0.334916	0.1021	0.0042	1663	76	1139	40	876	40	47.30
90339 - 4	Disc. outlier	8.86	0.9	0.298	0.01	0.330914	3.355705	0.112608	0.209	0.02	2898	155	2324	97	1681	50	41.98
90339 - 5	REE	4.57	0.23	0.2871	0.0066	0.393672	3.483107	0.080071	0.1155	0.0062	1888	97	1744	43	1627	33	13.81
90339 - 6		4.09	0.18	0.2525	0.0089	0.570134	3.960396	0.139594	0.1201	0.0061	1958	91	1652	37	1451	46	25.86
90339 - 7	Concordant	4.87	0.25	0.3127	0.0054	0.305179	3.197953	0.055225	0.1132	0.0061	1851	97	1797	44	1754	27	5.26
90339 - 8		4.54	0.23	0.268	0.0044	0.335802	3.731343	0.061261	0.1216	0.0056	1980	82	1738	43	1531	22	22.69
90339 - 9	Discordant	1.35	0.11	0.099	0.0032	0.387738	10.10101	0.326497	0.095	0.0073	1528	145	868	49	609	19	60.18
90339 - 10	Concordant	4.54	0.21	0.2997	0.0074	0.487491	3.33667	0.082387	0.1108	0.0049	1813	80	1738	39	1690	37	6.77
90339 - 11	Disc. outlier	4.88	0.31	0.234	0.011	0.837704	4.273504	0.200891	0.1501	0.0046	2347	52	1799	55	1355	58	42.25
90339 - 12		4.21	0.18	0.2659	0.0076	0.640493	3.760812	0.107492	0.1138	0.0039	1861	62	1676	36	1520	39	18.32
90339 - 13		4.68	0.27	0.2882	0.0042	0.282532	3.469813	0.050566	0.1152	0.0057	1883	89	1764	49	1633	21	13.30
90339 - 14	Alp.dose+ REE	1.884	0.083	0.1284	0.0032	0.475597	7.788162	0.194098	0.1063	0.0049	1737	85	1075	30	779	18	55.17
90339 - 15		3.87	0.18	0.2467	0.0057	0.41241	4.053506	0.093656	0.1156	0.0059	1889	92	1607	38	1421	30	24.76
90339 - 16	Discordant	2.17	0.15	0.1529	0.0056	0.445002	6.540222	0.239537	0.1004	0.0074	1632	137	1171	49	917	31	43.78

Sample 90341		Isotope ratios									Age estimates (Ma)						
		Concordia output					Tera-Wasserburg output										
Analysis #	Comments	Pb207 U235	2σ	Pb206 U238	2σ	roh	238/206	2σ	207/206	2σ	Pb207 Pb206	2σ	Pb207 U235	2σ	Pb206 U238	2σ	Disc.
90341 - 1	Discordant	3.28	0.34	0.219	0.015	0.688968	4.56621	0.312754	0.1027	0.0074	1673	133	1476	84	1277	80	23.72
90341 - 2	Discordant	4.44	0.19	0.2758	0.006	0.482251	3.625816	0.078879	0.1164	0.0046	1902	71	1720	36	1570	30	17.43
90341 - 3	REE	4.7	0.19	0.298	0.0071	0.536042	3.355705	0.079951	0.1146	0.0043	1874	68	1767	34	1681	35	10.26
90341 - 4	Alp.dose+REE	3.34	0.11	0.2241	0.0041	0.513712	4.462294	0.081639	0.108	0.0033	1766	56	1490	26	1304	22	26.19
90341 - 5		4.8	0.16	0.3143	0.0033	0.304979	3.181674	0.033406	0.1098	0.0036	1796	60	1785	28	1762	16	1.91
90341 - 6		3.62	0.11	0.2414	0.0043	0.493143	4.142502	0.073789	0.1082	0.0034	1769	57	1554	24	1394	22	21.21
90341 - 7		4.86	0.23	0.3252	0.0057	0.346844	3.075031	0.053898	0.1076	0.0051	1759	87	1795	41	1815	28	-3.18
90341 - 8		4.74	0.19	0.3169	0.0055	0.360164	3.15557	0.054767	0.109	0.0049	1783	82	1774	34	1775	27	0.46
90341 - 9		3.98	0.18	0.2659	0.0056	0.386681	3.760812	0.079205	0.1095	0.0055	1791	91	1630	37	1520	29	15.14
90341 - 10		3.65	0.16	0.2462	0.009	0.772528	4.061738	0.14848	0.1065	0.0032	1740	55	1561	36	1419	47	18.47
90341 - 11	Alpha dose	2.918	0.075	0.1994	0.002	0.332919	5.015045	0.050301	0.1056	0.003	1725	52	1387	20	1172	11	32.04
90341 - 12	Disc. outlier	3.62	0.69	0.178	0.0048	0.234199	5.617978	0.151496	0.134	0.015	2151	195	1554	164	1056	26	50.91
90341 - 13		4.04	0.11	0.2731	0.0039	0.503143	3.661662	0.05229	0.106	0.0026	1732	45	1642	22	1557	20	10.12
90341 - 14		4.38	0.17	0.2978	0.004	0.321592	3.357958	0.045104	0.1062	0.0042	1735	73	1709	33	1680	20	3.16
90341 - 15		4.79	0.22	0.3036	0.0052	0.339776	3.293808	0.056416	0.1139	0.0054	1863	86	1783	39	1709	26	8.24
90341 - 16	Discordant	4.49	0.26	0.2741	0.0071	0.4948	3.648304	0.094502	0.1187	0.0054	1937	81	1729	49	1562	36	19.37
90341 - 17	Alp. dose+REE	4.08	0.12	0.2629	0.0035	0.402225	3.803728	0.050639	0.1122	0.0034	1835	55	1650	24	1505	18	18.02
90341 - 18		3.93	0.11	0.2624	0.0028	0.347604	3.810976	0.040666	0.1077	0.0031	1761	53	1620	23	1502	14	14.69
90341 - 19		4.4	0.16	0.2867	0.0052	0.426214	3.487967	0.063263	0.1117	0.0043	1827	70	1712	31	1625	26	11.07
90341 - 20	REE	4.27	0.12	0.292	0.0041	0.453526	3.424658	0.048086	0.1051	0.0029	1716	51	1688	23	1652	20	3.76
90341 - 21	Disc.Outlier+REE	1.72	0.15	0.1303	0.0048	0.464212	7.674597	0.282717	0.0939	0.0066	1506	133	1016	58	790	27	47.57
90341 - 22		4.12	0.15	0.2784	0.0044	0.380691	3.591954	0.056769	0.1068	0.0041	1746	70	1658	30	1583	22	9.29
90341 - 23		2.94	0.14	0.2082	0.005	0.559529	4.803074	0.115348	0.1012	0.0036	1646	66	1392	37	1219	27	25.94
90341 - 24		4.38	0.22	0.2882	0.0053	0.330921	3.469813	0.06381	0.1106	0.0058	1809	95	1709	42	1633	27	9.77
90341 - 25		4.45	0.19	0.2976	0.0065	0.538637	3.360215	0.073392	0.1083	0.0037	1771	62	1722	36	1679	32	5.17
90341 - 26	REE	4.37	0.17	0.281	0.004	0.391276	3.558719	0.050658	0.1135	0.0038	1856	60	1707	33	1596	20	14.00
90341 - 27	Disc. outlier	8.67	0.87	0.337	0.019	0.758606	2.967359	0.167299	0.1776	0.0086	2631	80	2304	96	1872	92	28.83
90341 - 28		4.78	0.18	0.3178	0.0044	0.323365	3.146633	0.043566	0.1086	0.0044	1776	74	1781	32	1779	22	-0.16
90341 - 29		4.58	0.16	0.3032	0.0044	0.367739	3.298153	0.047862	0.109	0.004	1783	67	1746	30	1707	22	4.24
90341 - 30	Alpha dose	4.6	0.11	0.3069	0.003	0.343197	3.25839	0.031851	0.1084	0.0029	1773	49	1749	20	1725	15	2.67
90341 - 31		4.62	0.35	0.2955	0.0077	0.32662	3.384095	0.088181	0.1114	0.0084	1822	137	1753	65	1669	38	8.42

Sample 90342		Isotope ratios									Age estimates (Ma)						
		Concordia output					Tera-Wasserburg output										
Analysis_#	Comments	Pb207 U235	2σ	Pb206 U238	2σ	roh	238/206	2σ	207/206	2σ	Pb207 Pb206	2σ	Pb207 U235	2σ	Pb206 U238	2σ	Disc.
90342 - 1		4.67	0.19	0.3141	0.0056	0.376692	3.183699	0.056761	0.1072	0.0047	1752	80	1762	35	1761	28	-0.48
90342 - 2		4.01	0.13	0.257	0.0033	0.371546	3.891051	0.049963	0.1122	0.0036	1835	58	1636	27	1474	17	19.66
90342 - 3		4.13	0.13	0.2806	0.0039	0.416247	3.563792	0.049532	0.1054	0.0032	1721	56	1660	26	1594	20	7.37
90342 - 4		4.51	0.13	0.3025	0.004	0.415851	3.305785	0.043713	0.1072	0.0031	1752	53	1733	24	1704	20	2.78
90342 - 5		4.34	0.17	0.276	0.005	0.399617	3.623188	0.065637	0.1131	0.0047	1850	75	1701	33	1571	25	15.06
90342 - 6		4.1	0.16	0.2725	0.005	0.451657	3.669725	0.067334	0.1076	0.0039	1759	66	1654	32	1553	25	11.69
90342 - 7	REE	4.37	0.12	0.2928	0.0039	0.430088	3.415301	0.045491	0.1073	0.003	1754	51	1707	23	1656	19	5.62
90342 - 8	REE	3.071	0.098	0.2057	0.0027	0.356329	4.861449	0.063811	0.1075	0.0037	1757	63	1425	25	1206	14	31.39
90342 - 9		4.48	0.13	0.2973	0.0034	0.359212	3.363606	0.038467	0.1077	0.0032	1761	54	1727	24	1678	17	4.71
90342 - 10	Discordant	3.57	0.18	0.2417	0.0094	0.774829	4.13736	0.160907	0.104	0.0033	1697	58	1543	41	1396	49	17.75
90342 - 11	Disc. Outlier	5.97	0.44	0.3029	0.0068	0.315583	3.30142	0.074116	0.1437	0.0097	2272	116	1971	66	1706	34	24.94
90342 - 12	REE	3.39	0.21	0.2269	0.0077	0.608499	4.407228	0.149562	0.1062	0.0047	1735	81	1502	50	1318	41	24.03
90342 - 13	Discordant	4.49	0.15	0.2804	0.0042	0.39552	3.566334	0.053419	0.115	0.004	1880	63	1729	28	1593	21	15.24
90342 - 14	REE	3.46	0.15	0.2275	0.0071	0.678158	4.395604	0.137182	0.1094	0.0037	1789	62	1518	35	1321	37	26.16
90342 - 15		3.87	0.12	0.2588	0.0032	0.373323	3.863988	0.047777	0.1074	0.0033	1756	56	1607	25	1484	16	15.50
90342 - 16	REE	3.63	0.15	0.2371	0.0045	0.510214	4.21763	0.080048	0.1094	0.0035	1789	58	1556	33	1372	23	23.35
90342 - 17	REE	3.71	0.16	0.2295	0.006	0.559194	4.357298	0.113916	0.1161	0.0045	1897	70	1574	35	1332	32	29.79
90342 - 18		3.56	0.12	0.2425	0.0051	0.548317	4.123711	0.086725	0.106	0.0034	1732	59	1541	27	1400	27	19.17
90342 - 19	REE	4.19	0.16	0.2801	0.0051	0.448067	3.570154	0.065005	0.1046	0.0038	1707	67	1672	32	1592	26	6.76
90342 - 20	REE	3.68	0.18	0.2428	0.0081	0.673007	4.118616	0.1374	0.1091	0.004	1784	67	1567	40	1401	42	21.47

Sample 90345		Isotope ratios								Age estimates (Ma)						
		Concordia output					Tera - Wasserburg output									
Analysis #	Comments	Pb207 U235	26	Pb206 U238	26	roh	238/206	26	207/206	26	Pb207 Pb206	26	Pb207 U235	26	Pb206 U238	26	Disc.
90345 - 1		4.84	0.19	0.3191	0.0044	0.305475	3.133814	0.043211	0.1092	0.0046	1786	77	1792	34	1785	22	-0.04
90345 - 2		4.86	0.21	0.319	0.005	0.332327	3.134796	0.049135	0.1096	0.0048	1793	80	1795	37	1785	24	-0.44
90345 - 3		4.77	0.16	0.3243	0.0053	0.374556	3.083565	0.050394	0.1066	0.0041	1742	70	1780	29	1811	26	3.79
90345 - 4		4.61	0.19	0.3166	0.0048	0.313152	3.15856	0.047887	0.106	0.0046	1732	80	1751	35	1773	24	2.33
90345 - 5	Disc. outlier	4.53	0.22	0.291	0.0058	0.373268	3.436426	0.068492	0.1101	0.0054	1801	89	1736	41	1647	29	-9.39

Sample 140808		Isotope ratios									Age estimates (Ma)						
		Concordia output					Tera-Wasserburg output										
Analysis_#	Comments	Pb207/U235	2σ	Pb206/U238	2σ	roh	238/206	2σ	207/206	2σ	Pb207/Pb206	2σ	Pb207_U235	2σ	Pb206 U238	2σ	Disc.
140808 - 1		4.82	0.26	0.3221	0.0058	0.30055	3.104626	0.055904	0.1085	0.0062	1774	104	1788	46	1800	28	-1.44
140808 - 2		4.85	0.37	0.327	0.011	0.356787	3.058104	0.102872	0.1124	0.0099	1839	159	1794	66	1824	54	0.80
140808 - 3		4.96	0.34	0.3209	0.0086	0.339417	3.116236	0.083514	0.1131	0.0084	1850	134	1813	60	1794	42	3.01
140808 - 4	REE	4.79	0.22	0.3124	0.0067	0.392119	3.201024	0.068652	0.1113	0.0056	1821	91	1783	39	1753	33	3.75
140808 - 5	Disc. Outlier.	6.56	0.54	0.318	0.011	0.396878	3.144654	0.108777	0.15	0.012	2346	137	2054	75	1780	54	24.13
140808 - 6	Disc.+REE	5	0.17	0.3012	0.004	0.360972	3.320053	0.044091	0.1195	0.0041	1949	61	1819	29	1697	20	12.91
140808 - 7	Disc.+ REE	4.55	0.2	0.2784	0.0058	0.403104	3.591954	0.074832	0.1184	0.0056	1932	85	1740	37	1583	29	18.06
140808 - 8		4.55	0.34	0.3151	0.008	0.294969	3.173596	0.080574	0.107	0.0088	1749	151	1740	64	1766	39	-0.96
140808 - 9	Disc.+REE	4.27	0.26	0.2552	0.0043	0.277931	3.918495	0.066025	0.1202	0.007	1959	104	1688	51	1465	22	25.21
140808 - 10	Disc. Outlier.	6.95	0.59	0.3147	0.0064	0.258656	3.177629	0.064623	0.158	0.012	2434	129	2105	78	1764	31	27.55
140808 - 11		4.58	0.23	0.3085	0.0055	0.337538	3.241491	0.05779	0.1066	0.0053	1742	91	1746	43	1733	27	0.50
140808 - 12		4.68	0.21	0.3184	0.0064	0.39876	3.140704	0.06313	0.106	0.0049	1732	85	1764	38	1782	31	-2.90
140808 - 13		4.77	0.16	0.3122	0.0047	0.391441	3.203075	0.048221	0.1102	0.0039	1803	64	1780	29	1752	23	2.84
140808 - 14	REE	4.89	0.28	0.3208	0.0073	0.35766	3.117207	0.070934	0.1094	0.0065	1789	108	1801	49	1794	36	-0.23
140808 - 15		4.82	0.23	0.3192	0.0053	0.319092	3.132832	0.052018	0.1095	0.0054	1791	90	1788	41	1786	26	0.30
140808 - 16	Disc.+ REE	3.34	0.3	0.217	0.012	0.646281	4.608295	0.254837	0.1118	0.0073	1829	118	1490	73	1266	64	30.78
140808 - 17		5.16	0.43	0.3381	0.0097	0.341363	2.957705	0.084856	0.1076	0.0085	1759	144	1846	73	1878	47	-6.73
140808 - 18		4.59	0.24	0.3131	0.0055	0.317953	3.193868	0.056104	0.105	0.0055	1714	96	1747	45	1756	27	-2.43
140808 - 19		4.7	0.32	0.3227	0.0076	0.321391	3.098853	0.072982	0.1052	0.0073	1718	128	1767	59	1803	37	-4.95
140808 - 20		4.63	0.2	0.3072	0.0053	0.394803	3.255208	0.056161	0.1071	0.0043	1751	73	1755	37	1727	26	1.36
140808 - 21	REE	4.7	0.21	0.303	0.0039	0.270205	3.30033	0.04248	0.1112	0.0051	1819	83	1767	38	1706	19	6.21
140808 - 22		4.94	0.33	0.3069	0.0073	0.328973	3.25839	0.077505	0.1157	0.0079	1891	123	1809	58	1725	36	8.75
140808 - 23		4.73	0.29	0.3137	0.0061	0.293638	3.187759	0.061987	0.109	0.0069	1783	115	1773	53	1759	30	1.34
140808 - 24		4.6	0.32	0.31	0.0082	0.347275	3.225806	0.085328	0.1078	0.0077	1763	131	1749	60	1741	40	1.24
140808 - 25		4.73	0.24	0.3133	0.0058	0.324406	3.191829	0.059089	0.1093	0.0059	1788	98	1773	43	1757	29	1.73
140808 - 26	Discordant	4.4	0.39	0.3159	0.0087	0.275348	3.165559	0.087181	0.104	0.01	1697	177	1712	76	1770	43	-4.30
140808 - 27	Disc.	4.04	0.16	0.2737	0.0039	0.339535	3.653635	0.052061	0.1064	0.0042	1739	72	1642	33	1560	20	10.30
140808 - 28	Discordant	5.08	0.47	0.36	0.014	0.350916	2.777778	0.108025	0.106	0.011	1732	190	1833	82	1982	67	-14.46
140808 - 29		4.94	0.4	0.321	0.0088	0.31022	3.115265	0.085403	0.1107	0.0093	1811	153	1809	71	1795	43	0.90
140808 - 30	Disc.+REE	4.35	0.31	0.268	0.013	0.65455	3.731343	0.180998	0.1178	0.0066	1923	100	1703	61	1531	66	20.41
140808 - 31		4.92	0.24	0.3313	0.007	0.380795	3.018412	0.063776	0.1072	0.0055	1752	94	1806	42	1845	34	-5.27

Sample 140813		Isotope ratios									Age estimates (Ma)						
		Concordia output					Tera-Wasserburg output										
Analysis_#	Comments	Pb207 U235	2σ	Pb206 U238	2σ	roh	238/206	2σ	207/206	2σ	Pb207 Pb206	2σ	Pb207 U235	2σ	Pb206 U238	2σ	Disc.
140813 - 1		4.45	0.13	0.2924	0.0039	0.42556	3.419973	0.045615	0.1093	0.0031	1788	52	1722	1697	1654	19	7.51
140813 - 2	Disc. outlier	8.72	0.23	0.3673	0.0069	0.615401	2.72257	0.051145	0.1704	0.0041	2562	40	2309	2285	2017	33	21.27
140813 - 3	Common Pb?	3.41	0.16	0.2183	0.008	0.738875	4.580852	0.167874	0.1137	0.0038	1859	60	1507	1469	1273	42	31.54
140813 - 4		3.89	0.11	0.2536	0.0029	0.410412	3.943218	0.045092	0.1102	0.0028	1803	46	1612	1589	1457	15	19.18
140813 - 5		3.56	0.15	0.229	0.0045	0.49816	4.366812	0.085811	0.1111	0.0038	1817	62	1541	1507	1329	24	26.86
140813 - 6	Common Pb?	2.71	0.12	0.1669	0.0033	0.453794	5.991612	0.118468	0.1159	0.0045	1894	70	1331	1298	995	18	47.46
140813 - 7		4	0.11	0.2623	0.0029	0.35413	3.812429	0.04215	0.1096	0.0032	1793	53	1634	1612	1502	15	16.24
140813 - 8		5.28	0.22	0.33	0.0054	0.342642	3.030303	0.049587	0.1159	0.0052	1894	81	1866	1829	1838	26	2.93
140813 - 9		4.05	0.16	0.2586	0.0073	0.652301	3.866976	0.109161	0.1128	0.0037	1845	59	1644	1612	1483	37	19.64
140813 - 10	Common Pb?	3.62	0.11	0.2235	0.0068	0.626865	4.474273	0.13613	0.119	0.0045	1941	68	1554	1529	1300	36	33.02
140813 - 11	Common Pb?	4.11	0.13	0.2469	0.0052	0.535418	4.050223	0.085302	0.1204	0.004	1962	59	1656	1630	1422	27	27.50
140813 - 12		3.88	0.11	0.2608	0.0029	0.36926	3.834356	0.042637	0.1072	0.003	1752	51	1610	1586	1494	15	14.75
140813 - 13	Common Pb?	4.6	0.23	0.2639	0.0054	0.431241	3.789314	0.077538	0.1238	0.0053	2012	76	1749	1707	1510	28	24.95
140813 - 14	Common Pb?	3.44	0.12	0.1972	0.0022	0.286331	5.070994	0.056573	0.1259	0.0047	2041	66	1514	1486	1160	12	43.17
140813 - 15		4.7	0.15	0.2907	0.006	0.588569	3.439972	0.071	0.1164	0.0033	1902	51	1767	1740	1645	30	13.50
140813 - 16		3.97	0.13	0.2611	0.0052	0.586932	3.82995	0.076276	0.1092	0.003	1786	50	1628	1601	1495	27	16.27

Sample 140814		Isotope ratios									Age estimates (Ma)						
		Concordia output					Tera-Wasserburg output										
Analysis_#	Comments	Pb207 U235	2σ	Pb206 U238	2σ	roh	238/206	2σ	207/206	2σ	Pb207 Pb206	2σ	Pb207 U235	2σ	Pb206 U238	2σ	Disc.
140814 - 1		11.03	0.29	0.4636	0.0059	0.451983	2.157032	0.027451	0.1712	0.0043	2569	42	2526	25	2455	26	4.44
140814 - 2	Disc. outlier.	3.323	0.099	0.2061	0.0023	0.33786	4.852014	0.054147	0.1158	0.0036	1892	56	1486	24	1208	12	36.16
140814 - 3		4.14	0.18	0.2663	0.0087	0.73104	3.755163	0.122681	0.1115	0.0034	1824	55	1662	36	1522	44	16.56
140814 - 4		5.98	0.34	0.303	0.011	0.71312	3.30033	0.119814	0.1401	0.005	2228	62	1973	51	1706	55	23.44
140814 - 5		9.04	0.2	0.3915	0.0054	0.56913	2.554278	0.035231	0.1656	0.0033	2514	33	2342	20	2130	25	15.27
140814 - 6		3.23	0.13	0.2198	0.004	0.469183	4.549591	0.082795	0.1051	0.0036	1716	63	1464	32	1281	21	25.36
140814 - 7		4.29	0.14	0.2781	0.0034	0.330221	3.595829	0.043962	0.1116	0.0039	1826	63	1691	27	1582	17	13.36
140814 - 8		3.59	0.13	0.237	0.0051	0.580754	4.219409	0.090797	0.1094	0.0033	1789	55	1547	29	1371	27	23.38
140814 - 9		3.92	0.19	0.255	0.0077	0.665663	3.921569	0.118416	0.1093	0.0037	1788	62	1618	40	1464	40	18.10
140814 - 10		2.88	0.15	0.2098	0.006	0.54497	4.766444	0.136314	0.1	0.0044	1624	82	1377	40	1228	32	24.40
140814 - 11		8.05	0.33	0.3639	0.0094	0.6625	2.748008	0.070985	0.1575	0.0046	2429	50	2237	38	2001	45	17.64
140814 - 12		9.39	0.35	0.404	0.013	0.816484	2.475248	0.079649	0.167	0.0038	2528	38	2377	35	2187	60	13.46
140814 - 13		6.93	0.59	0.344	0.014	0.543539	2.906977	0.118307	0.1432	0.009	2266	108	2103	79	1906	68	15.90
140814 - 14		3.75	0.24	0.2413	0.0089	0.610282	4.144219	0.152854	0.1107	0.0053	1811	87	1582	53	1393	46	23.05
140814 - 15		3.91	0.16	0.2579	0.0073	0.630323	3.877472	0.109754	0.109	0.0038	1783	64	1616	34	1479	38	17.03
140814 - 16		3.33	0.19	0.2305	0.0059	0.394784	4.338395	0.111048	0.1024	0.0061	1668	110	1488	46	1337	31	19.84

Sample 140818		Isotope ratios									Age estimates (Ma)						
		Concordia output					Tera-Wasserburg output										
Analysis_#	Comments	Pb207 U235	2σ	Pb206 U238	2σ	roh	238/206	2σ	207/206	2σ	Pb207 Pb206	2σ	Pb207 U235	2σ	Pb206 U238	2σ	Disc.
140818 - 1	REE	4.66	0.33	0.3178	0.0088	0.337291	3.146633	0.087131	0.1061	0.0082	1733	142	1760	61	1779	43	-2.63
140818 - 2	REE	4.4	0.26	0.29	0.0058	0.312339	3.448276	0.068966	0.1085	0.0066	1774	111	1712	50	1642	29	7.49
140818 - 3		4.9	0.36	0.3222	0.0079	0.307974	3.103662	0.076098	0.1109	0.0084	1814	138	1802	64	1800	39	0.76
140818 - 4		4.71	0.35	0.3176	0.0088	0.355295	3.148615	0.087241	0.107	0.0078	1749	133	1769	64	1778	43	-1.66
140818 - 5		4.8	0.39	0.326	0.01	0.338164	3.067485	0.094095	0.1066	0.0091	1742	156	1785	71	1819	49	-4.41
140818 - 6	Disc.	4.27	0.31	0.304	0.0077	0.315572	3.289474	0.083319	0.1011	0.0077	1644	141	1688	62	1711	38	-4.06
140818 - 7		4.59	0.3	0.3209	0.009	0.417138	3.116236	0.087398	0.1031	0.0063	1681	113	1747	56	1794	44	-6.75
140818 - 8		4.67	0.47	0.315	0.012	0.350324	3.174603	0.120937	0.108	0.011	1766	186	1762	88	1765	59	0.04
140818 - 9		4.57	0.42	0.303	0.013	0.426479	3.30033	0.141598	0.1077	0.0098	1761	166	1744	80	1706	65	3.11
140818 - 10		4.75	0.23	0.3107	0.0066	0.38665	3.218539	0.068369	0.1125	0.0057	1840	92	1776	41	1744	33	5.22
140818 - 11	Disc.	4.43	0.36	0.2922	0.0085	0.325616	3.422313	0.099554	0.1101	0.0093	1801	154	1718	70	1653	43	8.25
140818 - 12	REE	4.75	0.39	0.311	0.011	0.389821	3.215434	0.113729	0.1125	0.0094	1840	151	1776	71	1746	54	5.14
140818 - 13		4.69	0.31	0.3188	0.0065	0.285847	3.136763	0.063955	0.1068	0.0073	1746	125	1765	57	1784	32	-2.20
140818 - 14	Disc	4.95	0.47	0.309	0.0094	0.305467	3.236246	0.098449	0.116	0.011	1895	171	1811	84	1736	46	8.42
140818 - 15		4.53	0.34	0.307	0.01	0.383161	3.257329	0.106102	0.1057	0.0083	1727	144	1736	64	1726	50	0.03
140818 - 16		4.41	0.33	0.3102	0.0086	0.326331	3.223727	0.089375	0.1046	0.0084	1707	148	1714	64	1742	42	-2.01
140818 - 17		4.59	0.38	0.3069	0.0092	0.329948	3.25839	0.097677	0.1096	0.0094	1793	156	1747	71	1725	46	3.76
140818 - 18	Disc.	4.35	0.46	0.2548	0.0091	0.299384	3.924647	0.140166	0.123	0.014	2000	202	1703	91	1463	47	26.85
140818 - 19		4.32	0.27	0.3041	0.007	0.332358	3.288392	0.075695	0.1041	0.0068	1698	120	1697	53	1712	35	-0.77
140818 - 20	Disc.	4.56	0.39	0.302	0.011	0.384136	3.311258	0.120609	0.1108	0.0097	1813	159	1742	74	1701	55	6.14
140818 - 21		4.44	0.34	0.3069	0.0092	0.351034	3.25839	0.097677	0.1063	0.0085	1737	147	1720	66	1725	46	0.66
140818 - 22	Disc.	4.39	0.39	0.304	0.012	0.396729	3.289474	0.129848	0.1073	0.0098	1754	167	1710	76	1711	60	2.45
140818 - 23	REE	4.49	0.18	0.2986	0.005	0.361711	3.348962	0.056078	0.1089	0.0047	1781	79	1729	34	1684	25	5.43
140818 - 24	Disc.	4.47	0.44	0.33	0.011	0.295306	3.030303	0.10101	0.102	0.011	1661	200	1725	85	1838	54	-10.69
140818 - 25	REE	4.78	0.26	0.3062	0.0066	0.365365	3.265839	0.070394	0.1129	0.0062	1847	99	1781	47	1722	33	6.75
140818 - 26		4.82	0.24	0.3232	0.006	0.34438	3.094059	0.057439	0.1067	0.0054	1744	93	1788	43	1805	29	-3.53
140818 - 27	Disc.outlier	3.78	0.41	0.273	0.012	0.340914	3.663004	0.161011	0.099	0.012	1605	226	1589	91	1556	61	3.07
140818 - 28	Disc. Outlier	5.61	0.53	0.314	0.01	0.291577	3.184713	0.101424	0.134	0.014	2151	182	1918	85	1760	49	18.16
140818 - 29	REE	4.36	0.23	0.2784	0.0082	0.442825	3.591954	0.105798	0.1157	0.0069	1891	107	1705	45	1583	41	16.26
140818 - 30		4.69	0.36	0.3216	0.0086	0.325057	3.109453	0.083151	0.1054	0.0082	1721	143	1765	66	1798	42	-4.43

Sample 140819		Isotope ratios									Age estimates (Ma)						
		Concordia output					Tera-Wasserburg output										
Analysis #	Comments	Pb207 U235	2σ	Pb206 U238	2σ	roh	238/206	2σ	207/206	2σ	Pb207 Pb206	2σ	Pb207 U235	2σ	Pb206 U238	2σ	Disc.
140819 - 1	Disc.	3.45	0.38	0.211	0.017	0.774351	4.739336	0.381842	0.1124	0.0074	1839	119	1516	91	1234	91	32.88
140819 - 2	Disc.	1.81	0.24	0.145	0.011	0.421858	6.896552	0.523187	0.092	0.015	1467	310	1049	91	873	62	40.52
140819 - 3	Disc.	3.42	0.42	0.171	0.014	0.767268	5.847953	0.47878	0.1359	0.0093	2176	119	1509	101	1018	78	53.23
140819 - 4	Disc.	6.13	0.46	0.275	0.013	0.714231	3.636364	0.171901	0.1619	0.0075	2476	78	1995	68	1566	66	36.74
140819 - 5	Disc.	3.86	0.33	0.261	0.016	0.737816	3.831418	0.234876	0.1052	0.0059	1718	103	1605	71	1495	82	12.97

Sample RAF505		Concentrations				Isotope ratios								Age estimates (Ma)				
Spot no.	Grain .spot	238U (ppm)	232Th (ppm)	232Th /238U	f204 (%)	238U/ 206Pb	±1σ	207Pb/ 206Pb	±1σ	238U 206Pb*	±1σ	207Pb*/ 206Pb*	±1σ	238U/206Pb* date	±1σ	207Pb*/206Pb* date	±1σ	Disc (%)
RAF505-1	505-4.4	221.82	152.64	0.71	0.065	3.096	0.028	0.10885	0.00051	3.098	0.028	0.10828	0.00055	1803	14	1771	9	-1.83
RAF505-2	505-4.2	181.72	77.02	0.44	0.050	3.049	0.029	0.10911	0.00057	3.050	0.029	0.10867	0.00060	1828	15	1777	10	-2.86
RAF505-3	505-5.1	140.67	58.75	0.43	0.061	3.060	0.031	0.10953	0.00063	3.062	0.031	0.10899	0.00067	1822	16	1783	11	-2.21
RAF505-4	505-5.4	505.43	438.85	0.90	0.035	3.070	0.023	0.10952	0.00034	3.071	0.023	0.10921	0.00035	1817	12	1786	6	-1.73
RAF505-5	505-4.1	220.02	102.84	0.48	0.076	3.088	0.027	0.10994	0.00050	3.091	0.028	0.10927	0.00054	1807	14	1787	9	-1.11
RAF505-6	505-5.3	528.42	454.24	0.89	0.028	3.006	0.023	0.10958	0.00034	3.007	0.023	0.10934	0.00035	1851	12	1788	6	-3.49
RAF505-7	505-2.2	252.68	119.18	0.49	0.036	3.090	0.027	0.10968	0.00049	3.091	0.027	0.10937	0.00051	1807	14	1789	8	-1.00
RAF505-8	505-6.1	338.09	268.69	0.82	0.027	3.129	0.025	0.10965	0.00041	3.130	0.025	0.10942	0.00043	1787	13	1790	7	0.13
RAF505-9	505-5.5	231.46	145.72	0.65	-0.056	3.043	0.027	0.10900	0.00051	3.042	0.027	0.10949	0.00054	1832	14	1791	9	-2.31
RAF505-10	505-5.2	466.43	390.40	0.86	0.013	3.044	0.024	0.11003	0.00037	3.044	0.024	0.10992	0.00038	1831	13	1798	6	-1.84
RAF505-11	505-4.3	176.60	78.98	0.46	0.089	3.047	0.029	0.11087	0.00057	3.050	0.029	0.11009	0.00063	1828	15	1801	10	-1.51
RAF50512	505-2.3	246.43	122.88	0.52	-0.007	3.166	0.027	0.11047	0.00048	3.166	0.027	0.11053	0.00049	1769	13	1808	8	2.15

Sample RAF465		Concentrations				Isotope ratios								Age estimates (Ma)				
Spot no.	Grain .spot	238U (ppm)	232Th (ppm)	232Th /238U	f204 (%)	238U/ 206Pb	±1σ	207Pb/ 206Pb	±1σ	238U 206Pb*	±1σ	207Pb*/ 206Pb*	±1σ	238U/206Pb* date	±1σ	207Pb*/206Pb* date	±1σ	Disc (%)
RAF465-1	465-6.2	70.96	27.96	0.41	0.228	3.045	0.037	0.10793	0.00089	3.052	0.037	0.10595	0.00111	1827	19	1731	19	-5.55
RAF465-2	465-7.5	71.49	13.43	0.19	0.426	3.040	0.041	0.11045	0.00096	3.053	0.041	0.10675	0.00136	1827	22	1745	23	-4.70
RAF465-3	465-6.1	50.69	22.26	0.45	0.193	3.158	0.047	0.10878	0.00110	3.164	0.047	0.10710	0.00133	1770	23	1751	23	-1.12
RAF465-4	465-2.1	74.88	26.12	0.36	0.324	3.196	0.041	0.11008	0.00090	3.207	0.041	0.10726	0.00119	1750	20	1753	20	0.20
RAF465-5	465-1.2	45.81	21.16	0.48	-0.039	3.200	0.049	0.10793	0.00111	3.198	0.049	0.10826	0.00116	1754	24	1770	19	0.94
RAF465-6	465-5.2	44.45	34.92	0.81	0.267	3.168	0.050	0.11092	0.00121	3.177	0.050	0.10860	0.00155	1764	25	1776	26	0.67
RAF465-7	465-4.1	86.20	55.12	0.66	0.087	3.112	0.037	0.10938	0.00084	3.115	0.038	0.10863	0.00093	1795	19	1776	16	-1.02
RAF465-8	465-7.1	57.27	21.93	0.40	0.062	3.067	0.042	0.10927	0.00100	3.069	0.042	0.10873	0.00107	1818	22	1778	18	-2.24
RAF465-9	465-8.4	103.08	71.92	0.72	0.055	3.261	0.036	0.10947	0.00077	3.263	0.036	0.10899	0.00082	1724	17	1783	14	3.32
RAF465-10	465-8.1	73.09	42.44	0.60	-0.097	3.203	0.040	0.10848	0.00088	3.200	0.040	0.10932	0.00098	1753	20	1788	16	1.96
RAF465-11	465-8.2	102.01	66.52	0.67	-0.054	3.054	0.034	0.10889	0.00076	3.052	0.034	0.10936	0.00081	1827	18	1789	13	-2.13
RAF465-12	465-7.3	315.78	339.79	1.11	0.043	3.223	0.027	0.10978	0.00047	3.224	0.027	0.10940	0.00049	1742	13	1789	8	2.68
RAF465-13	465-6.5	198.93	114.40	0.59	0.056	3.141	0.029	0.10991	0.00055	3.143	0.029	0.10942	0.00058	1781	14	1790	10	0.51
RAF465-14	465-9.1	73.45	48.71	0.68	0.557	2.997	0.038	0.11431	0.00090	3.014	0.039	0.10945	0.00136	1847	21	1790	23	-3.16
RAF465-15	465-6.3	172.42	88.61	0.53	0.042	3.130	0.030	0.10992	0.00059	3.131	0.030	0.10956	0.00061	1787	15	1792	10	0.31
RAF465-16	465-7.4	99.50	70.85	0.74	-0.015	3.195	0.035	0.10960	0.00072	3.194	0.035	0.10974	0.00073	1756	17	1795	12	2.19
RAF465-17	465-3.1	259.85	241.89	0.96	0.035	3.137	0.027	0.11012	0.00047	3.138	0.027	0.10982	0.00049	1783	14	1796	8	0.73
RAF465-18	465-5.1	118.00	75.87	0.66	0.053	3.147	0.035	0.11034	0.00075	3.148	0.035	0.10988	0.00080	1778	17	1797	13	1.07
RAF465-19	465-6.2	76.73	30.71	0.41	0.165	3.112	0.039	0.11133	0.00089	3.118	0.039	0.10989	0.00105	1793	20	1798	17	0.23
RAF465-20	465-1.1	117.07	76.05	0.67	0.048	3.187	0.035	0.11039	0.00072	3.188	0.035	0.10996	0.00076	1759	17	1799	13	2.23
RAF465-21	465-6.6	90.64	49.80	0.57	-0.058	3.112	0.036	0.10947	0.00079	3.111	0.036	0.10998	0.00085	1797	18	1799	14	0.12
RAF465-22	465-6.4	200.20	115.68	0.60	0.018	3.142	0.029	0.11024	0.00054	3.143	0.029	0.11008	0.00055	1781	14	1801	9	1.10
RAF465-23	465-7.2	63.28	28.62	0.47	0.028	3.235	0.043	0.11161	0.00096	3.236	0.043	0.11136	0.00099	1736	20	1822	16	4.71
RAF465-24	465-8.3	90.92	60.15	0.68	-0.077	3.066	0.035	0.11077	0.00079	3.064	0.035	0.11144	0.00086	1821	19	1823	14	0.11

Appendix A4: Zircon trace element data

Sample: 90332	REE														
Analysis_#	La	Ce	Pr	Nd	Sm	Eu	Gd	Dy	Yb	Lu	Pb	Th	U	Alpha dose	Th/U
90332 - 1	-	8.27	1.21	11	12.1	3.29	39.9	114.8	249.4	49.8	205	38.2	37.5	3.52234E+17	1.02
90332 - 2	0.01	6.2	0.5	6.1	6.3	1.37	19.4	61	143	28.9	106	19.9	23.4	1.97302E+17	0.85
90332 - 3	0.02871	5.27	0.101	1.39	3.08	0.66	10.24	35.9	99.9	21.13	70.4	12.23	17.5	1.57025E+17	0.70
90332 - 4	-0.009	8.31	0.65	6.56	9.8	1.73	26	79.4	174.9	34.08	217	28.05	30.63	2.59737E+17	0.92
90332 - 5	-0.009	4.12		0.85	1.4	0.317	4.85	21.1	65	14.24	86	8.47	13.39	1.15646E+17	0.63
90332 - 6	-0.002	6.9	0.121	1.35	2.17	0.5	8.16	34.5	106	22.07	197	19.82	30.4	2.1864E+17	0.65
90332 - 7	0.019	4.97		0.71	1.6	0.54	7.74	28.2	82.8	17.29	91	8.97	14.46	1.0795E+17	0.62
90332 - 8	0.015	5.54		0.78	1.3	0.19	6.19	22.9	74.8	15.69	139	12.6	24.8	1.65877E+17	0.51
90332 - 9	0.014	5.36	0.148	1.58	3.07	0.48	11	37.8	105.6	21	159	14.1	20.2	1.55968E+17	0.70
Sample:90334	**REE**														
Analysis_#	La	Ce	Pr	Nd	Sm	Eu	Gd	Dy	Yb	Lu	Pb	Th	U	Alpha dose	Th/U
90334 - 10	0.008	17.32	0.49	6.49	10.9	0.108	41.3	162.6	397.6	80.3	-	140.2	309.9	2.18637E+18	0.45
90334 - 8	-	15.72	0.5	5.94	7.1	0.27	29.5	109	291.1	60	-	145.1	267.9	2.02718E+18	0.54
90334 - 6	-	22.6	2.1	14.7	11.7	0.25	47.7	177.3	450.1	90.2	-	172.7	366.7	2.77121E+18	0.47
90334 - 7	-	18	1.2	9.5	10	0.223	34	118.6	284.7	55.7	-	95.6	200	1.49593E+18	0.48
90334 - 3	-	20.8	3.38	19.2	15.4	0.38	56.5	190.5	422.7	82.6	-	121.4	225	1.73088E+18	0.54
90334 - 1	-	13.61	1.26	11.3	13	0.47	43.6	157.8	381	76.5	-	123.2	248	1.8673E+18	0.50
90334 - 14	-	14.77	0.46	8.2	10.2	0.293	41.4	147	340	66.9	-	125	233	1.75234E+18	0.54
90334 - 12	-	18.35	0.58	7.49	10.4	0.234	40.8	163.2	401.7	76.8	-	152.6	320.9	2.4714E+18	0.48
90334 - 13	-	5.96	0.47	6.06	7.8	0.63	27.2	86.4	201.3	41.3	-	38.8	77.8	5.95403E+17	0.50
90334 - 2	-	18.11	0.12	2.76	3.94		20.1	80	228	44.76	-	97.9	239.9	1.76551E+18	0.41
90334 - 4	-	13.62	0.307	3.47	4.57	0.158	18.5	74.4	216.6	45.4	-	97.9	190.7	1.46569E+18	0.51
90334 - 11	-	6.02	0.86	8.05	10	0.49	30	97	244	50.8	-	50.65	110.7	8.52587E+17	0.46
90334 - 9	-	173	40	152	34.7	0.64	52	145.4	325.1	64.5	-	112.5	225.7	1.78767E+18	0.50
90334 - 5	-	22.8	1.45	12.3	11.4	0.268	47.2	174.4	412.3	79.6	-	151.3	310	2.42474E+18	0.49

Sample:90335	REE														
Analysis_#	La	Ce	Pr	Nd	Sm	Eu	Gd	Dy	Yb	Lu	Pb	Th	U	Alpha dose	Th/U
90335 - 1	0.029	4.57	0.41	4.04	6.4	0.42	21.2	69.7	161.8	33.6	-	25.3	51.7	3.80878E+17	0.49
90335 - 2	-	7.9	0.72	9.3	13.2	0.98	42.7	139.7	324.1	66.5	-	90.7	149.9	1.15632E+18	0.61
90335 - 3	-	24	5.8	24.6	6.4	0.29	16.7	55	140.2	31.24	-	25.53	74.4	5.57004E+17	0.34
90335 - 4	-	17.7	1.62	9.4	7.11	0.69	23.6	94.7	250.2	51.7	-	132.1	283.2	2.11825E+18	0.47
90335 - 5	-	189	55	227	42.6	0.97	44.7	81.6	182.1	38.69	-	82.1	170.6	1.2257E+18	0.48
90335 - 6	-	10.08	1.43	11.8	11.4	1.02	43.6	141.7	332	68.3	-	107.1	189.1	1.50199E+18	0.57
90335 - 7	-	6.18	0.6	6.29	7.9	0.88	25.8	84.7	212	44.3	-	61.2	130	9.65874E+17	0.47
90335 - 8	-0.035	8.53	0.48	5.63	9	0.54	32.5	111.8	278.9	58.4	-	93.9	197.8	1.43563E+18	0.47
90335 - 9	-	54.5	11.1	49	15.2	0.31	35.4	121.5	304.5	58.6	-	136.9	329.2	2.38442E+18	0.42
90335 - 10	0.019	4.19	0.15	3.13	3.67	0.27	14.7	55	144.3	31.22	-	29.95	67.4	5.10954E+17	0.44
90335 - 11	-	10.3	0.75	7.2	8.7	0.5	26.1	91.6	227	47.15	-	63.8	128.1	9.98501E+17	0.50
90335 - 12	-0.033	4.82	0.148	1.34	2.85	0.181	12.34	45.9	130.3	27.72	-	31.73	76	5.4305E+17	0.42
90335 - 13	-	27.9	4.6	17.5	4.9	0.161	14	49.9	142.6	29.94	-	45.2	113.1	8.18062E+17	0.40
90335 - 14	-	12.2	0.78	5.2	5.3	0.86	17.5	63	184	38.5	-	71.2	190.7	1.33203E+18	0.37
90335 - 15	-	21.9	2.66	13.1	8.7	0.69	28.5	103.8	264.9	53.6	-	119.1	246.6	1.76398E+18	0.48
90335 - 16	-	75	12.5	45	13.7	0.51	32.7	108.5	266	52.6	-	87.6	186	1.38835E+18	0.47
Sample:90336	**REE**														
Analysis_#	**La**	**Ce**	**Pr**	**Nd**	**Sm**	**Eu**	**Gd**	**Dy**	**Yb**	**Lu**	**Pb**	**Th**	**U**	**Alpha dose**	**Th/U**
90336 - 1	-	8.72		0.44	1.29	0.162	4.58	26.5	153.4	35	-	104.2	197		0.53
90336 - 2	-	153	26	71	9.7	0.75	13.1	49.3	214.7	46	-	188	249	1.99039E+18	0.76
90336 - 3	0.023	11.54		0.84	1.44	0.17	8.55	39.6	179.7	38.2	-	107.7	155.6	1.24267E+18	0.69
90336 - 4	-0.008	9.24	1.34	13.3	15	2.88	41.9	132.9	301.5	58.38	-	80.72	50.63	5.03337E+17	1.59
90336 - 5	-	8.8	0.92	12.3	13	2.35	36.7	113.1	262.3	51.4	-	65.3	43.8	4.71671E+17	1.49
90336 - 6	0.034	7.49	0.36	4.09	4.98	0.98	16.9	56.7	157.9	31.1	-	48.36	40.1	3.70023E+17	1.21
90336 - 7	-56	40.7	12.6	41.9	11.7	1.43	21.9	75.9	270	57.8	-73.6	171	227	1.94363E+18	0.75
90336 - 8	-	21.2	3.4	20.7	13.4	1.6	33.7	107.8	268.9	52.4	-	70.9	69.4	6.07533E+17	1.02
90336 - 9	-	8.89	0.98	10.6	13	2.66	37.6	117.1	264.5	51.3	-	67.7	45.1	4.31175E+17	1.50
90336 - 10	-	18.01	0.259	3.26	4.36	0.6	16.2	63.8	194.2	38.9	-	107.6	117.8	9.93667E+17	0.91
90336 - 11	-	8.8	0.94	11	12.6	2.53	34.1	102.5	233.2	44.97	-	71.5	40.01	4.31162E+17	1.79
90336 - 12	-	65	11.6	38.9	11.4	0.8	22.8	80.4	285.2	59.1	-	266.8	275.5	2.28179E+18	0.97
90336 - 13	-	431	95	330	55.1	22.2	47.7	80.6	247.3	50.9	-	151.3	209.6	1.70697E+18	0.72
90336 - 14	-	166	47.1	213	64.2	6.09	80.5	168.1	326	61.2	-	44.8	44.2	4.189E+17	1.01
90336 - 15	-	12.04	0.79	8.8	11.9	2.05	40.6	153.3	400.7	76.1	-	90	107.4	8.81945E+17	0.84

Sample:90339	REE														
Analysis_#	La	Ce	Pr	Nd	Sm	Eu	Gd	Dy	Yb	Lu	Pb	Th	U	Alpha dose	Th/U
90339 - 1	-	-	-	-	-	-	-	-	-	-	-	-	-	-	-
90339 - 2	-	36.9	0.53	3.59	6.14	0.64	20.8	75	233	48.3	2818	188.8	162.7	1.45541E+18	1.16
90339 - 3	-	27.7	2.85	10.8	6.8	1.1	13	48.7	257.5	56.3	2650	249	606	4.10815E+18	0.41
90339 - 4	-	-	-	-	-	-	-	-	-	-	-	-	-	-	-
90339 - 5	-	156	54.8	135	15.1	2.25	34.3	121.3	354.9	71	2470	108.1	89	8.74491E+17	1.21
90339 - 6	-	25.9	2.18	8.6	6.2	1	20.9	74.9	261	58.3	-	83.6	199	1.64597E+18	0.42
90339 - 7	-	19.3	1.81	11.5	11.8	1.93	36.6	115.8	287.8	57.1		139.7	118.8	1.12808E+18	1.18
90339 - 8	-	42.1	3.38	11.4	4.98	0.64	10.5	42.9	195.2	42.5	-	326	386.2	3.66315E+18	0.84
90339 - 9	-	9.74	0.9	4.7	2.29	0.19	8.8	50.8	383.7	84	-	129.3	561.2	3.26745E+18	0.23
90339 - 10	-	17.2	1.44	8.3	8	0.49	22.2	92	279	55.9		139	148.1	1.28959E+18	0.94
90339 - 11	-	20.69	1.53	9.1	7.4	1.05	19.3	54.1	197.1	43.82		110.9	460	4.48986E+18	0.24
90339 - 12	-	27.2	4.8	16.5	5.1	0.57	14.9	62.1	271	57.3		176	359	2.85139E+18	0.49
90339 - 13	-	27.8	1.8	5.1	1.75	0.33	8.1	45.2	220.2	47.3		183	295	2.46893E+18	0.62
90339 - 14	-	139.3	27.7	107.4	40.4	5.34	66.3	181.6	522	107.8	-	781	679	5.91348E+18	1.15
90339 - 15	-	17.61	2.11	13	15.9	1.56	55.8	224	621	127.4	-	221	212.7	2.0021E+18	1.04
90339 - 16	-	38.5	4.6	24.9	10.6	2.21	18.4	59.6	287.2	68.3	-	369	575	4.06893E+18	0.64

Sample:90341	REE														
Analysis_#	La	Ce	Pr	Nd	Sm	Eu	Gd	Dy	Yb	Lu	Pb	Th	U	Alpha dose	Th/U
90341 - 1	-0.03	14.30	-	1.61	2.5	-	10.5	46.3	184	41	270	162	200	1.52663E+18	0.81
90341 - 2	-	16.8	0.74	4.89	5.8	0.42	18.8	67.1	199.2	43.1	289	183	180.4	1.70137E+18	1.01
90341 - 3	-	43	6.5	19.2	5.4	0.48	15.6	52.5	179	38.6	292	141	184.2	1.59578E+18	0.77
90341 - 4	-	48.1	6.1	21	4.87	0.34	12.9	53.7	225.2	49.33	466	304.2	427.3	3.39167E+18	0.71
90341 - 5	-	11.92	0.24	1.54	1.19	0.272	6.52	37.2	189.4	43.49	270.6	133.4	225.3	1.76544E+18	0.59
90341 - 6	-	7.24	0.182	2.28	1.88	0.34	4.39	15.3	82.2	20.11	132	72.9	385	2.62405E+18	0.19
90341 - 7	-0.038	17.28	0.78	9.1	11.1	1.58	42.9	152.1	365.9	71.8	406	177	110.2	1.0838E+18	1.61
90341 - 8	-	9.96	0.54	8.86	13	2.22	47.1	149.8	336.8	67.1	481	211.6	136.7	1.34991E+18	1.55
90341 - 9	0.014	9.4	0.55	7.3	9.5	1.69	35.8	116	277	56.8	340	156	143	1.27531E+18	1.09
90341 - 10	-	41.7	1.46	12.4	13.6	1.31	52.5	190	517	105.2	1067	664	380	3.8007E+18	1.75
90341 - 11	-	19.84	0.84	3.57	3.02	0.38	8.51	44	201.6	44.41	487	286.2	494.3	3.67446E+18	0.58
90341 - 12	-	9.92	0.53	3.83	4.23	0.79	12.9	42.9	148.1	32.34	500	92.2	454.6	3.9314E+18	0.20
90341 - 13	-	34.4	3.75	11.6	3.73	0.69	10.57	46.3	199.2	44.4	520	241.6	338.7	2.62612E+18	0.71
90341 - 14	0.005	6.55		0.76	1.06	0.186	4.23	24.6	139.2	31.1	226.8	97.3	204.5	1.4865E+18	0.48
90341 - 15	-	35	3.7	15.6	8.5	1.07	21.5	55.7	162.1	34.8	334	145.9	140.8	1.30079E+18	1.04
90341 - 16	-	21.2	1.89	12.6	9.2	1.89	28.8	93.9	281.2	58.3	560	241	228	2.22504E+18	1.06
90341 - 17	-	55	8.4	23.9	7	1.08	14.8	55.1	224.6	49.1	582	274	355	3.00315E+18	0.77
90341 - 18	-	12.64	0.184	1.19	2.48	0.138	9.05	43.9	211.2	45.58	550	221.4	370.4	2.83809E+18	0.60
90341 - 19	-	27.5	1.64	9.4	8.9	1.27	24.5	81.5	241.2	48.4	581	198.8	204	1.81108E+18	0.97
90341 - 20	-	53.2	5.7	17.3	5.59	0.47	14.4	56.4	214.2	44.58	725	265.3	316.4	2.50888E+18	0.84
90341 - 21	-	462	102	342	45.6	4.9	35.5	71.3	359	81.5	695	541	507	3.63496E+18	1.07
90341 - 22	-	27.4	2.01	9.2	3.56	0.46	9.9	39.3	158.3	33.4	650	191	239.7	1.91933E+18	0.80
90341 - 23	-	13.55	0.42	4.29	3.03	0.5	6.87	27.1	127.2	28.4	425	121.9	263.8	1.79401E+18	0.46
90341 - 24	-0.001	17.6	0.38	4.02	6.9	0.98	21.2	74.6	215	43.5	427	106	97.9	8.82406E+17	1.08
90341 - 25	-	21.1	1.95	18.7	27.6	3.51	85.5	282	682	130.4	1290	312	228	2.14317E+18	1.37
90341 - 26	-	294	68	182	31.2	4.28	19.8	37.2	132.5	28.97	436	102.1	236.7	1.84144E+18	0.43
90341 - 27	-	9.2	0.32	1.54	2.69	0.69	10.9	47.5	192.6	42.5	670	73.4	269	3.07062E+18	0.27
90341 - 28	0.002	7.22	0.095	1.59	5.38	0.225	17.9	75.5	247.6	50.37	544	117.4	230.6	1.74055E+18	0.51
90341 - 29	0.001	22	0.178	2.45	4.38	0.34	15.5	61.8	212.6	43.4	861	202	200.1	1.7382E+18	1.01
90341 - 30	-	31.6	0.63	3.46	5.52	0.63	18.5	74.9	262.8	54.17	1311	277.7	385.5	3.0813E+18	0.72
90341 - 31	-0.086	7.3		0.72	1.35	0.17	4	23.5	120	26.5	394	79.8	187.5	1.42422E+18	0.43

Sample:90342	REE														
Analysis_#	**La**	**Ce**	**Pr**	**Nd**	**Sm**	**Eu**	**Gd**	**Dy**	**Yb**	**Lu**	**Pb**	**Th**	**U**	**Alpha dose**	**Th/U**
90342 - 1	-	34.4	3.14	15.7	12.5	1.13	40.1	142	356	71.4	-	224	161	1.5012E+18	1.39
90342 - 2	-	18.9	1.23	6.15	2.61	0.64	8.07	40.4	183.6	41.7	-	222	274.3	2.34419E+18	0.81
90342 - 3	-	13.24	0.144	1.89	2.31	0.83	8.88	39.9	196.9	43.83	-	185.3	307.9	2.29798E+18	0.60
90342 - 4	0.0249	12.49		1.2	1.81	0.186	10.8	51.7	243	52.2	-	206	311	2.41227E+18	0.66
90342 - 5	-	21.6	0.85	7.8	8.6	1	26.2	89.5	266	56.1	-	228	185	1.77917E+18	1.23
90342 - 6	-	13	0.34	2.14	2.16	0.34	9.9	49.6	221	47.9	-	173	266	2.06607E+18	0.65
90342 - 7	-	30.4	5.13	22.7	5.9	0.275	13.1	54.1	235.1	50.9	-	218.1	336.8	2.60473E+18	0.65
90342 - 8	-	110	24.1	91	21.1	2.64	24.8	59.1	223.2	48.3	-	267.2	368.8	2.92023E+18	0.72
90342 - 9	-	15.66	0.135	1.98	2.82	0.36	10.13	49.2	215.8	46.6	-	238.3	335.1	2.64994E+18	0.71
90342 - 10	-	13.32	0.54	4.22	3.41	2.9	10.6	48.1	221	49.6	-	202	347	2.53131E+18	0.58
90342 - 11	-	39.2	3.79	27.2	14.1	2.57	46.1	149	362	72.5	-	311	190	2.6402E+18	1.64
90342 - 12	-	70	16.3	64	15.9	1.45	30.3	86.4	287	61.6	-	183	350	2.57904E+18	0.52
90342 - 13	-	15.35	0.57	3.62	2.82	0.98	11.5	46.9	195	42.6	-	172	262	2.21092E+18	0.66
90342 - 14	-	138	22	77	11.8	1.77	17.1	61.8	260.6	56.5	-	273	382	3.08381E+18	0.71
90342 - 15	-	22.9	1.2	5.7	4.73	0.58	16.5	66.3	264.3	58.1	-	280.5	356.1	2.86488E+18	0.79
90342 - 16	-	39.3	5.7	28.2	7.9	1.95	16.7	71.1	295.9	64.8	-	278.4	407	3.25796E+18	0.68
90342 - 17	-	73	14	57	21.9	2.86	47.3	143	373	76.7	-	409	335	3.3175E+18	1.22
90342 - 18	-	17.5	0.28	4.67	3.82	2.56	11.5	51.2	232.2	51.32	-	231.9	350	2.6762E+18	0.66
90342 - 19	-	93	24.2	106	24.1	2.09	29.4	66.5	227.1	48.4	-	191.5	244	1.89563E+18	0.78
90342 - 20	-	42.5	7.1	29.6	12.2	1.5	34.3	126.9	342	71	-	233	261	2.20251E+18	0.89
Sample:90345	**REE**														
Analysis_#	**La**	**Ce**	**Pr**	**Nd**	**Sm**	**Eu**	**Gd**	**Dy**	**Yb**	**Lu**	**Pb**	**Th**	**U**	**Alpha dose**	**Th/U**
90345 - 1	-	13.89	1.08	12	11.8	1.23	45.1	174	401.8	76.8	-	301.3	186.5	1.87401E+18	1.62
90345 - 2	-	12.1	0.65	8.1	12	0.95	38	137.4	299.6	56.2	-	260.1	130.6	1.42788E+18	1.99
90345 - 3	-0.022	14.82	0.84	9.6	12.5	1.19	50.8	181	368	69.2	-	288	176	1.7209E+18	1.64
90345 - 4	-	14.54	1.26	12	19.1	2.3	73.1	258	536	103.1	-	360	183.8	1.90877E+18	1.96
90345 - 5	-	25.6	2.57	21.2	27.3	3.12	96.4	325	596	111.4	-	407	168	2.01012E+18	2.42

Sample:140808	REE														
Analysis_#	La	Ce	Pr	Nd	Sm	Eu	Gd	Dy	Yb	Lu	Pb	Th	U	Alpha dose	Th/U
140808 - 1	-0.005	16.86	0.93	10.4	11.3	0.72	42.1	138.4	323	63.9	-	111.5	110.5	9.54159E+17	1.01
140808 - 2	-	14.2	1.2	5.3	2.84	0.266	11	43.1	116.8	24.08	-	28.46	36.09	3.07367E+17	0.79
140808 - 3	-	12.17	0.32	2.82	3.13	0.268	13.8	50.6	137.5	28.62	-	39.52	55.26	4.64726E+17	0.72
140808 - 4	-	137	38	159	43	4.6	66	151	324	64.5	-	123	136	1.1803E+18	0.90
140808 - 5	-	680	90	177	20	2.53	35.3	85.6	192.4	38.6	-	38.64	34.23	4.37752E+17	1.13
140808 - 6	-	1350	180	334	18.1	1.49	18.2	52.1	208	45.43	-	142.2	253.9	2.17824E+18	0.56
140808 - 7	-	510	70	158	20	2.51	46.3	126.2	293.4	60.5	-	179	146.3	1.48428E+18	1.22
140808 - 8	-	22.3	2.55	12.5	7.4	0.64	27.7	91.2	224.2	46.1	-	62.9	66	5.51854E+17	0.95
140808 - 9	-	201	29.8	92	21.6	1.14	52.8	154	391	79.5	-	200	253.8	2.33935E+18	0.79
140808 - 10	-	162	24.2	63	12.4	0.9	32.9	98.5	266.1	54.7	-	169.4	212.4	2.60081E+18	0.80
140808 - 11	-	19.23	0.5	3.88	4.77	0.3	16.8	66	187.3	38.8	-	90.6	123.9	9.72381E+17	0.73
140808 - 12	-0.013	13.22	0.82	10.5	11.2	0.55	38.1	121.9	280.2	56.3	-	84.2	105.9	8.39398E+17	0.80
140808 - 13	-0.023	18.71	0.52	7.3	9.4	0.58	37.7	131.3	326.6	66.1	-	161.1	207.6	1.71972E+18	0.78
140808 - 14	-	38.2	5.68	18.7	5.46	0.29	14.8	50.1	144.9	30.34	-	67.6	97.5	7.82482E+17	0.69
140808 - 15	0.013	17.75		2.22	2.81	0.172	14.4	54.7	159.2	33.67	-	80.25	120.2	9.58891E+17	0.67
140808 - 16	-	88	12.5	38.1	9.7	1.11	26.1	81.7	227	47.9	-	83.5	141	1.12951E+18	0.59
140808 - 17	-	38.1	6.2	27.1	11.4	1.46	37.2	106.8	232.1	46.99	-	50.8	49.7	4.25998E+17	1.02
140808 - 18	-	21.3	3.03	19.6	15.5	0.81	47.8	148.7	320	64.2	-	100.5	106.8	8.68602E+17	0.94
140808 - 19	-0.044	11.3	0.42	6.3	6.6	0.79	29.6	92.6	216	44.3	-	62.7	72.1	5.77112E+17	0.87
140808 - 20	-	30.4	3.2	11.6	7.41	0.45	25.6	93.2	251	52	-	125.7	149	1.21235E+18	0.84
140808 - 21	-	118	19.7	63	12.2	1.39	25.7	68.2	213.9	44.96	-	151.3	235.5	1.90118E+18	0.64
140808 - 22	0.002	11.89	0.116	1.76	3.41	0.34	12.6	50.6	152.1	32.18	-	45.69	68.9	5.86699E+17	0.66
140808 - 23	-	19.6	1.72	8.4	5.08	0.45	18	60.9	165.2	34.61	-	66.5	84.7	6.93818E+17	0.79
140808 - 24	0.001	12.16	0.81	8.9	10.2	1.03	34.7	105.3	240	46.9	-	60.6	60.3	5.15849E+17	1.00
140808 - 25	0.018	18.13	0.125	2.33	3.48	0.175	14.3	53.7	160	32.3	-	80.5	121.7	9.6699E+17	0.66
140808 - 26	0	8.62	0.7	6.9	8	0.87	27	87.2	195.8	40.1	-	42.9	41.7	3.42377E+17	1.03
140808 - 27	-0.004	5.55	0.162	2.85	3.47	0.51	12.3	43.3	129.8	28.92	-	30.88	213	1.40218E+18	0.14
140808 - 28	-0.003	8.13	0.31	3.51	4.06	0.62	15.2	48.7	121.5	25.14	-	25.59	26.75	2.21161E+17	0.96
140808 - 29	-	13.5	0.87	9.8	9.6	1.01	35.3	100.4	228.9	45.5	-	50.4	49.5	4.39446E+17	1.02
140808 - 30	-	73	10.4	31	10.1	0.98	23.1	74.5	217.1	46.5	-	121	119.3	1.14118E+18	1.01
140808 - 31	-0.041	19.3	0.56	7	9.5	0.38	38.6	129	318	62.7	-	141	150	1.25304E+18	0.94
140808 - 32	-	20.3	2.9	16.5	12.1	1.24	39.9	118.4	255.9	52.7	-	60.7	60.4	4.89158E+17	1.00
140808 - 33	-	60.6	12.7	48.5	9.4	0.54	16.3	47.4	195.3	42.63	-	131.6	256.5	2.00817E+18	0.51
140808 - 34	-	104	16.6	57	15.4	1.23	37.6	107.1	263.2	53.9	-	110.1	211.8	1.57604E+18	0.52
140808 - 35	0.021	13	0.167	2.6	3.8	0.36	18.5	62	165.5	34.2	-	60.21	82	6.74606E+17	0.73
140808 - 36	-	122	28.9	101	18.2	0.78	26.4	63.4	158	33.36	-	61.3	79.6	6.06682E+17	0.77

Sample:140813	REE														
Analysis_#	La	Ce	Pr	Nd	Sm	Eu	Gd	Dy	Yb	Lu	Pb	Th	U	Alpha dose	Th/U
140813 - 1	-	13.3	0.8	3.12	3.1	0.84	10	40.4	235.2	58.6	-	65.4	397	2.71736E+18	0.16
140813 - 2	-	11.81	0.49	4.6	5.44	1.09	24.4	108.2	409	88.9	-	88.5	285.2	3.18814E+18	0.31
140813 - 3	-	22.6	2.78	12	4.12	1.47	11.6	44.1	258.3	64.2	-	102.7	498	3.61855E+18	0.21
140813 - 4	-	14.66	0.45	2.77	1.91	0.71	7.34	30.6	173.6	43.8	-	100.3	460.3	3.23647E+18	0.22
140813 - 5	-	29.3	3.9	11.7	3.3	2.04	7.68	32.5	183.6	46	-	79.1	422.4	2.96936E+18	0.19
140813 - 6	-	24.8	2.37	10	6.8	0.91	15.6	57.7	208.3	47	-	247	553	4.42877E+18	0.45
140813 - 7	-	25	3.13	11.5	4.24	1.21	12.7	52.1	281.5	67.6	-	82.9	420.4	2.91733E+18	0.20
140813 - 8	-	19.4	1.31	6.2	5.07	1.29	17.5	68.5	242.1	54.4	-	81.2	150.8	1.24121E+18	0.54
140813 - 9	-	15.4	1.92	6	2.85	1.34	8.93	39	211.8	52.01	-	70.1	382.5	2.73346E+18	0.18
140813 - 10	-	20.5	2.14	10.3	4.44	1.42	11.4	41.7	238.5	61.3	-	84.2	479	3.62709E+18	0.18
140813 - 11	-	98	18.4	50.5	7.5	3.76	12.6	36.5	198.7	48.6	-	72.6	403	3.09533E+18	0.18
140813 - 12	-	12.05	0.32	1.18	1.59	0.88	9.01	46.8	214	46.9	-	184.5	492.6	3.51589E+18	0.37
140813 - 13	-	12.2	1.05	4.2	0.74	0.54	4.7	29.3	166.7	37.4	-	47.4	379.4	2.94672E+18	0.12
140813 - 14	-	47.7	6.4	19.3	3.31	1.7	7.6	29.8	170.4	40.33	-	92.6	524	4.21577E+18	0.18
140813 - 15	-	67	10	28	5	1.18	10.9	42.4	225.6	56.2	-	66.7	361	2.67525E+18	0.18
140813 - 16	-	9.71	0.45	2.19	2.28	1.08	7.78	35.9	213.6	53	-	67.8	414	2.82973E+18	0.16
Sample:140814	**REE**														
Analysis_#	**La**	**Ce**	**Pr**	**Nd**	**Sm**	**Eu**	**Gd**	**Dy**	**Yb**	**Lu**	**Pb**	**Th**	**U**	**Alpha dose**	**Th/U**
140814 - 1	0.0294	16.36	-	1.85	2.74	0.62	12.21	48.4	173.1	37.2	-	69	152.8	1.80118E+18	0.45
140814 - 2	-	14.12	0.55	4.28	3.42	1.09	13.2	54.5	267.3	62.8	-	130.9	643	4.76665E+18	0.20
140814 - 3	-	14.6	1.16	7.3	2.52	3.97	8.48	32.7	178.2	42.85	-	54.4	394	2.73716E+18	0.14
140814 - 4	-	6.26	0.87	4.56	1.94	0.54	8.8	37.1	132.7	29.43	-	43.3	287	2.54511E+18	0.15
140814 - 5	-	15.57	0.39	2.15	1.83	0.55	7.65	35.8	144.9	30.51	-	83.2	316.5	3.39515E+18	0.26
140814 - 6	-	12.4	1.04	4.5	3.17	0.74	11.5	52.7	306.2	73.3	-	85.5	563	3.65837E+18	0.15
140814 - 7	-	9.24	0.28	2.32	3	0.61	11	44.2	240.8	58.9	-	69.6	403	2.83455E+18	0.17
140814 - 8	-	36	5.5	20.6	5	1.03	11.5	45.9	249.1	61.6	-	89.4	522	3.58442E+18	0.17
140814 - 9	-	6.81	0.068	1.24	1.86	0.38	9.46	48.3	297	67.4	-	55.33	419	2.83759E+18	0.13
140814 - 10	-	15.9	0.61	3.02	2.52	1.14	10.3	47.2	266.5	64.9	-	103.6	655.7	4.00495E+18	0.16
140814 - 11	-	3.57	0.202	1.62	2.06	0.203	8.89	39.5	175.7	39.4	-	72.5	248	2.5734E+18	0.29
140814 - 12	-	59.9	7.3	28.6	7.8	2.08	13.5	30.4	97.7	22.25	-	184	253	3.19013E+18	0.73
140814 - 13	-	10.99	0.32	1.54	1.67	0.69	12.9	67.5	213.1	45.5	-	102.8	346	3.29541E+18	0.30
140814 - 14	-	20.5	1.24	10.1	2.35	8	12	46.9	262.1	62.9	-	88.8	570	3.9494E+18	0.16
140814 - 15	-	11.5	1.13	4.3	1.69	0.64	6.9	33.6	214.9	52	-	46.1	418	2.80147E+18	0.11
140814 - 16	-	28.6	2.85	10.8	3.2	9.1	7.2	35.2	224.7	56.5	-	60.7	523	3.25089E+18	0.12

Sample:140818	REE														
Analysis_#	La	Ce	Pr	Nd	Sm	Eu	Gd	Dy	Yb	Lu	Pb	Th	U	Alpha dose	Th/U
140818 - 1	-	33	7.7	24	7.3	0.76	17	50.6	122.8	25.7	-	40.2	55.6	4.32761E+17	0.72
140818 - 2	-	104	24.5	101	26.1	2.51	51.2	137	265	51.9	-	67.1	95	7.57292E+17	0.71
140818 - 3	0.014	3.06	0.301	2.99	4.67	0.31	17.8	57.4	148.6	30.41	-	19.41	52.04	3.86953E+17	0.37
140818 - 4	-	4.18	0.78	9.4	10.9	0.72	32.4	103.6	217.5	42.4	-	28.33	50.1	3.77268E+17	0.57
140818 - 5	0.011	3.67		0.81	2.36	0.164	8.66	35	98.7	20.15	-	14.55	37.13	2.64536E+17	0.39
140818 - 6	-	5.2	1.18	10.3	10.6	0.76	39.4	121.8	252.6	50.6	-	32.87	60.9	4.2287E+17	0.54
140818 - 7	-	4.09	1.13	10.3	12.8	0.95	44.2	130.8	268.6	53.2	-	36	61.8	4.45768E+17	0.58
140818 - 8	-	4.18	0.14	1.27	1.8	0.33	6.42	24.9	69.3	14.83	-	10.91	35.1	2.47973E+17	0.31
140818 - 9	0.01	3.15	0.26	3.26	3.78	0.33	13.8	45.1	113.8	23.7	-	15.33	40.8	2.92996E+17	0.38
140818 - 10	-	13.8	1.73	13.3	12.1	0.75	46.3	145.9	310	59.8	-	79.8	123.2	1.01021E+18	0.65
140818 - 11	0.004	3.52		0.98	1.1	0.125	8.95	33.5	93.1	19.81	-	16.53	44.5	3.27866E+17	0.37
140818 - 12	-	175	35.3	113	19.5	3.1	22.7	50.1	110.2	22.59	-	22.5	40	3.20096E+17	0.56
140818 - 13	-	13.6	1.26	6.3	4.75	0.49	20.2	65.1	168.5	35.73	-	44	71.9	5.47297E+17	0.61
140818 - 14	-	5.22	0.35	4.4	6.8	0.72	25.5	88.7	200.3	39.5	-	34.5	60	4.99656E+17	0.58
140818 - 15	-	8.3	0.88	10.2	12.1	0.55	38.1	120.2	257	50.8	-	57.9	101	7.50493E+17	0.57
140818 - 16	-	5.75	0.57	6.44	7.9	0.49	25.2	77	171.8	34.93	-	34.1	54.9	4.07922E+17	0.62
140818 - 17	-	4.46	0.228	1.78	3.02	0.62	10.32	40.1	108.2	21.61	-	18.29	44.36	3.29072E+17	0.41
140818 - 18	0.013	4.44	0.3	3.7	4.5	0.28	16.4	55.1	137.5	27.2	-	19.9	61	5.02896E+17	0.33
140818 - 19	-	10.6	0.7	8.3	10.9	0.69	36.4	121.8	269.8	54.4	-	74.5	124	9.10449E+17	0.60
140818 - 20	-	3.56	0.141	1.72	2.75	0.28	11.2	39.8	108.6	21.81	-	16.63	45.8	3.39162E+17	0.36
140818 - 21	-	4.59	0.78	8.6	8.6	0.72	34.3	106.6	227	44.6	-	33	55.7	4.19155E+17	0.59
140818 - 22	-	75	16.6	60	12.7	2.68	21.1	54.4	124.2	24.99	-	18.33	37.2	2.7529E+17	0.49
140818 - 23	-	132	33.2	134	37	5.6	59.2	138.5	287.3	56.9	-	102.4	189.9	1.45086E+18	0.54
140818 - 24	0.014	3.37		1.09	2.07	0.259	9.92	36.8	96.6	19.8	-	14.86	34.15	2.32854E+17	0.44
140818 - 25	-	46	8.3	22.9	10.4	1.51	28	90.2	219.3	45.1	-	73.2	133	1.0651E+18	0.55
140818 - 26	-	9.47	0.54	8.2	8.9	0.3	31	105.4	237	45.9	-	61.6	114	8.49298E+17	0.54
140818 - 27	-	3.67	0.53	5.9	7	0.43	26.2	82.7	184.5	37	-	27.3	57.2	3.79257E+17	0.48
140818 - 28	0	3.08	0.43	4.79	5.4	0.42	20.2	63.3	139	28.2	-	17.9	37.2	3.52358E+17	0.48
140818 - 29	-	299	65	222	38.4	3.32	41.2	79.2	173.5	35.1	-	48.7	86.3	7.14277E+17	0.56
140818 - 30	-	4.45	0.292	2.9	5.06	0.244	16.4	55.5	134.2	27.46	-	17.76	42.6	3.01443E+17	0.42

Sample:140818	REE														
Analysis_#	La	Ce	Pr	Nd	Sm	Eu	Gd	Dy	Yb	Lu	Pb	Th	U	Alpha dose	Th/U
140819 - 1	-0.09	11.7	1.14	11.2	12.8	1.69	45	143	365	72.7		143	323.1	2.49322E+18	0.44
140819 - 2	-	-	-	-	-	-	-	-	-	-		-	-	-	-
140819 - 3	-	-	-	-	-	-	-	-	-	-		-	-	-	-
140819 - 4	-	-	-	-	-	-	-	-	-	-		-	-	-	-
140819 - 5	-	31	0.29	4.3	7.6	1.56	22.8	79.3	267	58.6		123.5	234.4	1.70847E+18	0.53

Appendix A5 – Lu-Hf isotope data

Sample	Project	Age(Ma)	1s	176Hf/177Hf	1s	176Lu/177Hf	1s	t		177/176t	2s	eHf(t)	2s	tDM	2s
90341 - 1	KN90341	1770	8	0.281416	0.000021	0.00072	0.000075	1.77	0.008	0.281392	4.2E-05	-9.38373	1.312249	2.546915	0.023462
90341 - 2	KN90341	1770	8	0.28139	0.000016	0.000748	0.000013	1.77	0.008	0.281365	3.2E-05	-10.3402	1.105123	2.58402	0.020807
90341 - 3	KN90341	1770	8	0.28138	0.0000155	0.000663	0.000028	1.77	0.008	0.281358	3.1E-05	-10.5939	1.033832	2.591862	0.019066
90341 - 4	KN90341	1770	8	0.281409	0.0000135	0.000772	3.8E-06	1.77	0.008	0.281383	2.7E-05	-9.69393	0.94955	2.559832	0.018062
90341 - 5	KN90341	1770	8	0.281396	0.000018	0.00064	4.7E-06	1.77	0.008	0.281374	3.6E-05	-9.99838	1.266941	2.568693	0.024017
90341 - 6	KN90341	1770	8	0.281402	0.000016	0.000346	1.65E-06	1.77	0.008	0.28139	3.2E-05	-9.43453	1.132201	2.541252	0.021364
90341 - 7	KN90341	1770	8	0.281434	0.00002	0.001562	0.000015	1.77	0.008	0.281382	4E-05	-9.74905	1.384385	2.578801	0.02667
90341 - 8	KN90341	1770	8	0.281458	0.0000195	0.00143	0.000025	1.77	0.008	0.28141	3.9E-05	-8.73949	1.325024	2.536658	0.025246
90341 - 9	KN90341	1770	8	0.281432	0.0000195	0.001116	3.95E-05	1.77	0.008	0.281395	3.9E-05	-9.28804	1.29043	2.551415	0.02404
90341 - 10	KN90341	1770	8	0.28148	0.0000175	0.00229	0.00009	1.77	0.008	0.281403	3.5E-05	-8.98426	1.027933	2.564533	0.018454
90341 - 11	KN90341	1770	8	0.281394	0.0000175	0.000681	8E-07	1.77	0.008	0.281371	3.5E-05	-10.1185	1.240742	2.574139	0.023625
90341 - 12	KN90341	1770	8	0.281395	0.000017	0.000591	6.5E-06	1.77	0.008	0.281375	3.4E-05	-9.97544	1.191639	2.566793	0.022517
90341 - 13	KN90341	1770	8	0.281385	0.000014	0.0007	4.45E-06	1.77	0.008	0.281361	2.8E-05	-10.4599	0.983504	2.587544	0.018648
90341 - 14	KN90341	1770	8	0.281416	0.0000185	0.000468	0.00001	1.77	0.008	0.2814	3.7E-05	-9.08312	1.289801	2.530388	0.024254
90341 - 15	KN90341	1770	8	0.281358	0.000018	0.000638	0.000013	1.77	0.008	0.281337	3.6E-05	-11.3452	1.24714	2.619911	0.023419
90341 - 16	KN90341	1770	8	0.281434	0.0000155	0.001108	1.85E-05	1.77	0.008	0.281397	3.1E-05	-9.20748	1.056497	2.548141	0.01998
90341 - 17	KN90341	1770	8	0.28142	0.0000155	0.000775	0.000009	1.77	0.008	0.281394	3.1E-05	-9.30732	1.079161	2.545121	0.020438
90341 - 18	KN90341	1770	8	0.281399	0.0000125	0.000684	0.000005	1.77	0.008	0.281376	2.5E-05	-9.94436	0.875679	2.567558	0.016584
90341 - 19	KN90341	1770	8	0.28141	0.0000175	0.000924	2.85E-05	1.77	0.008	0.281379	3.5E-05	-9.8401	1.174656	2.568627	0.021912
90341 - 20	KN90341	1770	8	0.281382	0.00002	0.000744	9.5E-06	1.77	0.008	0.281357	4E-05	-10.6195	1.397507	2.594594	0.026451
90341 - 22	KN90341	1770	8	0.28137	0.0000145	0.000542	1.25E-05	1.77	0.008	0.281352	2.9E-05	-10.8046	0.999803	2.597255	0.018697
90341 - 23	KN90341	1770	8	0.281376	0.0000185	0.000429	1.35E-05	1.77	0.008	0.281362	3.7E-05	-10.4568	1.281451	2.581645	0.023958
90341 - 24	KN90341	1770	8	0.281355	0.0000165	0.00079	0.000065	1.77	0.008	0.281328	3.3E-05	-11.633	1.016568	2.634311	0.017894
90341 - 25	KN90341	1770	8	0.281555	0.000024	0.0027	0.0001	1.77	0.008	0.281464	4.8E-05	-6.81052	1.465631	2.48597	0.027486
90341 - 26	KN90341	1770	8	0.281439	0.0000165	0.000412	0.000005	1.77	0.008	0.281425	3.3E-05	-8.19972	1.159713	2.4958	0.021877
90341 - 27	KN90341	1770	8	0.281082	0.000018	0.000647	0.00002	1.77	0.008	0.28106	3.6E-05	-21.1551	1.23044	2.992105	0.022592
90341 - 28	KN90341	1770	8	0.281285	0.000019	0.000802	4.5E-06	1.77	0.008	0.281258	3.8E-05	-14.1331	1.338427	2.73001	0.025395
90341 - 29	KN90341	1770	8	0.281405	0.0000205	0.000779	2.45E-05	1.77	0.008	0.281379	4.1E-05	-9.84465	1.397225	2.565746	0.026166
90341 - 30	KN90341	1770	8	0.281316	0.000021	0.000921	3.6E-06	1.77	0.008	0.281285	4.2E-05	-13.174	1.482591	2.696328	0.028275
90341 - 31	KN90341	1770	8	0.281381	0.000016	0.000422	0.000009	1.77	0.008	0.281367	3.2E-05	-10.2709	1.114666	2.57446	0.020902
90332 - 1	KN90332	1809	10	0.281492	0.0000235	0.001142	2.15E-05	1.809	0.01	0.281453	4.7E-05	-6.32176	1.616404	2.47085	0.03084
90332 - 2	KN90332	1809	10	0.2815	0.000019	0.00066	0.00006	1.809	0.01	0.281477	3.8E-05	-5.4498	1.202919	2.429151	0.021955
90332 - 3	KN90332	1809	10	0.281444	0.00002	0.000441	2.55E-06	1.809	0.01	0.281429	4E-05	-7.17122	1.414079	2.490935	0.026767

90332 - 4	KN90332	1809	10	0.281483	0.0000215	0.000701	2.7E-06	1.809	0.01	0.281459	4.3E-05	-6.10319	1.520235	2.454798	0.028996	
90332 - 5	KN90332	1809	10	0.28149	0.000014	0.000284	1.3E-06	1.809	0.01	0.28148	2.8E-05	-5.34614	0.991038	2.419146	0.01872	
90332 - 6	KN90332	1809	10	0.281461	0.0000165	0.000419	4.8E-06	1.809	0.01	0.281447	3.3E-05	-6.54076	1.160038	2.466636	0.02191	
90332 - 7	KN90332	1809	10	0.281454	0.0000195	0.000353	0.000008	1.809	0.01	0.281442	3.9E-05	-6.70869	1.365276	2.471858	0.025694	
90332 - 8	KN90332	1809	10	0.281481	0.0000225	0.000299	6.5E-06	1.809	0.01	0.281471	4.5E-05	-5.68412	1.58198	2.432175	0.029807	
90332 - 9	KN90332	1809	10	0.281445	0.000023	0.00042	0.000019	1.809	0.01	0.281431	4.6E-05	-7.10998	1.586995	2.488237	0.029724	
90339 - 2	KN90339	1811	26	0.281398	0.000018	0.000783	0.000012	1.811	0.026	0.281371	3.6E-05	-9.17662	1.248969	2.575512	0.023612	
90339 - 5	KN90339	1811	26	0.281571	0.0000225	0.001478	0.000014	1.811	0.026	0.28152	4.5E-05	-3.88246	1.563653	2.383316	0.030316	
90339 - 6	KN90339	1811	26	0.281511	0.00002	0.001085	2.55E-05	1.811	0.026	0.281474	4E-05	-5.53303	1.35803	2.44111	0.025774	
90339 - 7	KN90339	1811	26	0.281387	0.0000295	0.00114	2.85E-05	1.811	0.026	0.281348	5.9E-05	-10.0031	2.025349	2.614661	0.038391	
90339 - 8	KN90339	1811	26	0.281398	0.0000185	0.000642	1.85E-06	1.811	0.026	0.281376	3.7E-05	-9.00494	1.309265	2.566148	0.024886	
90339 - 9	KN90339	1811	26	0.281482	0.000019	0.001154	0.000021	1.811	0.026	0.281442	3.8E-05	-6.647	1.298005	2.485358	0.024695	
90339 - 10	KN90339	1811	26	0.281523	0.000021	0.00096	0.00008	1.811	0.026	0.28149	4.2E-05	-4.9543	1.295947	2.416735	0.023612	
90339 - 11	KN90339	1811	26	0.281132	0.000016	0.000742	9.5E-06	1.811	0.026	0.281106	3.2E-05	-18.5716	1.113044	2.932161	0.020816	
90339 - 12	KN90339	1811	26	0.281419	0.000023	0.000766	4.05E-05	1.811	0.026	0.281393	4.6E-05	-8.4102	1.534443	2.545883	0.028501	
90339 - 14	KN90339	1811	26	0.281433	0.0000165	0.002052	0.000022	1.811	0.026	0.281362	3.3E-05	-9.48341	1.118024	2.614134	0.021594	
140813 - 1	KN140813	1900	50	0.281455	0.000016	0.001181	0.000019	1.9	0.05	0.281412	3.2E-05	-5.65968	1.087745	2.524199	0.020692	
140813 - 2	KN140813	1900	50	0.281171	0.000016	0.001408	3.15E-05	1.9	0.05	0.28112	3.2E-05	-16.037	1.055685	2.930071	0.019485	
140813 - 3	KN140813	1900	50	0.281442	0.0000185	0.001141	1.25E-05	1.9	0.05	0.281401	3.7E-05	-6.07007	1.281992	2.539378	0.024517	
140813 - 4	KN140813	1900	50	0.281409	0.0000185	0.000812	0.000009	1.9	0.05	0.28138	3.7E-05	-6.82015	1.290969	2.562512	0.02452	
140813 - 5	KN140813	1900	50	0.281484	0.000023	0.000767	1.35E-05	1.9	0.05	0.281456	4.6E-05	-4.09882	1.599061	2.457659	0.030386	
140813 - 7	KN140813	1900	50	0.281437	0.0000225	0.001189	0.000016	1.9	0.05	0.281394	4.5E-05	-6.30921	1.557134	2.54944	0.02979	
140813 - 8	KN140813	1900	50	0.281379	0.0000195	0.001141	0.000021	1.9	0.05	0.281338	3.9E-05	-8.30752	1.33122	2.625681	0.025227	
140813 - 9	KN140813	1900	50	0.2815	0.0000205	0.001	0.000005	1.9	0.05	0.281464	4.1E-05	-3.82939	1.443288	2.450737	0.027715	
140813 - 10	KN140813	1900	50	0.281439	0.00002	0.001276	0.000031	1.9	0.05	0.281393	4E-05	-6.34975	1.341086	2.552523	0.025404	
140813 - 11	KN140813	1900	50	0.281418	0.000017	0.000852	1.45E-05	1.9	0.05	0.281387	3.4E-05	-6.55181	1.170317	2.552938	0.022146	
140813 - 12	KN140813	1900	50	0.281447	0.000016	0.000697	1.25E-05	1.9	0.05	0.281422	3.2E-05	-5.3231	1.104417	2.503385	0.02087	
140813 - 14	KN140813	1900	50	0.281429	0.0000185	0.000655	4.4E-06	1.9	0.05	0.281405	3.7E-05	-5.90825	1.302767	2.525023	0.024747	
140813 - 15	KN140813	1900	50	0.281455	0.0000275	0.001099	0.000032	1.9	0.05	0.281415	5.5E-05	-5.55452	1.871246	2.518779	0.035521	
140813 - 16	KN140813	1900	50	0.281442	0.0000215	0.001033	0.000015	1.9	0.05	0.281405	4.3E-05	-5.93157	1.488669	2.53221	0.028383	
140808 - 1	KN140808	1767.6	4.65	0.281348	0.000022	0.001169	3.75E-05	1.7676	0.00465	0.281309	4.4E-05	-12.3869	1.472838	2.670054	0.027453	
140808 - 2	KN140808	1767.6	4.65	0.281324	0.0000215	0.000462	5.5E-07	1.7676	0.00465	0.281309	4.3E-05	-12.3967	1.525366	2.653742	0.028841	
140808 - 3	KN140808	1767.6	4.65	0.281341	0.0000185	0.000514	0.000006	1.7676	0.00465	0.281324	3.7E-05	-11.8552	1.299357	2.634427	0.024483	
140808 - 4	KN140808	1767.6	4.65	0.281334	0.0000155	0.00109	0.00005	1.7676	0.00465	0.281297	3.1E-05	-12.7898	0.981505	2.683658	0.01763	

140808 - 5	KN140808	1767.6	4.65	0.281385	0.000021	0.000778	0.000011	1.7676	0.00465	0.281359	4.2E-05	-10.6075	1.464965	2.592814	0.027729
140808 - 6	KN140808	1767.6	4.65	0.281332	0.0000185	0.000641	7E-07	1.7676	0.00465	0.281311	3.7E-05	-12.3257	1.311984	2.65521	0.024919
140808 - 7	KN140808	1767.6	4.65	0.281358	0.000019	0.001116	3.15E-05	1.7676	0.00465	0.281321	3.8E-05	-11.9687	1.274109	2.652681	0.023764
140808 - 8	KN140808	1767.6	4.65	0.281341	0.0000195	0.000803	1.05E-05	1.7676	0.00465	0.281314	3.9E-05	-12.1994	1.359644	2.654184	0.025701
140808 - 9	KN140808	1767.6	4.65	0.281388	0.0000195	0.001354	4.15E-05	1.7676	0.00465	0.281343	3.9E-05	-11.1871	1.285788	2.628024	0.023938
140808 - 10	KN140808	1767.6	4.65	0.281302	0.000023	0.000889	9.5E-06	1.7676	0.00465	0.281272	4.6E-05	-13.6865	1.610555	2.713084	0.030533
140808 - 11	KN140808	1767.6	4.65	0.281327	0.000021	0.000657	1.05E-05	1.7676	0.00465	0.281305	4.2E-05	-12.5226	1.466156	2.663073	0.027618
140808 - 12	KN140808	1767.6	4.65	0.281378	0.000018	0.001003	1.75E-05	1.7676	0.00465	0.281344	3.6E-05	-11.124	1.236455	2.617589	0.023339
140808 - 13	KN140808	1767.6	4.65	0.281352	0.000015	0.001116	5.5E-06	1.7676	0.00465	0.281315	3E-05	-12.1817	1.052019	2.660884	0.020115
140808 - 14	KN140808	1767.6	4.65	0.281346	0.00002	0.000519	2.9E-06	1.7676	0.00465	0.281329	4E-05	-11.6832	1.413255	2.628015	0.02672
140808 - 15	KN140808	1767.6	4.65	0.281331	0.0000235	0.000552	6.5E-07	1.7676	0.00465	0.281312	4.7E-05	-12.2549	1.667144	2.650444	0.031596
140808 - 16	KN140808	1767.6	4.65	0.281346	0.0000205	0.000883	2.75E-05	1.7676	0.00465	0.281316	4.1E-05	-12.1172	1.390151	2.652912	0.02593
140808 - 17	KN140808	1767.6	4.65	0.281338	0.0000165	0.000922	6.5E-06	1.7676	0.00465	0.281307	3.3E-05	-12.4477	1.156149	2.666485	0.021976
140808 - 18	KN140808	1767.6	4.65	0.281347	0.0000185	0.00122	3.35E-05	1.7676	0.00465	0.281306	3.7E-05	-12.4831	1.23384	2.674997	0.022976
140808 - 19	KN140808	1767.6	4.65	0.281365	0.000019	0.000828	0.000043	1.7676	0.00465	0.281337	3.8E-05	-11.3771	1.24671	2.623338	0.02283
140808 - 20	KN140808	1767.6	4.65	0.281362	0.000017	0.000887	3.25E-05	1.7676	0.00465	0.281332	3.4E-05	-11.5539	1.12971	2.631443	0.020862
140808 - 21	KN140808	1767.6	4.65	0.281336	0.000018	0.00068	3.1E-06	1.7676	0.00465	0.281313	3.6E-05	-12.2301	1.270762	2.652476	0.024105
140808 - 22	KN140808	1767.6	4.65	0.281366	0.0000155	0.000571	1.9E-06	1.7676	0.00465	0.281347	3.1E-05	-11.0358	1.0961	2.604614	0.020772
140808 - 23	KN140808	1767.6	4.65	0.281337	0.0000225	0.000621	6.5E-06	1.7676	0.00465	0.281316	4.5E-05	-12.1246	1.582198	2.647105	0.029904
140808 - 24	KN140808	1767.6	4.65	0.28139	0.00002	0.000918	0.000015	1.7676	0.00465	0.281359	4E-05	-10.5967	1.384427	2.595461	0.026197
140808 - 25	KN140808	1767.6	4.65	0.281341	0.00002	0.000544	4.45E-06	1.7676	0.00465	0.281323	4E-05	-11.8904	1.409562	2.636437	0.026626
140808 - 26	KN140808	1767.6	4.65	0.281362	0.0000225	0.00079	1.95E-05	1.7676	0.00465	0.281335	4.5E-05	-11.4383	1.551227	2.62482	0.02916
140808 - 27	KN140808	1767.6	4.65	0.281341	0.000015	0.000404	4.2E-06	1.7676	0.00465	0.281327	3E-05	-11.7244	1.055117	2.626998	0.019844
140808 - 28	KN140808	1767.6	4.65	0.281332	0.0000215	0.000514	1.65E-06	1.7676	0.00465	0.281315	4.3E-05	-12.1747	1.522745	2.646539	0.028809
140808 - 29	KN140808	1767.6	4.65	0.281369	0.000022	0.000874	0.000018	1.7676	0.00465	0.28134	4.4E-05	-11.2899	1.519296	2.62104	0.028653
140808 - 30	KN140808	1767.6	4.65	0.281356	0.000017	0.000753	2.45E-05	1.7676	0.00465	0.281331	3.4E-05	-11.6073	1.148769	2.63043	0.021339
140808 - 31	KN140808	1767.6	4.65	0.281341	0.0000145	0.00106	0.00007	1.7676	0.00465	0.281305	2.9E-05	-12.5056	0.862848	2.672004	0.014871
140808 - 32	KN140808	1767.6	4.65	0.281346	0.0000255	0.001046	3.05E-05	1.7676	0.00465	0.281311	5.1E-05	-12.3114	1.738044	2.664205	0.032631
140808 - 33	KN140808	1767.6	4.65	0.281344	0.000018	0.000592	9.5E-07	1.7676	0.00465	0.281324	3.6E-05	-11.8416	1.275884	2.635685	0.024205
140808 - 34	KN140808	1767.6	4.65	0.281333	0.000016	0.00083	0.000016	1.7676	0.00465	0.281305	3.2E-05	-12.5156	1.098012	2.666897	0.020582
140808 - 35	KN140808	1767.6	4.65	0.281343	0.00002	0.000576	3.4E-06	1.7676	0.00465	0.281324	4E-05	-11.8575	1.412063	2.635917	0.026721
140808 - 36	KN140808	1767.6	4.65	0.281349	0.0000155	0.000568	3.6E-06	1.7676	0.00465	0.28133	3.1E-05	-11.6353	1.09205	2.627307	0.020644
140814 - 1	KN140814	2656	25	0.281121	0.000021	0.000677	0.000005	2.656	0.025	0.281087	4.2E-05	0.345987	1.476167	2.94203	0.027833
140814 - 2	KN140814	1939	46	0.281288	0.000021	0.00098	4.1E-06	1.939	0.046	0.281252	4.2E-05	-10.4589	1.481025	2.738525	0.028257

140814 - 3	KN140814	1939	46	0.281486	0.0000225	0.000744	7.5E-06	1.939	0.046	0.281459	4.5E-05	-3.11793	1.578676	2.453474	0.030079
140814 - 4	KN140814	2656	25	0.281121	0.000021	0.000394	0.000008	2.656	0.025	0.281101	4.2E-05	0.857841	1.465314	2.920709	0.027414
140814 - 5	KN140814	2656	25	0.28106	0.000018	0.000437	1.35E-06	2.656	0.025	0.281038	3.6E-05	-1.39088	1.275905	3.00539	0.023901
140814 - 6	KN140814	1939	46	0.281442	0.000018	0.001339	0.000028	1.939	0.046	0.281393	3.6E-05	-5.4598	1.205329	2.552627	0.022898
140814 - 8	KN140814	1939	46	0.281421	0.0000205	0.001135	2.15E-05	1.939	0.046	0.281379	4.1E-05	-5.93857	1.399941	2.567758	0.026617
140814 - 9	KN140814	1939	46	0.281415	0.0000195	0.001104	0.000035	1.939	0.046	0.281374	3.9E-05	-6.11109	1.293552	2.573887	0.024304
140814 - 11	KN140814	2656	25	0.281076	0.000018	0.000526	0.000013	2.656	0.025	0.281049	3.6E-05	-0.98189	1.233763	2.990833	0.023062
140814 - 12	KN140814	2656	25	0.281074	0.000016	0.00034	5.5E-06	2.656	0.025	0.281057	3.2E-05	-0.71663	1.118583	2.979277	0.020873
140814 - 13	KN140814	2656	25	0.28115	0.0000285	0.000627	0.000005	2.656	0.025	0.281118	5.7E-05	1.468167	2.009828	2.899299	0.037891
140818 - 1	KN140818	1766	7	0.281483	0.000023	0.000599	0.000014	1.766	0.007	0.281463	4.6E-05	-6.95098	1.599859	2.448336	0.030227
140818 - 2	KN140818	1766	7	0.281504	0.0000245	0.00128	0.00006	1.766	0.007	0.281461	4.9E-05	-7.01586	1.59688	2.463292	0.029815
140818 - 3	KN140818	1766	7	0.281506	0.0000215	0.000812	5.5E-06	1.766	0.007	0.281479	4.3E-05	-6.38788	1.513579	2.430584	0.028918
140818 - 4	KN140818	1766	7	0.281444	0.0000245	0.001074	1.65E-05	1.766	0.007	0.281408	4.9E-05	-8.90094	1.70042	2.532189	0.032416
140818 - 5	KN140818	1766	7	0.281468	0.000019	0.000458	1.65E-06	1.766	0.007	0.281453	3.8E-05	-7.31561	1.345223	2.459663	0.025506
140818 - 6	KN140818	1766	7	0.281502	0.000021	0.001282	1.75E-05	1.766	0.007	0.281459	4.2E-05	-7.08925	1.449512	2.466178	0.027783
140818 - 7	KN140818	1766	7	0.281471	0.0000205	0.001348	3.75E-05	1.766	0.007	0.281426	4.1E-05	-8.26842	1.366403	2.513247	0.025759
140818 - 8	KN140818	1766	7	0.281491	0.000025	0.000351	7.5E-06	1.766	0.007	0.281479	5E-05	-6.37179	1.757346	2.421972	0.033153
140818 - 9	KN140818	1766	7	0.281538	0.0000285	0.000541	1.25E-05	1.766	0.007	0.28152	5.7E-05	-4.92923	1.993973	2.370277	0.037784
140818 - 10	KN140818	1766	7	0.281492	0.000022	0.001383	0.000041	1.766	0.007	0.281446	4.4E-05	-7.56449	1.464584	2.486568	0.02766
140818 - 11	KN140818	1766	7	0.281496	0.000022	0.000454	4.2E-06	1.766	0.007	0.281481	4.4E-05	-6.31698	1.552177	2.42166	0.029408
140818 - 12	KN140818	1766	7	0.281465	0.000021	0.000555	0.000011	1.766	0.007	0.281446	4.2E-05	-7.53768	1.464984	2.469886	0.027665
140818 - 13	KN140818	1766	7	0.281498	0.0000245	0.000904	3.8E-06	1.766	0.007	0.281468	4.9E-05	-6.78116	1.730649	2.44732	0.033178
140818 - 16	KN140818	1766	7	0.281473	0.0000215	0.000845	0.000006	1.766	0.007	0.281445	4.3E-05	-7.59878	1.512389	2.477629	0.028878
140818 - 17	KN140818	1766	7	0.281465	0.0000265	0.00051	1.15E-06	1.766	0.007	0.281448	5.3E-05	-7.48365	1.878973	2.466994	0.035688
140818 - 20	KN140818	1766	7	0.281502	0.000023	0.000501	0.000009	1.766	0.007	0.281485	4.6E-05	-6.15977	1.61176	2.416485	0.030494
140818 - 21	KN140818	1766	7	0.281548	0.000029	0.001181	1.95E-05	1.766	0.007	0.281508	5.8E-05	-5.33587	2.012815	2.396372	0.038646
140818 - 22	KN140818	1766	7	0.281501	0.0000185	0.000599	0.000013	1.766	0.007	0.281481	3.7E-05	-6.3119	1.282703	2.423965	0.024225
140818 - 23	KN140818	1766	7	0.281507	0.000029	0.001141	0.000011	1.766	0.007	0.281469	5.8E-05	-6.74393	2.033047	2.45019	0.039092
140818 - 24	KN140818	1766	7	0.281503	0.000023	0.000481	2.1E-06	1.766	0.007	0.281487	4.6E-05	-6.1001	1.628184	2.41387	0.030915
140818 - 25	KN140818	1766	7	0.281519	0.0000255	0.000905	2.05E-05	1.766	0.007	0.281489	5.1E-05	-6.03701	1.761907	2.41873	0.033497
140818 - 26	KN140818	1766	7	0.281495	0.00002	0.00088	0.00005	1.766	0.007	0.281466	4E-05	-6.85935	1.301146	2.449894	0.024046
140818 - 29	KN140818	1766	7	0.281489	0.000019	0.000697	0.000017	1.766	0.007	0.281466	3.8E-05	-6.85458	1.308686	2.446413	0.024692
140818 - 30	KN140818	1766	7	0.281498	0.0000255	0.000722	1.15E-05	1.766	0.007	0.281474	5.1E-05	-6.5648	1.783329	2.435776	0.033891
90342 - 1	KN90342	1764	10	0.28145	0.000021	0.00131	0.00008	1.764	0.01	0.281406	4.2E-05	-9.01298	1.30096	2.539661	0.023516

90342 - 2	KN90342	1764	10	0.281375	0.00002	0.000642	1.25E-05	1.764	0.01	0.281354	4E-05	-10.8817	1.390433	2.597213	0.026174
90342 - 3	KN90342	1764	10	0.281386	0.00002	0.000649	2.35E-06	1.764	0.01	0.281364	4E-05	-10.4999	1.414565	2.582839	0.026875
90342 - 4	KN90342	1764	10	0.281379	0.0000235	0.000758	2.15E-05	1.764	0.01	0.281354	4.7E-05	-10.8776	1.617563	2.599603	0.030379
90342 - 5	KN90342	1764	10	0.281396	0.000023	0.000896	2.85E-05	1.764	0.01	0.281366	4.6E-05	-10.438	1.565416	2.58581	0.029351
90342 - 6	KN90342	1764	10	0.28142	0.0000185	0.000713	0.000023	1.764	0.01	0.281396	3.7E-05	-9.36842	1.258958	2.541031	0.02354
90342 - 7	KN90342	1764	10	0.281387	0.0000195	0.000755	1.05E-05	1.764	0.01	0.281362	3.9E-05	-10.59	1.359685	2.588557	0.025718
90342 - 8	KN90342	1764	10	0.281396	0.0000175	0.000762	0.000008	1.764	0.01	0.28137	3.5E-05	-10.2788	1.223613	2.576822	0.023189
90342 - 9	KN90342	1764	10	0.281394	0.0000255	0.000703	0.000008	1.764	0.01	0.28137	5.1E-05	-10.2796	1.791674	2.575592	0.033979
90342 - 10	KN90342	1764	10	0.281411	0.0000195	0.000725	2.65E-05	1.764	0.01	0.281387	3.9E-05	-9.70221	1.321645	2.554023	0.024655
90342 - 11	KN90342	1764	10	0.281431	0.000021	0.00129	0.00008	1.764	0.01	0.281388	4.2E-05	-9.66378	1.30096	2.564472	0.023439
90342 - 12	KN90342	1764	10	0.28145	0.0000205	0.00102	0.00005	1.764	0.01	0.281416	4.1E-05	-8.66825	1.336781	2.520414	0.024692
90342 - 13	KN90342	1764	10	0.281423	0.0000205	0.000635	2.85E-05	1.764	0.01	0.281402	4.1E-05	-9.16918	1.387897	2.531847	0.025841
90342 - 14	KN90342	1764	10	0.281369	0.0000205	0.000866	1.85E-05	1.764	0.01	0.28134	4.1E-05	-11.361	1.411672	2.620495	0.026577
90342 - 15	KN90342	1764	10	0.281384	0.0000185	0.000915	0.000018	1.764	0.01	0.281353	3.7E-05	-10.8867	1.270846	2.603425	0.023943
90342 - 16	KN90342	1764	10	0.28135	0.000021	0.000946	0.000009	1.764	0.01	0.281318	4.2E-05	-12.1307	1.469762	2.651822	0.027945
90342 - 17	KN90342	1764	10	0.281451	0.000022	0.001437	0.000036	1.764	0.01	0.281403	4.4E-05	-9.12845	1.476577	2.546801	0.027942
90342 - 18	KN90342	1764	10	0.281417	0.0000175	0.0008	3.25E-06	1.764	0.01	0.28139	3.5E-05	-9.57859	1.234906	2.550862	0.023547
90342 - 19	KN90342	1764	10	0.281406	0.0000185	0.000768	1.35E-05	1.764	0.01	0.28138	3.7E-05	-9.93085	1.281544	2.563657	0.024188
90342 - 20	KN90342	1764	10	0.281458	0.0000225	0.001341	0.000042	1.764	0.01	0.281413	4.5E-05	-8.7658	1.497816	2.530708	0.028178
90345 - 1	KN90345	1785	5.5	0.281547	0.000021	0.001641	0.000017	1.785	0.0055	0.281491	4.2E-05	-5.503	1.450323	2.427083	0.028126
90345 - 2	KN90345	1785	5.5	0.281522	0.000019	0.001196	0.000017	1.785	0.0055	0.281481	3.8E-05	-5.85522	1.308301	2.433098	0.025035
90345 - 3	KN90345	1785	5.5	0.281508	0.0000195	0.0013	0.000065	1.785	0.0055	0.281464	3.9E-05	-6.47743	1.2283	2.459074	0.022634
90345 - 4	KN90345	1785	5.5	0.281587	0.000028	0.00234	0.000075	1.785	0.0055	0.281508	5.6E-05	-4.92381	1.80783	2.416298	0.034758
90345 - 5	KN90345	1785	5.5	0.281579	0.0000215	0.00234	0.000115	1.785	0.0055	0.2815	4.3E-05	-5.20786	1.250003	2.427655	0.022873
90335 - 1	KN90335	1794	15.5	0.281442	0.000027	0.000823	1.85E-05	1.794	0.0155	0.281414	5.4E-05	-8.04484	1.87259	2.518386	0.035477
90335 - 2	KN90335	1794	15.5	0.2815	0.0000245	0.001572	0.000018	1.794	0.0155	0.281446	4.9E-05	-6.89131	1.696268	2.48793	0.032801
90335 - 3	KN90335	1794	15.5	0.281459	0.0000225	0.000789	0.000014	1.794	0.0155	0.281432	4.5E-05	-7.40012	1.563919	2.493058	0.029659
90335 - 4	KN90335	1794	15.5	0.281421	0.000019	0.001089	2.15E-05	1.794	0.0155	0.281384	3.8E-05	-9.11217	1.297234	2.564666	0.024537
90335 - 5	KN90335	1794	15.5	0.281461	0.000023	0.00082	3.85E-06	1.794	0.0155	0.281433	4.6E-05	-7.3666	1.623975	2.492347	0.031029
90335 - 6	KN90335	1794	15.5	0.281479	0.0000255	0.00156	0.000055	1.794	0.0155	0.281426	5.1E-05	-7.62243	1.677786	2.516277	0.031647
90335 - 7	KN90335	1794	15.5	0.28146	0.0000225	0.00102	4.05E-05	1.794	0.0155	0.281425	4.5E-05	-7.64398	1.499821	2.506742	0.028075
90335 - 8	KN90335	1794	15.5	0.281426	0.000022	0.001247	1.45E-05	1.794	0.0155	0.281384	4.4E-05	-9.12572	1.527203	2.568445	0.029233
90335 - 9	KN90335	1794	15.5	0.281479	0.0000215	0.001034	0.000017	1.794	0.0155	0.281444	4.3E-05	-6.98629	1.48565	2.481664	0.0283
90335 - 10	KN90335	1794	15.5	0.281495	0.000028	0.000742	1.25E-05	1.794	0.0155	0.28147	5.6E-05	-6.06505	1.958115	2.441118	0.037233

90335 - 11	KN90335	1794	15.5	0.281467	0.000024	0.001024	8.5E-06	1.794	0.0155	0.281432	4.8E-05	-7.40027	1.683741	2.497431	0.032254	
90335 - 12	KN90335	1794	15.5	0.281481	0.000021	0.000657	3.6E-06	1.794	0.0155	0.281459	4.2E-05	-6.45886	1.482555	2.454699	0.028227	
90335 - 13	KN90335	1794	15.5	0.281466	0.00002	0.000604	9.5E-06	1.794	0.0155	0.281445	4E-05	-6.92784	1.397272	2.471662	0.026444	
90335 - 14	KN90335	1794	15.5	0.281451	0.0000215	0.000758	4.35E-06	1.794	0.0155	0.281425	4.3E-05	-7.6468	1.516247	2.501923	0.028903	
90335 - 15	KN90335	1794	15.5	0.281443	0.0000175	0.001096	0.000018	1.794	0.0155	0.281406	3.5E-05	-8.3395	1.199181	2.535017	0.022755	
90335 - 16	KN90335	1794	15.5	0.281478	0.0000225	0.00108	0.00005	1.794	0.0155	0.281441	4.5E-05	-7.07743	1.476843	2.486023	0.027529	
90334 - 1	KN90334	1801	10	0.281496	0.0000175	0.001492	0.000024	1.801	0.01	0.281445	3.5E-05	-6.78262	1.184457	2.488202	0.022643	
90334 - 2	KN90334	1801	10	0.281521	0.0000155	0.00142	0.000075	1.801	0.01	0.281472	3.1E-05	-5.80753	0.918581	2.448888	0.016556	
90334 - 3	KN90334	1801	10	0.281481	0.000018	0.000853	0.00001	1.801	0.01	0.281452	3.6E-05	-6.53935	1.253962	2.467248	0.023868	
90334 - 4	KN90334	1801	10	0.281484	0.0000215	0.001652	2.95E-05	1.801	0.01	0.281428	4.3E-05	-7.40297	1.455155	2.515478	0.027897	
90334 - 5	KN90334	1801	10	0.281481	0.0000205	0.000917	0.00002	1.801	0.01	0.28145	4.1E-05	-6.61705	1.407212	2.471365	0.026663	
90334 - 6	KN90334	1801	10	0.281511	0.00002	0.001511	1.15E-05	1.801	0.01	0.281459	4E-05	-6.27309	1.392346	2.46866	0.026964	
90334 - 7	KN90334	1801	10	0.281458	0.000022	0.001097	0.000017	1.801	0.01	0.28142	4.4E-05	-7.65227	1.521017	2.514537	0.029	
90334 - 8	KN90334	1801	10	0.281487	0.000018	0.001936	1.05E-05	1.801	0.01	0.281421	3.6E-05	-7.64129	1.252747	2.53041	0.024496	
90334 - 9	KN90334	1801	10	0.281501	0.0000195	0.00174	1.95E-05	1.801	0.01	0.281441	3.9E-05	-6.90621	1.337412	2.497675	0.025874	
90334 - 10	KN90334	1801	10	0.281472	0.000017	0.001246	0.00001	1.801	0.01	0.281429	3.4E-05	-7.33609	1.182948	2.50513	0.022718	
90334 - 11	KN90334	1801	10	0.28147	0.000023	0.001182	7.5E-06	1.801	0.01	0.28143	4.6E-05	-7.32939	1.615101	2.503668	0.03108	
90334 - 12	KN90334	1801	10	0.281461	0.000027	0.001249	0.000034	1.801	0.01	0.281418	5.4E-05	-7.73031	1.834803	2.52046	0.034841	
90334 - 13	KN90334	1801	10	0.281497	0.0000215	0.00142	7.5E-06	1.801	0.01	0.281448	4.3E-05	-6.65969	1.50858	2.482086	0.029225	
90334 - 14	KN90334	1801	10	0.28148	0.0000245	0.000978	0.000014	1.801	0.01	0.281447	4.9E-05	-6.72663	1.705837	2.476668	0.032555	
90336 - 1	KN90336	1785	19	0.281353	0.0000195	0.000517	3.25E-06	1.785	0.019	0.281335	3.9E-05	-11.039	1.376894	2.618496	0.026028	
90336 - 2	KN90336	1785	19	0.281388	0.0000165	0.000737	0.00002	1.785	0.019	0.281363	3.3E-05	-10.0607	1.123554	2.585994	0.021003	
90336 - 3	KN90336	1785	19	0.281374	0.00002	0.000599	8.5E-06	1.785	0.019	0.281354	4E-05	-10.3917	1.399766	2.595679	0.026416	
90336 - 4	KN90336	1785	19	0.281432	0.000019	0.001234	0.000005	1.785	0.019	0.28139	3.8E-05	-9.09644	1.337178	2.559325	0.025758	
90336 - 5	KN90336	1785	19	0.281452	0.0000235	0.001044	0.000017	1.785	0.019	0.281417	4.7E-05	-8.15772	1.627851	2.51926	0.031004	
90336 - 6	KN90336	1785	19	0.281426	0.000023	0.000632	0.000006	1.785	0.019	0.281405	4.6E-05	-8.58515	1.618815	2.527592	0.030709	
90336 - 7	KN90336	1785	19	0.281381	0.0000235	0.000901	1.55E-05	1.785	0.019	0.28135	4.7E-05	-10.5066	1.63146	2.606558	0.030899	
90336 - 8	KN90336	1785	19	0.28146	0.0000205	0.000987	2.65E-05	1.785	0.019	0.281427	4.1E-05	-7.80509	1.391957	2.504582	0.02625	
90336 - 9	KN90336	1785	19	0.281446	0.000017	0.001075	0.000013	1.785	0.019	0.28141	3.4E-05	-8.40805	1.175905	2.529518	0.022397	
90336 - 10	KN90336	1785	19	0.281373	0.0000185	0.000667	0.000009	1.785	0.019	0.28135	3.7E-05	-10.5091	1.292047	2.601597	0.024399	
90336 - 11	KN90336	1785	19	0.281404	0.000025	0.000951	0.000006	1.785	0.019	0.281372	5E-05	-9.75009	1.760837	2.578614	0.033657	
90336 - 12	KN90336	1785	19	0.281344	0.0000205	0.000961	8.5E-06	1.785	0.019	0.281311	4.1E-05	-11.8924	1.435272	2.661027	0.027304	
90336 - 13	KN90336	1785	19	0.281365	0.0000205	0.000856	1.65E-05	1.785	0.019	0.281336	4.1E-05	-11.0205	1.416021	2.625247	0.026703	
90336 - 14	KN90336	1785	19	0.281474	0.0000175	0.001236	0.000025	1.785	0.019	0.281432	3.5E-05	-7.60761	1.182533	2.501721	0.022407	
90336 - 15	KN90336	1785	19	0.281502	0.0000225	0.001375	0.000016	1.785	0.019	0.281455	4.5E-05	-6.7807	1.559246	2.472231	0.030016	

9.3 Appendix C – Whole-rock geochemistry and Sm-Nd isotope data

Appendix C1: Whole-rock major elements

Sample	SiO2 (wt.%)	Al2O3	Fe2O3	TiO2	MgO	CaO	Na2O	K2O	MnO	P2O5	BaO	Cr2O3	CuO	NiO	PbO	SrO	ZnO	V2O5	ZrO2	SO3	Total
90328	48.0	14.2	6.98	0.782	7.02	19.1	1.40	0.388	0.252	0.031	<0.025	<0.02	0.012	0.012	<0.01	0.043	<0.01	0.056	<0.02	0.10	99.0
90329	25.0	14.0	8.58	0.141	2.29	33.1	0.20	0.200	0.174	0.010	<0.025	<0.02	<0.01	<0.01	<0.01	<0.04	<0.01	<0.02	<0.02	<0.1	99.5
90331	52.3	18.8	9.99	1.59	1.72	6.79	5.34	1.16	0.169	0.329	0.175	<0.02	<0.01	<0.01	<0.01	0.088	0.018	<0.02	<0.02	<0.1	98.6
90332	52.8	17.6	10.3	1.30	1.90	6.26	5.24	2.04	0.169	0.450	0.243	<0.02	<0.01	<0.01	<0.01	0.083	0.017	<0.02	0.029	0.18	98.8
90333	48.9	14.5	12.9	2.20	5.43	9.90	3.82	0.589	0.224	0.186	0.031	<0.02	<0.01	0.012	<0.01	<0.04	0.016	0.083	<0.02	<0.1	98.9
90334	61.6	17.6	4.87	0.566	0.360	1.81	5.24	6.90	0.103	0.090	0.137	<0.02	<0.01	<0.01	<0.01	<0.04	<0.01	<0.02	0.148	<0.1	99.1
90335	60.6	17.4	5.33	0.663	0.773	2.32	5.19	5.57	0.132	0.155	0.177	<0.02	<0.01	<0.01	<0.01	<0.04	0.012	<0.02	0.102	<0.1	98.5
90336	68.8	15.0	3.21	0.268	0.398	1.44	3.80	5.59	0.060	0.080	0.172	<0.02	<0.01	<0.01	<0.01	<0.04	<0.01	<0.02	0.046	<0.1	99.0
90337	74.9	11.9	2.47	0.276	0.390	0.896	3.00	4.59	0.036	0.079	0.064	<0.02	<0.01	<0.01	<0.01	<0.04	<0.01	<0.02	0.028	<0.1	98.8
90339	72.1	14.0	1.73	0.210	0.337	0.945	3.61	5.66	0.022	0.044	0.084	<0.02	<0.01	<0.01	<0.01	<0.04	<0.01	<0.02	0.023	<0.1	98.9
90340	69.2	13.6	3.19	0.316	1.28	2.12	3.41	4.95	0.054	0.102	0.082	<0.02	<0.01	<0.01	<0.01	<0.04	<0.01	<0.02	0.030	<0.1	98.6
90341	63.2	13.9	4.93	0.468	3.13	4.58	3.55	4.76	0.085	0.162	0.081	0.024	<0.01	<0.01	<0.01	<0.04	<0.01	<0.02	0.027	<0.1	99.1
90342	67.6	15.1	3.13	0.420	0.473	1.72	3.79	5.78	0.045	0.128	0.152	<0.02	<0.01	<0.01	<0.01	<0.04	<0.01	<0.02	0.038	<0.1	98.4
90343	67.0	15.1	3.65	0.529	0.809	1.98	3.99	5.32	0.076	0.177	0.118	<0.02	<0.01	<0.01	<0.01	<0.04	<0.01	<0.02	0.035	<0.1	99.0
90344	51.1	15.1	13.7	1.98	3.49	6.13	3.60	2.50	0.186	0.468	0.138	<0.02	<0.01	<0.01	<0.01	0.043	0.017	0.045	0.028	<0.1	98.8
90345	49.4	16.3	13.0	1.40	6.40	7.58	2.97	1.38	0.163	0.362	0.086	<0.02	<0.01	<0.01	<0.01	0.057	0.014	0.032	<0.02	<0.1	99.3
140808	68.3	13.75	4.51	0.43	0.46	1.4	3.27	5.38	0.07	0.1	0.14	0.003				0.02					98.24
140809	62.2	17.2	3.75	0.42	0.68	1.53	3.68	8.07	0.09	0.19	0.31	0.005				0.03					98.48
140810	61.3	16.35	5.65	0.89	0.95	2.79	4.56	5.04	0.12	0.23	0.2	0.004				0.03					98.7
140811	52.5	1.52	6.76	0.1	14.65	23.6	0.34	0.23	0.41	0.02	0.01	0.002				<0.01					100.75
140812	50.8	3.08	7.92	0.13	13.15	23.2	0.41	0.14	0.4	0.04	<0.01	0.004				0.01					100.54
140813	56.8	15.45	9.67	0.63	2.56	6.68	4.28	2.94	0.21	0.23	0.1	0.011				0.02					100.02
140814	60.3	17.9	6.82	0.43	1.56	2.36	6.01	3.41	0.07	0.12	0.08	0.002				0.03					99.77
140815	58.9	21.3	3.93	0.18	2.04	6.02	6.17	0.22	0.08	0.1	0.01	0.004				0.04					99.5
140816	65.1	17.25	3.81	0.41	0.36	1.38	5.1	6.56	0.09	0.06	0.09	0.002				0.01					100.67
140817	49.7	13.35	8.01	1.02	5.97	19.2	1.83	0.21	0.24	0.1	0.01	0.013				0.02					100.26
140818	64	16.65	5.11	0.55	0.34	1.62	4.9	6.11	0.15	0.1	0.13	0.003				0.01					99.92
140819	68.9	14.2	3.88	0.46	1.91	3.6	4.33	2.92	0.12	0.13	0.11	0.008				0.06					100.99
140820	58.8	16.3	8.42	1.19	2.09	4.28	4.24	4.02	0.13	0.35	0.15	0.004				0.03					100.48
140821	75.3	13	2.03	0.14	0.27	1.89	5.58	0.37	0.03	0.05	0.02	0.002				0.02					98.88

Sample	SiO2 (wt.%)	Al2O3	Fe2O3	TiO2	MgO	CaO	Na2O	K2O	MnO	P2O5	BaO	Cr2O3	CuO	NiO	PbO	SrO	ZnO	V2O5	ZrO2	SO3	Total
140822	56.4	15.05	7.93	0.75	4.14	6.78	4.38	2.73	0.13	0.28	0.08	0.014				0.06					99.2
140824	48.6	15.25	10.55	0.91	8.57	9.53	3.18	0.58	0.2	0.07	0.02	0.054				<0.01					98.33
140825	53.6	16.25	9.38	1.1	2.58	8.82	4.17	1.94	0.13	0.24	0.07	0.021				0.02					99.14
140826	77.5	12.35	2.2	0.25	0.23	2.11	4.61	0.67	0.03	<0.01	0.02	0.002				0.02					100.5
140827	73.7	13.75	2.18	0.24	0.38	1	3.22	5.34	0.04	0.02	0.08	0.004				0.02					100.55
140828	71.3	14.3	3.22	0.36	0.54	1.42	3.29	5.34	0.04	0.09	0.11	0.002				0.02					100.78
140829	49.1	13.35	16.3	1.37	7.11	8.84	2.98	1.08	0.3	0.13	0.02	0.016				0.01					101.24
140831	63.8	15.1	5.88	0.64	2.32	3.91	3.5	4.23	0.09	0.24	0.11	0.014				0.04					100.62
140832	67.9	15.55	3.74	0.49	0.41	1.47	4.05	6.06	0.08	0.07	0.12	0.002				0.02					100.28
140833	64.2	17.1	5.92	1	1.32	4.06	6	1.32	0.17	0.31	0.03	0.003				0.04					101.99
140834	96.5	0.43	1.43	0.01	0.74	1.17	0.09	0.05	0.05	<0.01	<0.01	0.006				<0.01					100.62
140835	46.5	13.9	13.5	0.9	10.25	11.25	2.03	0.31	0.19	0.04	0.02	0.021				0.02					100.19
140838	60.2	17.95	6.33	0.79	0.79	2.79	4.82	5.71	0.13	0.17	0.23	<0.002				0.04					100.25

Appendix 2C: Whole-rock trace elements

Sample	Ag (ppm)	As	Ba	Cd	Ce	Co	Cr	Cu	Ga	La	Mo	Nb	Nd	Ni	Pb	Rb	Sb	Sc	Sn	Sr	Th	U	V	Y	Zn	Zr	Cl	F
90328	<10	<10	231	<10	<15	21.2	125	88.0	16.1	<15	<3	<5	<10	85.3	5.1	7.2	<15	40.1	<5	353	<3	<5	274	12.3	82.3	33.2	<0.02	<0.2
90329	<10	<10	37	<10	<15	<4	6.6	<5	14.3	<15	<3	<5	<10	<5	9.0	<5	<15	<5	<5	66.7	<3	<5	19.6	8.9	48.8	54.7	<0.02	<0.2
90331	<10	<10	1660	<10	39	17.0	28.9	44.4	26.6	26	<3	6.4	23	13.1	8.2	<5	<15	24.1	<5	743	<3	<5	106	20.6	142	82.9	<0.02	<0.2
90332	<10	<10	2170	<10	59	13.3	24.9	24.3	25.1	30	<3	6.9	28	8.1	8.1	14.2	<15	20.7	<5	664	<3	<5	77.7	25.7	124	183	0.042	<0.2
90333	<10	<10	286	<10	17	60.7	90.2	<5	18.7	<15	<3	8.0	15	87.7	<5	<5	<15	43.9	<5	239	<3	<5	448	28.2	128	75.5	0.060	<0.2
90334	<10	<10	1130	<10	23	<4	13.8	<5	22.4	<15	3.4	7.7	15	<5	11.4	58.2	<15	8.7	<5	147	<3	<5	13.8	17.4	43.9	864	<0.02	<0.2
90335	<10	<10	1550	<10	50	4.5	9.6	<5	22.1	25	3.4	13.6	21	6.3	16.1	50.5	<15	7.4	<5	268	<3	<5	23.9	21.2	91.2	557	<0.02	<0.2
90336	<10	<10	1450	<10	173	<4	<5	<5	23.0	104	<3	27.1	62	5.1	28.8	205	<15	6.0	<5	181	21.4	<5	<5	44.3	58.4	307	<0.02	<0.2
90337	<10	<10	503	<10	140	<4	39.7	<5	17.5	82	<3	15.6	54	<5	18.8	191	<15	<5	<5	123	37.6	6.0	14.7	20.2	33.0	194	<0.02	<0.2
90339	<10	<10	705	<10	83	<4	8.0	<5	17.5	45	<3	8.6	30	<5	16.5	229	<15	<5	<5	151	21.7	<5	11.4	6.6	14.7	169	<0.02	<0.2
90340	<10	<10	701	<10	138	7.0	57.8	5.4	18.1	84	<3	17.9	47	15.8	20.4	180	<15	6.9	<5	160	28.3	<5	31.5	22.5	35.0	219	<0.02	<0.2
90341	<10	<10	725	<10	102	12.9	162	15.6	17.4	52	3.2	15.1	42	34.8	19.9	139	<15	11.6	<5	238	22.0	<5	69.9	20.4	48.2	167	<0.02	<0.2
90342	<10	<10	1300	<10	127	<4	48.9	<5	19.3	72	6.9	16.8	36	5.8	18.5	174	<15	6.8	<5	207	18.8	<5	18.5	22.9	40.3	274	<0.02	<0.2
90343	<10	<10	1020	<10	96	7.8	7.0	5.1	21.0	39	<3	39.9	68	7.9	19.2	236	<15	8.6	<5	183	20.5	5.2	29.6	75.4	38.6	232	<0.02	<0.2
90344	<10	<10	1320	<10	80	39.8	12.0	11.4	22.6	32	<3	12.0	25	9.4	9.6	47.5	<15	30.3	<5	365	<3	<5	240	31.6	137	182	0.073	<0.2
90345	<10	<10	835	<10	53	47.7	44.5	23.1	20.2	25	<3	8.1	25	57.6	8.6	28.1	<15	25.1	<5	467	<3	<5	169	23.3	114	121	0.024	<0.2
140808							<10		27.8							149.5			2	205			12					
140809							20		22.4							126			1	319			36					
140810							10		25.5							80.5			1	296			27					
140811							<10		6.1							18.2			5	41			61					
140812							20		11.1							8.2			12	132.5			62					
140813							60		18.6							59.8			1	182.5			122					
140814							<10		20.4							86.6			1	263			48					
140815							10		26.1							4.7			<1	402			32					
140816							<10		26.6							95.4			1	80.7			<5					
140817							80		17.2							3.3			1	202			324					
140818							<10		23							63			1	80			<5					
140819							40		17							66.8			<1	472			61					
140820							10		23.7							92.4			2	289			112					

Sample	Ag (ppm)	As	Ba	Cd	Ce	Co	Cr	Cu	Ga	La	Mo	Nb	Nd	Ni	Pb	Rb	Sb	Sc	Sn	Sr	Th	U	V	Y	Zn	Zr	Cl	F
140821						<10		20.5								11.7			2	250			11					
140822						80		19.4								95.2			1	482			160					
140824						400		16.5								21.7			<1	128.5			292					
140825						140		22.1								46.4			2	234			219					
140826						<10		22.1								19.7			1	141.5			<5					
140827						10		20.7								194			3	128.5			10					
140828						<10		21.3								255			5	163			25					
140829						100		19.3								40.1			1	107.5			377					
140831						80		20.5								173			3	292			86					
140832						<10		22.1								96.1			1	139.5			8					
140833						10		25.9								48.7			1	297			39					
140834						30		2.3								2.4			<1	5.6			41					
140835						140		16.2								4.5			<1	174.5			364					
140838						<10		25.1								56.4			<1	300			17					

Sample	S	Hf	Be	Y	Zr	Nb	Cs	Ba	La	Ce	Pr	Nd	Sm	Eu	Gd	Tb	Dy	Ho	Er	Tm	Yb	Lu	Hf	Ta	W	Bi	Th	U
90328	0.12	<5	<1	11.0	32.6	1.33	<0.4	220	3.24	8.43	1.36	6.62	1.96	0.964	2.13	0.399	2.18	0.452	1.30	0.176	1.17	0.187	1.24	0.143	0.24	<0.5	0.153	0.167
90329	<0.1	5.5	<1	6.16	44.5	2.51	<0.4	44.9	0.56	1.22	0.201	1.27	0.88	0.614	0.98	0.178	1.01	0.192	0.493	0.066	0.37	0.051	1.80	0.222	<0.2	1.04	0.046	1.35
90331	<0.1	<5	<1	22.1	122	5.17	<0.4	1790	31.0	55.7	7.45	33.1	6.84	4.82	5.70	0.878	4.49	0.883	2.37	0.305	1.78	0.272	2.64	0.238	<0.2	<0.5	0.424	0.150
90332	<0.1	6.0	<1	30.5	267	4.13	0.53	2470	46.5	81.1	10.6	46.0	9.48	5.12	7.97	1.20	5.71	1.09	2.97	0.366	2.16	0.323	5.05	0.186	<0.2	<0.5	0.627	0.190
90333	<0.1	<5	<1	23.3	72.6	7.26	<0.4	311	7.27	16.8	2.55	13.4	4.22	1.49	4.27	0.778	4.49	0.892	2.56	0.341	2.25	0.320	2.04	0.451	0.63	<0.5	0.102	0.082
90334	<0.1	17.7	<1	15.8	1160	7.06	<0.4	1280	19.2	38.4	5.00	22.5	4.84	2.24	3.93	0.609	3.20	0.656	1.99	0.300	2.12	0.358	21.6	0.245	0.25	<0.5	0.956	0.875
90335	<0.1	10.7	<1	21.3	842	12.0	0.44	1800	35.9	68.9	8.91	37.2	7.36	2.51	5.78	0.875	4.45	0.884	2.62	0.373	2.40	0.393	16.5	0.371	<0.2	<0.5	1.63	0.809
90336	<0.1	7.6	5.2	46.2	375	28.8	1.25	1620	122	230	24.8	88.6	15.4	3.20	11.1	1.76	9.13	1.85	5.41	0.803	5.07	0.748	9.70	1.20	0.34	<0.5	23.0	2.04
90337	<0.1	<5	2.3	13.4	152	15.7	1.50	429	50.8	109	9.86	31.2	4.89	0.524	3.25	0.422	2.34	0.496	1.49	0.236	1.59	0.237	4.59	0.754	0.38	<0.5	27.3	3.19
90339	<0.1	6.9	2.5	5.12	118	7.40	1.38	567	25.1	59.2	5.00	15.6	2.12	0.381	1.24	0.146	0.76	0.171	0.554	0.097	0.72	0.122	3.40	0.566	0.24	<0.5	14.1	2.42
90340	<0.1	<5	2.9	20.0	210	18.0	0.99	707	69.0	148	13.9	47.1	7.52	0.963	4.81	0.686	3.68	0.712	1.98	0.294	2.05	0.324	5.82	1.25	0.22	<0.5	25.4	2.99
90341	<0.1	6.9	2.7	23.0	226	17.3	0.75	798	67.6	132	13.8	49.0	7.97	1.25	5.47	0.763	4.13	0.831	2.34	0.336	2.23	0.329	5.95	0.998	<0.2	<0.5	23.5	3.36
90342	<0.1	7.7	2.6	21.3	284	16.7	0.97	1350	77.7	163	16.2	54.3	8.25	1.46	5.53	0.788	4.04	0.759	2.09	0.295	1.73	0.275	6.18	0.665	<0.2	<0.5	17.9	2.09
90343	<0.1	5.4	4.4	81.5	288	45.6	2.26	1150	41.5	118	16.1	73.0	19.6	1.14	16.7	2.75	15.4	3.18	8.42	1.14	7.02	0.909	7.61	4.27	0.24	<0.5	21.6	5.24
90344	<0.1	<5	1.0	28.0	188	10.8	0.89	1360	32.3	72.0	8.10	34.2	7.11	2.80	5.99	0.917	5.30	1.10	2.93	0.410	2.59	0.380	4.32	0.450	0.98	<0.5	1.48	0.400
90345	<0.1	<5	<1	18.9	119	7.40	0.41	803	24.0	53.8	5.93	25.4	5.07	1.81	4.35	0.674	3.60	0.740	2.04	0.288	1.83	0.274	3.14	0.318	<0.2	<0.5	1.88	0.387
140808				46	410	21.3	0.68	1285	1040	1820	172	513	49	3	22.9	2.47	11.15	1.95	4.75	0.66	3.79	0.6	11.5	0.8	1		110	2.36
140809				18.8	309	5.8	0.75	2960	33.4	65	8.24	34.4	6.59	3.24	5.4	0.74	3.7	0.73	1.99	0.28	1.71	0.25	7.6	0.2	1		1.65	0.77
140810				30.7	769	17.5	0.66	1870	46.4	91.9	11.55	47.4	9.38	2.71	7.71	1.16	6.1	1.21	3.2	0.48	3.04	0.47	17.9	0.7	1		4.67	1.59
140811				14.9	23	3.9	0.26	63.7	11.8	29.9	3.96	16	3.21	0.45	2.68	0.45	2.37	0.51	1.52	0.26	1.9	0.31	0.7	0.1	1		3.24	1.03
140812				25.2	59	9.7	0.18	47.2	15	34.7	4.44	17.2	3.68	0.56	3.49	0.54	3.59	0.8	2.48	0.45	3.48	0.59	1.8	0.5	1		8.98	2.55
140813				14.7	93	5.8	0.41	900	20.8	40.9	4.89	18.6	3.37	1.08	3.21	0.47	2.63	0.54	1.51	0.22	1.37	0.22	2.5	0.1	1		0.52	0.5
140814				8.4	128	19.1	1.66	734	21.3	37.9	4	13.9	2.19	0.84	1.87	0.28	1.43	0.35	0.91	0.16	1.15	0.19	3.4	0.6	<1		7.12	1
140815				7.2	77	3.1	0.17	109	20.3	33.4	3.47	12.1	1.93	1.83	1.57	0.23	1.26	0.28	0.77	0.12	0.79	0.12	2.1	0.1	1		2.56	0.49
140816				20.3	868	7.1	0.31	804	28.7	56.2	7.02	28.2	5.45	1.85	4.39	0.66	3.63	0.75	2.18	0.34	2.25	0.41	18.4	0.3	<1		2.64	1.19
140817				18.6	67	4.3	0.15	48.3	7.8	18.7	2.64	11.8	2.97	1.13	3.61	0.56	3.58	0.79	2.11	0.33	1.83	0.27	1.7	0.2	<1		0.69	0.55
140818				21.3	1440	12.7	0.53	1145	27.9	57.1	7.13	30.5	6.04	2.38	5.19	0.77	4.26	0.84	2.39	0.38	2.4	0.44	26.6	0.5	1		4.33	1.14
140819				21.2	214	10.3	0.86	961	32.9	65.4	7.77	29.7	5.55	0.99	4.69	0.73	3.85	0.81	2.18	0.37	2.28	0.35	6.1	0.7	1		2.68	2.07
140820				31.7	431	19.3	1.32	1400	53.2	109.5	13.25	54.1	9.29	2.23	8.39	1.13	6.37	1.25	3.4	0.49	2.91	0.45	10.7	0.6	1		3.13	0.91
140821				15.9	76	21.2	0.12	184.5	21.3	47.4	5.5	20.3	4.56	0.31	3.98	0.67	3.67	0.72	1.74	0.26	1.68	0.24	3.4	0.9	1		44.6	3.58
140822				17.4	153	10.6	0.42	732	47.7	94.7	10.6	38.2	6.35	1.26	4.48	0.64	3.43	0.69	1.91	0.27	1.81	0.28	4.2	0.4	1		14.8	2.49
140824				16.9	47	2.7	0.72	209	2.6	7.2	1.15	6.1	2.1	0.66	2.49	0.45	3.1	0.65	1.81	0.27	1.79	0.28	1.4	<0.1	2		0.31	0.21
140825				28.2	121	13	0.2	690	33.2	76.2	9.21	36.1	6.74	1.87	5.92	0.93	5.11	1.05	2.98	0.49	2.85	0.41	3.6	0.6	1		5.19	1.99

Sample	S	Hf	Be	Y	Zr	Nb	Cs	Ba	La	Ce	Pr	Nd	Sm	Eu	Gd	Tb	Dy	Ho	Er	Tm	Yb	Lu	Hf	Ta	W	Bi	Th	U
140826				23	417	23.4	0.27	150	70.7	141	14.45	50.9	8.23	0.3	5.21	0.75	4.14	0.89	2.47	0.39	2.6	0.42	10.9	1.3	<1		24	4.16
140827				22.3	249	17.8	0.49	718	66.7	134	14.05	47.2	8.05	0.83	5.54	0.74	4.09	0.78	2.39	0.39	2.42	0.36	7.3	1.3	1		34.6	3.57
140828				22.7	343	19.3	1.93	993	39.9	105.5	9.04	33.2	6.58	1.01	5.1	0.71	4.09	0.77	2.43	0.37	2.44	0.4	9.4	1.2	<1		23.4	3.07
140829				23.5	65	4.9	1.26	218	5.3	13.7	1.92	9.2	2.87	1.08	3.63	0.66	4.47	0.95	2.65	0.41	2.57	0.41	2	0.2	<1		0.4	0.29
140831				21.9	265	16.7	1.19	930	56.4	113.5	12.6	45.1	7.69	1.28	5.49	0.71	4.04	0.83	2.28	0.37	2.3	0.4	7.2	0.9	<1		17.1	3.19
140832				18.6	664	9.7	0.58	1015	39.8	77.1	8.67	35.3	6.15	1.74	4.83	0.61	3.43	0.72	1.95	0.3	2.06	0.35	15.1	0.4	<1		3.42	1.12
140833				40.4	522	31.4	0.92	270	87.4	167.5	18	67.7	12.55	2.12	9.69	1.37	7.95	1.52	4.28	0.65	4.33	0.72	12	1.6	<1		11.85	2.2
140834				0.7	13	0.3	0.04	9.2	0.7	1.2	0.14	0.5	0.09	<0.03	0.09	0.02	0.08	0.02	0.06	0.02	0.07	0.01	<0.2	<0.1	<1		0.07	0.18
140835				10.6	14	0.7	0.27	134.5	2.4	6	0.94	4.7	1.46	0.83	2.04	0.34	2.18	0.44	1.14	0.18	0.95	0.15	0.5	<0.1	<1		0.08	<0.05
140838				18.8	747	5.6	0.37	2100	29.3	57.4	7.37	31.9	6.49	3.11	5.37	0.66	3.78	0.76	2.01	0.29	1.96	0.34	15.5	0.2	<1		1.14	0.65

Appendix B2 : Sm-Nd isotope data

Sample	Age (Ma)	Rock unit	Sm(ppm)	Nd(ppm)	147Sm/144Nd	143Nd/144Nd	±2s	εNd(t)	e^(lt)-1	Rock (t)	CHUR(t)	Rock(t)/ CHUR(t)	-1	TDM Ga	Two-stage model
90332	1800	Diorite/Gabbro	9.48	46.00	0.124556	0.511411	0.000009	-7.30	0.011842	0.509936	0.510309	0.999270	-0.000730	2649	2611
90335	1800	Granite	7.36	37.20	0.119575	0.511333	0.000009	-7.68	0.011842	0.509917	0.510309	0.999232	-0.000768	2636	2639
90336	1800	Granite	15.40	88.60	0.105045	0.511152	0.000010	-7.85	0.011842	0.509908	0.510309	0.999215	-0.000785	2544	2653
90339	1800	Granite	2.12	15.60	0.082123	0.510835	0.000008	-8.74	0.011842	0.509863	0.510309	0.999126	-0.000874	2471	2720
90341	1800	Granite	7.97	49.00	0.098297	0.511086	0.000009	-7.58	0.011842	0.509922	0.510309	0.999242	-0.000758	2486	2632
90342	1800	Granite	8.25	54.30	0.091818	0.511027	0.000009	-7.23	0.011842	0.509940	0.510309	0.999277	-0.000723	2432	2606
90345	1800	Gabbro	5.07	25.40	0.120640	0.511439	0.000008	-5.85	0.011842	0.510010	0.510309	0.999415	-0.000585	2506	2502

9.4 Appendix D - Petrographic descriptions

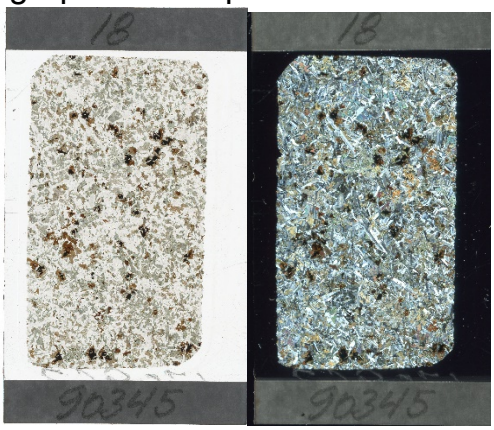

Sample: 90345 (meta-gabbro)

Hand specimen:

Massive, fine-grained gabbro. Mainly dark grey in colour, with white plagioclase and brown pyroxene crystals.

Minerals:

Plagioclase (50%), clinopyroxene (35%), biotite (10%) and oxides (5%). Accessory minerals are garnet and apatite.

Petrographic description:

This sample shows a coarse-grained igneous rock. The plagioclase and clinopyroxene both show sub- to anhedral grains and form an ophitic texture, where large pyroxene grains enclose small random oriented plagioclase laths. Based on the inclusion relationship it is evident that the plagioclase must have crystallized before the clinopyroxene. The clinopyroxene grains also show exsolution lamellae, indicating an unmixing of a solid solution phase to form two separate phases in solid state. The oxides appear sub to anhedral and is observed as inclusions in the pyroxene grains- often rimmed by biotite. The sample can be described as a coarse-grained, inhomogeneous, massive mafic rock.

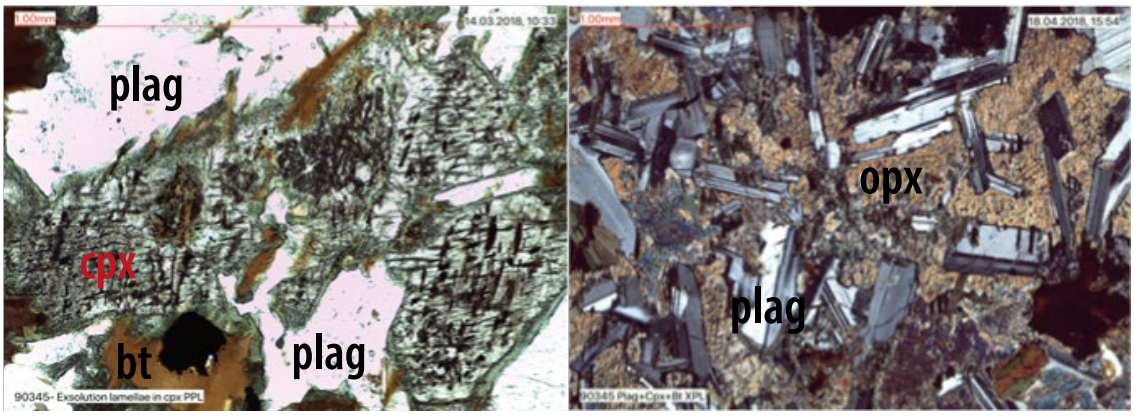

The first microphotograph (PPL) show exsolution lamellae in a clinopyroxene grain. The second microphotograph (XPL) shows the ophitic texture formed by plagioclase and pyroxene.

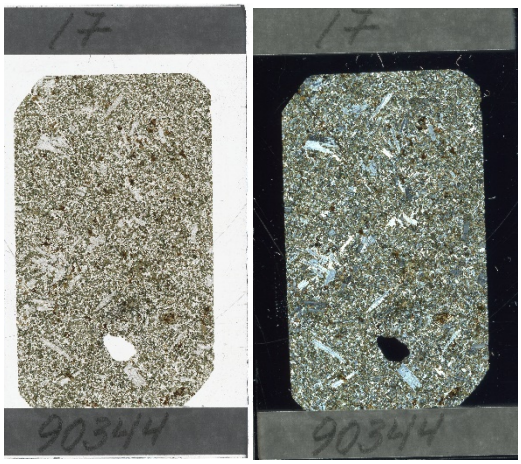

Sample: 90344 (amphibolite)

Hand specimen:

Fine-grained, massive amphibolite. Black in colour, rich in amphibole and plagioclase.

Minerals:

Hornblende (55%), plagioclase (40%) and biotite (5%). Accessory minerals are epidote, apatite, titanite and oxides.

Petrographic description:

This sample is a fine- to medium-grained rock. The feldspar is subhedral and sodium-rich, showing alteration processes (saussuritization) forming euhedral grains of epidote. Some of the feldspar crystals also appear with internal zoning. The hornblende is sub- to anhedral in shape and appears with a deep green colour, resulting from a high-Al content. Some of the hornblende grains show uralite texture, resulting from a reaction where pyroxene form hornblende. The biotite is again found together with the oxides and often appear as glomerocrysts together with hornblende. Oxides are found with rimming of biotite, but also with rimming of radial growing titanite. This rim texture is interpreted to have formed by metamorphic processes.

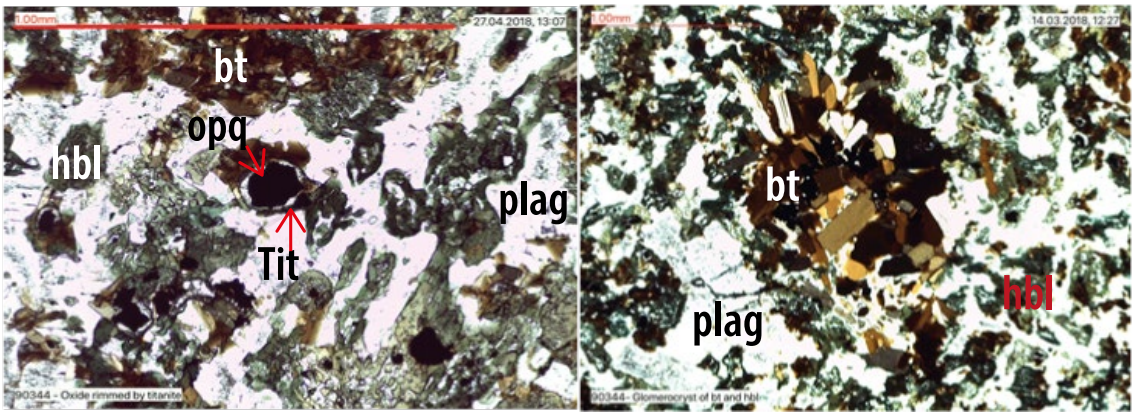

The first microphotograph (PPL) shows an oxide crystal with a rim of radial growing titanite. The second microphotograph (PPL) shows a glomerocrysts of biotite.

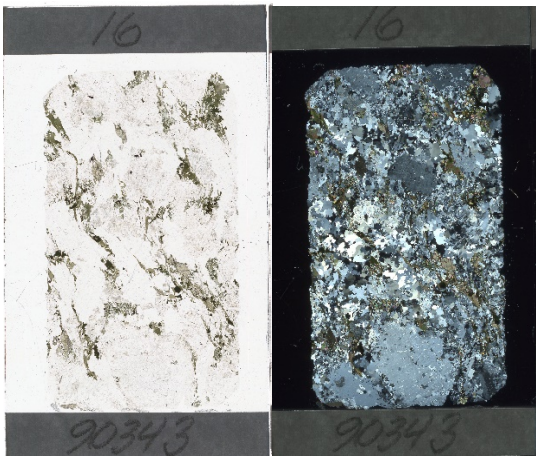

Sample: 90343 (granite)

Hand specimen:

Coarse-grained, non-foliated granitic rock. Light grey colour showing phenocrysts of feldspar crystals, with black mafic minerals.

Minerals:

Quartz (55%), microcline (25%) and biotite (10%), muscovite (5%) and orthoclase (5%). Accessory minerals are epidote and titanite.

Petrographic description:

The anhedral coarse-grained quartz grains shows grain boundaries with textures suggesting some deformation, features of bulging can be observed. The feldspar is presented both as phenocrysts (perthitic orthoclase and microcline) and part of a groundmass (plagioclase and microcline). Some of the plagioclase grains are heavily altered by saussuritization, forming epidote crystals. The epidote crystals are also found as inclusions in the clusters formed by biotite. The biotite shows a mineral alignment that in some cases can be described as a weak foliation and sometimes terminates into larger clusters of tabular grains. The accessory titanite appears in various sizes and is sometimes seen with polygonal twinning.

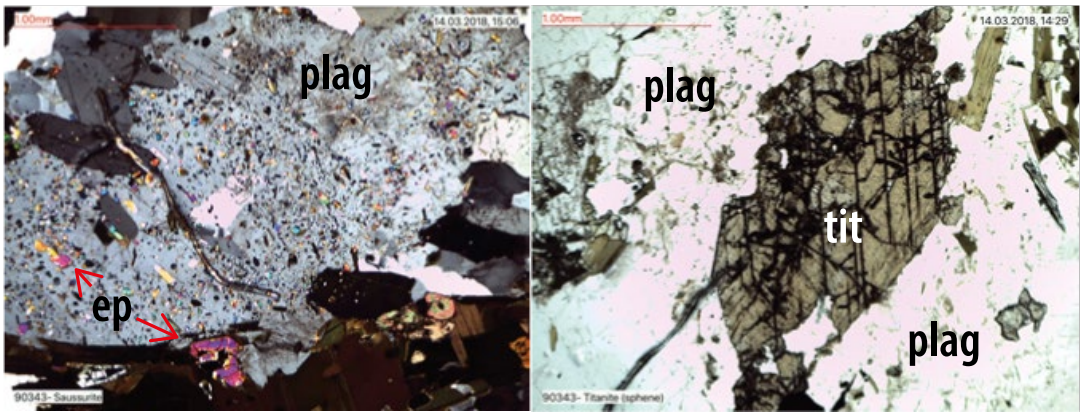

The first microphotograph (XPL) shows saussuritization of a feldspar grain. The second microphotograph (PPL) shows a titanite grain with twinning.

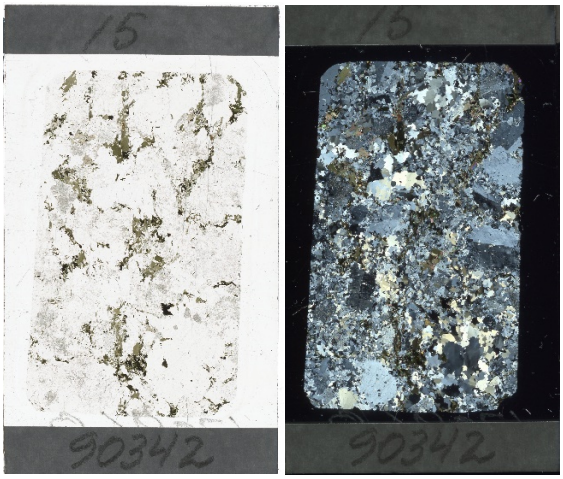

Sample: 90342 (granite)

Hand specimen:

Coarse-grained, non-foliated granitic rock. Light grey colour showing phenocrysts of feldspar crystals, with black mafic minerals.

Minerals:

Quartz (40%), biotite (20%), microcline (15%), plagioclase (10%) and epidote (5%). Accessory mineral is allanite.

Petrographic description:

This sample is very similar to samples 90343. Plagioclase grains appear with saussuritization forming the alteration product of epidote. The sample lacks amphibole, but shows non-foliated, coarse grains of biotite. The most interesting observation in this sample is the appearance of allanite. This mineral is often found in metamorphic felsic rocks. The coarse-grained elongated allanite show a weak zonation but appear mostly as metamict. The allanite is also observed with a rim of very fine-grained epidote. The sample can be described as a coarse-grained, non-foliated, granitic rock.

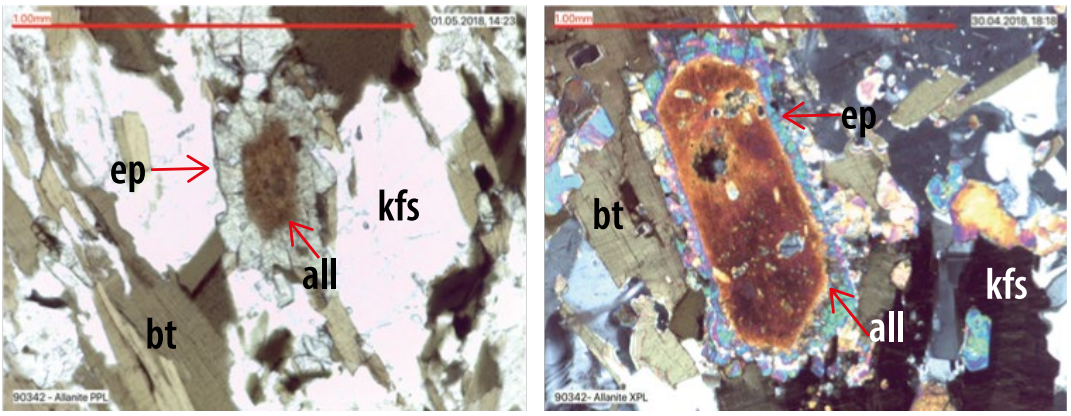

The first microphotograph (PPL) shows an allanite grain with a rim of epidote. The second microphotograph (XPL) shows the same picture in XPL.

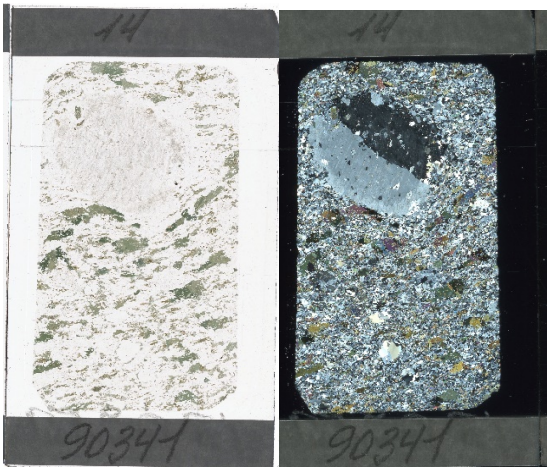

Sample: 90341 (granite)

Hand specimen:

Porphyritic rock with phenocrysts of feldspar grains. Appear with a dark grey colour with phenocrysts of feldspar in a fine-grained matrix.

Minerals:

Quartz (40%), orthoclase (40%) and hornblende (20%). Accessory minerals are epidote, apatite, titanite and allanite.

Petrographic description:

This sample shows a striking porphyritic texture, where large phenocrysts of k-feldspar (orthoclase) are found in a matrix with medium to fine-grained crystals of quartz and hornblende. The orthoclase shows perfect Carlsbad twinning, with alteration processes giving the k-feldspar a dusty appearance. The sub- to anhedral hornblende grains show a deep green colour and show a high frequency of inclusions of both apatite, epidote and quartz. Subhedral, prismatic grains of allanite is observed also in this thin-section. The allanite has a brown colour and show no internal textures. Fragmental coarse-grained titanite is also observed.

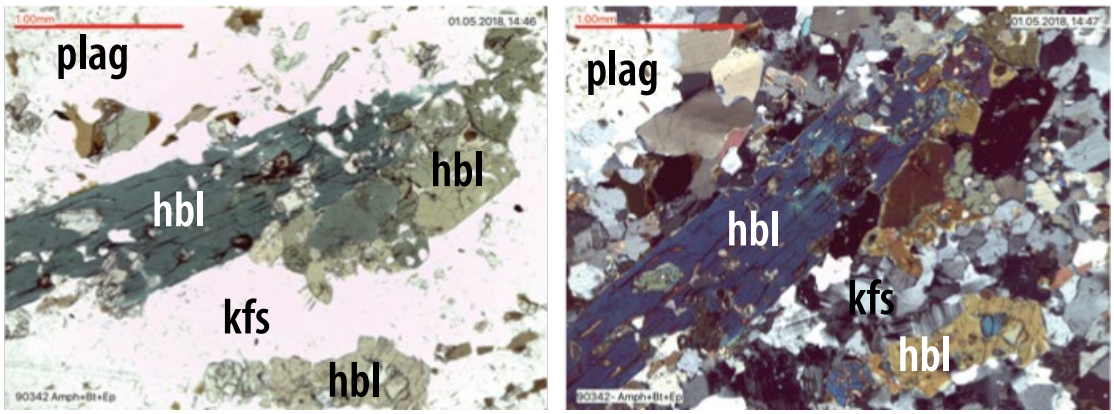

The first microphotograph (PPL) shows a large grain of hornblende with zircon inclusions. The second microphotograph shows the same grain in XPL.

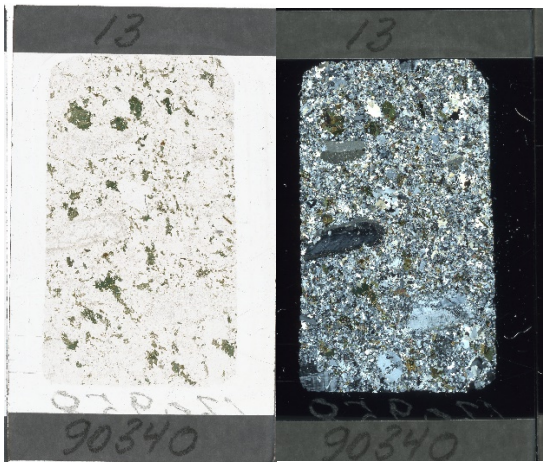

Sample: 90340 (granite)

Hand specimen:

Fine-grained inequigranular porphyritic rock, that shows a light grey colour in field. Phenocrysts of feldspar in a finer-grained matrix. Clusters of amphibole.

Minerals:

Quartz (40%), orthoclase (20%), hornblende (20%), biotite (10%) and microcline (10%). Accessory minerals are epidote, allanite, titanite and muscovite.

Petrographic description:

This sample shows a porphyritic texture with phenocrysts of perthitic orthoclase, with some of the feldspar grains showing zonation with a core rich in K. The rims of the orthoclase grains are altered and shows formation of very fine-grained needles of epidote. Very metamict grain of allanite shows the same rims of epidote. Hornblende appear with a dark green colour and anhedral grains forming glomerocrysts. Neither the hornblende or biotite grains show any orientation. The titanite grains in this sample show an euhedral shape, looking like diamonds.

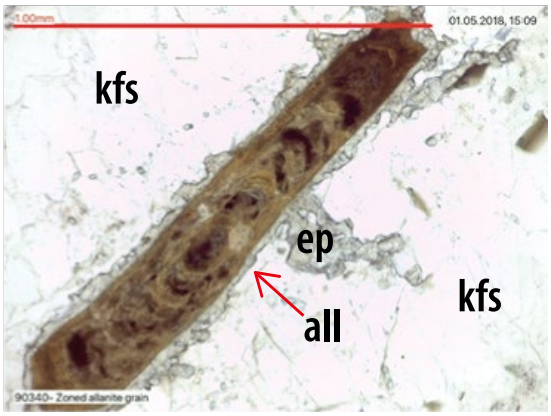

The microphotograph (PPL) shows a concentric zoning in an allanite grain.

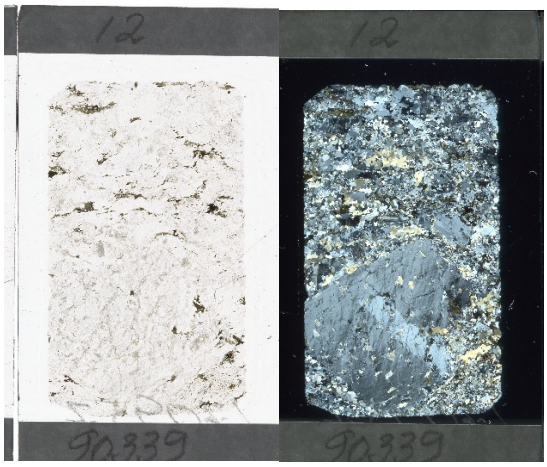

Sample: 90339 (granite)

Hand specimen:

Porphyritic rock with phenocrysts of feldspar grains. Appear with a dark grey colour with phenocrysts of feldspar in a fine-grained matrix.

Minerals:

Quartz (40%), microcline and orthoclase (40%), plagioclase (10%) and biotite (10%). Accessory minerals are epidote and iron oxides.

Petrographic description:

This sample shows phenocrysts of orthoclase with characteristic Carlsbad twinning. The matrix is rich in coarse-grained anhedral quartz, anhedral smaller grains of both orthoclase and microcline. The biotite found in thin-section show a random orientation, interstitial with the feldspar grains. Alteration of the feldspar grains gives a dusty look in ppl and forms fine-grained epidote.

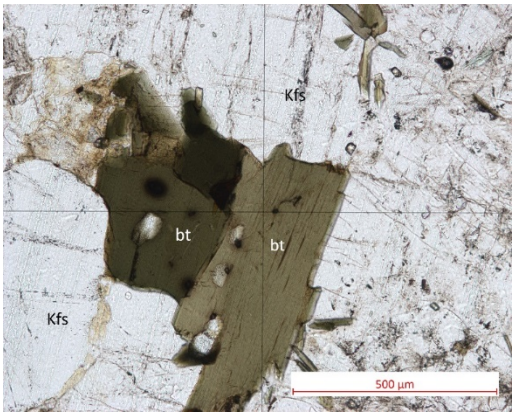

Microphotograph (PPL) showing a biotite grain with zircon inclusions, the zircon shows dark haloes.

Sample: 90338 (granite)

Hand specimen:

Porphyritic rock with phenocrysts of feldspar grains. Appear with a dark grey colour with phenocrysts of feldspar in a fine-grained matrix.

Minerals:

Quartz (40%), microcline and orthoclase (40%), plagioclase (10%) and biotite (10%). Accessory minerals are epidote and iron oxides.

Petrographic description:

This sample shows an inequigranular, non-foliated rock. The phenocrysts of k-feldspar and plagioclase all show alteration. The plagioclase grains show saussuritization forming nice, euhedral grains of epidote. The biotite found in this sample are coarse-grained, anhedral and randomly oriented, with possibly inclusions of zircon showing black haloes in the grains.

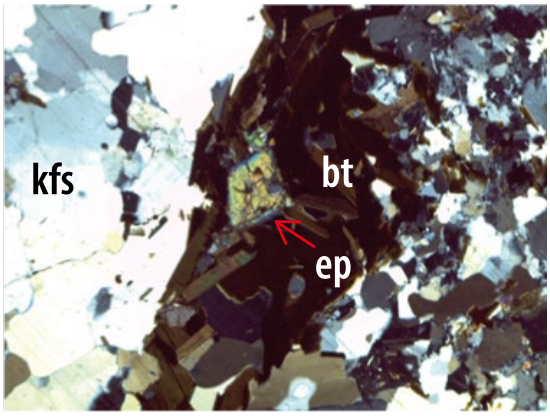

Microphotograph (XPL) showing a nice growing euhedral crystal of epidote in a mush of biotite.

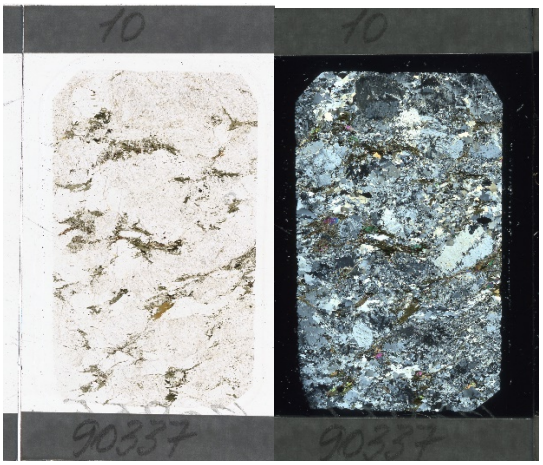

Sample: 90337 (granite)

Hand specimen:

Porphyritic rock with phenocrysts of feldspar grains. Appear with a dark grey colour with phenocrysts of feldspar in a fine-grained matrix.

Minerals:

Quartz (40%), microcline and orthoclase (40%), plagioclase (10%) and biotite (10%). Accessory minerals are epidote, muscovite and iron oxides.

Petrographic description:

This sample shows a highly deformed rock with phenocrysts of orthoclase and plagioclase. The rock shows a foliated texture formed by biotite grains. Muscovite grains are observed with an orientation sometimes parallel to the biotite grains but most often oblique, interpreted to be pre-tectonic. The sample shows veins of quartz with bulging texture, suggesting deformation.

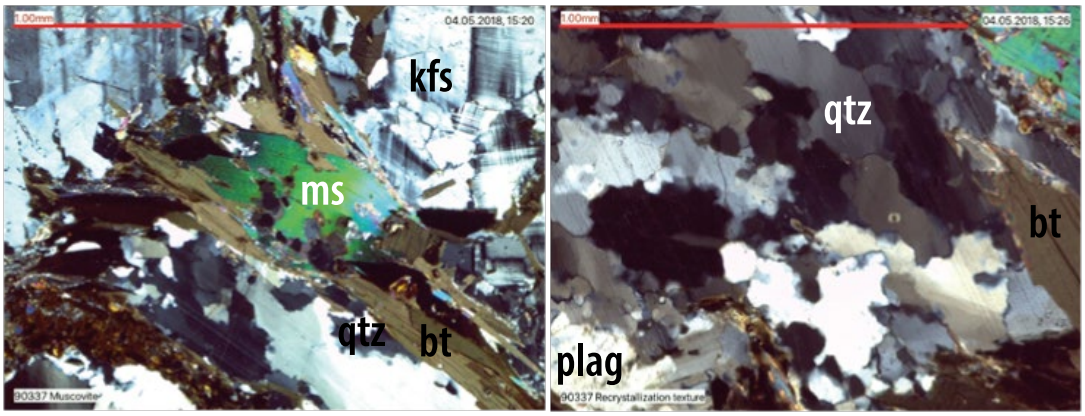

The first microphotograph (XPL) shows a flaky grain of muscovite. The second microphotograph (XPL) shows recrystallization growing quartz.

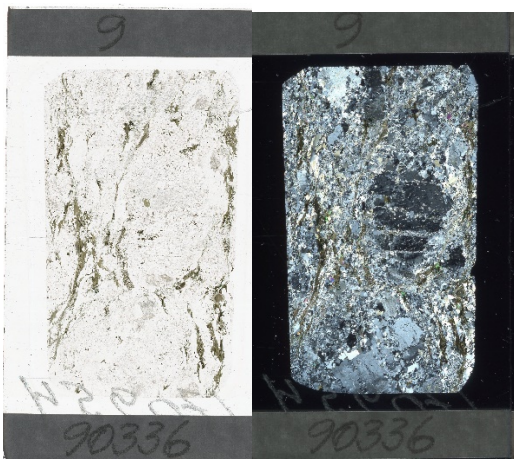

Sample: 90336 (granite)

Hand specimen:

Porphyritic granitic rock, with a deformation texture giving it an "eye" texture. Light grey colour with pink phenocrysts of k-feldspar.

Minerals:

Microcline and orthoclase (55%), quartz (25%) and biotite (20%). Accessory minerals are epidote, muscovite and allanite.

Petrographic description:

This is a coarse-grained sample with large phenocrysts of orthoclase. The matrix consists of coarse-grained microcline, quartz and biotite. Where the biotite is aligned, forming an interstitial texture with the k-feldspar. The few grains of allanite observed in this thin section appear as inclusions in the biotite grains. Subhedral grains of flaky muscovite is observed growing oblique to the orientation of the biotite. The sample show an overall deformed texture, and most of the feldspar grains are altered by saussuritization forming fine-grained epidote.

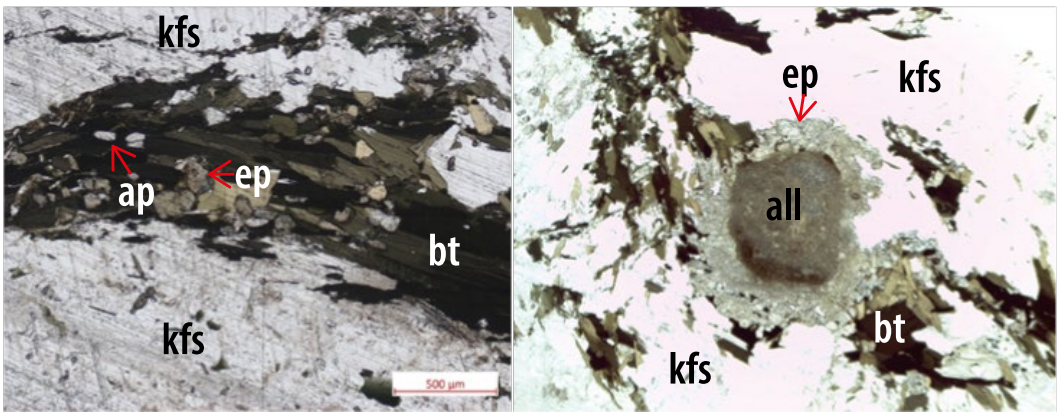

The first microphotograph (PPL) shows aligned grains of green-coloured biotite grains, with inclusions of epidote. The second microphotograph (PPL) shows an allanite grain with a rim of epidote.

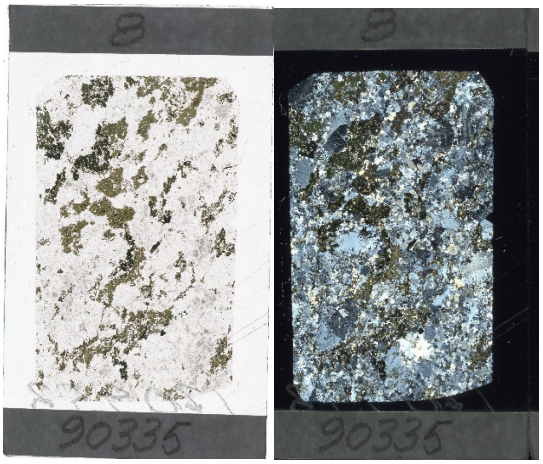

Sample: 90335 (granite)

Hand specimen:

Coarse-grained, inequigranular rock. It shows a light-grey colour with pink k-feldspar and grey quartz grains, with dark mafic minerals.

Minerals:

Microcline and orthoclase (50%), hornblende (40%) and quartz (10%). Accessory minerals are epidote, titanite and garnet.

Petrographic description:

This is a coarse-grained, highly deformed sample. It shows large an- to subhedral grains of orthoclase that are highly altered. Some of the orthoclase grains show perthitic textures. The hornblende makes up almost half of the sample with subhedral deep green coloured grains that shows random orientation and clustering. Quartz and fragmented titanite grains are found as inclusions mainly in the hornblende. The accessory fine-grained epidote grains are observed in the altered feldspar grains. Euhedral, fine-grained crystals of garnet appear as an accessory mineral.

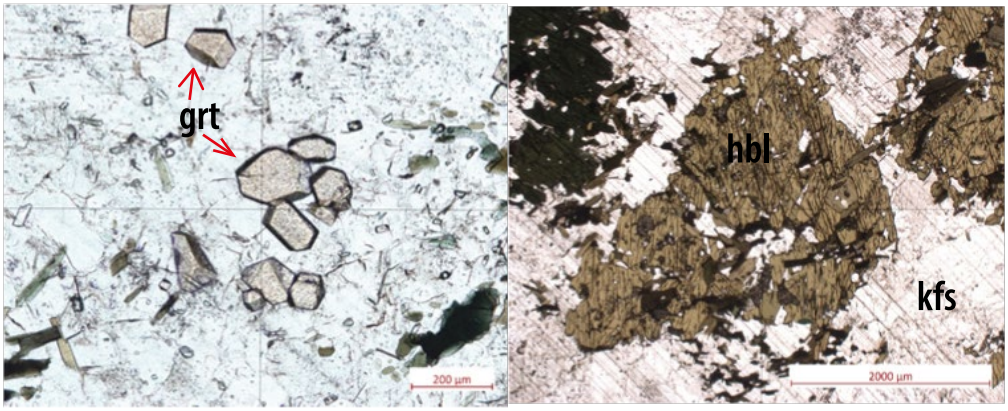

The first microphotograph (PPL) microphotograph shows euhedral, pink garnet crystals. The second microphotograph (PPL) shows an anhedral altered grain of hornblende.

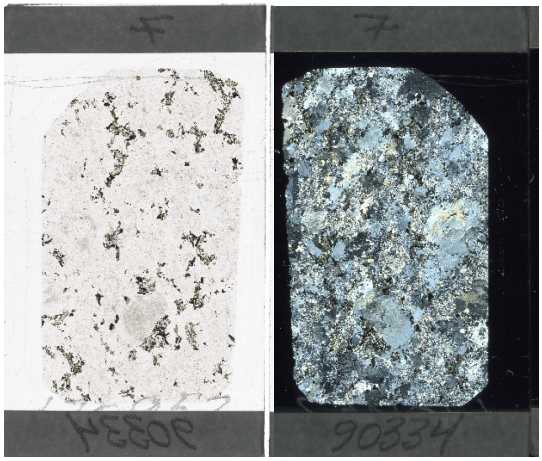

Sample: 90334 (granite)

Hand specimen:

Coarse-grained, inequigranular rock. It shows a light-grey colour with pink k-feldspar and grey quartz grains, with dark mafic minerals.

Minerals:

Microcline and orthoclase (50%), hornblende (30%), plagioclase (10%) and quartz (10%). Accessory minerals are epidote, titanite, plagioclase and garnet.

Petrographic description:

This sample shows a very deformed rock. It is rich in k-feldspar, represented by large perthitic orthoclase grain, weakly showing Carlsbad twinning. The highly altered orthoclase grain has a dusty appearance in ppl and shows fine-grained needles of epidote. The fine-grained matrix consists of mainly quartz and hornblende. The hornblende grains are randomly oriented and show inclusions of anhedral oxides, rimmed by titanite. It is therefore reasonable to believe that this rock has experienced some degree of metamorphism.

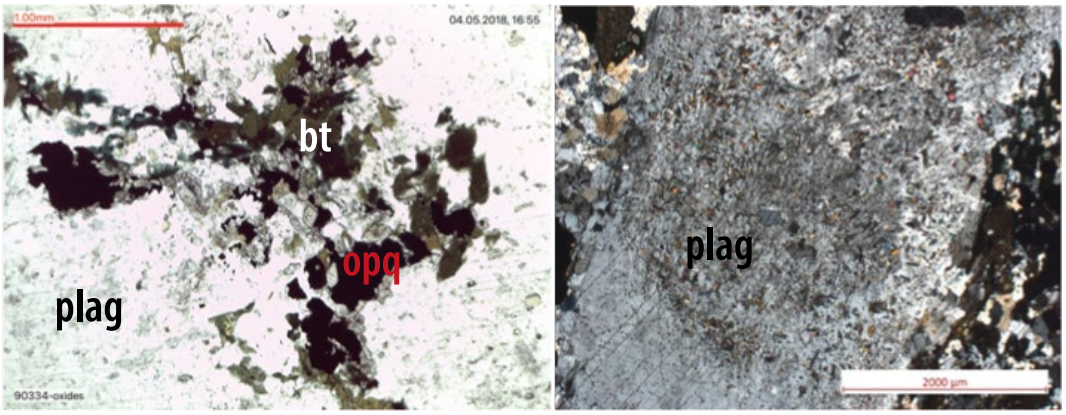

The first microphotograph (PPL) shows a much of oxide minerals and hornblende, with the oxides showing a rim of titanite. The second microphotograph (PPL) shows an altered feldspar grain forming fine-grained epidote.

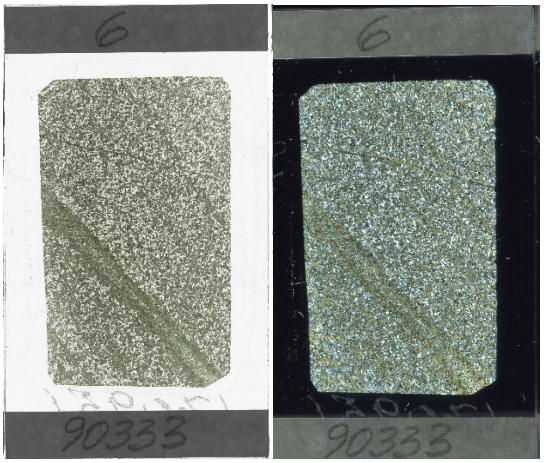

Sample: 90333 (amphibolitic dyke)

Hand specimen:

Very fine-grained homogenous rock, showing a dark green colour. A mm-wide green layering (vein) cuts through the massive texture.

Minerals:

Hornblende (60%) and plagioclase (40%). Accessory mineral is titanite.

Petrographic description:

This sample shows a very-fine grained equigranular texture of anhedral grains of hornblende and plagioclase, with medium-grained fragments of titanite. The thin-section show mm-wide hydrous veins formed by aligned hornblende grains.

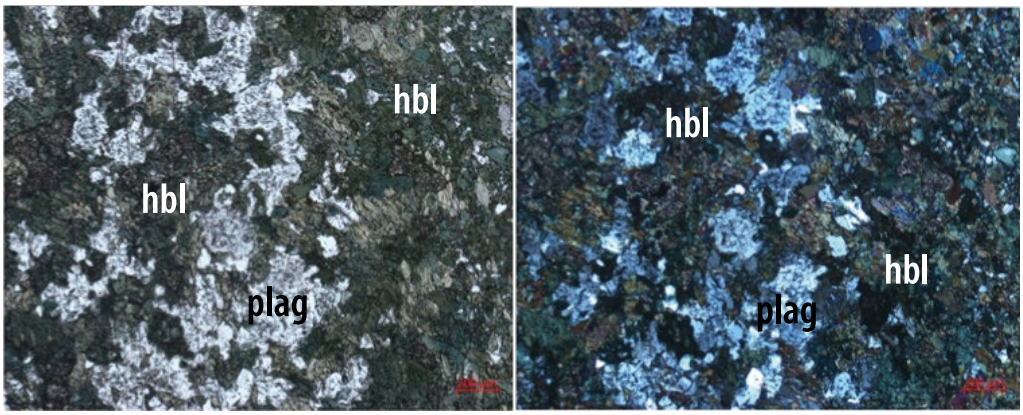

The first microphotograph (PPL) shows fine-grained hornblende and plagioclase randomly oriented. The second microphotograph shows the same feature in XPL. Scale is 200µm.

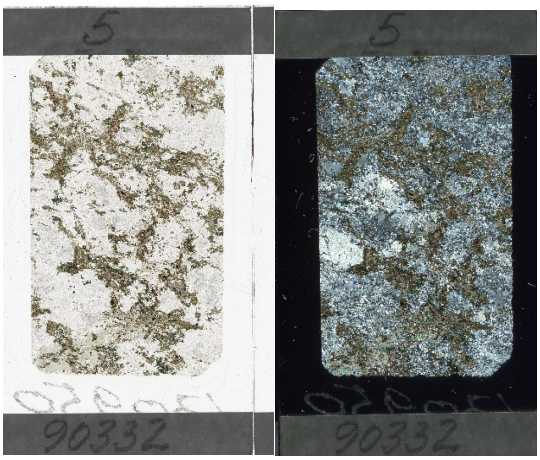

Sample: 90332 (granodiorite)

Hand specimen:

Porphyritic, coarse-grained, inhomogenous rock. White colour from plagioclase grains and dark mafic minerals of amphibole and biotite.

Minerals:

Plagioclase (50%), hornblende (20%), biotite (20%) and epidote (10%). Accessory minerals are quartz, oxides and titanite.

Petrographic description:

This sample shows very altered phenocrysts of plagioclase, with fine-grained interstitial textures formed by hornblende, biotite, plagioclase and quartz. The biotite and hornblende forms glomerocrysts, almost like a rose texture where the orientation of the grains is random. Epidote appear as inclusions in the hornblende, showing a distinct higher relieff in ppl. Coarse-grained oxide crystals are found as inclusions in the glomerocrysts of biotite, showing a rim of titanite. The appearance of radial growth of titanite along a rim on the oxides is interpreted to be part of a metamorphic phase. The non-foliated biotite and hornblende grains would in that case limit the metamorphic exposure to amphibolite facies.

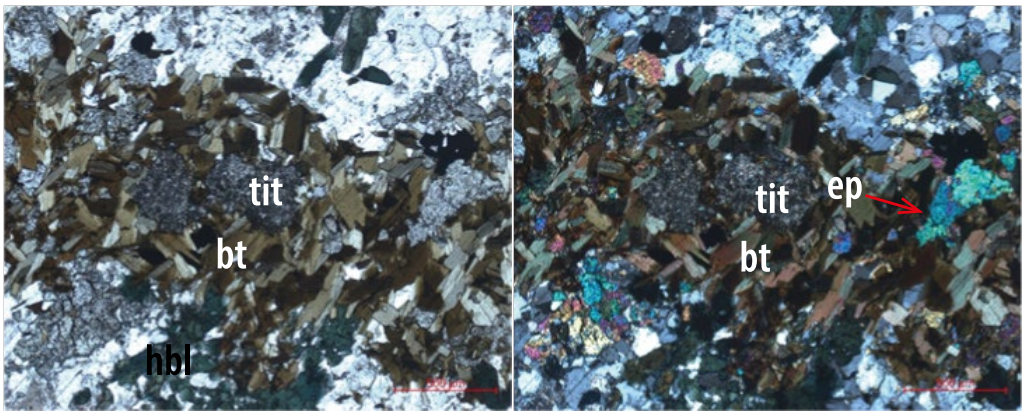

The first microphotograph (PPL) shows a glomerocrystic texture, where a fragmental titanite grain is rimmed by flaky biotite. Hydrothermal alteration has formed medium-grained epidote. The second microphotograph shows the same event in XPL. Scale is 500µm.

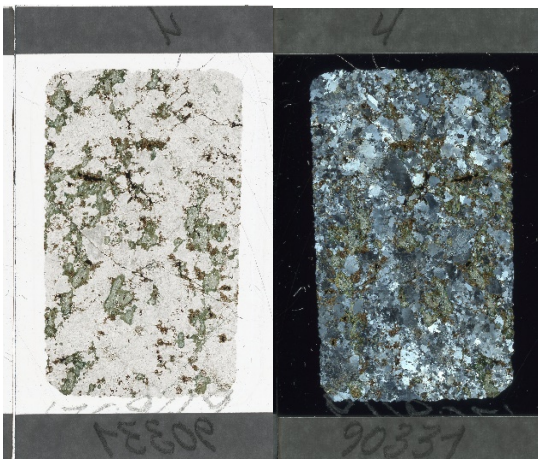

Sample: 90331 (granodiorite)

Hand specimen:

Medium-grained inequigranular rock with 50% light minerals and 50% dark minerals.

Minerals:

Plagioclase (60%), hornblende (20%) and biotite (20%). Accessory minerals are epidote and oxides.

Petrographic description:

This sample is similar to sample 90332. It shows coarse-grained phenocrysts of altered plagioclase. The plagioclase shows deformation lamellae and shows a somewhat dusty look in ppl. The hornblende and biotite are randomly oriented and forms a rim around larger replaced grains of pyroxene. The replacing texture of what is interpreted to be pyroxene grains can be described as poikolitic or a graphic texture, it's being replaced by plagioclase and hornblende. The oxides are found as inclusions in glomerocrysts of biotite.

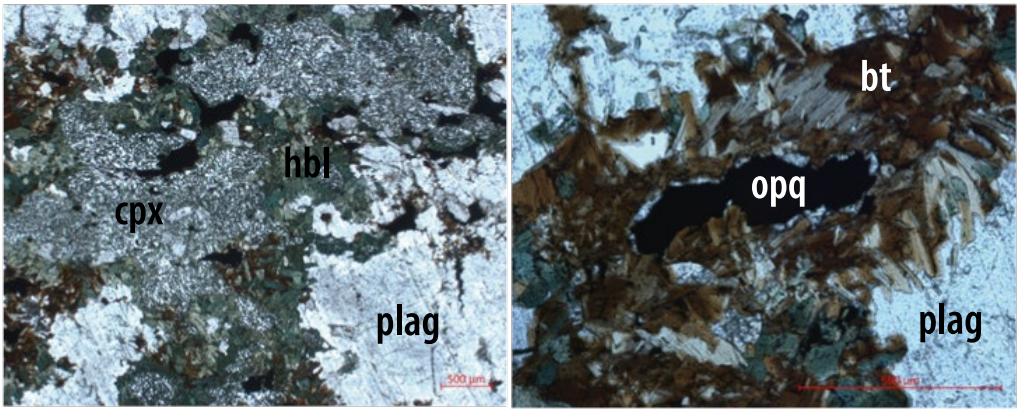

The first microphotograph (PPL) shows hardly altered replaced pyroxene grains with a poikilitic texture, with the grain showing a rim of hornblende. The second microphotograph (PPL) shows an oxide grain with a rim of radial growing biotite. Scale is 500µm.

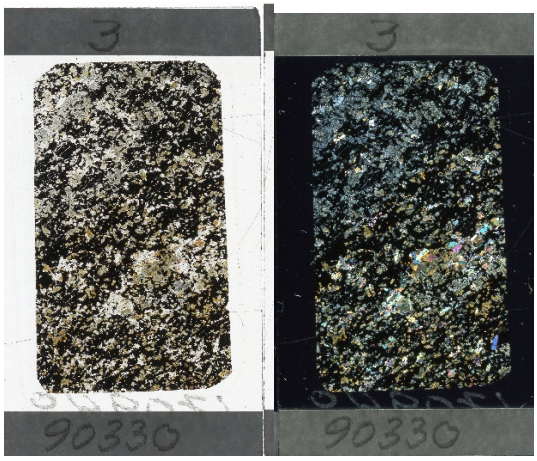

Sample: 90330 (Meta-sediment with magnetite)

Hand specimen:

Coarse-grained inequigranular rock with a grey colour in field.

Minerals:

Pyroxene (50%), oxides (30%) and feldspar (20%).

Petrographic description:

This sample is mainly consisting of anhedral pyroxene grains appearing interstitial with grains of oxides. The oxides appear black in both ppl and xpl and cannot be described from transmitted light. The clinopyroxene grains are coarse-grained and appear with a skeletal texture, similar to the one typical for olivine grains- formed by serpentinization. The interpretation is that this is a mafic rock with mineralisation of iron oxides.

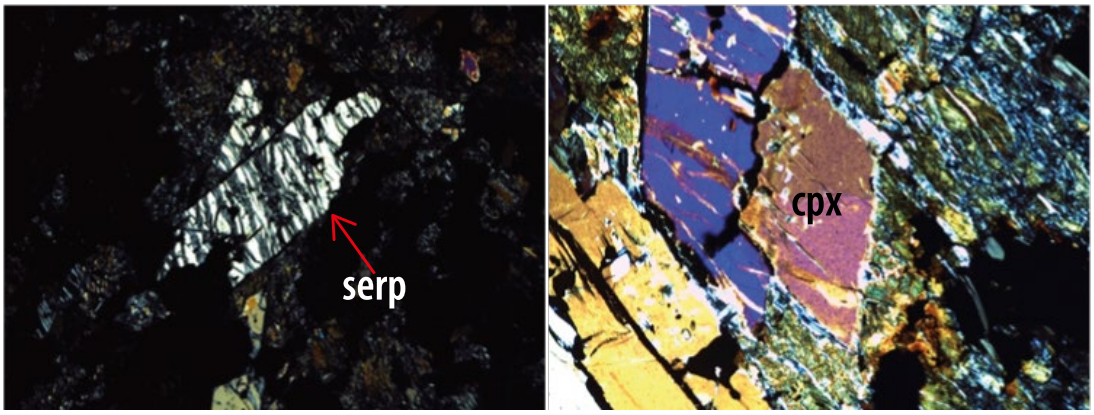

The first microphotograph (XPL) shows serpentinization. The second microphotograph (XPL) shows colourful pyroxene grains.

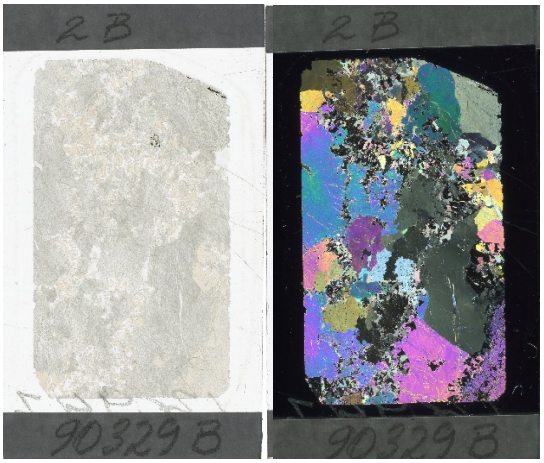

Sample: 90329B (skarn)

Hand specimen:

A coarse-grained, homogenous sedimentary rock with a shiny look.

Minerals:

Pyroxene (70%) and calcite (30%).

Petrographic description:

This sample show large grains of diopside and carbonate grains. The diopside grains show Carlsbad twinning, interpreted to be a replacive texture of feldspar. The carbonate minerals are either calcite or dolomite, in thin-section they are not possible to differentiate. The carbonate mineral shows symmetric twinning.

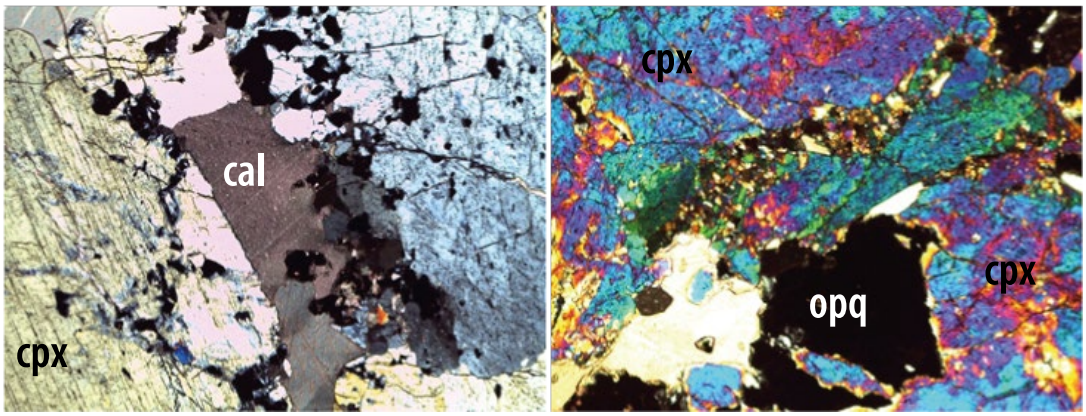

The first microphotograph (XPL) shows an interstitial grain of calcite, with distinct symmetrical twinning. The second microphotograph (XPL) shows oxide crystals together with diopside grains.

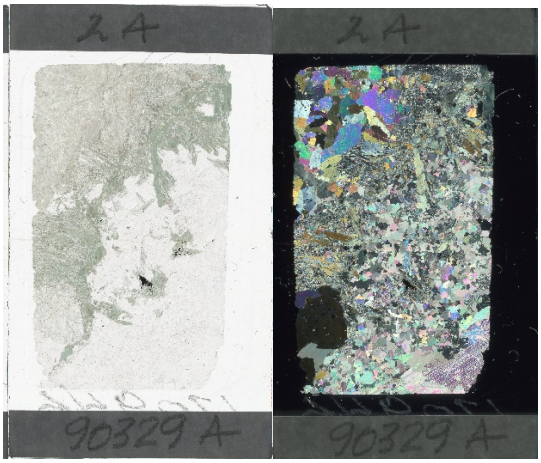

Sample: 90329A (skarn)

Hand specimen:

A coarse-grained, homogenous sedimentary rock with a shiny look.

Minerals:

Pyroxene (30%), chlorite (20%) and carbonate(50%).

Petrographic description:

This sample is another part of the same rock in sample 90329B. It shows coarse-grained carbonate minerals with symmetric twinning, together with coarse-grained clino- and orthopyroxene. Most of the clinopyroxene grains are altered in the process of serpentinite, giving the grains a skeletal texture. Another interesting mineral that is observed in this sample is vesuvian, This mineral is typically found in metamorphic rocks and this rock is by field observations called a meta-sediment, indicating that metamorphic processes have been active in this rock.

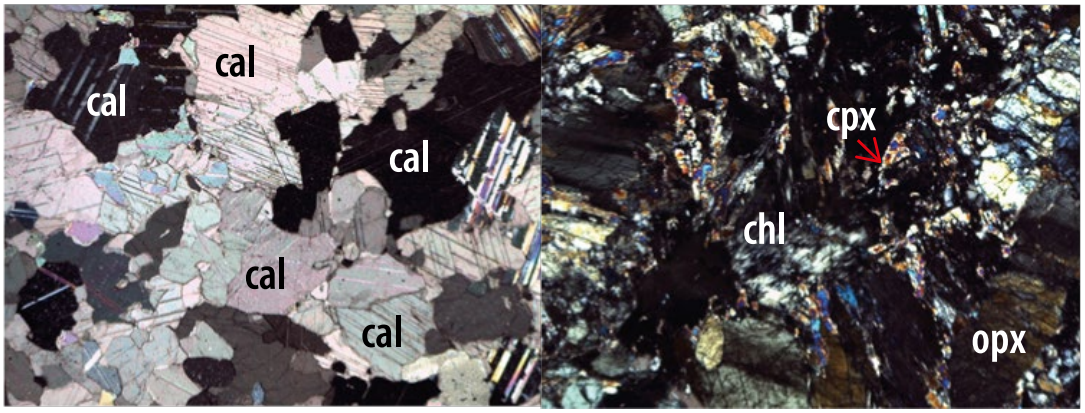

The first microphotograph (XPL) shows anhedral crystals of calcite with symmetrical twinning. The second microphotograph (XPL) shows heavily chloritized pyroxene grains.

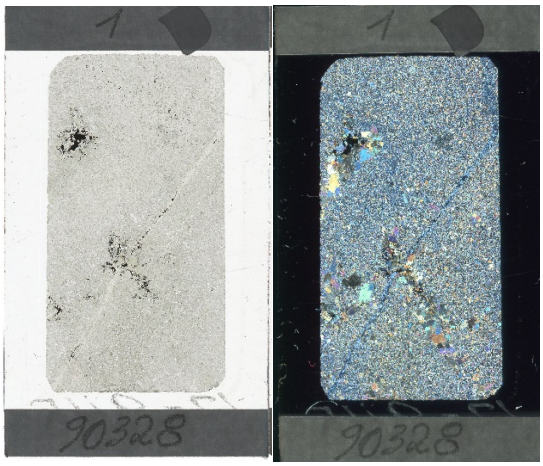

Sample: 90328 (metasediment)

Hand specimen:

Fine grained shiny rock. Appear inequigranular as there are clusters of coarse-grained minerals, with a network of small veins.

Minerals:

Pyroxene (60%) and plagioclase (40%). Accessory minerals are vesuvian and oxides.

Petrographic description:

This sample shows a fine-grained rock. The fine-grained minerals constituting in this rock are clinopyroxene and plagioclase. The texture is inequigranular as some of the clinopyroxene grains are coarse-grained, the rock shows a mosaic texture. Small mm-wide veins cut the texture of the rock, showing oxides aligned parallel to the orientation of the veins- with a rim of vesuvian. The interpretation is therefore that the texture of the rock is metamorphic.

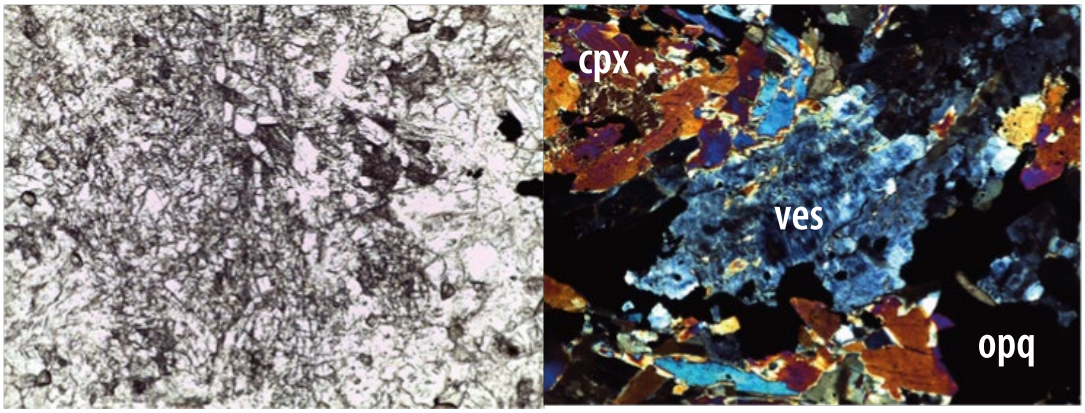

The first microphotograph (PPL) shows an altered texture of diopside and plagioclase grains. The second microphotograph (XPL) shows a grain of vesuvian, surrounded by diopside.

Sample: 140808 (granite)

Hand specimen:

Porphyritic, inequigranular heterogenous coarse-grained rock. An overall light-grey colour with pink phenocrysts of k-feldspar, white to grey plagioclase and quartz, with black mafic minerals of amphibole and biotite.

Minerals:

Quartz (40%), microcline (30%) plagioclase (10%), orthoclase (10%) biotite (5%) and hornblende (5%). Accessory minerals are epidote, apatite and allanite.

Petrographic description:

This sample shows coarse-grained k-feldspar phenocrysts of microcline and orthoclase in a matrix of intermediate to fine-grained replaced crystals of plagioclase, anhedral microcline and orthoclase, green-coloured hornblende, yellow to brown-coloured biotite, epidote and titanite. The orthoclase is characterized by the perthitic texture and albite twinning, whilst the microcline shows distinct tartan twins. The amphibole and biotite grain are randomly oriented (non-foliated) and can be observed in coarse-grained clusters where the epidote appear as inclusions in the biotite. The titanite grains are often shown with inclusions of oxides. The feldspar grains are altered by saussuritization to form fine-grained needles of epidote. Apatite and allanite are accessory minerals, with the allanite being metamict. The texture can be described as coarse-grained, porphyritic and slightly deformed.

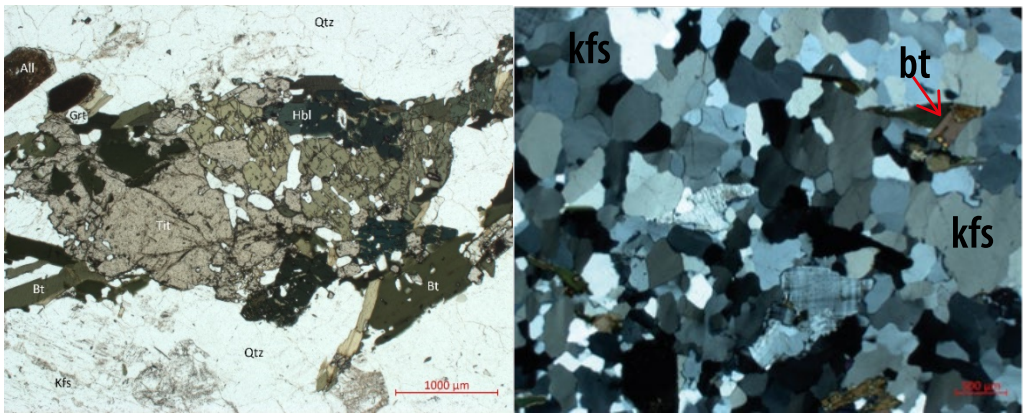

The first microphotograph (PPL) shows an altered titanite grain, with hornblende and biotite growing at the rims. The second microphotograph (XPL) shows deformation textures in quartz (scales is 500µm).

Sample: 140809 (granite)

Hand specimen:

A fine-grained, inequigranular rock. Appear with a light-grey colour showing fine-grained amphibole in a matrix of feldspar and quartz, with rusty-colored oxides.

Minerals:

K-feldspar (55%), plagioclase (15%), quartz (10%), bitotite (10%) and hornblende (10%). Accessory minerals are epidote, titanite and allanite.

Petrographic description:

This is a porphyritic rock with phenocrysts of both microcline and orthoclase, in a matrix consisting of anhedral grains of microcline, plagioclase, hornblende and quartz. The microcline grains show distinct tartan twinning, whilst the orthoclase shows perthitic twinning. All the feldspar grains show alteration by the process of saussuritization, forming fine-grained epidote. The hornblende and biotite grains are medium-grained and randomly oriented, often seen with inclusions of titanite and epidote. The quartz in this sample show a recrystallization texture growing in veins between the larger feldspar grains. The quartz show bulging, indication some degree of deformation.

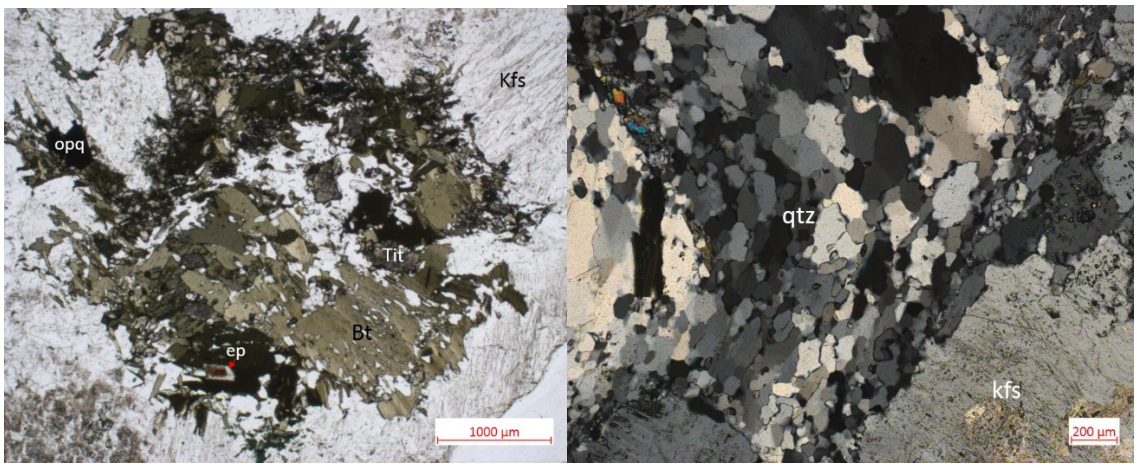

The first microphotograph (PPL) shows a much of biotite and hornblende grains. The second microphotograph (XPL) shows a recrystallization texture formed by quartz.

Sample: 140810 (granite)

Hand specimen:

Coarse-grained, porphyritic, inequigranular rock. Large pink phenocrysts of k-feldspar with black mafic minerals forming randomly oriented clusters, forming a rim around brown-coloured oxides.

Minerals:

K-feldspar (45%), plagioclase (30%), hornblende (15%), quartz (10%) and biotite (5%). Accessory minerals are titanite, epidote and oxides.

Petrographic description:

The sample show coarse-grained phenocrysts of both k-feldspar (microcline and orthoclase) and plagioclase. Coarse-grained hornblende is observed in what seems to be former feldspar crystals, as they show albite twinning, this is interpreted to be a replacive texture. The colour of the hornblende is dark green with two very distinct cleavage and it has inclusions of anhedral titanite grains. The biotite is yellow in colour and appear with a finer grainsize and more platy in shape than the hornblende. Oxides appear as inclusions in the titanite grains and show a close to euhedral shape compared to the other minerals which are subhedral to anhedral. The feldspar grains are altered with saussuritization forming very fine-grained epidote crystals. The texture can be described as coarse-grained, deformed and allotriomorphic.

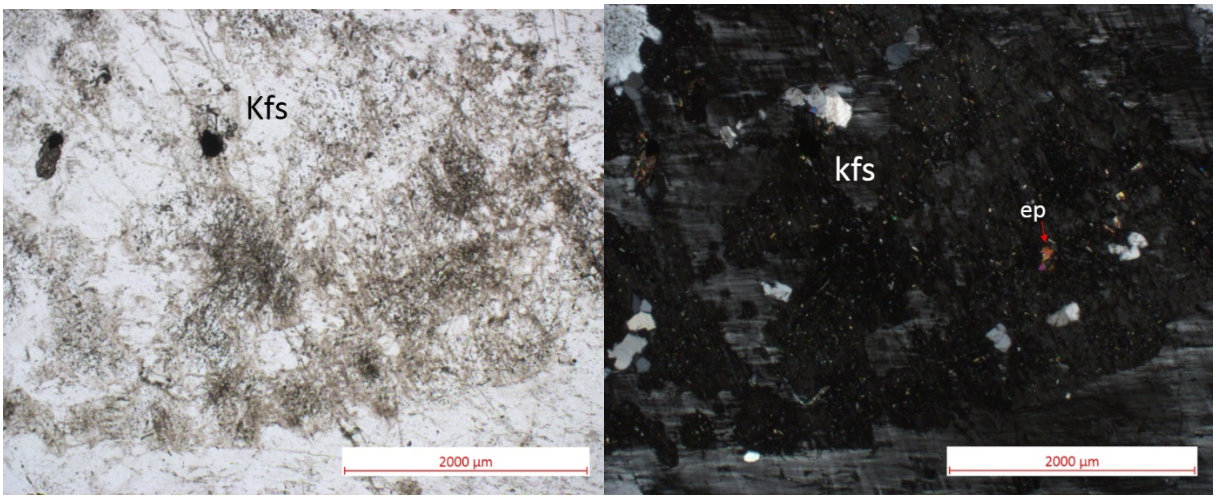

The first microphotograph (PPL) shows the dusty look which is described for many of the feldspar grains in this study. The second microphotograph shows the same feldspar grain in XPL, with epidote inclusions formed by the alteration.

Sample: 140811 (metasediment)

Hand specimen:

A coarse-grained inequigranular green coloured rock with no foliation. Appear massive with a small network of veins.

Minerals:

Diopside (80%), carbonate (15%) and hornblende (5%).

Petrographic description:

This sample consist of both coarse-grained and fine-grained anhedral diopside, showing varying interference colours. The carbonate grains are coarse-grained and show distinct symmetric twins. The hornblende is found to grow in the space between the larger grains of diopside and as a replacive mineral in some of the diopside grains. The texture is …

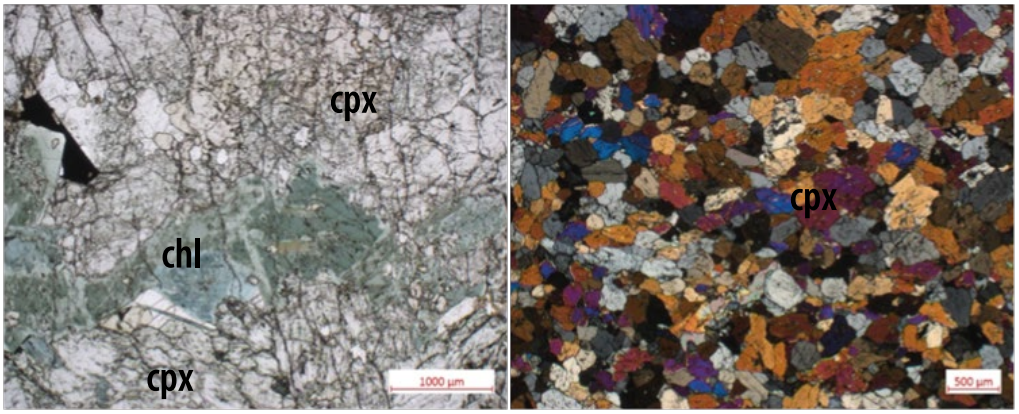

The first microphotograph (PPL) shows chloritization of diopside grains. The second microphotograph (XPL) shows the mosaic texture formed by anhedral medium-grained diopside crystals.

Sample: 140812 (metasediment)

Hand specimen:

A coarse-grained inequigranular green coloured rock.

Minerals:

Diopside (50%), hornblende (30%) and oxides (20%). Accessory mineral is titanite and chlorite.

Petrographic description:

This sample was taken from a skarn found on Bjarkøya. It shows a large amount of coarse-grained hornblende that appears with a green colour. Half of the thin section consists of colourless, fine-grained, high-relieff crystals of the pyroxene diopside that shows a pale green pleochroism. The crystals form a mosaic texture in xpl, showing several 2. order colours varying from yellow, blue to purple. Coarse-grained colourless clinopyroxene grains of augite is observed with micro-cracks within it. Coarse-grained oxides are also observed and is identified to be the copper iron-sulfide chalcopyrite.

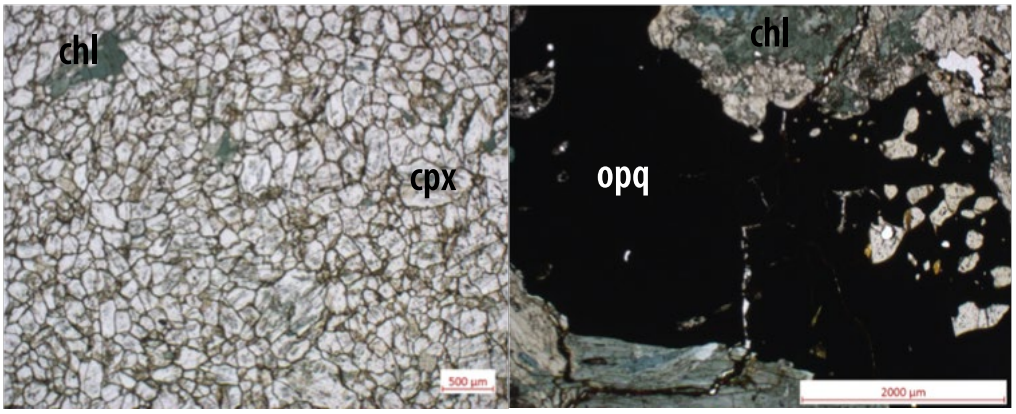

The first microphotograph (PPL) shows a recrystallization texture of anhedral diopside grains. The second microphotograph (PPL) shows a large grain of chalcopyrite.

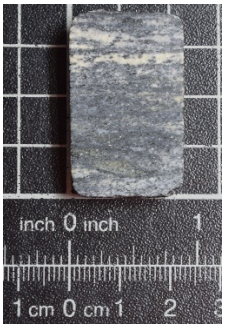

Sample: 140813 (gneiss)

Hand specimen:

A fine-grained, inequigranular gneissic rock. The colour is dark grey, with distinct leucosomes of plagioclase and melanosomes of amphibole. Pebbles of diopside are oriented in the same direction as the leuco- and melanosomes.

Minerals:

K-feldspar (40%), hornblende (30%), diopside (15%) and quartz (15%).

Petrographic description:

This sample show an inequigranular fine-grained texture. The microcline shows anhedral, varying size grains with distinct tartan twinning. The hornblende appears with a dark green colour as fine-grained, anhedral grains. Both the microcline and hornblende show a strong foliation, where larger grains of epidote can be observed as inclusions in mainly the clusters of hornblende. The feldspar grains show saussuritization forming very fine-grained epidote grains.

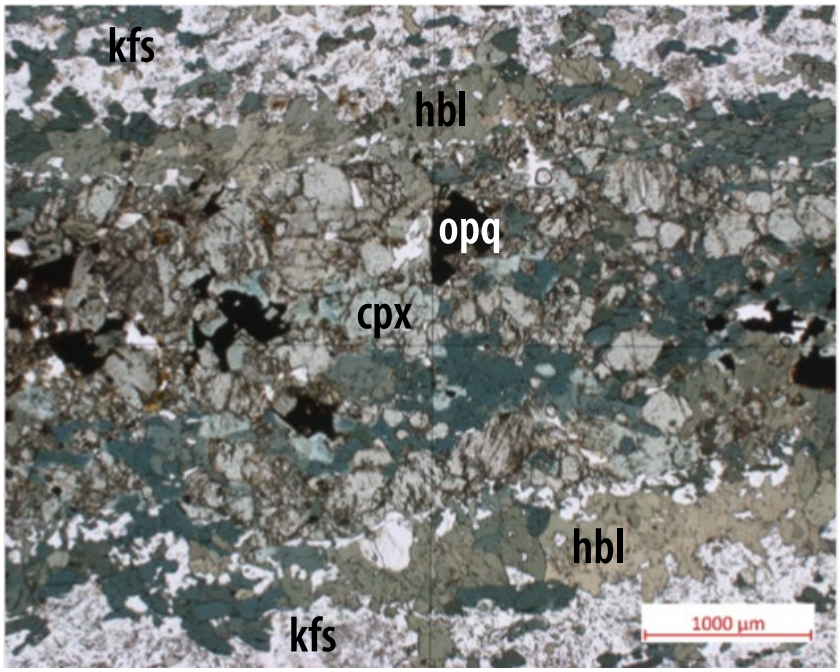

The microphotograph (PPL) shows a hydrothermal vein. From the edge to the centre: altered alkali-feldspar grains together with green randomly oriented anhedral grains of hornblende, iron oxides and diopside forms the centre of the vein.

Sample: 140814 (gneiss)

Hand specimen:

A medium-grained, equigranular foliated rock. The colour is light grey with light feldspar grains together with dark amphibole grains. The texture can be described as gneissic.

Minerals:

Plagioclase (40%), biotite (30%), quartz (20%) and diopside (10%). Accessory minerals are epidote and zircon.

Petrographic description:

The sample shows an inequigranular grain distribution. The plagioclase appear anhedral with albite twins and is observed with the alteration process of saussuritization forming very fine-grained epidote. The biotite shows a deep green colour in this thin-section, with a platy shape of the grains and a distinct bird-eye texture. The biotite is growing in a certain direction, creating a foliation of the rock. The foliated biotite show inclusions of randomly oriented anhedral grains of diopside, suggesting that the biotite is a later phase of crystallization. Quartz is evenly distributed between the foliation of biotite and the plagioclase grains and show no specific texture. Zircon is accessory and appear as small inclusions in the biotite, showing a clear black halo.

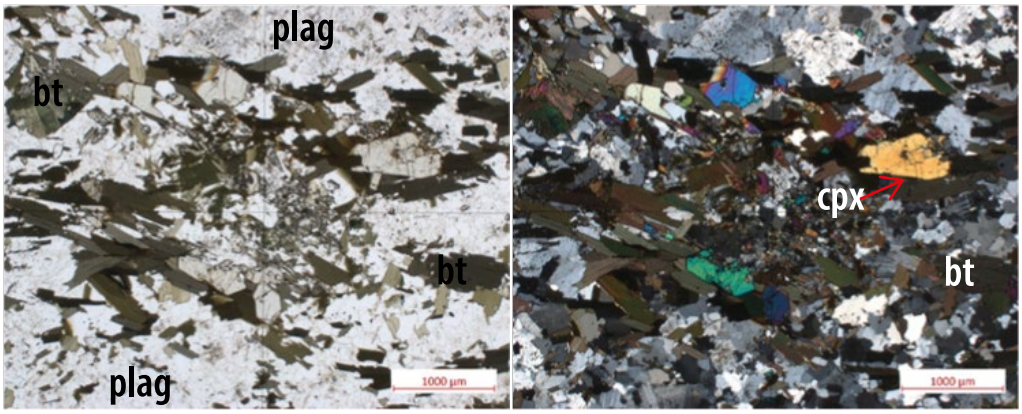

The first microphotograph (PPL) shows slightly oriented biotite in a groundmass of quartz, plagioclase. The second microphotograph (XPL) shows the same feature, with evidently subhedral colourful crystals of diopside.

Sample: 140815 (granodioritic dyke)

Hand specimen:

Coarse-grained inequigranular leucocratic rock, with coarse-grained pyroxene growing with a rim or halo of amphibole surrounded by feldspar and quartz. Small pink garnet crystals can be observed.

Minerals:

Plagioclase (60%), Omphacite (30%) and quartz (10%). Accessory minerals are epidote and garnet.

Petrographic description:

This sample shows large plagioclase anhedral plagioclase grains, that has deformation lamellae parallel to the albite twins. The plagioclase show saussuritization resulting in small needles of epidote, and inclusions of both garnet, quartz and omphacite. The omphacite appear with a clear green pleochroism and are found in a glomerocrystic texture found with euhedral grains of epidote. The omphacite appear with a pokolitic texture and in rims around the larger plagioclase grains. Garnet shows euhedral shapes with a pink colour in ppl. The mineral assemblage, if the interpretation of omphacite is true- witnesses high degree metamorphism.

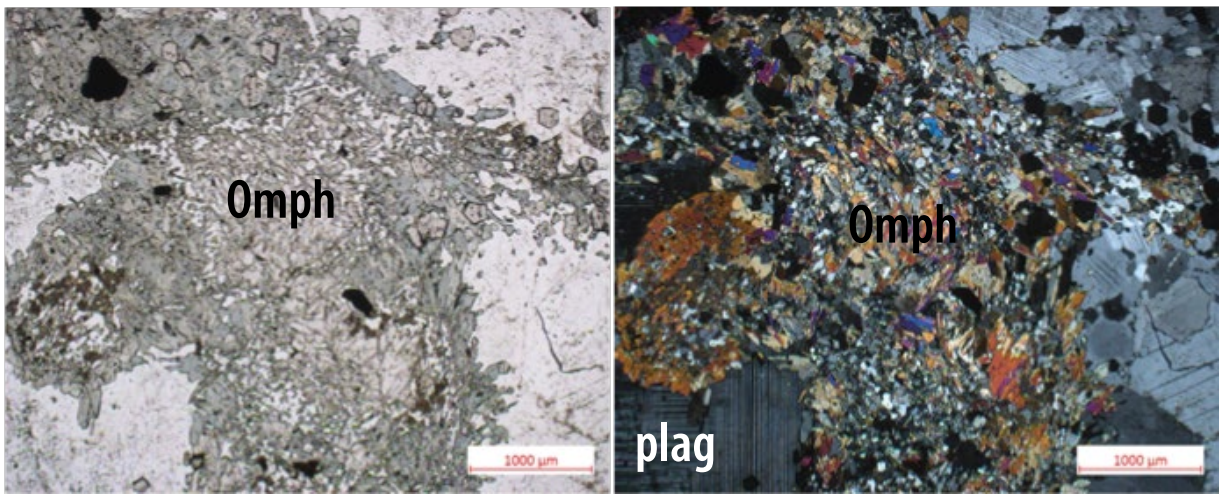

The microphotographs in PPL and XPL shows the interpreted high-grade metamorphism mineral omphacite.

Sample: 140816 (granite)

Hand specimen:

Coarse-grained porphyritic rock. Large crystals of feldspar with less content of dark-mafic minerals of amphibole and biotite.

Minerals:

K-feldspar (40%), quartz (30%), hornblende (15%), plagioclase (10%) and biotite (5%). Accessory minerals are titanite, epidote and garnet.

Petrographic description:

Altered coarse feldspar grains, both alkali feldspar (microcline and orthoclase) and plagioclase. The orthoclase shows a perthitic texture with exsolution lamellae on both sides of the albite twinning. Plagioclase show deformation lamellae and saussuritization forming fine-grained epidote. Hornblende and biotite appear randomly oriented in coarse-grained clusters, often with remnants of titanite inclusions. The sample is rich in fine-grained anhedral quartz and euhedral garnet crystals appearing with a pink colour and high relieff in ppl. Epidote is not just represented as saussuritization products but appears as small inclusions in the hornblende and biotite grains.

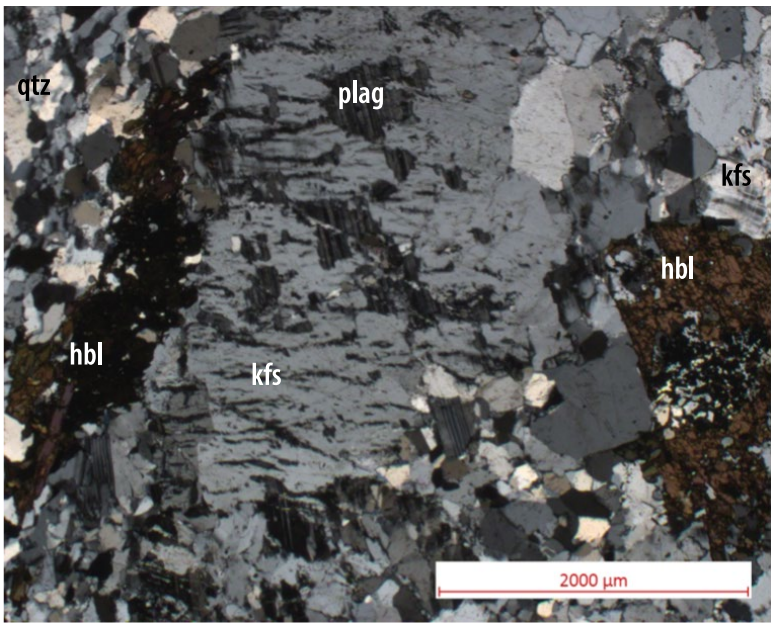

The microphotograph (XPL) shows a plagioclase-grain that was first replaced by an orthoclase grain, and now it's altered and replaced by quartz.

Sample: 140817 (metasediment)

Hand specimen:

Very fine-grained dark grey rock, with a network of green very fine-grained veins. The rock appears massive and inequigranular.

Minerals:

Pyroxene (50%) and plagioclase (50%).

Petrographic description:

This sample shows large pyroxene phenocrysts in a very fine-grained matrix of anhedral pyroxene and plagioclase. The pyroxene grains are both clinopyroxene and orthopyroxene. The pyroxenes appear anhedral with internal cracks, sometimes looking like exsolution lamellaes. Throughout the thin-section, veins of green coloured amphibole can be observed, indicating hydrous conditions. A needle-shaped mineral with a colourless display in ppl and a grey colour in xpl is not possible to identify without chemical analyses. It appears randomly oriented and is interpreted to reflect static metamorphism. This unidentified mineral forms a skeletal texture of the matrix. The rock can be described as a non-foliated, homogenous metamorphosed mafic rock.

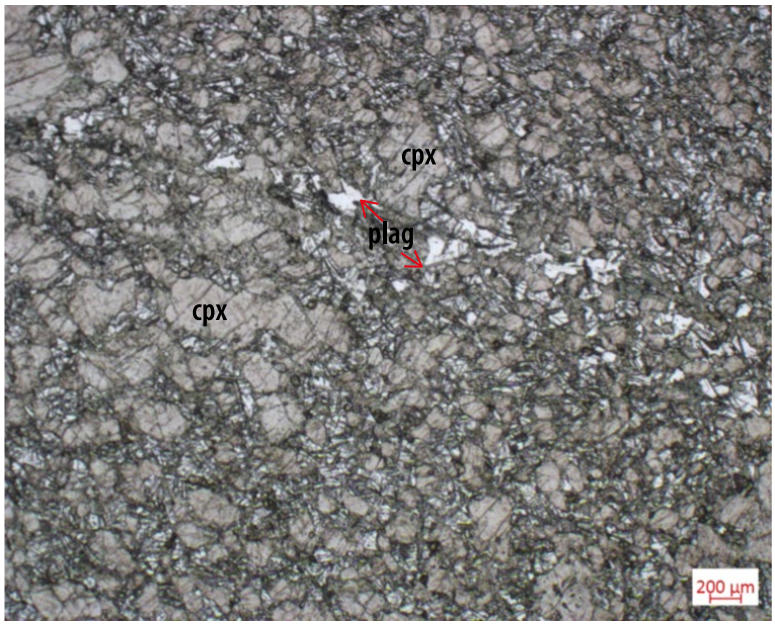

The microphotograph (PPL) shows a thin-section with coarse-grained diopside-grains surrounded by smaller grains of plagioclase.

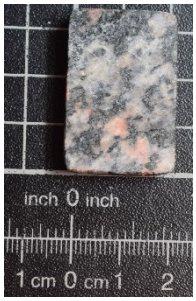

Sample: 140818 (granite)

Hand specimen:

Coarse-grained, inequigranular heterogenous rock. The colour is light grey, with pink crystals of k-feldspar and black amphibole and biotite.

Minerals:

K-feldspar (50%), hornblende (20%), plagioclase (10%), biotite (10%) and quartz (10%). Accessory minerals are epidote, titanite and oxides.

Petrographic description:

This sample shows a highly altered mineral assemblage. The coarse-grained orthoclase has a mesoperthitic texture and the plagioclase show alteration by saussuritization. Orthoclase crystals are observed to be partly altered to microcline. The feldspar grains appear with a dusty look in ppl, and this is a result of high degree of alteration. The hornblende grains are anhedral and shows a poikilitic texture with inclusions of quartz. Accessory titanite appear in corona textures along the rim of the accessory oxides.

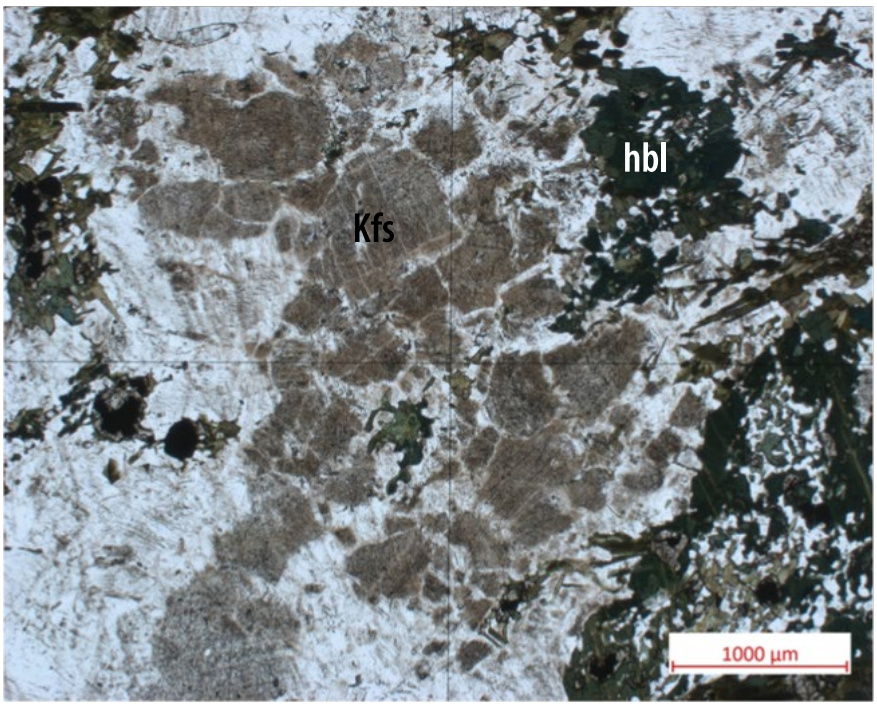

Microphotograph (PPL) showing an altered grain of feldspar giving it a dusty appearance.

Sample: 140819 (metasediment)

Hand specimen:

Minerals:

Quartz (40%), hornblende (25%), plagioclase (20%), microcline (10%) and biotite (5%). Accessory mineral is epidote.

Petrographic description:

This sample shows a bimodal grain size distribution. Coarse grains of hornblende with a subhedral to euhdedral shape are observed with a deep green colour. The hornblende is randomly oriented and observed with pokolitic texture, with inclusions of quartz. The quartz, plagioclase and microcline are all constituting in a fine-grained matrix. The biotite is growing randomly oriented, but often in a circular pattern.

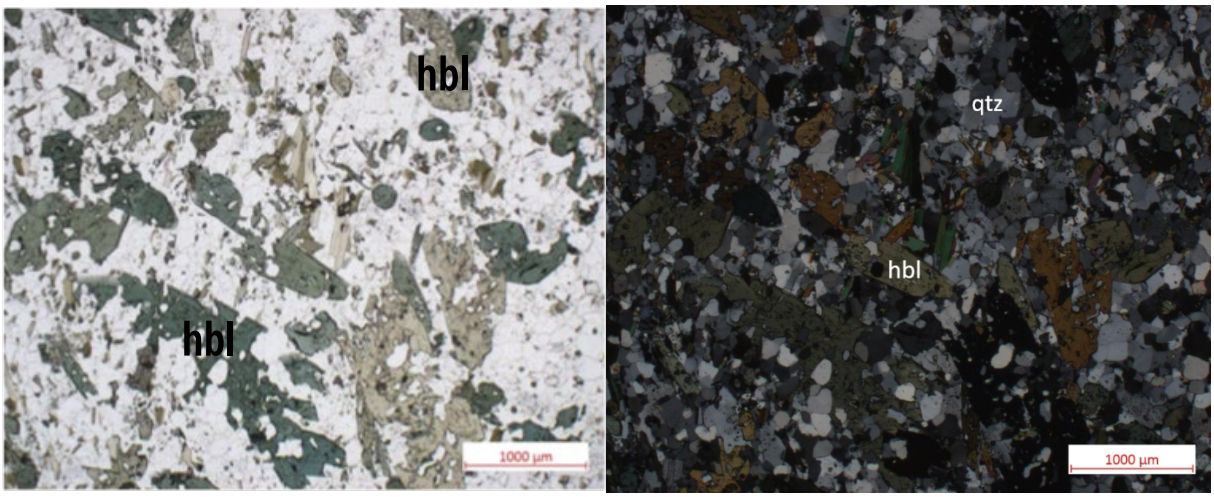

The first microphotograph (PPL) shows sub to anhedral, inclusion-rich (zircon with black haloes) hornblende grains. The second microphotograph (XPL) shows the same picture in XPL, highlighting the many inclusions which seem to be of quartz.

Sample: 140820 (granite)

Hand specimen:

Fine-grained dark grey coloured rock, with porphyroclasts of plagioclase. Inequigranular, massive non-foliated rock.

Minerals:

K-feldspar (40%), plagioclase (30%), hornblende (15%) and biotite (15%). Accessory minerals are titanite, oxides and epidote.

Petrographic description:

This sample shows a fine-grained rock with a mineral assemblage of hornblende, biotite, alkali-feldspar, plagioclase and quartz. All minerals appear anhedral, with the biotite grains growing in what appears to be veins. The hornblende grains are green coloured with a poikilitic texture. The thin section shows almost a dividing between one part very rich in alkali-feldspar (orthoclase) and one part very rich in plagioclase. The quartz is fine-grained and based on the interstitial growth it must have formed as one of the latest minerals. As for some of the granitic samples from Grytøya, this sample shows a corona texture formed by reactions including titanite forming around ilmenite. Accessory minerals are epidote and oxides. From thin-section observations the rock can be described as a fine-grained syenite.

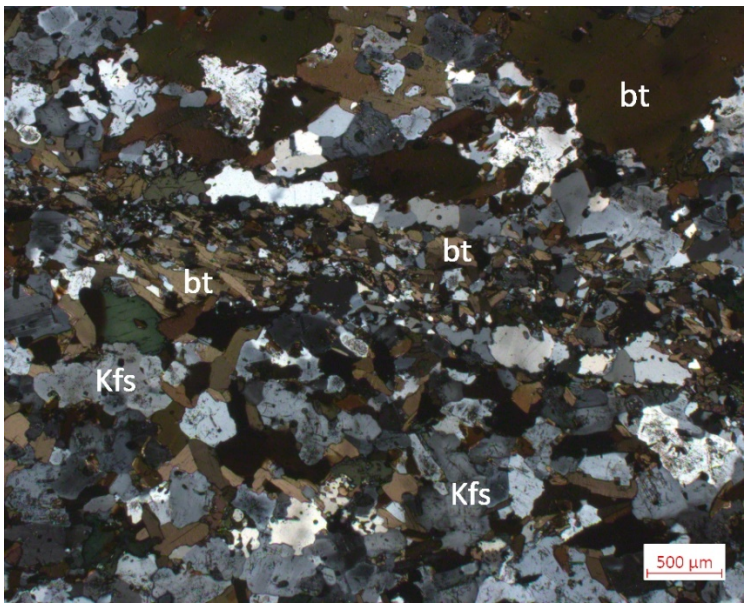

The microphotograph (XPL) shows a vein of oriented fine-grained biotite, surrounded by larger grains of biotite and orthoclase.

Sample: 140821 (leucocratic dyke)

Hand specimen:

Medium-grained, inequigranular rock. White in color, with black crystals of biotite.

Minerals:

Plagioclase (80%), quartz (10%) and biotite (10%). Accesory minerals are epidote, garnet and oxides.

Petrographic description:

This sample is taken from a leucocratic dyke and show a mineral assemblage of plagioclase and quartz, where the plagioclase appears both coarse-grained and fine-grained. The flaky biotite grains observed in the rock are very fine-grained, randomly oriented. Accessory epidote is observed as alteration products of the plagioclase. Garnet and oxides appear with subhedral to euhedral shape, in contrast to the anhedral plagioclase and quartz grains. The texture can be described as medium-grained inequigranular.

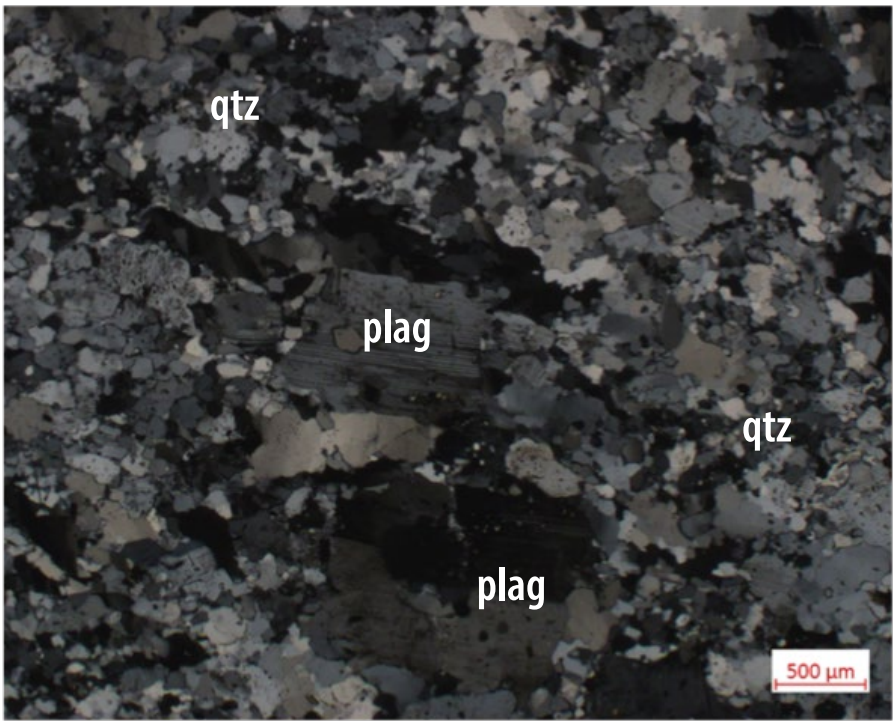

The microphotograph (XPL) shows the typical texture of this leucocratic dykes, larger anhedral grains of plagioclase surrounded by anhedral smaller grains of plagioclase and quartz.

Sample: 140822 (amphibolite)

Hand specimen:

Coarse-grained, inequigranular dark-coloured rock. Large crystals of black amphibole, with coarse-grained plagioclase gives it a leopard texture.

Minerals:

Amphibole (50%), microcline (30%), plagioclase (20%) and quartz (10%). Accessory minerals are titanite, epidote and biotite.

Petrographic description:

This sample appear coarse-grained and consists mainly of green coloured subhedral amphibole showing two perfect cleavages (hornblende), in a matrix of fine-grained anhedral grains of plagioclase, alkali-feldspar and quartz. Hornblende appears with a lot of inclusions; these inclusions are mainly of epidote and apatite. Titanite is found as fragmental grains with a clear euhedral shape, with beautiful twinning. The sample is rich in fine-grained, needle-shaped apatite showing a high relieff in ppl. Accessory minerals are zircons with pleochroic haloes and subhedral fine-grained epidote.

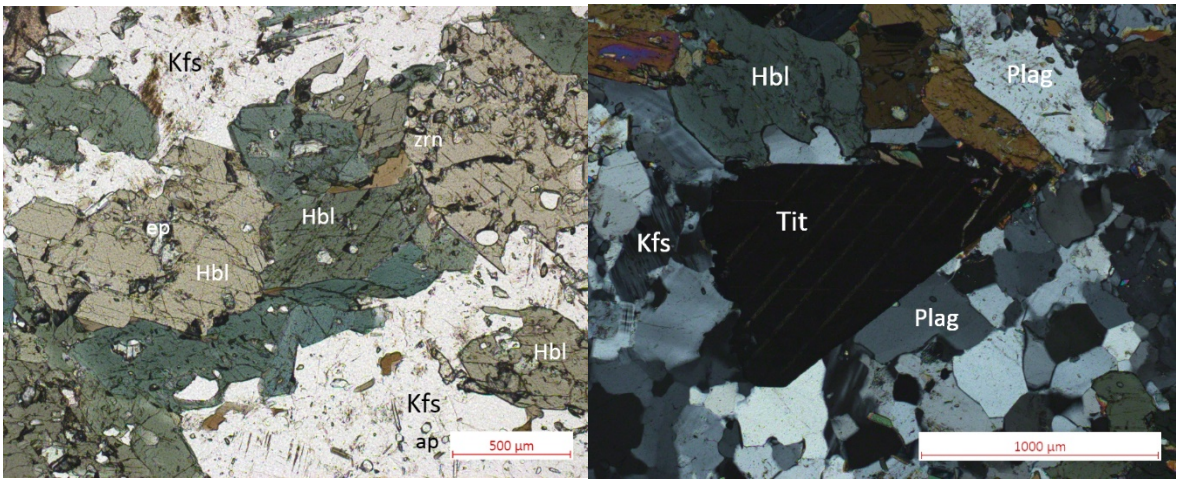

The first microphotograph (PPL) shows several grains of hornblende with inclusions of epidote, see the clear pleochroism. The second microphotograph (XPL) shows twinning in a titanite grain surrounded orthoclase and plagioclase.

Sample: 140823 (Leucocratic dyke)

Hand specimen:

Coarse-grained leucocratic dyke formed by plagioclase, cutting through a dark grey metasedimentary rock.

Minerals:

K-feldspar (30%) and quartz (70%).

Petrographic description:

This sample was picked from a plagioclase vein cutting through a metasedimentary rock, and this is reflected in the thin-section. One part consists of large grains of altered anorthoclase, intruded by small veins of calcite. The other part consists of a fine-grained groundmass of quartz and k-feldspar.

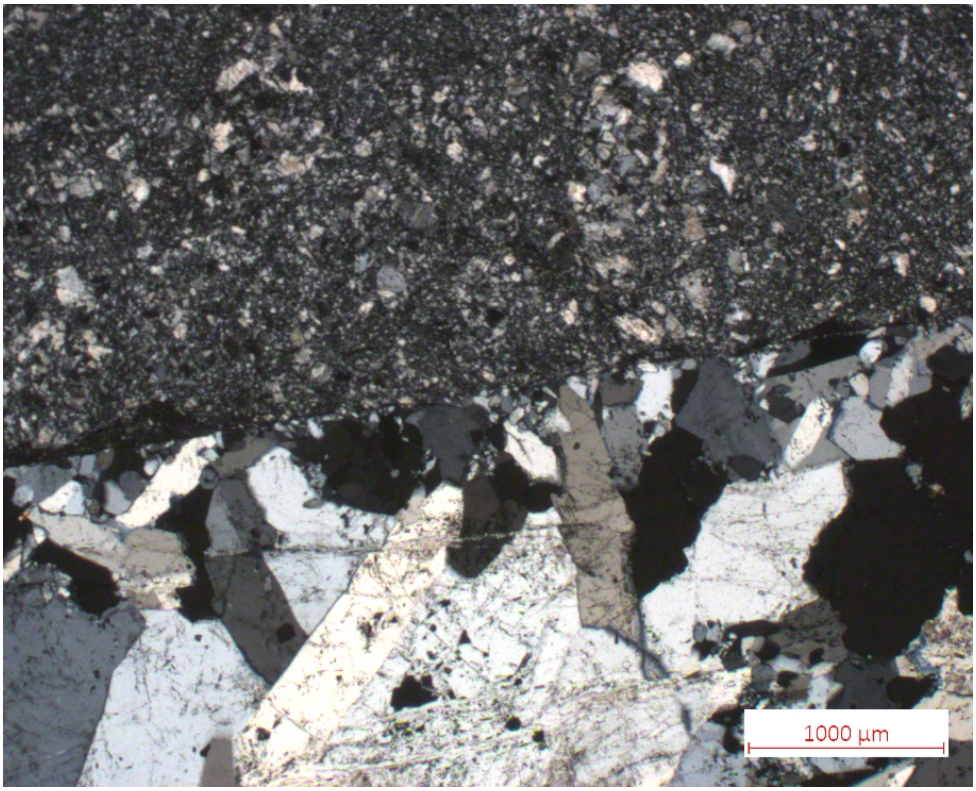

The microphotograph (PPL) shows a thin-section that consists of two distinct different textures, one very fine-grained texture consisting of feldspar and one fine-grained texture consisting of quartz and amphibole.

Sample: 140824 (amphibolite)

Hand specimen:

A very fine-grained dark coloured rock, showing tiny black spots of amphibole. It appears massive with no foliation.

Minerals:

Amphibole (50%), microcline (30%), plagioclase (20%) and quartz (10%). Accessory minerals are titanite, epidote and biotite.

Petrographic description:

This sample shows a fine grained, inequigranular rock consisting mainly of fine-grained hornblende-grains in a mushy groundmass of feldspar and quartz. As for sampled 140825, coarse-grained yellow biotite, oriented oblique to the hornblende orientation suggesting that the biotite is post-tectonic.

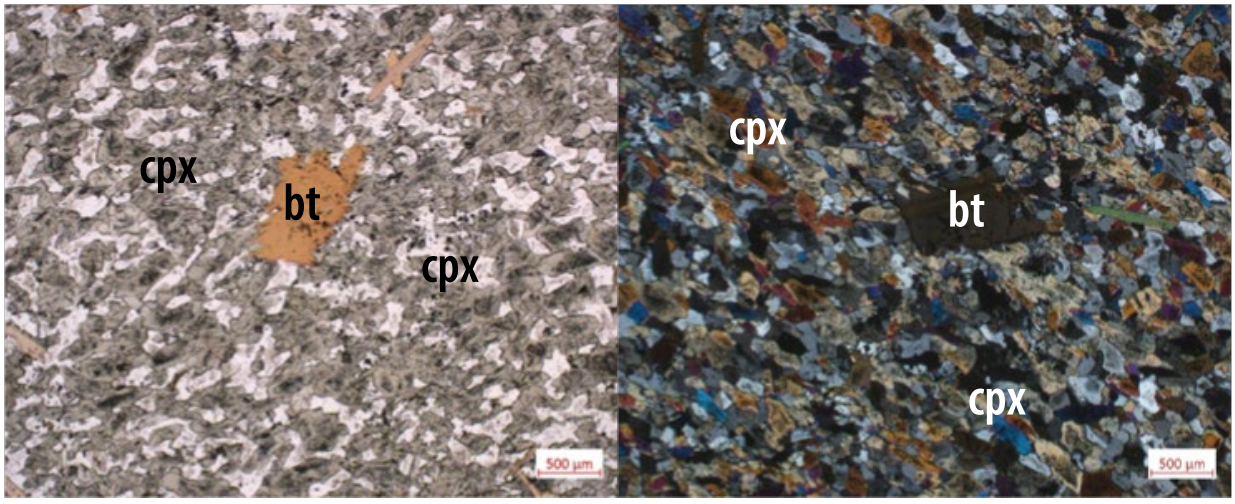

The first microphotograph (PPL) shows a large grain of biotite in a finer grained matrix. The second microphotograph (XPL) shows the same picture in xpl showing the finer grains of hornblende.

Sample: 140825 (Metabasalt)

Hand specimen:

Fine-grained, ineguigranular layered rock. The layers are light-coloured consisting of plagioclase and dark-coloured consisting of mainly hornblende.

Minerals:

Hornblende (50%), microcline (30%), plagioclase (25%) and quartz (5%). Accessory minerals are titanite, epidote, biotite and garnet.

Petrographic description:

This thin-section shows a fine-grained rock with a clear layering texture. The leucocratic layers consist of plagioclase and quartz, whilst the melanocratic layering are formed by hornblende. The plagioclase and microcline grain are anhedral and largely altered to form epidote. The hornblende grains are anhedral and fine-grained. The appearance of garnet in this layered rock suggest that the rock has been exposed to a high pressure during a metamorphic process that layered the rock.

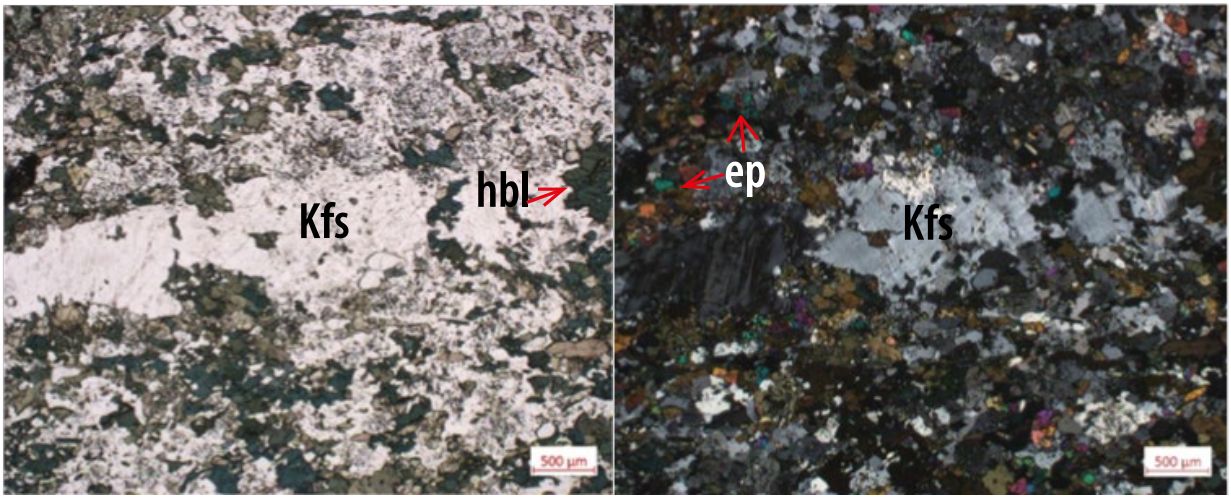

The first microphotograph (PPL) shows a large feldspar-phenocryst surrounded by smaller anhedral grains of hornblende, plagioclase and quartz. The second microphotograph (XPL) reveals the phenocryst as being a microcline grain surrounded by quartz, hornblende and epidote.

Sample: 140826 (quartzitic granite)

Hand specimen:

Coarse-grained, inequigranular

Minerals:

Quartz (60%), microcline (20%), plagioclase (20%). Accessory minerals are titanite, epidote and biotite.

Petrographic description:

This thin-section is showing highly altered coarse grains of feldspar with associated saussuritization forming epidote. Very few randomly oriented yellow grains of biotite with inclusions of zircon are observed, in a groundmass rich in quartz.

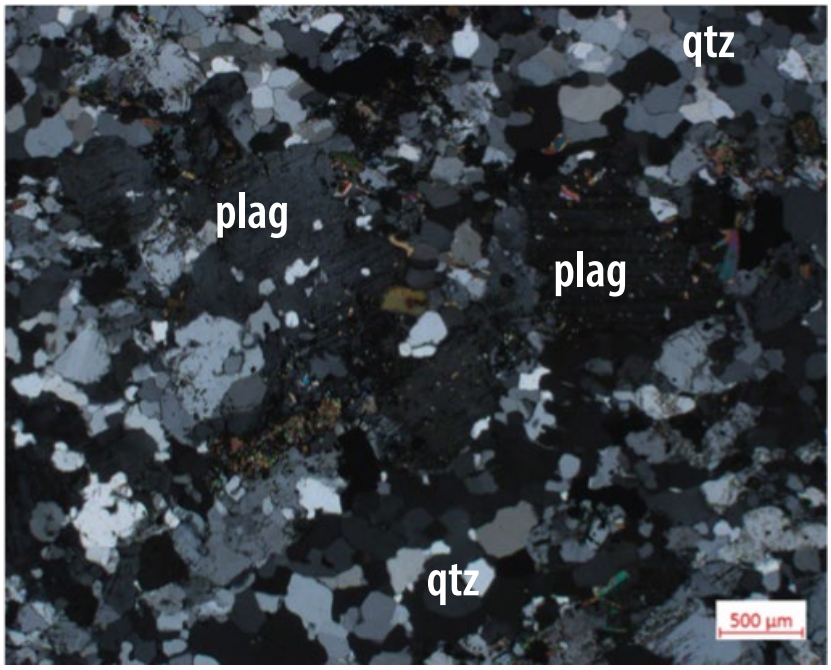

Microphotograph (XPL) showing saussuritization of plagioclase grains, and recrystallizing texture of quartz.

Sample: 140827 (granite)

Hand specimen:

This is a medium-grained, porphyritic light grey coloured rock. Phenocrysts of plagioclase are surrounded by weakly oriented grains of black biotite.

Minerals:

Plagioclase (40%), k-feldspar (30%), quartz (10%) and biotite (10%). Accessory minerals are epidote, muscovite and titanite.

Petrographic description:

This sample is collected not too far from the sample locality of sample 140828. The mineral assemblage is very similar, but this sample shows an overall higher degree of deformation. This is reflected in the less random and continuous foliation of the biotite grains. The biotite grains are subhedral, medium-grained and shows a dark green colour in ppl. The biotite shows small inclusions of the higher-relieff mineral epidote which shows a concentric zoning. The muscovite found in the thin section appear post-tectonic as it do not seem to follow the foliation and show a more euhedral shape than the biotite. The rest of the thin section consists of medium-grained, anhedral crystals of quartz and plagioclase. Accessory mineral is titanite. The rock can be described as an intermediate to coarse-grained, deformed, foliated rock.

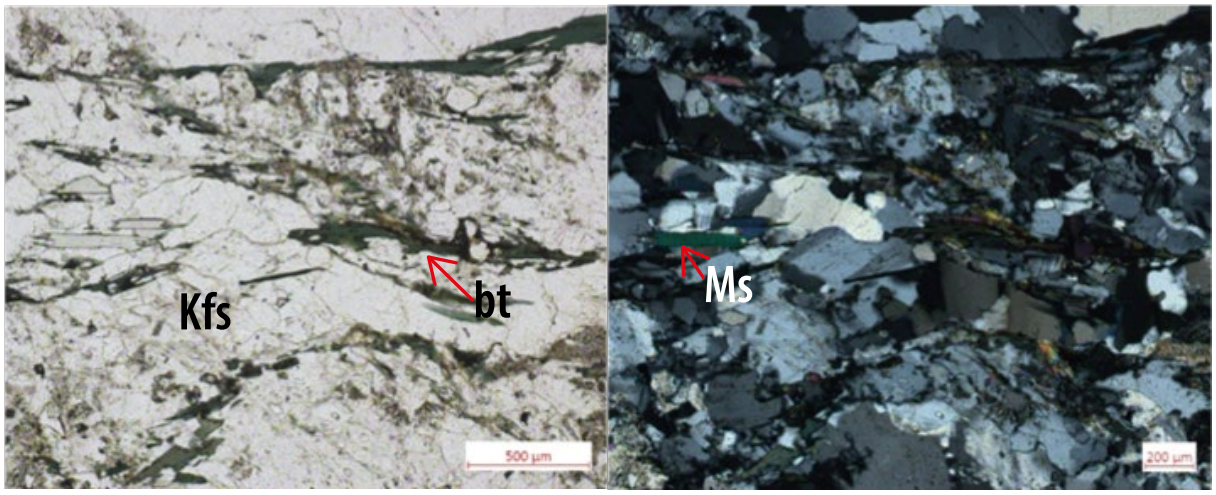

The first microphotograph (PPL) shows a foliation of green biotite grains. The second microphotograph (XPL) shows that the flaky colourless grains shown in the first photo is muscovite with bird-eye texture.

Sample: 140828 (granite)

Hand specimen:

This is a coarse-grained, inequigranular, porphyritic and weakly foliated rock. It appears with a light grey colour, with phenocrysts of k-feldspar making it pink. The dark biotite grains give the rock a slightly gneissic texture.

Minerals:

K-feldspar (50%), quartz (35%) and biotite (15%). Accessory minerals are epidote, titanite, muscovite, oxides and allanite.

Petrographic description:

This sample show a mineral assemblage of phenocrystic k-feldspar (microcline and orthoclase), coarse-grained plagioclase, biotite, metamict allanite and quartz. The thin section shows oxides also in this sample, that appear black in ppl and isotropic in xpl. The feldspar is altered in this sample, because of the fine grainsize of the alteration products it is hard to distinguish the alteration process, and both epidote and muscovite appear other places in the thin section. The alteration is mainly in plagioclase and is therefore interpreted to be saussuritization, indicating retrograde metamorphism of the rock. The allanite show a brown colour in both ppl and xpl as it masks its own colour, appearing with rimming as it is an inclusion in mostly epidote formed together with the biotite. The biotite grains appear subhedral with a flaky shape and forms a foliation of the granite, together with muscovite grains. The titanite show simple twinning. The texture can be described as coarse-grained and deformed. Accessory minerals are zircon, apatite and muscovite.

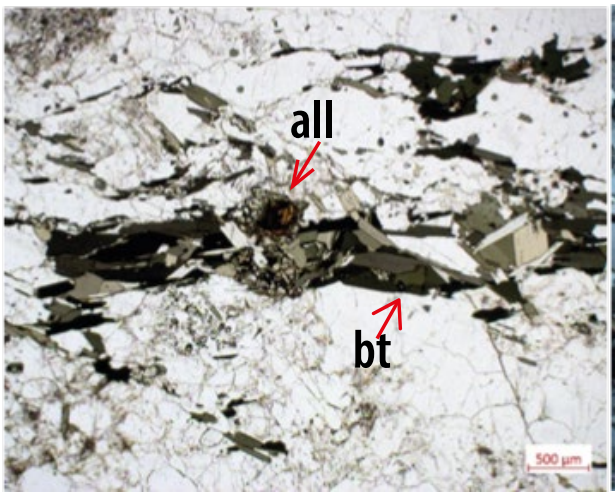

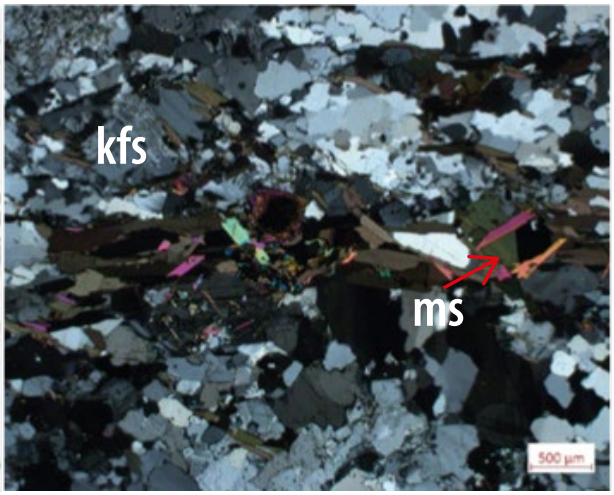

The first microphotograph (PPL) shows a grain of allanite with a rim of titanite in a cluster of green biotite. The second microphotograph (XPL) shows the same photo in XPL showing post-tectonic muscovite which grows across the foliation formed by the biotite.